

SECTION VII

LIST OF SYMBOLS

STABILIZATION AND ORIENTATION OF BALLOON-BORNE INSTRUMENTS

by

Russell A. Nidey

List of Symbols ii

List of Figures v

List of Tables v

A. INTRODUCTION 1

B. AZIMUTH STABILIZATION 3

1. Reaction Wheel 4

2. Motors 7

3. Perturbations 13

C. GIMBAL CONSIDERATIONS 17

D. ERROR SENSORS 19

E. EXAMPLES OF VARIOUS BALLOON-BORNE CONTROL SYSTEMS 29

1. The Solar Azimuth Pointing Platform 30

2. The Bi-axial Pointing Control 30

3. Stratoscope I 32

4. Coronascope 35

5. StratoLab 36

6. BAL-AST 39

7. Star Gazer 41

8. BBSP-200 44

9. Skytop 46

10. Polariscope 49

11. Stratoscope II 50

F. CONCLUSIONS 53

REFERENCES 54

<u>Symbol</u>	<u>Description</u>	<u>Dimensions</u>
A	subscript denoting aximuthal axis	
A_o	area of the objective	L^2
A_p	area of a photo-element	L^2
B	function used in the form $B(\lambda, \theta, \varphi)$ to indicate the rate at which photons arrive at a position analyzer from the background	
B	subscript denoting background	
D	function used in the form $D(t)$ to describe the action of a signal demodulator	
D	subscript denoting dark current	
E	efficiency of a telescope; $E(\lambda)$ is the efficiency of a telescope including the spectral character of the optics and the photo-element	
F	focal ratio of a Fabry lens	
g	acceleration due to gravity	LT^{-2}
G	fractional gradient in the background illumination	
G	subscript used with I to denote moment of inertia of the aximuthal gimbal	
I	moment of inertia. Subscripts are used to specify the axis about which I is taken	ML^2
L	length of pendulum	L
L	subscript denoting longitudinal axis	

M	a function used in the form $M(\theta, \varphi, t)$ to indicate the transmission of an analyzer	
n	an integer, e.g., 1, 2, 3	
N	cycles of the analyzer over which the signal has been integrated	
R	radius of prismatic suspension system	L
S	signal	
S_D	minimum signal due to the dark current	
t	time	T
T	period	T
T	function used in the form $T(\lambda, \theta, \varphi)$ to indicate the rate at which photons arrive at a position analyzer from a target	
T	subscript used to denote the transverse axis	
T	subscript used to denote target	
$(TE)_\lambda$	function defined as $\int_\lambda T(\lambda) E(\lambda) d\lambda$	
V	magnitude of target	
X	angular error	

Greek Letters

β	angular elevation of objective above the local horizon
γ	half amplitude (angular displacement) of a gondola about the horizontal axis which the line of sight from the gondola to the object projects onto the horizontal plane
δ	angular diameter (relative to the objective) of the circle of illumination produced on the analyzer by the target
Δ	half amplitude (angular displacement) of a gondola about its own azimuth axis
ΔX_B	statistical limiting accuracy due to photon noise in the signal from the background
ΔX_T	statistical limiting accuracy due to photon noise in the signal from the target
ϵ	error due to gradient in the background illumination
η	dark current of a photo-element
θ	angular displacement about the vertical axis
Θ	position angle measured about the optical axis
λ	wave length of light
φ	position angle measured about an axis transverse to the optical axis
φ_0	position angle (see φ) used as radius of the field of view
ω	rate of rotation T^{-1}

List of Figures

Fig. 1	The prismoidal multipoint suspension system	6
Fig. 2	Cross-spin forcing of the azimuth control system	16
Fig. 3	The solar azimuth pointing platform (photograph courtesy of Ball Brothers Research Corp.)	31
Fig. 4	The solar biaxial pointing control (model 3-4M) (photograph courtesy of Hi-Altitude Instrument Company, Inc.)	33
Fig. 5	Coronascope II at Palestine, Texas, prior to the flight of June 6, 1970	37
Fig. 6	The Johns Hopkins University 12-in. telescope mounted on the StratoLab gondola (photograph courtesy of Librascope, Inc.)	38
Fig. 7	The BAL-AST unmanned telescope system (line drawing courtesy of Johns Hopkins University).	40
Fig. 8	The photoelectric tracker used on BAL-AST shown in a test fixture (photograph courtesy of Impro Corporation)	42
Fig. 9	The balloon-borne bi-axial solar pointer shown with simulated instrument and gondola (photograph courtesy of Ball Brothers Research Corp.)	45
Fig. 10	Stratoscope II, the largest of the current balloon-borne telescopes, shown at Huntsville, Alabama, prior to the flight of September 9, 1971	54

List of Tables

Table 1	Rating of selected azimuth motors	9
---------	---	---

STABILIZATION AND ORIENTATION OF BALLOON-BORNE INSTRUMENTSA. INTRODUCTION

In the context of this section stabilization is defined as the reduction of the angular velocity of the instrument about one (or more) of the axes to a value appropriately near zero; and orientation is defined as the directing of the instrument toward a specific target. Whether stabilization or orientation is required depends upon the measurement being made by the instrument and upon the extent of the degradation of the measurement due to the motion of the balloon.

The balloon can be expected to be rotating some tens of degrees per minute in azimuth. This motion is generated primarily during ascent and descent of the balloon by windmill action of the gores. In addition to the azimuth rotation of the balloon (and gondola) there is a pendulous motion of the gondola beneath the balloon, with the balloon participating to a degree in this motion. The motion can be that of a simple pendulum in a single vertical plane, or a combination of two such motions with the gondola describing an elliptical or more complex path beneath the balloon.

The amplitude and character of the pendulous motion depends very much on the portion of the trajectory under consideration. The motion may be very severe during the launch phase, but should be very small at float altitude. Characteristically, at float, the amplitude is of the order of a few minutes of arc, with one degree representing a reasonable design limit. The period of the pendulous motion is directly related to the length of the pendulum:

$$T = 2\pi(L/g)^{\frac{1}{2}}$$

where T is the period; L, the length of the pendulum; and g, the acceleration of gravity. Thus, if the length is 100 m the period is about 20 sec.

The gondola will also oscillate about its center of mass as a compound pendulum. The period of this motion is characteristically much shorter, and the amplitude much less; moreover, this motion is more readily damped by the ambient air.

Inasmuch as differential motion of the ambient air relative to the balloon system continually excites the natural frequencies of the system, it is essential that all mechanical resonances including that of the compound pendulum, be well outside the critical band pass of the control sys-

tem. Hence, the gondola must be constructed as a simple, rigid system to reduce the number of resonant frequencies and to assure that these frequencies are above those critical to the control system.

Uniaxial control suffices if it is necessary only to have one side of the instrument turned, say, toward the sun. Biaxial control is necessary if the instrument, such as telescope, must be pointed at a celestial target; and triaxial control is indicated if the image of the target is not to be allowed to rotate in the focal plane of the instrument, as for high resolution photography of the moon.

Though the choices of the number and order of the axes of the gimbals, the motors that drive the gimbals, and the sensors that command the motors are clearly based on the specific instrument to be controlled, a number of generalizations can be made. Since the azimuthal motion of the balloon constitutes the most severe of the motions to be countered by the control system, virtually all control systems will have an azimuth stabilization gimbal as the first gimbal.

B. AZIMUTH STABILIZATION

To control the instrument there must be a source of reaction torque.

A propeller on the end of a lever could be used to react against the ambient air. Though the accuracy of such a system would be limited severely by the lag of the torque behind the control signal, coarse stabilization could be obtained. Higher speed of response and hence greater accuracy would be obtained by ejecting a gas or pellets; however, not only would the duration of the mission be bounded by the quantity of "fuel" carried, but also the accuracy of control would be limited by the method of metering the ejecta. Greater accuracy can be obtained by driving a reaction wheel, the chief limitation being that the total impulse available is determined by the size and maximum speed of the wheel.

1. Reaction Wheel

For a top speed of 500 rpm in a wheel 0.5 m in diameter, the maximum total impulse available would be less than 200 N m/kg. Without active in-flight balancing of the gondola it would be very difficult to reduce the residual azimuthal gravitational moment to less than 0.1 N m. Thus, a reaction wheel of one kg mass could be expected to be saturated in less than one-half hour. In contrast, a 280 kg balloon 60 m in diameter subjected to the same secular bias would accrete speed at the rate of only 15° per

minute per hour. Furthermore, any rotational speed of the balloon in excess of a few degrees per minute would be aerodynamically dampened by the ambient atmosphere. Consequently, the balloon constitutes an excellent source of reaction torque for the azimuth gimbal. However, the balloon is not rigid; thus, to avoid undue velocity in the control motor, it is usually expedient to incorporate a wheel intermediate between the gondola and the balloon. This wheel is generally coupled to the balloon with a prismatic multipoint suspension system as illustrated in Fig. 1. The parachute risers may be used conveniently as the multiple load lines.

If the maximum torque that the suspension train can transmit to the balloon is less than can be developed by the azimuth motor, it is necessary to incorporate a torque limiter between the reaction wheel and the balloon to avoid winding the parachute into an ineffective rope. The torque limiter may be viscous or non-viscous, obtained by using a Teflon or a neoprene shoe, respectively, on a steel wheel in a classical prony brake. The latter maximizes the momentum transfer; the former strongly dampens the torsional oscillation of the wheel relative to the balloon.

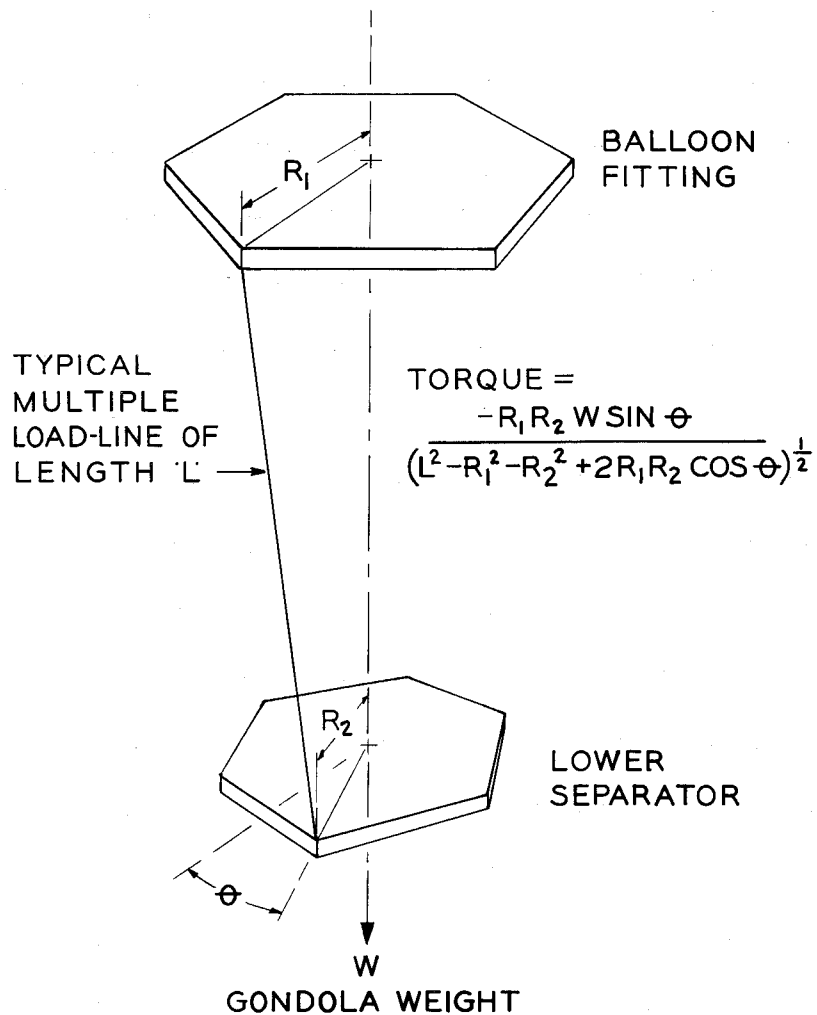


Fig. 1. The prismatic multipoint suspension system.

2. Motors

Consider now the selection of the motor. One can enumerate a number of ideal characteristics that this element should have:

- a. If the system is to be rather "tight," the torque produced by the motor must be proportional to the driving signal.
- b. The motor should also be non-viscous; i.e., the torque should be independent of the relative velocity between the reaction wheel and the gondola. Back emf (as well as any source of drag between the stator and the rotor) provides disadvantageous viscous reaction in the motor.
- c. To avoid inertial coupling of the wheel to the gondola, the motor should be directly coupled between the gondola and the wheel. Otherwise, oscillation of the wheel on the torsional suspension system will constitute a corresponding forcing function to the stabilization system.
- d. Since the balloon may make several revolutions during the flight, the motor must be able to accommodate a corresponding number of revolutions of the wheel relative to the gondola.

e. In addition, in some instances, power amplification may be required.

It may be necessary to derive relatively robust motion from a relatively weak power source.

f. Reliability of the motor is essential. The system must operate repeatedly in a predictable manner; the loop gain, adjusted on the ground for optimum performance, must not be grossly different at float altitude.

g. The motor should be easy to excite and to incorporate. A complex power output stage in the power amplifier, as a case in point, would be disadvantageous, as would a complex mounting involving many gears and bearings.

h. Finally, the motor must have a satisfactory frequency response; i.e., the torque output should be reasonably independent of the frequency of excitation (and without undue phase shift) to a suitably high frequency, the higher the better.

It is instructive to rate the three best suited motors (servomotors, torque motors, and electromagnetic clutches) on each of these factors

(Table 1).

Table 1

Rating of Selected Azimuth Motors

Characteristic	Servomotor	Clutches	Torque motor
Proportionality of torque to excitation	Excellent	Excellent	Excellent
Independence of torque with speed	Inferior	Superior	Mean
Adaptability to direct coupling	Inferior	Superior	Superior
Accommodation of multi-revolutions	Excellent	Excellent	Excellent
Power amplification	Mean	Superior	Inferior
Reliability	Superior	Inferior	Superior
Ease of excitation	Superior	Superior	Mean
Ease of incorporation	Mean	Mean	Superior
Frequency response	Superior	Inferior	Superior

The two-phase servomotor is perhaps the most highly developed of the three. A great deal of effort has been spent during the last three decades developing a servomotor exhibiting a high ratio of torque to moment of inertia. A large ratio is essential in control systems requiring high angular acceleration, but not particularly so in the balloon applications, where the angular acceleration required is relatively modest.

The servomotor exhibits excellent linearity, but is inferior in regard to viscous and inertial reaction. Further compromise is encountered with backlash between the bull gear and the drive pinion, usually necessitating anti-backlash gearing. The use of spring-loaded gears to eliminate the backlash introduces additional friction, as well as an asymmetry favoring one direction.

The servomotor is without peer in regard to reliability and exhibits a superior frequency response. It is more difficult to incorporate than the torque motor, but less difficult to excite.

The torque motor was initially developed for use on inertial navigation platforms, and has since been used to advantage on a number of balloon-borne instruments. The linearity of this motor is excellent. It exhibits

a more viscous response than the clutches, but less than the servomotor. It can be directly coupled, requiring no bull gear or bearings of its own. If it incorporates a commutator, it can be used without limit stops, but only at a moderate speed (less than 600 rpm). The commutator introduces some friction and limits the life of the motor, but neither is serious. Being a current device, it is wasteful of power, providing less than unity power gain. Hence, it is more difficult to excite than either the servomotor or the clutches; with transistors, however, a satisfactory output stage may be readily built.

Dual overrunning contra-rotating clutches have been used to avoid the viscous and inertial reactions and to obviate the difficulties pertaining to backlash in the gear train. By modulating the power from a separate prime mover, rather than converting electrical to mechanical energy directly, the electromagnetic clutch has a power amplification of about 50. By the same token, because the pair of clutches must be constantly overdriven by the prime mover (usually an electric motor), they are wasteful of power.

A single prime mover is usually used to drive the clutches in opposite directions, with the output shafts of the clutch pair coupled in opposition

directly to the bull gear. Because the pair is continuously opposed, the backlash is automatically removed. The output torque of a pair of clutches is proportional to the excitation independently of the speed of the output shaft. It is the absence of viscous, as well as inertial, reaction which makes the clutch particularly desirable as an azimuth motor. However, as far as reliability is concerned, the clutches are inferior. The output torque for a given excitation tends to decrease gradually with use.

The frequency response of the clutches is also inferior. The break frequency is about 2 cps; the mid-frequency attenuation, about 10 db per decade; the low frequency asymptotic phase shift, about 12 deg; and the high frequency asymptotic phase shift, about 60 deg, Stuart (1).

From a comparison of the ratings of these three motors, it is clear that no single one has all of the characteristics desired. A compromise on several factors must be made in each instance; the choice depends on the specific stabilization system. The choice will certainly be influenced by the magnitude of the perturbations encountered by the system during the flight.

3. Perturbations

Translational acceleration of the balloon gondola will result in perturbing torques if the center of mass of the gondola is not coincident with the axes of the stabilization system. During launch and ascent, this perturbation may be particularly severe, but should be of little consequence at float. At float, the gravitational bias resulting from an improperly balanced gondola or instrument may be significant. The bias in the azimuth degree of freedom may be conveniently alleviated by placing an aircraft universal joint at the base of the suspension train.

An asymmetric gondola will also be subject to aerodynamic perturbations. The aerodynamic moment is proportional to the square of the velocity of the air relative to the gondola and, save for gusts during ascent, is negligible, except for the excitation of mechanical oscillations.

Internal motion of components, such as the movement of a plateholder or the shifting of film from a supply spool to the take-up spool, may introduce inertial and gravitational perturbations of consequence depending upon the relative mass of the component and the gondola. On occasion, it may be necessary to provide counter-motion; i.e., if an object is moved, another

object would be moved in the opposite direction to compensate for the reaction.

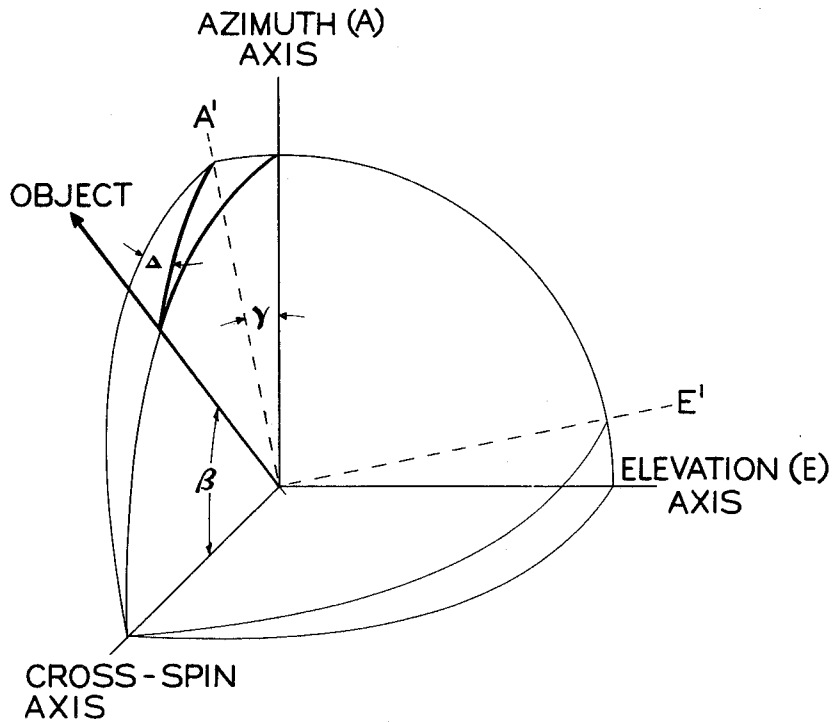
Friction in the gimbal bearings, both static and kinetic, constitutes a major perturbation. The static friction is the more troublesome, whereas the kinetic friction can be lumped with the viscous character of the motor. The friction noise, or stiction, characteristically contains frequencies higher than the bandpass of the stabilization system; hence, this noise must be attacked at the source by using floated bearings, by the use of dynamic bearings (in which an intermediate race is driven continually relative to both the outer and the inner race) or by the use of members that flex rather than slide. Because of the multi-revolution requirement, the flexure bearing is suitable only for gimbals other than azimuth (such as elevation) and then the design of the flexure member must be such that the suspension is virtually neutral.

Inertial and viscous reactions were mentioned earlier in connection with the discussion of the motor, but without explanation. The reaction wheel can be expected to be oscillating, whereas the stabilized instrument must not. Hence, if the motor is geared to the reaction wheel, the motor

must be accelerated in synchronism with the oscillation to avoid coupling the oscillation to the payload. The reflected inertia and the corresponding counter excitation of the motor is proportional to the square of the gear train ratio; consequently, the ratio should be selected to be the least possible consistent with the other considerations. This criterion is contrary to the usual practice of matching the reflected inertia to the load, as for maximum power transfer.

The viscous coupling is analogous to the inertial coupling and can likewise be lessened by the choice of the motor, by minimizing the gear train ratio, or by both.

The pendulous motion of the gondola introduces a gimbal restraint. Suppose the payload is to be oriented in azimuth relative to an object which has an elevation of β above the horizon, while the gondola is pendulously oscillating about the projection on the horizontal plane of the line of sight to the object (or cross-spin axis in Fig. 2) with a half amplitude of γ . Then the azimuth control system will be forced to cyclically drive the gondola about the azimuth axis with a half amplitude, Δ , given by the following expression:



$$\tan \Delta = \sin \gamma \tan \beta$$

β = ELEVATION ANGLE OF OBJECT

Fig. 2. Cross-spin forcing of the azimuth control system.

$$\Delta = \arctan (\sin \gamma \tan \beta)$$

for $\beta \approx 45^\circ$ and $\gamma < 1^\circ$, $\Delta \approx \gamma$.

Hence, the azimuth control system may suffer appreciable forcing due to the gimbal restraint. The restraint may be obviated by the use of at least three gimbals.

Virtually all that has been said about the azimuth control system also applies to the second and third control gimbals, except that in these gimbals, limited travel is required and the azimuth (or intermediate) gimbal, restrained by the gravitational field, constitutes sufficient reaction reference.

C. GIMBAL CONSIDERATIONS

The second gimbal to be added is logically an elevation gimbal since, to avoid inter-axis coupling, the second gimbal axis should be orthogonal to the first and, to point the instrument, the second axis should be transverse to the axis of the instrument. If, however, the azimuth error sensor is mounted on the instrument and senses the motion of the target relative to an axis transverse to the instrument, as is usually the case, the azimuthal sensor gain is proportional to the cosine of the elevation angle, β .

Moreover, if the longitudinal and transverse moments of inertia of the instrument (I_L and I_T , respectively) are unequal, the azimuthal moment of inertia, I_A , also varies with β .

Specifically,

$$I_A = I_T \cos^2 \beta + I_L \sin^2 \beta + I_G$$

where I_G is the moment of inertia of the azimuthal gimbal.

Hence, the loop-gain is proportional to

$$\cos \beta / (I_T \cos^2 \beta + I_L \sin^2 \beta + I_G)$$

and the azimuthal gain-margin may be minimum at an intermediate elevation angle requiring that the loop-gain be adjusted at the intermediate position to avoid oscillation of the control system during flight.

The third gimbal to be added may be either cross-elevation or cross-azimuth. If it is cross-elevation, the gain margin on two of the three gimbals, elevation and cross-elevation, will be constant; but, since the cross-elevation axis will not in general be orthogonal to the azimuth axis, inter-axis coupling will be obtained. On the other hand if the third gimbal is cross-azimuth, added between the azimuth and elevation gimbals, inter-axis coupling is obviated but the loop-gain on two of the three axes, azi-

imuth and cross-azimuth will not be constant. The choice between the two alternatives is not obvious. Thus, when the third gimbal is dictated (to avoid rotation of the image of the target, to obviate the gimbal restraint, or to accommodate offset guiding) a detailed study of the trade-offs should be made.

In some instances, redundant gimbals may be incorporated to avoid having one gimbal interfere with another, to maintain three independent degrees of freedom, or to utilize limited travel on one or more gimbals.

Moreover the gimbal system may be conventional, i.e., with the azimuth gimbal on the outside, or inside-out. The inside-out configuration is lighter, but affords less protection for the instrument. In addition, the counter-balances tend to be more complex and all testing must be done with the gondola suspended as during flight.

D. ERROR SENSORS

Any field sensing device can be used as the error sensor to excite the motor to control the gimbal. An example is a compass which senses the magnetic field. A compass is not a good choice for a precise control system, but may well serve as a coarse sensor to establish initial orientation.

The magnetic field also varies with geographic position as does the gravitational field. Hence, these fields are of primary value in conjunction with geophysical instruments and to control the third or fourth gimbal.

In addition, it is difficult to distinguish the gravitational field from the linear and angular accelerations of the gondola. In particular, a bubble level cannot be used to measure local vertical in the presence of pendulous motion, a point that has often been overlooked by balloonists.

Electromagnetic flux can also be used as a source of orientation signals. The emitted (or reflected) light from the sun, a planet, or a star can be detected by a photoelectric telescope to derive two control signals per celestial source. Though a third signal can, in principle, be derived from a source of finite angular size, which has surface features, such as the moon, it is expedient in general to use a second celestial source or another sensor, such as a gyroscope, to obtain the third signal.

A photoelectric guide telescope incorporates four elements to derive the control signals: An objective element, an image position analyzer, a field defining element, and the photo-element. The objective element collects the light from the celestial target and usually forms an image of the

target on the analyzer. The analyzer modulates the light energy as a function of the position of the image on the analyzer. The field element, by defining the field of view, rejects the stray light around the target enhancing the signal-to-noise ratio. Except in instances in which an extra-focal analyzer is used to increase the linear range of the telescope, it is advantageous to use a Fabry lens as the field element. The Fabry lens is used to form an image of the aperture of the objective element on the photo-element obviating local variations in the quantum efficiency of the photo-element. The photo-element may be a phototube, a photodiode, a photoconductor, a photomultiplier, or a photovoltaic device, depending on the intensity of the light and many other factors.

The "objective" element may range from a shadow casting aperture for a solar sensor to a large mirror for a stellar sensor with the error resolution ranging from a fraction of a degree to a millisecond of arc. The analyzer may be a fixed knife-edge, a prism, a split field polarizer, a mosaic of photodetectors or a rotating knife edge to name a few that have been used. Of these, the rotating knife-edge provides the greatest accuracy.

The accuracy of a guide-telescope is a function of the brightness and angular size of the image of the target, the efficiency of the telescope, the temperature and character of the photocathode, the time interval during which the signal is integrated, and the size and celestial position of the field of view of the telescope. The interplay of these factors can perhaps best be illustrated by considering a specific example. Let (1) θ and φ be the two position angles designating an element on the position analyzer (θ being measured about the optical axis and φ , transverse to the optical axis) where φ_0 is the radius of the field of view; (2) $A_0 T(\lambda, \theta, \varphi)$ and $A_0 B(\lambda, \theta, \varphi)$ be the rate at which photons of wave length λ arrive at the position analyzer from the target and from the background, respectively, where A_0 is the area of the objective; (3) $E(\lambda)$ be the efficiency of the telescope including the spectral character of the optics and of the photo-element; (4) $M(\theta, \varphi, t)$ be the transmission of the analyzer, a function not only of the position of the element on the analyzer, but also of time t ; (5) $D(t)$ be the function describing the action of the signal demodulator; and (6) η and A_p be the specific dark current and area of the photo-element,

respectively (the former, of course, depends upon the temperature at which the element is used). The signal from the telescope is then given by the expression:

$$dS = \int_0^{\varphi_0} \int_0^{2\pi} \int_{\lambda} \{ [T(\lambda, \theta, \varphi) + B(\lambda, \theta, \varphi)] [A_0 E(\lambda) M(\theta, \varphi, t) D(t) d\lambda d\theta d\varphi] + \eta A_p \} dt$$

For a rotating knife-edge and a synchronous demodulator $M(\theta, \varphi, t)$ and $D(t)$ are simple double-valued periodic functions: $M(\theta, \varphi, t) = 1$ for $\omega t - n\pi \leq \theta \leq \omega t - (n-1)\pi$ and $\varphi \leq \varphi_0$ and $M = 0$ for all other values of θ and φ , where n is an integer and ω is the rate of rotation of the knife-edge; and $D(t) = 1$ for $2\pi n \leq \omega t \leq 2\pi(n+1)$ and $D = -1$ for all other values of ωt . Thus, neglecting the background and dark current for the moment and considering a small angular error, X , where the image of the target is nearly bisected by the knife-edge, the target signal is sinusoidally modulated and full-wave rectified to give the following expression for the signal due to the target:

$$S_T = A_0 (TE)_{\lambda} N \left[\int_0^{\pi/\omega} \{ (4\delta X/\pi\delta^2) \sin \omega t + \frac{1}{2} \} dt \right]$$

$$- \int_{\pi/\omega}^{2\pi/\omega} \{ (4\delta X/\pi\delta^2) \sin \omega t + \frac{1}{2} \} dt]$$

$$= A_o (TE)_\lambda N [16X/\pi\delta\omega + \pi/2\omega - \pi/2\omega]$$

where $(TE)_\lambda \equiv \int_{\lambda} T(\lambda) E(\lambda) d\lambda$, δ is the angular diameter (relative to the objective) of the circle of illumination produced on the analyzer by the target (the circle is assumed here to be uniformly illuminated) and the signal has been integrated for N cycles of the analyzer (N must not be less than 20 for reasonably satisfactory demodulation). The latter two terms in the expression cancel in the absence of photon noise. With photon noise, the noise component may not cancel and the statistical limiting accuracy due to the photon noise in the signal from the target, ΔX_T , is given by the expression:

$$S_T = 0 = [16 A_o (TE)_\lambda N/\pi\delta\omega] \Delta X_T + \pi A_o (TE)_\lambda N/2\omega$$

$$+ [\pi A_o (TE)_\lambda N/2\omega]^{1/2} - \pi A_o (TE)_\lambda N/2\omega$$

$$+ [\pi A_o (TE)_\lambda N/2\omega]^{1/2}$$

or

$$\Delta X_T = [\pi^3 \delta^2 \omega / 128 A_o (TE)_\lambda N]^{1/2}$$

If $A_o (TE)_\lambda = 3.87 \times 10^5$ electrons sec^{-1} as for a target of magnitude $V = 0.00$ observed by a telescope with $A_o = 20 \text{ cm}^2$ ($\sim 3 \text{ in}^2$), an efficiency of 0.02 electrons photon^{-1} and an effective bandpass of 1,000 \AA (see Code 1962), and if $\delta = 12 \text{ sec of arc}$ and $\omega/N = 40\pi \text{ sec}^{-1}$ as for an integration time of (1/20) sec and a modulation frequency of 400 cps, the limiting accuracy due to photon noise in the target signal is 0.1 sec of arc. This limiting accuracy can be reduced by increasing the integration time (with attendant reduction of the speed of response of the control system), by increasing the area of the objective and by reducing the size of the image (with attendant increased difficulty in target acquisition). The size of the image cannot, however, be reduced to a value less than the larger of the diffraction limit of the objective or the angular diameter of the target.

If the background around the target produces a uniform gradient in the illumination of the analyzer, the signal due to the background is also sinusoidally modulated and rectified to give the following expression for the maximum signal from the background:

$$\begin{aligned}
S_B &= A_0 (BE)_\lambda N \left[\int_0^{\pi/\omega} \int_0^{\varphi_0} \{2GX(\varphi_0^2 - X^2)^{\frac{1}{2}} \sin \omega t \, dX + (\pi\varphi_0^2/2)\} dt \right. \\
&\quad \left. - \int_{\pi/\omega}^{2\pi/\omega} \int_0^{\varphi_0} \{2GX(\varphi_0^2 - X^2)^{\frac{1}{2}} \sin \omega t \, dX + (\pi\varphi_0^2/2)\} dt \right] \\
&= A_0 (BE)_\lambda N \left[8 \varphi_0^3 G/3\omega + \pi^2 \varphi_0^2/2\omega - \pi^2 \varphi_0^2/2\omega \right]
\end{aligned}$$

where $(BE)_\lambda \equiv \int_{\lambda} B(\lambda) E(\lambda) \, d\lambda$ and G is the fractional gradient in the background illumination. As before, the latter two terms in the expression cancel in the absence of photon noise. With photon noise the statistical limiting accuracy is given by the expression

$$\Delta X_B = [\pi^4 \varphi_0^2 A_0 (BE)_\lambda \delta^2 \omega / 128 A_0^2 (TE)_\lambda^2 N]^{\frac{1}{2}}$$

Assuming that $\varphi_0 = \tan^{-1}(0.1)$, $A_0 (BE)_\lambda = 1.04 \times 10^4$ electrons $\text{sec}^{-1} \text{deg}^{-2}$ as for the zodiacal light in the ecliptic some 80 deg from the sun, Allen (2), and the other parameters have the same values as before, the limiting accuracy due to the background photon noise will be 1.1 sec of arc. This error can be reduced by increasing the integration time and objective area, by reducing the field of view (with attendant increased difficulty in finding the target) and by observing a target in a less brightly illuminated portion of the sky.

The error due to the gradient in the background illumination is given by the expression

$$\epsilon = \pi \delta A_0 (BE)_\lambda \varphi_0^3 G / 6 A_0 (TE)_\lambda$$

If $A_0 (BE)_\lambda G = 2.32 \times 10^3$ electrons $\text{sec}^{-1} \text{deg}^{-3}$ again as for the zodiacal light in the ecliptic some 80 deg from the sun and the other parameters have the same values as before, the error is 0.7 sec of arc. This error can be reduced by observing a target in the region of the sky with a lesser gradient, by reducing the field of view, and by reducing the size of the image of the target.

If a Fabry lens is used, the minimum area of the photo-element is given by the expression

$$A_p = A_0 [2F \tan \varphi_0 / (1 - 2F \tan \varphi_0)]^2$$

where F is the focal ratio of the Fabry lens. Since $F \geq 1.5$, $A_p \geq 0.18 A_0$ (assuming $\varphi_0 = \tan^{-1} 0.1$ as before). The minimum signal due to the dark current is then given by the following expression

$$S_D = 0.18 A_0 \pi N [\pi/\omega - \pi/\omega]$$

As before, these two terms cancel in the absence of noise. The statistical limiting accuracy due to the noise in the dark current from a photo-element

of minimum size is then given by the expression

$$\Delta X_D = [0.18\pi^3 \eta A_o \delta^2 \omega / 64 A_o^2 (TE)_\lambda^2 N]^{1/2}$$

If $\eta = 4 \times 10^4$ electrons $\text{in.}^{-2} \text{ sec}^{-1}$ as for an S-11 photocathode used at room temperature and the other parameters have the same values as before, the limiting accuracy is 0.02 sec of arc. Though it would hardly be worthwhile in this example, this error can be reduced by cooling the photocathode, by reducing the size of the image, and by increasing the integration time and objective area.

It should be appreciated that in actual practice, the limiting accuracies, defined as in this example, can be approached only with difficulty. As a rule of thumb, it would be expedient to include a comfortable margin, say, an order of magnitude, between the design goal and the limiting accuracy due to each factor.

The photoelectric guide telescopes are used chiefly on orientation systems. For stabilization systems the floated rate integrating gyro is more appropriate, though equally expensive. This form of gyro, combining very low drift with high sensitivity (better than one deg per hr and 30 milli-

volts per milliradian, respectively), can be used for relatively long periods of time without assistance from an external reference. The low drift rate and the fact that the reference direction can be changed conveniently (as by remotely commanded torqueing) make this element particularly suited to multiple target missions.

Other gyroscopic elements may also be useful for providing coarse reference (such as the magnetically slaved free gyro) or for rate limiting (such as the spring restrained rate gyros).

E. EXAMPLES OF VARIOUS BALLOON-BORNE CONTROL SYSTEMS

There are as many different control systems for balloon-borne instruments as there are investigators that have seriously undertaken scientific measurements from balloons. This is true not only because of the individual preferences, but also because of the unique requirements of the various instruments. Most of the control systems have been designed to work automatically; of late, however, the tendency has been to invoke control by a radio system from the ground. Following the pattern of our previous discussions, I will first describe an automatic, single-axis stabilization system and progress to the more sophisticated multi-gimbaled and ground-commanded systems.

1. The Solar Azimuth Pointing Platform

Several single-axis orientation systems were built in 1959 for the Air Force Cambridge Research Laboratories by the Ball Brothers Research Corporation, Boulder, Colorado. These were intended to turn a variety of instruments mounted on the platform toward the sun with an accuracy of a fraction of a degree for several days. Special solar sensors, including one to activate the control system at sunrise and deactivate it at sunset, were incorporated. Two test flights were made in 1959, Dolder and Johnson (3).

A torque motor excited by a transistorized amplifier was used to drive the platform against the trapeze bar suspended below the platform. No torsional coupling to the balloon was used, windage on the trapeze bar and associated payload being deemed sufficient to prevent excessive speed of the torque motor. Universal joints on both ends of the azimuth shaft served to bound the gravitational bias on the control system. This system is shown in Fig. 3.

2. The Bi-axial Pointing Control

The first balloon-borne control system to be flown was developed at the

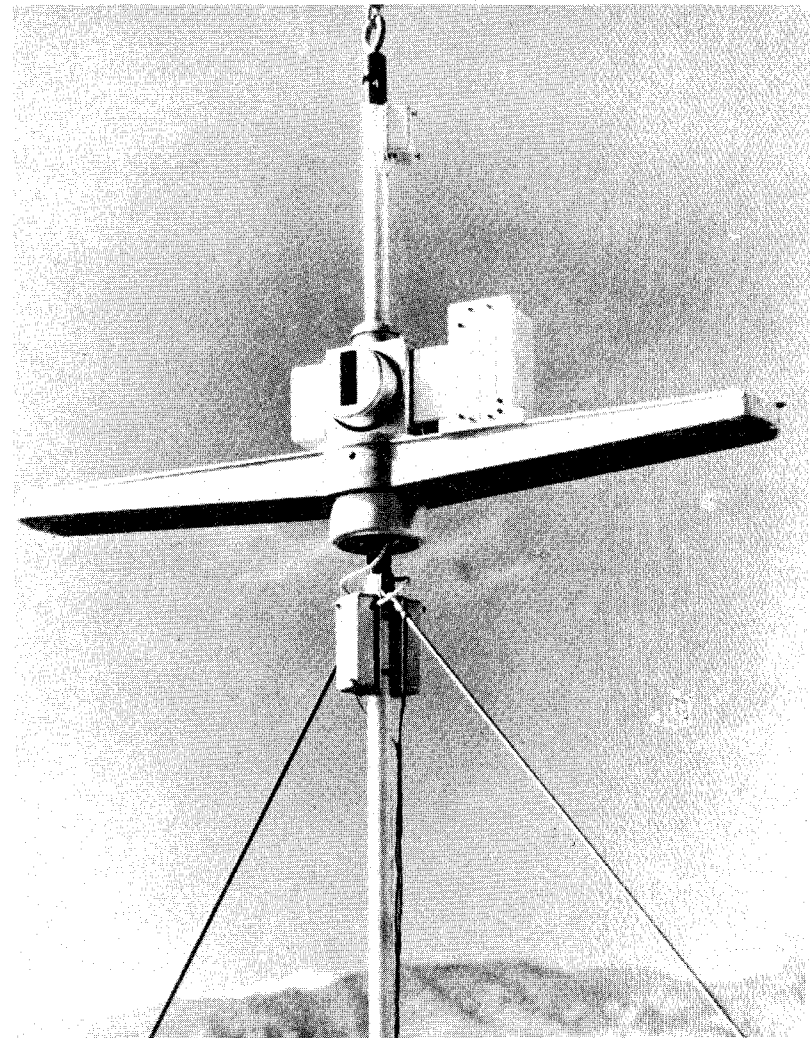


Fig. 3. The solar azimuth pointing platform (photograph courtesy of Ball Brothers Research Corp).

University of Denver, Edwards, et al. (4). It has since been improved and manufactured by the Hi-Altitude Instrument Company, Golden, Colorado.

Several designs are available, including lunar as well as solar versions.

One of these designs is shown in Fig. 4.

In general, counter-rotating clutches incorporating magnetically clamped disks have been used. Though these do not have the desired non-viscous character, they are much less wasteful of power than the magnetic particle clutches discussed earlier.

The accuracy is 0.1 deg or better in both azimuth and elevation. This system is relatively light in weight and low in cost. Several dozen flights have been made with it.

With the gondola suspended from the balloon by fine wires, complete freedom in azimuth has been obtained without undue occultation of the instrument and without use of the more complex reaction wheel system.

3. Stratoscope I

An explicit reaction wheel was first used on Stratoscope I in 1957.

Dr. Martin Schwarzschild of the Princeton University Observatory photographed the granulation of the solar photosphere with a very high resolu-

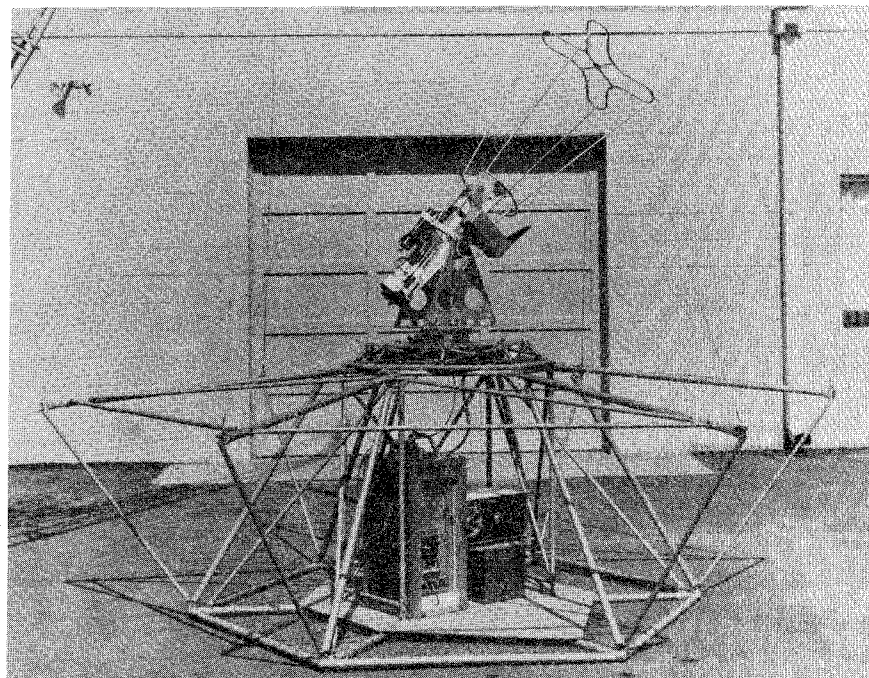


Fig. 4. The solar biaxial pointing control (model 3-4M) (photograph courtesy of Hi-Altitude Instrument Company, Inc.)

tion 12-in. telescope from above the stratosphere, Schwarzschild and Schwarzschild (5). Several sub-contractors were associated in the effort, including the University of Colorado, who developed the solar orientation system, borrowing heavily from the design of the earlier Aerobee-borne solar pointing control, Stacey, et al. (6). The azimuth and elevation drive units were constructed as rugged integral packages interconnected by welded tubular trusses; hence, remarkable longevity was obtained. Three flights were made in 1957, four in 1959, and many since as a part of "Coronascope." As originally built, both drive units used magnetic clutches. Inasmuch as the gears between the prime mover and the clutches generated undue high frequency vibrations of the telescope during flight, the clutches were replaced with geared servomotors prior to the second series of flights. In addition, a video-command link was incorporated in conjunction with an articulated guide-telescope assembly to permit selective observation of the solar photosphere, Danielson (7).

The accuracy obtained was a fraction of a minute of arc, though degradation of the accuracy was observed at higher elevation angles of the sun due to the gimbal restraint. Simple solar sensors, Nidey and Stacey (8),

were used with passive lead-lag networks for dampening.

4. Coronascope

The principal investigator with Coronascope has been Dr. Gordon Newkirk of the High-Altitude Observatory. Several flights have been made, Newkirk and Eddy (9) and Newkirk and Bohlen (10). Prior to a flight in 1964, a guide telescope sensing the limb of the sun was added to increase the absolute pointing accuracy to $\pm 1/3$ min of arc. Also, prior to a 1965 flight, the gear train in each of the servomotor drives was replaced with a steel-on-steel friction drive and the diameter of the objective of the guide telescope was increased from 1 cm to 5 cm to increase the accuracy to ± 5 sec of arc. At this accuracy, flexure of the instrument in the gravitational field of the earth became a problem. Thus, particular care was taken to assure that the guide telescope exhibited the same flexure as the coronagraph.

As the accuracy has increased, the difficulties with mechanical resonances have been compounded. In addition to the incorporation of an automatic gain control circuit to compensate for the loss of azimuth gain at high elevation angles of the sun, notched T filters in the compensation cir-

cuit and viscous dampeners on the servomotors have been tried with moderate success.

Coronascope is shown in Fig. 5.

5. StratoLab

With characteristic ingenuity Dr. John Strong of the Johns Hopkins University devised a novel optical system, Strong (11), to negate the majority of the motion of the manned StratoLab gondola. By use of his "monocentric" telescope design, using a servo-controlled secondary, the target image was stabilized to within ± 3 sec of arc in spite of motion of the telescope as large as ± 1 deg of arc. His 12-in. telescope was mounted on top of the gondola in an alt-azimuth mount (see Fig. 6). The elevation gimbal was controlled by an electrically powered Saginaw worm drive and the azimuth gimbal, by a variable-speed spur gearmotor. Both were operated by the observer located inside the gondola. The gondola was coupled to the balloon by a large diameter multipoint suspension system.

After many delays, due in main to failures of the balloons, the system was flown in 1959, Strong, et al. (12). Even with the monocentric telescope design, the gondola motion was sufficiently deleterious that the observer

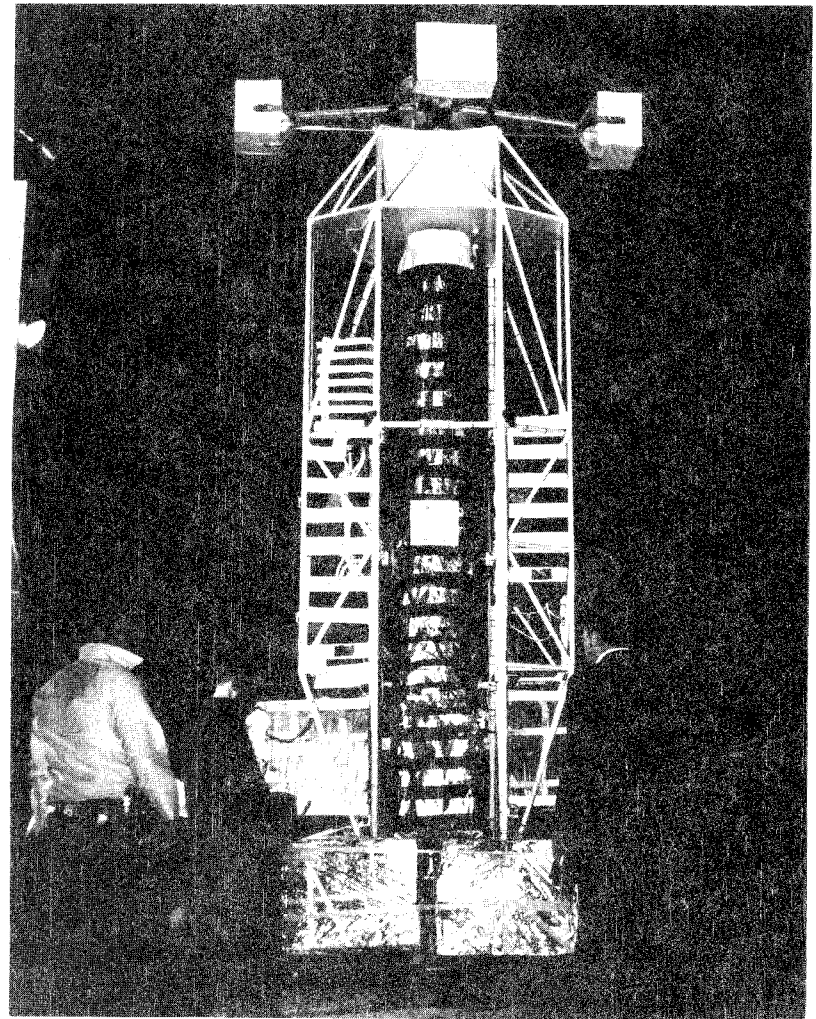


Fig. 5. Coronascope II at Palestine, Texas, prior to the flight of June 6, 1970.

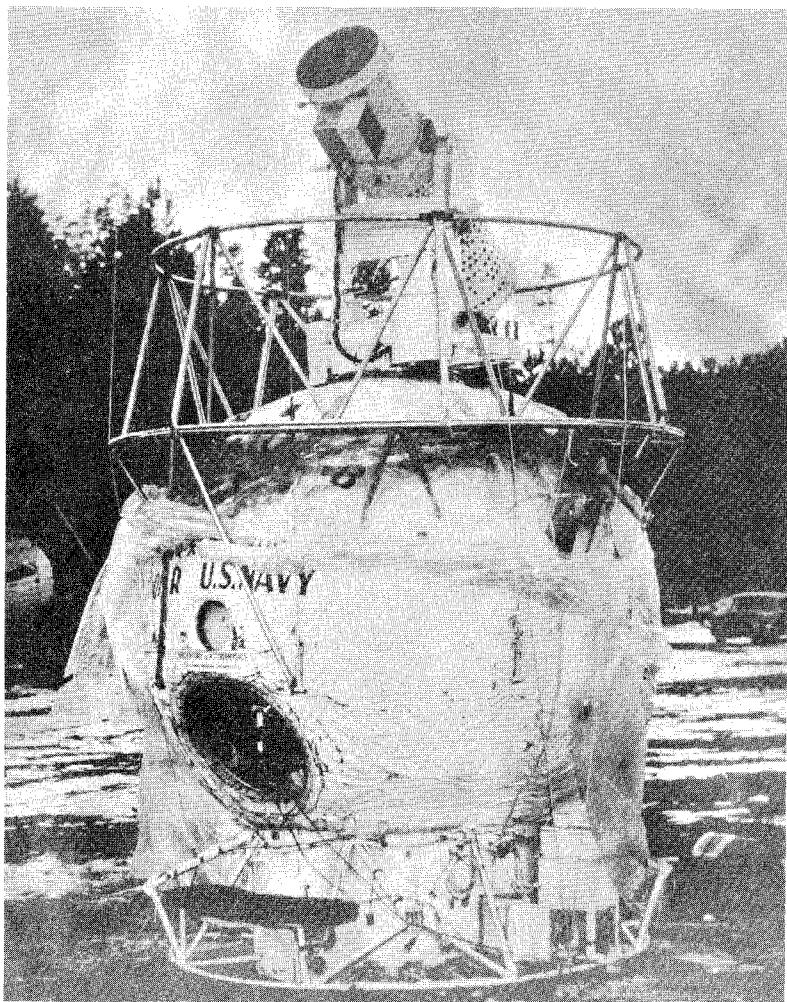


Fig. 6. The Johns Hopkins University 12-in. telescope mounted on the StratoLab gondola (photograph courtesy of Librascope, Inc.).

was barely able to gather the scientific data.

6. BAL-AST

In the Johns Hopkins BAL-AST System the gondola has been replaced with a reaction wheel and the initial acquisition is accomplished automatically with a clock-driven, offset-guiding system, Strong and Bottema (13) and Strong (14), rather than by command. Torsional coupling of the reaction wheel to the balloon has been obtained by use of an off-axis mount for the telescope with a spectrometer serving as a counterbalance. Thus, the risers do not interfere with the light beam as on StratoLab nor is the heavy reaction wheel above the telescope as on Stratoscope. This system is shown in Fig. 7. Though the Saginaw elevation drive of the StratoLab design has been retained, the azimuth drive has been improved by the substitution of a torque motor for the gearmotor and solar sensors for the observer command. The accuracy of azimuth stabilization is now a few minutes of arc. The star-tracker has also been much improved. The current version, built by the Impro Corporation, Pasadena, California, uses an image dissector tube to obtain a large acquisition field of view with a small instantaneous field of view, the latter to achieve daytime tracking. In the acquisition mode the instantaneous

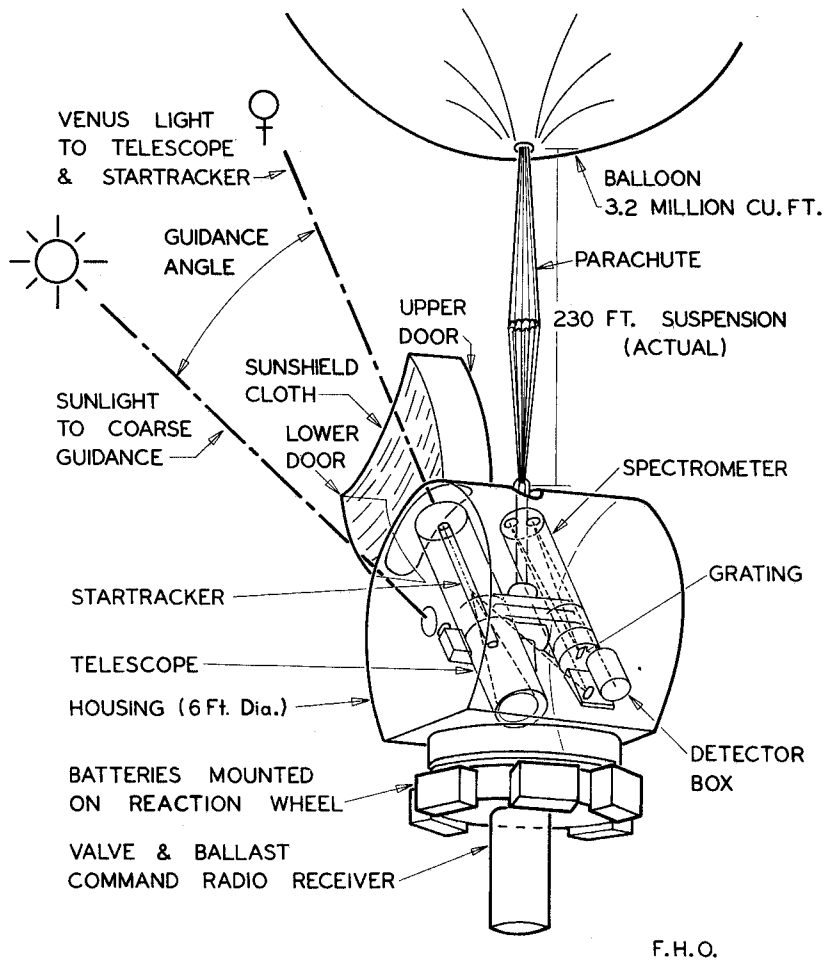


Fig. 7. The BAL-AST unmanned telescope system (line drawing courtesy of Johns Hopkins University).

field of view, some 10 min of arc in diameter, is electrically swept in a decaying spiral pattern from the circumference of the acquisition field of view, some 8 deg in diameter, to the center in about a second of time. After acquisition, the scan is switched to a cross pattern which generates the signals for the star-tracker actuators. These are two-phase 400 cps servomotors that tilt the star-tracker about elevation and cross-elevation axes. The gimballed tracker with a strap-down star-tracker is shown in a test fixture in Fig. 8. The test fixture simulates the azimuth and elevation drives of the primary telescope. The strap-down star-tracker in conjunction with a magnetometer can be used for nighttime acquisition of a bright target.

The BAL-AST System was flown twice in 1963: on the first flight the star-tracker malfunctioned because of high voltage arcing and on the second, the balloon burst at the tropopause, Strong (15). It was also flown successfully twice in 1964 and once in 1965.

7. Star Gazer

Under the guidance of Dr. J. Allen Hynek, then of the Smithsonian Astrophysical Observatory, the Massachusetts Institute of Technology built two balloon-borne control systems for a 12-in. telescope. The first of these,

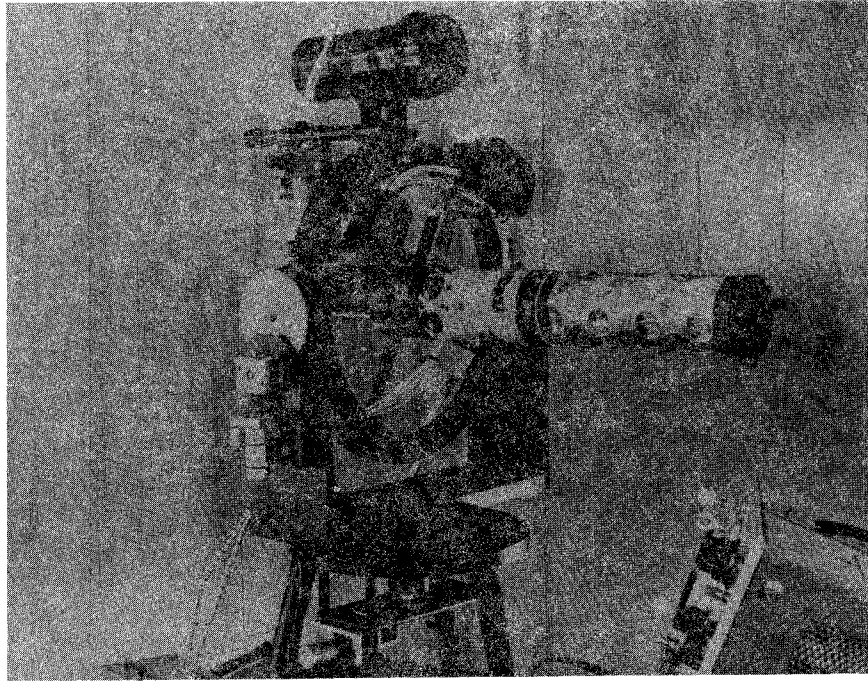


Fig. 8. The photoelectric tracker used on BAL-AST shown in a test fixture (photograph courtesy of Impro Corporation).

an unmanned tri-axial system, was wrecked at launch on its maiden flight. The second, a bi-axial system, was flown once in 1962, Markey, et al. (16). On this flight high-voltage arcing in the guide-telescope caused difficulties in tracking.

The manned system was superficially much like that used on StratoLab. Two gimbals were used, azimuth (or train) and elevation. Both were driven by torque motors. Though a guide telescope was used to trim the gyros, primary control of the telescope was vested in two floated rate integrating gyros. Initial acquisition was made by torquing the gyros from a console mounted inside the gondola.

The guide telescope used a 1P21 photomultiplier in conjunction with a rotating knife edge. The control accuracy obtained during pre-launch testing was ± 25 sec of arc with moderate gimbal motion and ± 2 min of arc with rolling and pitching motion of the order of 10 deg amplitude and 5 sec period. During flight, the stabilization accuracy was ± 30 sec of arc and some scientific data were obtained in spite of the tracker failure.

As on StratoLab, the Star Gazer gondola was coupled to the balloon with risers that occulted the telescope to a minor degree. The gondola served

as the azimuth reaction wheel. Initial acquisition of brighter objects was made by pre-setting the elevation angle of the telescope and then slewing the telescope in azimuth until the object to be observed appeared in the field of view of the telescope. Objects in the field of the telescope could be observed in the gondola by a mirror geared to the elevation gimbal which reflected light from the telescope through a window in the top of the gondola.

8. BBSP-200

Based on their earlier work on the Solar Azimuth Pointing Platform, the Ball Brothers Research Corporation has since developed a balloon-borne bi-axial solar pointer for the Air Force Cambridge Research Laboratories, Greeb (17). This system, shown in Fig. 9, an off-axis alt-azimuth system, has been built to point a 36-kg instrument up to 0.9 m in length to an accuracy of about ± 2 min of arc in both axes. Torque motors are used in both axes with fine and coarse solar sensors providing telemetry signals as well as control signals. Average power consumption is 17 watts from a 26-volt power source. The control system has a mass of 59 kg and is intended for use with a gondola having a mass of not more than 450 kg and a moment of inertia about the azimuth axis of not less than 70 kg m^2 .

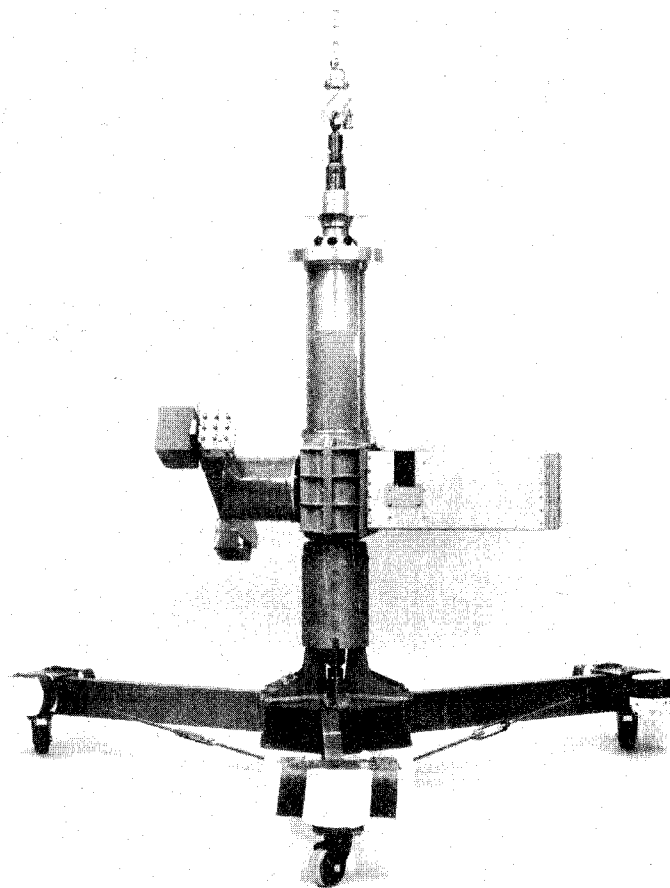


Fig. 9. The balloon-borne bi-axial solar pointer shown with simulated instrument and gondola (photograph courtesy of Ball Brothers Research Corporation).

The azimuth gimbal completely encloses the azimuth axle permitting electrical leads (as for load line severance) to be connected directly to the balloon from the gondola through the azimuth axle without the use of sliprings. Universal joints are used at the top and bottom of the azimuth axle to bound the gravitational bias.

9. Skytop

Dr. Alvin Howell's group at Tufts University has built and extensively used a unique orientation system for a 12-in. telescope. Three gimbals were used: coarse azimuth (initially controlled by a north-seeking gyro for target acquisition) and azimuth and elevation (controlled by a photoelectric guide telescope). The coarse azimuth motor was a simple gearmotor, whereas the azimuth and elevation gimbals each used a dual contra-rotating free gyroscope combining the reaction wheel and torquer in a single unit. The gyroscopes were constructed by Tufts expressly for the control system. At 12,000 rpm each gyro provided 3.0 SI units of angular momentum. The elevation and azimuth torques were derived by precessing the rotors; hence, the system had a relatively short operating time. This time was extended indefinitely, however, by appropriately off-setting a traveling weight

driven by an electric motor to trim the elevation gyroscope and by twisting the shroud lines of the parachute against the balloon with the coarse azimuth drive to trim the azimuth gyroscope.

The accuracy obtained was about ± 1 min of arc. Eleven flights were made. On the last, in March 1964, the system was expended in a freak fail.

10. Polariscope

Under the direction of Dr. T. Gehrels, a group at the University of Arizona has developed a 28-in. telescope system intended primarily for photoelectric photometry and polarization studies. A geared servomotor is used on each of the gimbals, azimuth, elevation, and cross-elevation. The latter two motors are controlled by floated rate integrating gyros. The gyros are torqued initially by signals from the command receiver for target acquisition and subsequently by signals from a photoelectric guide telescope for fine tracking. A television camera is used to identify the target. Multiple targets are to be observed on each flight. Control accuracy of ± 1 min of arc in elevation and cross-elevation was achieved during the maiden flight on May 27, 1966, from Palestine, Texas.

11. Stratoscope II

Since the completion of the 1959 series of flights with Stratoscope I, the balloon astronomy group at Princeton has developed the 36-in. (~ 0.91 m) Stratoscope II system. The telescope and gimbal system have been built by the Perkin-Elmer Corporation, Norwalk, Connecticut, and the television, telemetry, and ground command system by the RCA Corporation, Princeton, New Jersey. This system is by far the most sophisticated of all the systems yet built. It has seven control axes in an inside-out gimbal system: azimuth, fine cross-azimuth, fine elevation, coarse cross-azimuth, coarse elevation, ultrafine elevation, and ultrafine cross-elevation. Torque motors are used on three of the gimbals (azimuth, fine cross-azimuth, and fine elevation); spur-gear motors on two (coarse cross-azimuth and coarse elevation); and magnetic coil drivers on two (ultrafine elevation and ultrafine cross-elevation). The first five gimbals provide orientation of the telescope to an accuracy of about 1 sec of arc and the other two, stabilization of the image to about 0.03 sec of arc.

The azimuth gimbal is supported on a mercury bearing to bound the friction noise in the azimuth gimbal. As on Stratoscope I, a reaction wheel is

used to limit the speed of the azimuth motor.

Flexure bearings are used in the fine cross-azimuth and fine elevation gimbals. These bearings, designed to have virtually zero torsional constants while supporting the entire weight of the telescope, necessarily have very limited travel, ± 5 deg. Thus, as the target is tracked, these gimbals must be returned continually to the null position by driving the corresponding coarse gimbals. These gimbals are equipped with inertially compensated gearmotors. (The rotors in the motors rotate in directions opposing those of the gimbals and the gear train ratios are equal to the ratios of the moments of inertia of the gimbals to the moments of inertia of the rotors.) Thus, the telescope is scarcely disturbed during resetting of the flexure bearings. The coarse gimbals, as well as an elaborate set of counterbalances, are driven by ground command. The three fine gimbals are driven by signals derived from two stars in the field of the primary telescope. Inasmuch as the sensing axes are not collinear with the control axes, a rather complex coordinate transformation is required, Schlesinger (18).

The ultrafine control is accomplished by driving a spring-restrained wiggle lens transverse to the optical axis of the telescope by an orthogonal pair of magnetic coils. Signals for the coil drivers are derived from two pairs of photomultipliers mounted around the lens receiving light through the primary telescope from a guide star in the field (9th magnitude or brighter).

Guide stars in the field of view of the telescope for both the fine and ultrafine gimbals can be selected by ground commanded retrodividers driven on carriages by electric motors.

Six flights have been made. On the first two, the wiggle lens system was not used. The first flight, made early in 1963, was successful though fraught with harrowing malfunctions, Danielson, et al. (19). The second flight, made late in 1963, was somewhat more gratifying, Woolf, et al. (20). The third flight, made in July 1965, was unsuccessful because of excessive unbalance in the gimbal system caused by a malfunction in the cooling system for the primary mirror. The fourth flight in May 1966 was unsuccessful because of a malfunction in the latch mechanism for the tele-

scope occasioned by strain in the gondola due to unjetisoned ballast. Successful flights were made on 26 March 1970 and 9 September 1971. Figure 10 shows Stratoscope II at Huntsville, Alabama, prior to the flight of 9 September 1971.

F. CONCLUSIONS

It should be obvious to the reader that there is no pat solution to the problem of controlling a balloon-borne instrument. The solutions to the problem are legion. There is a wide variety of components, all far from ideal, from which to choose. Compromises must be made not only in the choice of the components, but also in the number and configuration of the gimbals. The compromises that best suit a given application must, of necessity, be determined by a careful evaluation of the trade-offs in the specific case.

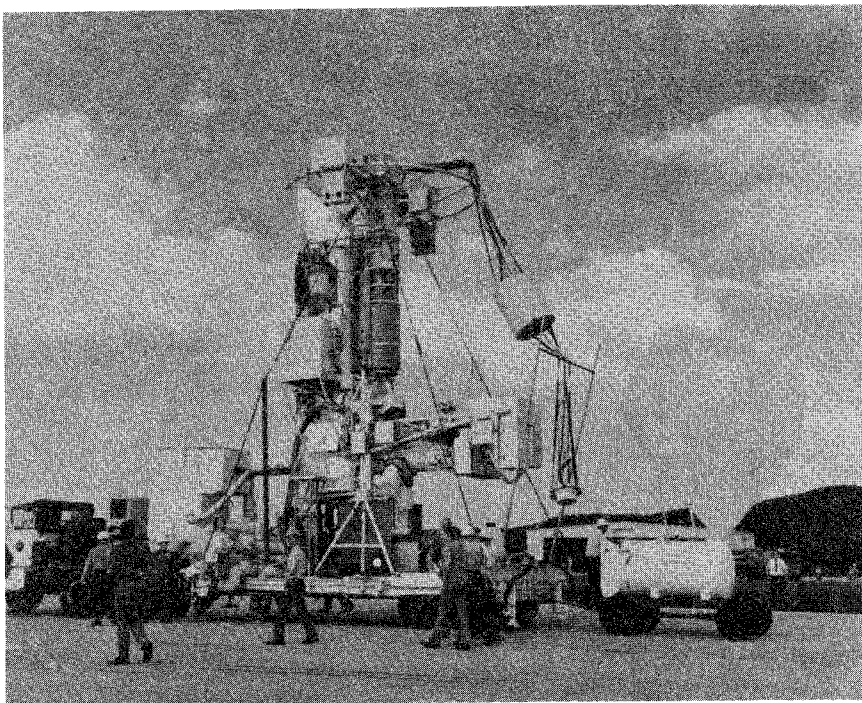


Fig. 10. Stratoscope II, the largest of the current balloon-borne telescopes, shown at Huntsville, Alabama, prior to the flight of 9 September, 1971.

REFERENCES

- (1) Stuart, F. E., 1965: Private communication.
- (2) Allen, C. W., 1955: Astrophysical Quantities, Athlone Press, London, p. 171
- (3) Dolder, F. P. and D. S. Johnson, 1960: Solar Azimuth Pointing Platform. Final Engineering Report by Ball Brothers Research Corp. under Contract No. AF19(604)-5543 from the Air Force Cambridge Research Center.
- (4) Edwards, Howard D., A. Goddard, Jr., M. Juza, T. Maher, F. Speck, 1956: Balloon-Borne Systems for Tracking the Sun, Review of Scientific Instruments, Vol. 27, No. 6, 381-385.
- (5) Schwarzschild, M. and B. Schwarzschild, 1959: Balloon Astronomy, Scientific American, Vol. 200, 52-59.
- (6) Stacey, D. S., G. A. Stith, R. A. Nidey, W. B. Pietenpol, 1954: Rocket-borne Servo Tracks the Sun, Electronics, Vol. 27, 149-151.
- (7) Danielson, R. E., 1961: The Structure of Sunspot Penumbrae I. Observations, J. Astrophys., Vol. 134, 275-288.
- (8) Nidey, R. A. and D. S. Stacey, 1956: Photoelectric Angular Error Sensors, Rev. Sci. Inst., Vol. 27, 216-218.
- (9) Newkirk, G. A., Jr. and J. A. Eddy, 1962: A Coronagraph Above the Atmosphere, Sky and Telescope, Vol. 24, 3-7.
- (10) Newkirk, G. A., Jr. and J. D. Bohlen, 1964: The First Flight of Corona-scope II, Sky and Telescope, Vol. 28, 1-4.

- (11) Strong, J. D., 1957: Interferometry for the Infrared, J. Opt. Soc. Am., Vol. 47, 354-357.
- (12) Strong, J. D. and associates, 1961: Astronomical Observations Using the ONR StratoLab. Technical report by the Johns Hopkins Univ. under Contract No. NONR 248(52) from the Office of Naval Research and Grants G-4880 and G-9262 from the National Science Foundation.
- (13) Strong, J. D. and M. Bottema, 1964: A Daytime Acquisition System for Balloon Astronomy, Mémoires Soc. R. Sc. Liège, Vol. 9, 528-532.
- (14) Strong, J. D., 1965: Infrared Astronomy by Balloon, Scientific American, Vol. 212, 28-37.
- (15) Strong, J. D., 1964: Balloon-Astronomy Program at the Johns Hopkins Univ. Final report by the Laboratory of Astrophysics and Physical Meteorology under Contract No. AF19(628)-202 from the Air Force Cambridge Research Laboratories.
- (16) Markey, W. R., J. B. Searcy, C. L. Lothrop, 1964: Final Report: Project Star Gazer, Experimental Astronomy Laboratory, Massachusetts Institute of Technology.
- (17) Greeb, M. E., 1965: Design and Development of the Balloon-Borne Solar Pointer BBSP-200. Final report by the Ball Brothers Research Corp. under Contract No. AF19(628)-4314 from the Air Force Cambridge Research Laboratories.
- (18) Schlesinger, E. R., 1963: Aiming a 3-Ton Telescope Hanging from a Balloon, Electronics, Vol. 36, 47-51.
- (19) Danielson, R. E., J. E. Gaustad, M. Schwarzschild, H. F. Weaver, N. J. Woolf, 1964: Mars Observations from Stratoscope II, Astronomical J., Vol. 69, 344-352.

- (20) Woolf, N. J., M. Schwarzschild, W. K. Rose, 1964: Infrared Spectra of Red-Giant Stars, J. Astrophys., Vol. 140, 833-852.

SECTION VIII.

SUPERPRESSURE BALLOONS

by

Vincent E. Lally

List of Symbols iii

List of Figures iv

List of Tables vi

A. INTRODUCTION 1

B. BALLOON SHAPES AND STRESSES 1

1. The Sphere 1

2. The Cylinder 3

3. The Tetroon 3

C. FREE LIFT AND SUPERTEMPERATURE STRESSES 4

1. Superpressure Due to Free Lift and Supertemperature 4

a. The free lift ratio 5

b. Superpressure 8

2. Stresses Produced by Superpressure 13

D. BALLOON LIFE 13

1. Diffusion 13

2. Leakage 19

E. BALLOON STABILITY 20

1. Diurnal Changes in Altitude Due to Supertemperature 20

2. Change in Altitude Resulting from Gas Loss 25

3. Creep 28

4. Altitude Variation Caused by Vertical Currents 30

F. NATURAL OSCILLATION PERIOD OF A SUPERPRESSURE BALLOON 32

G. BALLOON MATERIALS. 35

1. Desired Characteristics for Balloon Materials 35

2. Minimum Specifications for Balloon Materials 36

a. Modulus of elasticity 37

b. Strength of the balloon material 38

c. Transparency 38

d. Formability 40

e. Brittleness 41

f. Sealability 42

g. Permeability 43

REFERENCES 45

LIST OF SYMBOLS

<u>Symbol</u>	<u>Description</u>	<u>Dimensions</u>			
a	subscript indicating air		R	universal gas constant	$L^2 T^{-2} \theta^{-1}$
A	balloon surface area	L^2	s	subscript identifying values with level z_s	
A_D	balloon cross section	L^2	S	stress in psi	$ML^{-1} T^{-2}$
C_D	coefficient of drag		S*	Stress in Nm^{-2}	$ML^{-1} T^{-2}$
E	modulus of elasticity	$ML^{-1} T^{-2}$	t	thickness of balloon envelope in mils (0.001 in.)	L
f	free lift ratio		t*	thickness of balloon envelope in m	L
F	free lift	MLT^{-2}	T	temperature of enclosed gas or air. Subscripts identify the symbol with gas or air	θ
g	subscript indicating gas		T_o	temperature at z_o	θ
g	acceleration due to gravity	LT^{-2}	T_s	temperature at z_s	θ
G	mass of gross load (including mass of lifting gas)	M	V	volume of air or gas	L^3
l	cylinder length	L	V_i	nominal balloon volume	L^3
$\Delta l/l$	fractional change in length, strain		w	vertical wind velocity	LT^{-2}
m_f	mass of gas which provides free lift	M	$\Delta V/V$	fractional change in volume	
M_a	molecular weight of air	$M(M\text{-mol})^{-1}$	z_o	altitude at which balloon becomes fully inflated	L
M_g	molecular weight of lifting gas	$M(M\text{-mol})^{-1}$	z_s	altitude at which balloon is in static equilibrium, i.e., floating altitude	L
n	number of moles of gas		Δz	incremental change in altitude	L
p	pressure	$ML^{-1} T^{-2}$	<u>Greek letters</u>		
p'	partial pressure of gas	$ML^{-1} T^{-2}$	δ	permeability constant ($m^3 \text{ mil} / (m^2 \text{ mb day})$)	$L^3 TM^{-1}$
$P_{a,o}$	atmospheric pressure at z_o	$ML^{-1} T^{-2}$	Θ	supertemperature ($T_g - T_a$)	θ
$P_{a,s}$	atmospheric pressure at z_s	$ML^{-1} T^{-2}$	Π	superpressure in mb	$ML^{-1} T^{-2}$
$P_{g,s}$	gas pressure at z_s	$ML^{-1} T^{-2}$	Π_f	superpressure due to free lift	$ML^{-1} T^{-2}$
r	balloon radius	L	Π_T	superpressure due to supertemperature	$ML^{-1} T^{-2}$
			Π^*	superpressure in Nm^{-2}	$ML^{-1} T^{-2}$

$\rho_{a,o}$	air density at z_o
$\rho_{a,s}$	air density at z_s
$\rho_{\Delta z}$	air density at $z_s \pm \Delta z$
τ	period of oscillation, sec

ML^{-3}
 ML^{-3}
 ML^{-3}
 T

List of Figures

Fig. 1	Diffusion of helium through a Mylar balloon. Balloon life in days per mil thickness is based on the assumption that a 6% loss will cause failures	18
Fig. 2	Creep as a function of stress for 2-mil bilaminated Mylar at 20-25°C	29

List of Tables

Table 1	Permeability* (δ) of films to gases at 25°C	16
Table 2	Permeability of Mylar to helium	17
Table 3	Relative leakage rates of gases for three types of leaks . .	21
Table 4	Altitude displacement of superpressure balloons as a function of vertical wind	33

SUPERPRESSURE BALLOONS

A. INTRODUCTION

The superpressure balloon is a non-extensible balloon which is sealed to prevent gas release. By the time float level is reached, the free lift gas has been converted into superpressure, i.e., an internal pressure greater than the ambient atmospheric pressure. The variations in the radiation environment produce significant changes in the superpressure but, generally, negligible changes in the balloon volume. As long as the balloon is superpressured, it will continue to float at a constant-density level.

B. BALLOON SHAPES AND STRESSES

1. The Sphere

A balloon can be manufactured in almost any desired shape. When the balloon is superpressured, the stress distribution will vary over the surface, with the highest stresses in areas of maximum radii of curvature. Only a sphere provides uniform stress distribution over the entire surface. Intuitively, it would appear that the sphere is the most efficient shape for providing the largest enclosed volume at a given maximum stress and a

given mass of material. However, constructional difficulties arise which can offset much of the geometric efficiency of the sphere. In addition, the application may be one where factors other than efficiency are of prime importance. For example, the cylinder is a simple structure which is less affected by vertical currents at low altitudes; the tetraon (tetrahedral balloon) provides a compromise between ease of construction and design efficiency which makes it suitable for low-cost flight programs where maximum performance is not required.

The stress on the envelope of a spherical balloon is

$$S^* = \frac{r\Pi^*}{2t^*} \quad (1)$$

where S^* is stress (Nm^{-2}), r is balloon radius (m), Π^* is superpressure (Nm^{-2}), and t^* is film thickness (m).

Since American manufacturers usually express film characteristics in mils (10^{-3} in.) for film thickness and psi (lb/sq in.) for stress, it is necessary to deviate from the SI units of Eq. (1) and express the stress on a spherical balloon as

$$S = \frac{286 r\Pi}{t} \quad (1a)$$

where S is stress (psi), r is balloon radius (m), Π is superpressure (mb), and t is film thickness (mils).

2. The Cylinder

The cylinder is an inefficient shape for a superpressure balloon, but it is simple to manufacture and a cylindrical balloon which is long compared to its diameter provides a low drag relative to an equivalent sphere for motion normal to its circular cross section. It has application to low-altitude flight with light payloads. The circumferential stress on a long cylinder is

$$S^* = \frac{r\Pi^*}{t^*} \quad (2)$$

These factors are the same as those used in Eq. (1). The stress in manufacturers' units is

$$S = \frac{572 r\Pi}{t} \quad (2a)$$

where S is stress (psi), r is radius (m), Π is superpressure (mb) and t is film thickness (mils).

3. The Tetron

The tetron is made from a cylinder whose circumference is equal to

2.31 times the cylinder length. The ends are sealed with the straight seams orthogonal to each others. A complete description of the tetron is given by Grass (1). The basic advantage of the tetron is manufacturing simplicity. Stresses on the triangular faces are much higher than the stresses on a sphere. The tetron is not considered further in this section.

C. FREE LIFT AND SUPERTEMPERATURE STRESSES

1. Superpressure Due to Free Lift and Supertemperature

A superpressure balloon is normally launched as a sealed container. It can be lifted to the desired altitude by a tow balloon, or it can be inflated with an excess of lift gas over that required to give the desired superpressure. The excess is then expelled through a valve after the balloon has reached its float altitude. This second alternative is undesirable for long duration flights since it adds a complicated device which may cause leakage. Fortunately, a free lift (an excess of buoyancy over weight) of 8 to 10% is sufficient to carry small (1.5-2 m in diameter) spherical balloons aloft without assistance at an ascent rate of about 1.5 m per sec. When a balloon reaches float altitude, the free lift gas becomes the reservoir of excess gas which is drawn upon to sustain flight for extended periods.

As it rises, the gas fills out the balloon. A height is reached at which the balloon is completely inflated and begins to overpressure. The balloon continues to rise to a height about 1 km above the zero superpressure altitude, losing lift and gaining overpressure.

a. The free lift ratio. According to Archimedes' principle the buoyant force on a balloon system in the atmosphere is equal to the weight of the air displaced by the balloon system. The sum of the buoyant and gravitational forces acting on a balloon are then

$$F = gm_a - g(m_G + m_g) \quad (3)$$

where m_a is mass of the displaced air (kg), m_G is total mass of the balloon system (kg) exclusive of the mass of the lift gas, m_g is mass of the lift gas (kg), F is the resultant of the buoyant and gravitational forces (N) acting on the balloon, usually called free lift, and g is acceleration due to gravity ($m \text{ sec}^{-2}$).

Let the free lift ratio for superpressure balloons, f , be defined by Eq. (4)

$$f \equiv \frac{F'}{g(m_G' + m_{g,f})} \quad (4)$$

where F' is the free lift of a balloon system under the following conditions:

$V_{g,f} = V_{a,f}$, $p_{g,f} = p_{a,f}$, $T_{g,f} = T_{a,f}$, and m_G' is the total mass exclusive of the mass of the gas which the balloon system will have when it has achieved an equilibrium float condition. Note that this excludes any ballast dropped during ascent. The subscript f is used to denote the conditions associated with the definition of the free-lift ratio, and $m_{g,f}$ is mass (kg) of the lift gas, $V_{g,f}$ is volume (m^3) of the lift gas, $V_{a,f}$ is volume of the displaced air, $p_{g,f}$ is pressure (Nm^{-2}) of the lift gas, $p_{a,f}$ is pressure of the air, $T_{g,f}$ is temperature ($^{\circ}K$) of the lift gas, and $T_{a,f}$ is temperature of the ambient air.

If a superpressure balloon is inflated so the defining restrictions of the free lift-ratio are fulfilled and if the balloon remains a closed container from inflation until it reaches float altitude, z_s , and achieves hydrostatic equilibrium, the total mass of the system at float altitude, including the mass of the lift gas, will be $(m_G' + m_{g,f})$. Since a balloon in a state of hydrostatic equilibrium has no free lift, the mass of the system must then equal the mass of the displaced air at level z_s , i.e.,

$(m'_G + m_{g,f}) = m_{a,s}$. If this mass is substituted in Eq. (3), the free lift

upon completion of inflation is found to be

$$F' = gm_{a,f} - gm_{a,s} \quad (5)$$

Substituting into Eq. (4) yields

$$f = \frac{m_{a,f} - m_{a,s}}{m_{a,s}} \quad (6)$$

Now $m_{a,f} = n_{a,f}M_a$ and $m_{a,s} = n_{a,s}M_a$; $n_{a,f}$ is the number of moles of air having molecular weight M_a making up the gas mass $m_{a,f}$ and filling the volume $V_{a,f}$. For the conditions under which the free lift ratio was defined $n_{a,f} = n_{g,f}$. Also in a closed balloon $n_{g,f} = n_{g,s}$. Therefore, Eq. (6) may also be written

$$f = \frac{n_{g,s} - n_{a,s}}{n_{a,s}} = \frac{\Delta n_s}{n_{a,s}} \quad (7)$$

where Δn is the difference in the number of moles of gas inside the balloon and the number of moles of air displaced by the balloon when it is in hydrostatic equilibrium with its environment. It was to achieve this convenient result, which will be used in the next sub-section, that f was defined as it was here.

In zero-pressure ballooning, a fractional free lift is defined by the equation

$$f' \equiv \frac{F'}{gm_G} \quad (8)$$

and by all of the conditions used in defining f , except that m_G in zero-pressure ballooning is normally the total mass of the balloon system at the time of launch, exclusive of the lift gas. Thus, m_G usually includes ballast and other masses which may be detached during ascent. It is convenient at times, however, to define f' by Eq. (9)

$$f' = \frac{F'}{gm_G} \quad (9)$$

and the conditions defining f . Then the following convenient relationship exists between f' and f :

$$f' = \frac{\frac{M_a}{M_g} f}{\left(\frac{M_a}{M_g} - 1\right) - f} \quad (10)$$

b. Superpressure. The superpressure of the balloon at z_s is defined as

$$p_{g,s} - p_{a,s} = \Pi_s \quad (11)$$

Then

$$\frac{\Pi_s}{P_{a,s}} = \frac{P_{g,s} - P_{a,s}}{P_{a,s}} \quad (12)$$

Both the air and the gas behave essentially like an ideal gas under all conditions in which a balloon might conceivably operate in the atmosphere.

One form of the gas law for an ideal gas is

$$pV = nRT \quad (13)$$

where R is the universal gas constant [$J (^\circ K)^{-1} (kg \cdot mol)^{-1}$]. The other variables (with appropriate subscripts) have already been introduced.

Remembering that $V_{a,s} = V_{g,s}$ and substituting from Eq. (13) in the right side of Eq. (12) and simplifying yields

$$\frac{\Pi_s}{P_{a,s}} = \frac{n_{g,s} T_{g,s} - n_{a,s} T_{a,s}}{n_{a,s} T_{a,s}} \quad (14)$$

Let the lift gas supertemperature be defined as follows:

$$\Theta_s = T_{g,s} - T_{a,s}$$

or

$$T_{g,s} = T_{a,s} + \Theta_s \quad (15)$$

Similarly, let

$$n_{g,s} = n_{a,s} + \Delta n_s \quad (16)$$

Substituting from Eqs. (16) and (17) into Eq. (14) permits one to write

$$\frac{\Pi_s}{P_{a,s}} = \frac{(n_{a,s} + \Delta n_s)(T_{a,s} + \Theta_s) - n_{a,s} T_{a,s}}{n_{a,s} T_{a,s}}$$

which may be simplified to

$$\frac{\Pi_s}{P_{a,s}} = \frac{T_{a,s} \Delta n_s + n_{a,s} \Theta_s + \Delta n_s \Theta_s}{n_{a,s} T_{a,s}}$$

or

$$\frac{\Pi_s}{P_{a,s}} = \frac{\Delta n_s}{n_{a,s}} + \frac{\Theta_s}{T_{a,s}} + \frac{\Delta n_s \Theta_s}{n_{a,s} T_{a,s}} \quad (17)$$

After substituting for $\Delta n_s/n_{a,s}$ from Eq. (7), one may state Eq. (17)

in any of the following equivalent forms:

$$\frac{\Pi_s}{P_{a,s}} = f + \frac{\Theta_s}{T_{a,s}} (1 + f) \quad (18)$$

$$\frac{\Pi_s}{P_{a,s}} = f \left(1 + \frac{\Theta_s}{T_{a,s}} \right) + \frac{\Theta_s}{T_{a,s}} \quad (18a)$$

$$\Pi_s = p_{a,s} \left[f + \frac{\Theta_s}{T_{a,s}} (1 + f) \right] \quad (18b)$$

If supertemperature is zero, it follows readily from Eq. (18) that

$$\left(\frac{\Pi_s}{p_{a,s}} \right)_{\Theta = 0} = f \quad (19)$$

That is, the fractional superpressure resulting from the free lift only is equal to the free-lift ratio. Also, if the free-lift ratio is zero, Eq.

(18a) shows clearly that

$$\left(\frac{\Pi_s}{p_{a,s}} \right)_{f = 0} = \frac{\Theta_s}{T_{a,s}} \quad (20)$$

There are then two causes of superpressure: the extra gas added to produce free lift and supertemperature.

If f and $\Theta_s/T_{a,s}$ are sufficiently small compared to 1, the two basic causes of superpressure act essentially independently and may be added to yield the total superpressure. Thus, when a free-lift ratio of 5% is added to a fractional supertemperature of 5% to yield a fractional superpressure of 10%, the error compared with the more nearly correct value of 10.25% is not large. It is not difficult to retain the more precise form, however, and for the stress analysis which follows, that is done.

Of course, the volume for any real balloon does not remain constant under conditions of superpressure and supertemperature, but we can ignore the change for stress analysis. Section VIII.E, in which balloon stability is analyzed, treats the change in volume and the consequent change in altitude resulting from changes of superpressure.

It should be clearly noted that changes in air temperature do not directly affect the superpressure. The balloon floats along a constant-density surface. If the air temperature decreases and that decrease is not accompanied by any change in supertemperature, the balloon floats at a lower pressure, but the superpressure does not change.

The supertemperature varies not only from night to day but also during the day as the radiation environment changes. The extremes for polyester (polyethylene terephthalate) balloons measured in flight range from -15% (tropics, 30 mb, nighttime) to +15% (tropics, 100 mb, daytime). The sunset effect on these balloons has been measured to be from 3 to 10%. A more detailed analysis of supertemperature variations is included in Section VIII.E.

2. Stresses Produced by Superpressure

The stress in a sphere caused by superpressure may be determined by Eqs. (1a) and (18b) as follows:

$$S \text{ (sphere)} = \frac{286 r p_{a,s}}{t} \left[f + (1 + f) \frac{p_s}{T_{a,s}} \right] \quad (21)$$

Similarly, the stress in a cylinder, obtained from Eqs. (2a) and (18b), is

$$S \text{ (cyl)} = \frac{572 r p_{a,s}}{t} \left[f + (1 + f) \frac{p_s}{T_{a,s}} \right] \quad (22)$$

D. BALLOON LIFE

1. Diffusion

For the purpose of this section, we shall distinguish between two methods of gas loss from a superpressure balloon: diffusion and leakage. We define diffusion as the gas loss through the wall of a balloon that is without defect in material or assembly.

Leakage is defined as gas loss through defects in the balloon, e.g., pinholes, defective seals, or abrasions, which permit a larger gas loss than through film without imperfection.

If a plastic film is used to contain a gas, the gas dissolves in the film and diffuses to the outside. The rate at which the gas passes through a barrier of area A varies directly with the permeability of the film to the gas, δ , and the difference in partial pressure, p' , of the gas across the film and inversely with the film thickness, t ,

$$\text{Rate of Loss} = \frac{\delta p' A}{t}$$

For a balloon, the percentage of loss of gas per day can be obtained by dividing the rate of loss by balloon volume

$$\% \text{ Volume Loss per Day} = \frac{100 \delta p' A}{tV} \quad (23)$$

For a spherical balloon, the percentage loss of gas per day is

$$\text{Sphere \% Volume Loss per Day} = \frac{300 \delta p'}{rt} \quad (24)$$

For a long cylindrical balloon, Eq. (23) becomes

$$\text{Cylinder \% Volume Loss per Day} = \frac{200 \delta p'}{rt} \quad (25)$$

The permeability of plastic films is a marked function of temperature. Permeability at low atmospheric temperatures (200°K) may be less than 1% of the value at high temperatures (300°K).

Table 1 shows permeability data for a number of gases and films at 25°C. Table 2 gives specific data on the permeability of the polyester Mylar to helium at various temperatures. The values used are derived from a number of sources. Since the permeability of Mylar to helium varies with the crystallinity of the Mylar film, the data available are not consistent. The data derived by Lally, Mellor, and Verstraete in extensive tests with inflated balloons indicate lower values than given by other sources with the exception of the General Mills, Inc. tests made in 1960. The values derived from balloon measurements are used in Table 2, since the combination of stressed film, bilamination, and taped areas appears to provide a lower overall diffusion than would be indicated from the other test results.

Figure 1 is a presentation of the expected life of balloons at several altitudes using permeability values from Table 2, Eqs. (24) and (25), and assuming 6% gas loss to failure.

Circled points on the 500-mb and 200-mb curves are the designs used in the initial GHOST (Global Horizontal Sounding Technique) test flights in the Southern Hemisphere. Life expectancies for balloons without defect are 120 days for a 2.5-mil balloon at 500 mb and over 600 days for a 1.5-mil

Table 1

Permeability* (δ) of Films to Gases at 25°C

Film	He	H ₂	O ₂	N ₂
Saran	7.5×10^{-7} (0.03)	2.5×10^{-7} (0.01)	1.2×10^{-8} (0.0005)	2.5×10^{-9} (0.0001)
Mylar	22×10^{-7} (0.088)	15×10^{-7} (0.06)	7.5×10^{-8} (0.003)	1.2×10^{-8} (0.0005)
Polyethylene	185×10^{-7} (0.74)	220×10^{-7} (0.86)	140×10^{-7} (0.55)	50×10^{-7} (0.20)

*First-line entries are δ in NCAR units; second-line entries are in "trade" units.

NCAR units: m³ mil/m² day mb.

Trade units: std cc cm 10⁻⁹/sec cm² cm Hg.

To convert Trade units to NCAR units multiply by 2.5×10^{-5} .

Table 2

Permeability of Mylar to Helium

$T_{\circ K}$	NCAR units ($\times 10^7$)	Trade units	$T_{\circ K}$	NCAR units ($\times 10^7$)	Trade units
300	22	0.090	250	3.8	0.015
295	19	0.076	245	3.0	0.012
290	16	0.067	240	2.4	0.0095
285	14	0.056	235	1.9	0.0076
280	12	0.047	230	1.5	0.0058
275	10	0.039	225	1.1	0.0044
270	8.2	0.033	220	0.87	0.0035
265	6.8	0.027	215	0.65	0.0026
260	5.5	0.022	210	0.50	0.0020
255	4.7	0.019			

See Table 1 for definition of units.

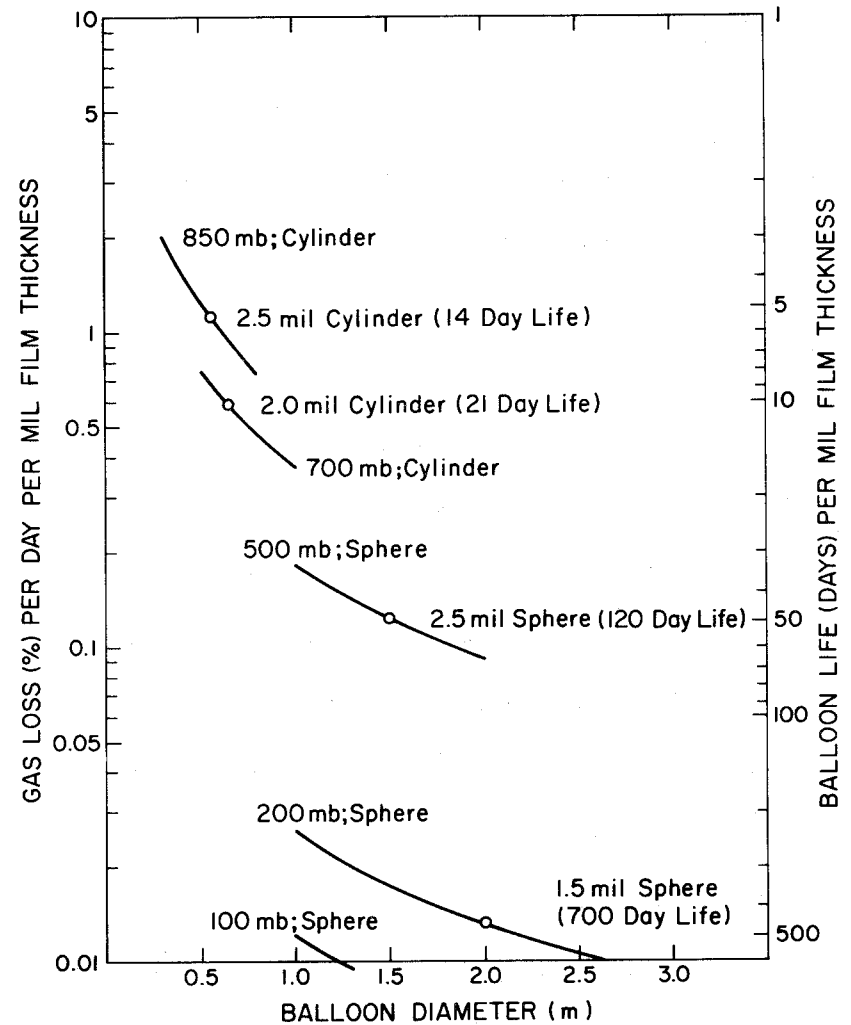


Fig. 1. Diffusion of helium through a Mylar balloon. Balloon life in days per mil thickness is based on the assumption that a 6% loss will cause failure.

balloon at 200 mb. Above 200 mb life expectancy is limited by ultra-violet deterioration, not by diffusion.

2. Leakage

Diffusion of gas through a plastic film is a function of the partial pressure of the gas contained within the film. Leakage is a function of the differential pressure, which we call either overpressure or superpressure, Π . For "small" leaks the flow through the orifice is molecular flow, and it is directly proportional to the overpressure. For "large" leaks the flow is turbulent, and flow rate is proportional to the square root of overpressure. Molecular flow occurs when the mean free path of the gas molecules exceeds the largest dimension of the hole. The mean free path for helium in the lower atmosphere is at all times less than 1 μm . A 1- μm hole will not produce a significant gas loss in a superpressure balloon in a period of a year. It is possible for a plastic film to have many hundreds of microholes, which would cause serious gas loss, but the technique of laminating together two sheets of film should eliminate such imperfections. The bilaminated film can develop holes during manufacture, packing, and testing, but the number of holes that are introduced should be few.

The characteristics of leaks in plastic films have not yet been investigated. Extensive data have been taken on leaks through vacuum systems. Table 3 is derived in part from a paper by Nerken (2). Data are provided on hydrogen, helium, air, and Freon 12, since they all may be used to test for leaks or as lifting gases for flight.

Empirical tests must be made to determine the nature of hole defects in balloons. Measurements as a function of pressure and for dissimilar gases such as air and helium will permit analysis of the holes which are introduced in balloons.

E. BALLOON STABILITY

1. Diurnal Changes in Altitude Due to Superpressure

The volume of a superpressure balloon does not remain constant. As the internal pressure increases, the stress on the film increases; consequently, volume increases. The expression relating stress, S , to strain, $\Delta l/l$, is the modulus of elasticity, E ,

$$E \equiv \frac{S}{\frac{\Delta l}{l}} \quad (26)$$

For a spherical balloon, the fractional volume change (for small changes) is three times the fractional change in linear dimension

Table 3

Relative Leakage Rates of Gases for Three Types of Leaks

Gas	Viscosity at 25°C (Air = 1)	Molecular Weight (Air = 1)	Flow Rate Relative to Air		
			Leak: Flow: Turbulent	Very Large Large Viscous	Small Molecular
Hydrogen	0.48	0.070	3.9	2.7	3.6
Helium	1.08	0.139	2.7	1.4	2.7
Air	1.00	1.00	1.00	1.00	1.00
Freon 12	0.67	4.20	0.49	0.97	0.62

$$\frac{\Delta V}{V} = \frac{3\Delta \ell}{\ell} \quad (27)$$

(For a long cylinder balloon, the fractional volume change is twice the fractional linear change.) The volume change for a spherical balloon can be expressed by combining Eqs. (26) and (27)

$$\frac{\Delta V}{V} = \frac{3S}{E} \quad (28)$$

Since we are concerned with changes in volume resulting from changes in stress rather than the total volume change from no stress, the equation can be written as

$$\frac{\Delta(\Delta V)}{V} = \frac{3\Delta S}{E} \quad (28a)$$

By combining Eqs. (1a) and (18b) and substituting in Eq. (28a), we can derive an expression for the volume change resulting from a change in super-temperature

$$\frac{\Delta(\Delta V)}{V} = \frac{3}{E} \times \frac{286r}{t} \times \frac{P_{a,s} \Delta \Theta (1+f)}{T_{a,s}} \quad (29)$$

If we assume a spherical balloon design which produces 10,000 psi stress at 25% superpressure, we can obtain a rough estimate of the variation of volume with supertemperature change. Thus, for the typical design we are

considering here, an increase of 1% in the superpressure produces a 400-psi increase in stress. We can express this mathematically as

$$\Delta S \approx 400 \times 100 \frac{\Delta(\Delta P)}{P} \approx 400 \times 100 \frac{\Delta\Theta}{T} \quad (30)$$

Substituting this value into Eq. (28a)

$$\frac{\Delta(\Delta V)}{V} \approx \frac{3 \times 4 \times 10^4}{E} \frac{\Delta\Theta}{T} \quad (31)$$

Using the value of 1.2×10^6 psi for the biaxial modulus of elasticity of Mylar, we have

$$\frac{\Delta(\Delta V)}{V} \approx \frac{1.2 \times 10^5}{1.2 \times 10^6} \frac{\Delta\Theta}{T} = 0.10 \frac{\Delta\Theta}{T} \quad (32)$$

A fractional change in volume will produce an equal but negative fractional change in density at the level at which the balloon floats. A 1% change in density causes a change of approximately $0.3T$ m in altitude, where T is the air temperature in $^{\circ}\text{K}$.

The altitude variation resulting from a supertemperature change on a spherical balloon can be roughly written as

$$\Delta z \approx -0.3 T \frac{\Delta\rho}{\rho} 100 \approx 0.3 T \frac{\Delta(\Delta V)}{V} 100 = 30 T \frac{\Delta(\Delta V)}{V} \quad (33)$$

Substituting from Eq. (32), we obtain

$$\Delta z \approx 30T \times 0.10 \frac{\Delta\Theta}{T} \quad (34)$$

Thus

$$\Delta z \approx 3.0 \Delta\Theta \quad (35)$$

To summarize, Eq. (29) provides a precise expression for the volume change resulting from a change in supertemperature. From the volume change, the altitude change can be computed using Eq. (33). However, as a sweeping approximation, we can state that a 1.0C° change in supertemperature will produce a 3.0 m change in altitude for a typical spherical balloon designed to reach a stress of 10,000 psi with 25% superpressure.

The average day-night supertemperature difference observed on GHOST test flights has been 10C° in the troposphere and 15C° in the stratosphere. The variation in density altitude between day and night is 30 to 50 m.

The variation in temperature during the day may be as much or greater for a Mylar balloon than the day-night effect. Maximum differences observed to date have been 20C° .

The diurnal changes in altitude resulting from supertemperature may be summarized as:

- a. A predictable day-night altitude change of 30 to 50 m.
- b. An unpredictable variation in the radiation environment on the order of ± 60 m.

2. Change in Altitude Resulting from Gas Loss

During inflation more gas is placed in a superpressure balloon than is required to provide buoyant equilibrium. The mass of this gas is

$$m_f = \frac{f V_i \rho_{a,s}}{\left(\frac{M_a}{M_g} - 1\right)} \quad (36)$$

where m_f = mass(kg) of gas which provides free lift.

During the life of the balloon this excess gas diffuses through the balloon. If we assume the balloon descends at the time that all free-lift gas has been lost, the change in balloon system mass during its life is

$$\Delta m_B = m_f \quad (37)$$

The percentage mass loss is

$$\frac{100 \Delta m_B}{m_B} = \frac{100 f V_i \rho_{a,s}}{V_i \rho_{a,s} \left(\frac{M_a}{M_g} - 1\right)} = \frac{100f}{\left(\frac{M_a}{M_g} - 1\right)} \quad (38)$$

For a helium-filled balloon having 10% free lift, the percentage mass loss is

$$\% \text{ Mass Loss} = \frac{100f}{\left(\frac{M_a}{M_g} - 1\right)} \approx \frac{100 \times 0.1}{\left(\frac{28.96}{4} - 1\right)} \approx 1.6\%$$

This 1.6% mass loss would cause the balloon to float (near the end of its useful life) at a level 1.6% lower in density than its original float level. However, the overpressure resulting from free lift decreases as the free lift gas is lost. This decrease in overpressure causes a reduction in volume which tends to balance out the mass loss.

We can design the balloon so that the mass loss exactly balances the loss in free lift superpressure. Basically, the technique requires that the fractional volume loss caused by a percentage reduction in overpressure equals the fractional mass loss produced by the same percentage loss in free lift. Combining Eq. (28) with (1a) and (19) and assuming $\theta_s = 0$, we get

$$\frac{\Delta V}{V} = \frac{3S}{E} = \frac{3}{E} \frac{286}{t} r f p_{a,s}$$

Equation (38) established that

$$\frac{\Delta m_B}{m_B} = \frac{f}{\left(\frac{M_a}{M_g} - 1\right)}$$

As discussed above, we want

$$\frac{\Delta m_B}{m_B} = \frac{\Delta V}{V}$$

Thus

$$\frac{858 r f p_{a,s}}{Et} = \frac{f}{\left(\frac{M_a}{M_g} - 1\right)} \quad (39)$$

For a helium-filled sphere in air

$$\frac{r}{t} = \frac{E}{858 \times p_{a,s} \left(\frac{M_a}{M_g} - 1\right)}$$

If we assume $E = 1.2 \times 10^6$, then

$$\frac{r}{t} = \frac{224}{p_{a,s}}$$

For example, the value of r/t needed to provide an exact balance of gas loss against volume decrease for a balloon floating at 200 mb would be $224/200$, or 1.12. A balloon constructed of 2.5-mil polyester having a radius of 2.8 m will meet this criterion; it will not vary in density altitude as a result of gas loss during the useful life of the balloon.

3. Creep

All plastic materials exhibit some degree of creep under stress.

Creep is the permanent elongation of the plastic film when stressed. The relationship between stress and strain is defined by the modulus of elasticity, which is a function of temperature. The non-elastic creep is a function of stress and temperature as well, but it also depends strongly on the prior history of the material.

Plastics exhibit markedly different characteristics above and below the "glass-transition" temperature. At higher temperatures they have "plastic" characteristics, and at lower temperatures the plastic behaves more like a glass. The "glass-transition" temperature for polyesters is about 350°K --thus, the polyesters are "glassy" substances at all temperatures of importance in ballooning.

Tests have been conducted at room temperature on bilaminated Mylar strips to measure creep. Results are shown in Fig. 2. Creep will be less at the lower temperatures which balloons experience at float altitude.

Tentative results for Mylar can be summarized as:

- a. Creep under moderate stress reduces with time, becoming negligible

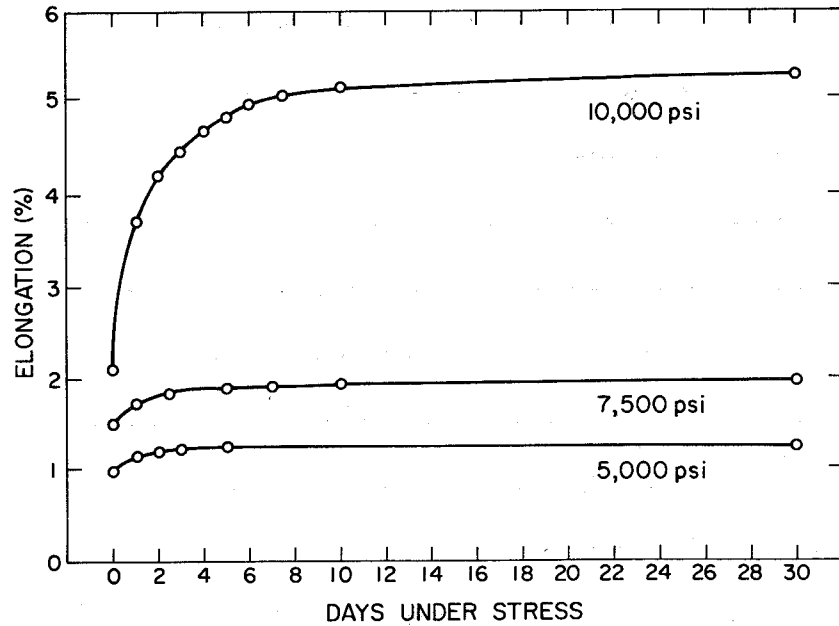


Fig. 2. Creep as a function of stress for 2-mil bilaminated Mylar at

20-25°C.

after two weeks. The time constant is about two days at room temperature for stresses between 5000 psi and 10,000 psi. Total creep is 3.3% at 10,000 psi and 0.25% at 5000 psi.

- b. A balloon may be prestressed to minimize creep. This procedure will also serve to relieve stresses produced in balloon manufacture.
- c. If a balloon is prestressed at 10,000 psi for one week at room temperature and is not stressed at float altitude beyond 7500 psi, creep will be negligible for one year.

The polyester material Cellanar has a higher modulus and a shorter time constant than Mylar.

4. Altitude Variation Caused by Vertical Currents

The drag on a balloon in a vertical current is

$$\text{Drag} = \frac{1}{2} C_D A_D \rho_{a,s} w^2 \quad (40)$$

where C_D is the coefficient of drag (dimensionless), A_D is the balloon cross section (m^2), and w is the vertical wind velocity (m/sec).

The restoring force can be expressed as

$$\text{Restoring Force} = V_i (\rho_{a,s} - \rho_{\Delta z}) g \quad (41)$$

where

$$\rho_{\Delta z} = \text{air density at } (z_s \pm \Delta z)$$

We can use the excellent approximation, derived from Eq. (33), that the

density difference at height Δz above or below the buoyant density $\rho_{a,s}$ is

$$\Delta\rho = \frac{\Delta z \rho_{a,s}}{30T_{a,s}}$$

Thus, we find that

$$\Delta\rho = (\rho_{a,s} - \rho_{\Delta z}) = \frac{\Delta z \rho_{a,s}}{30T_{a,s}} \quad (42)$$

Substituting Eq. (42) into (41) and equating Restoring Force to Drag,

we have

$$\frac{C_D A_D \rho_{a,s} w^2}{2} = \frac{V_i \Delta z \rho_{a,s} g}{30 T_{a,s}} \quad (43)$$

Solving for Δz , we obtain

$$\Delta z = \frac{15 C_D T_{a,s} w^2}{g} \frac{A_D}{V_i} \quad (44)$$

For a sphere this equation reduces to

$$\Delta z = \frac{1.15 C_D T_{a,s} w^2}{r} \quad (45)$$

For a cylinder balloon Eq. (44) becomes

$$\Delta z = \frac{1.53 C_D T_{a,s} w^2}{\ell} \quad (46)$$

where ℓ is cylinder length (m).

Table 4 provides data on the deviation from the buoyant altitude as a function of vertical wind velocity for typical spheres and cylinders.

The vertical excursion is negligible for vertical winds less than 0.5 m/sec (1 knot) but is quite serious for vertical winds greater than 1 m/sec (2 knots).

At the lower altitudes where convection may be severe, the balloon will move with the updrafts and downdrafts. The response of a cylinder-type superpressure balloon will, in general, be about 30% of the response of an equivalent spherical superpressure balloon. Because of this, the cylinder design is recommended for all altitudes up to 700 mb. Above 700 mb the cylinder design becomes too large and unwieldy.

F. NATURAL OSCILLATION PERIOD OF A SUPERPRESSURE BALLOON

If a superpressure balloon is displaced from its buoyant altitude, z_s , there is a restoring force which is proportional to the balloon volume and

Table 4

Altitude Displacement of Superpressure Balloons as a Function of Vertical Wind

Vertical Wind Speed (m/sec)	Δz (m)			
	700 mb sphere $C_D = 0.5$ $T_{a,s} = 269^\circ K$ $r = 0.75$ m	700 mb cylinder $C_D = 1.0$ $T_{a,s} = 269^\circ K$ $r = 0.3$ m $l = 7.0$ m	500 mb sphere $C_D = 0.5$ $T_{a,s} = 252^\circ K$ $r = 0.75$ m	200 mb sphere $C_D = 0.5$ $T_{a,s} = 217^\circ K$ $r = 1.0$ m
0.1	2	0.6	2	1.3
0.5	51	15	48	31
1.0	206	59	193	125
2.0	824	237	--	--
5.0	5150	1480	--	--

The value for $T_{a,s}$ is taken from the U.S. Standard Atmosphere, 1962.

and the density difference

$$G \frac{d^2 z}{dt^2} = -gV(\rho_{a,s} - \rho_a)$$

or

$$\frac{d^2 z}{dt^2} = -g \frac{(\rho_{a,s} - \rho_a)}{\rho_{a,s}}$$

Over a short vertical distance $d\rho/dz = \text{const}$, approximately, and

$$\frac{\rho_{a,s} - \rho_a}{\rho_{a,s}} = z \left[\frac{\left(p \frac{\partial T}{\partial z} - T \frac{\partial p}{\partial z} \right)}{pT} \right]_{a,s} = z \times \text{const}$$

$$\frac{d^2 z}{dt^2} = z \left[\frac{-g \left(\frac{\partial T}{\partial z} - \frac{T}{p} \frac{\partial p}{\partial z} \right)}{T} \right]_{a,s} = z \times \text{const}$$

This is the familiar equation for simple harmonic motion with the period

of oscillation, τ , equal to

$$\tau = 2\pi \sqrt{\left[\frac{T}{g \left(\frac{\partial T}{\partial z} - \frac{T}{p} \frac{\partial p}{\partial z} \right)} \right]_{a,s}}$$

or

$$\tau \approx 2 \sqrt{\left[\frac{T}{\frac{\partial T}{\partial z} + 3.42 \times 10^{-2}} \right]_{a,s}}$$

since

$$\frac{\partial P}{\partial z} = -3.48 \times 10^{-3} \frac{P}{T} \text{ g}$$

For an isothermal region ($\partial T/\partial z = 0$), the expression for period of oscillation simplifies to

$$\tau \approx 11\sqrt{T}$$

The natural oscillation period for a superpressure balloon in an isothermal atmosphere varies from 150 sec at -75°C to 180 sec at 0°C . An adiabatic lapse rate ($\partial T/\partial z = -10^{-2} \text{ }^{\circ}\text{C/m}$) will increase the period by approximately 15%.

G. BALLOON MATERIALS

1. Desired Characteristics for Balloon Materials

The ideal plastic film for balloon material would have a very large modulus of elasticity (10^7 psi) and would be transparent to the entire spectrum of radiation from infrared to ultraviolet. Such a material would not need to have a high ultimate strength since it would never be highly stressed. The material, in addition, should be easily formed so that a balloon could be manufactured out of few spherical sections. It should be readily sealed with seal strengths as high as the strength of the basic material. The

material should be impermeable to helium, oxygen, nitrogen, and water vapor.

In addition, it should be plastic in characteristics at room temperature so that it can be readily packed without damage. At the floating altitude of the balloon, the material could well have glassy characteristics so that it would shatter harmlessly into many pieces if struck by an aircraft.

No existing material comes close to meeting the above ideal specifications for balloon material. However, at least one material does come sufficiently close to providing an acceptable film for fabricating superpressure balloons. This is the polyester, polyethylene terephthalate.

2. Minimum Specifications for Balloon Materials

Most plastic materials fall short of the minimum specifications in some characteristic so that they cannot provide a long-lived, stable vehicle. The minimum specifications to permit flight are interrelated; for example, a material that has great strength but at the same time is highly absorbent of solar radiation, will be over-stressed by the pressure buildup caused by supertemperature. A weaker film may survive if it is sufficiently transparent.

The minimum specifications for a balloon material are indicated below.

a. Modulus of elasticity. A balloon with an insufficient modulus of elasticity will stretch as it superpressures, and if the volume increase due to stretch is sufficient to move the balloon to a higher altitude so that the stress is maintained, the balloon will continue to ascend until it bursts in the same fashion as neoprene and rubber balloons. The minimum modulus of elasticity for an acceptable balloon depends on the free lift introduced in the balloon and on the supertemperature which the balloon will realize at floating altitude. All materials with a modulus of elasticity less than 300,000 psi are unacceptable for superpressure use. This minimum modulus applies at the temperature at altitude. There are a number of film materials with too low a modulus at room temperature or at lower floating altitudes which are acceptable at higher altitudes where the film temperature is -30°C or lower. A realistic minimum modulus of elasticity for a plastic film with average transparency is 500,000 psi. The higher the modulus, the more stably the balloon will fly and the smaller the variation in altitude will be between night and day. A balloon with a modulus of 1.2×10^6 psi will undergo an altitude change of 30 to 50 m between day and

night. A modulus of 10^7 psi would reduce the altitude change between night and day to an insignificant amount.

b. Strength of the balloon material. The modulus of elasticity is a much more important characteristic of superpressure balloon film than the ultimate film strength, provided that the balloon is never stressed beyond its elastic limit. A lighter material may have a lower ultimate strength than a more dense material since a thicker film may be used. For example, polypropylene, which is 40% less dense than polyester, can provide a stronger material for balloon design than polyester, even though its strength is somewhat lower. An acceptable film strength for superpressure design depends on the altitude at which the balloon is to be flown, the payload weight, and the density of the film. As a general rule, the film material should be capable of stresses at 10,000 psi in its elastic range, while maintaining an acceptable modulus of elasticity.

c. Transparency. Balloon films vary markedly in their transparency to solar and infrared radiation. The ideal material should be transparent to the entire spectrum of solar and earth radiation. There are a number of plastic materials which approach this ideal. Polyethylene approaches this

ideal most closely, absorbing less than 6% of the radiation through the solar infrared band. Polyester film approaches polyethylene transparencies at the shorter solar wavelengths but is almost black in the infrared. As a result, a balloon made of this material shows larger variations in internal heating resulting from night and day differences.

It may be thought that a metalized balloon would have ideal characteristics. However, the best values of reflectivity achieved with metalized balloons have been on the order of 94% for solar radiation and 99% for infrared radiation. The infrared emissivity of the metalized film is 1%, so the balloon film becomes very hot in the region where the solar input is maximum. The metalized balloon, in general, is inferior in radiation characteristics to a clear balloon at the higher altitudes. For lower altitude flights, a metalized balloon will provide improved characteristics over a thick-walled semi-transparent balloon. In this case conduction is relied on as the basic mechanism to remove the excess heat caused by the inefficiency as an infrared emitter. Note that a metal capped balloon will increase both daytime and nighttime gas temperatures. A cap covering the upper third of the balloon has been used with dramatic success on flights near the tropopause

to overcome frost formation caused by nighttime cooling. The cap raises nighttime temperatures by 10 to 15 C° over those experienced by a clear balloon.

No complete theory has been worked out which will permit the theoretical computation of the amount of supertemperature experienced by a balloon in flight. The effectiveness of conduction and convection in removing heat from a balloon at float altitude can only be estimated at present. The simplest procedure for obtaining these data is to conduct flight tests of instrumented balloons with measurements of air temperature and lifting gas temperature.

d. Formability. The ideal film material should be readily formed into a hemisphere, or at least a large sector of a sphere, by heat or pressure in a die or mold. Most plastics can be so formed. However, the more readily they can be formed in this fashion the poorer they usually are as a balloon material in their characteristics. Polyethylene terephthalate film, a polyester, which is the best of the available balloon materials, is cast in sheet form and is drawn into other forms with great difficulty. As a result, the balloons used presently for superpressure flight are made from a large

number of flat gores to simulate a spherical form. The tapes required for sealing constitute a large increase in weight and an additional chance for leakage.

The optimum characteristic for formability would be a material which can be blown into a spherical shape in the same manner as rubber balloons or glass bulbs. However, attempts to blow large glass forms have failed because of the brittleness of the material. All the plastics which have been successfully formed by blowing have been completely inadequate in strength and modulus. It is not inconceivable that thin-walled glass balls may be blown using helium instead of air to provide a lighter-than-air sphere. We would need then only to enclose thousands of these balls in a netting to provide our superpressure balloon system.

e. Brittleness. Since superpressure balloons will be flown in the air lanes, it is essential that the material either shatter or tear easily. Actually, a number of plastic materials have a sufficiently high "glass transition temperature" that they exhibit glass-like characteristics at flight temperatures. Polyethylene terephthalate is one of these materials with a glass transition temperature above 70°C. Although this polyester

has ten times the strength of polyethylene, it has only about one-tenth the tear resistance. Since the balloon is never shocked during testing, inflation, launch, or flight there is no need for a high tear resistance. The glassy materials present a major problem in one general area, however. That is in the manufacture, packing, and unpacking. Creases in the material can cause holes. A double fold, one transverse to the other, in a glassy material makes a sharp point which can tear another section of the film or cause a pinhole at the point of intersection. To prevent such defects, the balloon can be assembled at the launch site. In most cases this does not provide a practical solution. The simplest procedure, which experience has proved to be adequate, is to ensure that the balloon is handled, packed and unpacked, and inflated at temperatures high enough (~30°C) so that the material has more plastic characteristics.

f. Sealability. Many of the plastics, such as polyethylene, can be heat-sealed using simple techniques. These seals have over 90% of the strength of the plastic material. Polyesters and polypropylene are materials which are not easily sealed to themselves and require tape seals with a thermal-setting adhesive. The tape seals are more difficult and costly, but they do provide additional strength to the balloon.

The desired specification for any seal is that it be gas tight and provide equivalent strength to the basic material.

g. Permeability. Most plastics serve as quite adequate gas barriers for a one-day flight. There are, however, few existing plastic materials which have low enough permeability to permit extended flight using either helium or hydrogen. It is not sufficient that the balloon film have low permeability for just helium and hydrogen. Its permeability for nitrogen, oxygen, and water vapor must also be sufficiently low so that there is no appreciable transfer of air into the balloon during flight. All of the materials under consideration as a balloon film do exhibit a much lower permeability to nitrogen and oxygen than to hydrogen and helium.

For extended flights of superpressure balloons, helium is the only acceptable filling gas. Too heavy a penalty is paid in balloon design if ammonia is used. Hydrogen is unacceptable because of the fire hazard not only during testing but after the balloon has finally returned to the ground at the end of its flight, when it becomes even a greater hazard with the possibility of an air mix with the hydrogen.

The best of the existing plastics for helium retention is cellophane. Saran ranks second, and polyethylene terephthalate ranks third. There are few other plastics with acceptable helium permeability characteristics at room temperature. However, because of the very great dependence of diffusion upon temperature among plastics, polyethylene and polypropylene become acceptable at temperatures below -30°C . As a rule of thumb, for long-duration flights, the rate of diffusion through a plastic material should be less than 10^{-6} m^3 mil per m^2 per day per mb (4×10^{-11} std cc cm per sec per cm^2 per cm Hg pressure).

REFERENCES

- (1) Grass, L. A., 1962: Superpressure Balloon for Constant Level Flight, AFCRL Res. Report 62-824 (Aug.), 9, 11, 12.
- (2) Nerkin, A., 1956: Experiments on Flows of Gases Through Leaks, 1956 National Symposium on Vacuum Technology Transactions, pp 4.
- (3) Lichfield, E. W. and R. W. Frykman, 1966: Ghost Balloons Riding the Skies Will Report the World's Weather, Electronics (Nov. 28), 98-106.
- (4) Anonymous, 1966: The Feasibility of a Global Observation and Analysis Experiment, Report of the Panel on International Meteorological Cooperation to the Committee on Atmospheric Sciences, NAS-NRC Publ. No. 1290, pp. 172.

SECTION IX

List of Figures

HOT-AIR BALLOONING

by

Richard G. McCarty

List of Figures ii

A. INTRODUCTION 1

B. PRINCIPLES OF HOT-AIR BALLOONING 2

C. FLIGHT LIMITATIONS AND CONTROLS 26

D. APPLICATIONS 32

Fig. 1. Specific lift vs balloon internal temperature for a balloon operating at sea level in the U.S. Standard Atmosphere, 1962 4

Fig. 2. Specific lift vs ambient temperature for a balloon with an internal gas temperature of 250°F (121°C) operating at a pressure of one atmosphere 5

Fig. 3. Specific lift vs altitude for a balloon operating in the U.S. Standard Atmosphere, 1962, with: 1) an average internal temperature of 250°F (121°C) and 2) an average internal temperature which differs by 191°F (88°C) from ambient air temperature 6

Fig. 4. Gas and skin temperatures as observed in static model hot-air experiment. Average temperature differential is 140°F 8

Fig. 5. Propane burner for a hot-air balloon 10

Fig. 6. Typical hot-air balloon in flight 14

Fig. 7. Payload vs diameter for hot-air balloons at sea level. It is assumed that the envelope is a metalized material, that specialized, light-weight, stainless steel tanks are used, that rigging weight is 10% of envelope weight, that fuel is carried for one-hour flight at sea level, and that 50% of the fuel will be used for ascent. Internal temperature is 250°F (121°C) 16

Fig. 8. Payload vs diameter for hot-air balloons at 20,000 ft (6 km) See caption of Fig. 7 for balloon system characteristics 17

Fig. 9	Volume vs diameter for a natural-shape hot-air balloon	18
Fig. 10	Surface area vs diameter for a natural-shape hot-air balloon .	19
Fig. 11	Gross lift vs diameter for balloon flying in the <u>Standard Atmosphere</u> with an internal temperature of 250°F	20
Fig. 12	Envelope weight vs diameter for a balloon made of available fabric. In flight at sea level in the <u>U.S. Standard Atmosphere, 1962</u> , with an internal temperature of 250°F; the safety factor is three	21
Fig. 13	Propane vapor pressure vs temperature	23
Fig. 14	Basic envelope heat loss rate vs gross lift for a balloon at sea level having an internal temperature of 250°F	25
Fig. 15	Double propane burner	28
Fig. 16	Inflated balloon with maneuvering vent open	29
Fig. 17	View of the removable cap inside a hot-air balloon	31
Fig. 18	An unmanned hot-air balloon. The white sectors are scoops which help the falling balloon to inflate before the burner is turned on. This balloon was dropped from an airplane . . .	36
Fig. 19	Performance of a hovering hot-air balloon.	38

HOT-AIR BALLOONING

A. INTRODUCTION

Any gas less dense than the surrounding atmosphere is capable of providing the buoyance necessary for balloon operation. Since the density of air diminishes as its temperature rises, "hot air" can serve as a pseudo lighter-than-air medium. Hot air, the most readily available buoyant gas, was used by the brothers Joseph and Etienne Montgolfier in the first demonstration of a balloon in November of 1782.

Within a year of the invention of the balloon, man was ready to fly. On the 21st of November, 1783, the Marquis d'Arlandes and Pilatre de Rozier went aloft carrying a fire with them. For fuel they used chopped wood and straw, which had the effect of quickly generating large amounts of heat and dense smoke, which was thought to be beneficial. At one point the upsurgent flame nearly turned their "globe volant" into a fiery bier.

Although hydrogen soon replaced hot air as the dominant balloon gas, hot-air balloons have been constructed and flown occasionally since 1782.

One well-publicized hot-air balloon was "L'Aigle" constructed by Eugene Godard in France in 1864. L'Aigle carried an 18-ft diameter stove which generated enough heat to fill its half-million-cu-ft envelope with hot air. A gondola, which surrounded the furnace, provided ample room for more than a half-dozen passengers. A series of flights was conducted between 1864 and 1866.

The current resurgence of interest in hot-air ballooning arises out of improvements in operational capabilities that are a direct result of gains in material technology. New materials mixed with modern engineering techniques are generally credited for the development of the modern hot-air balloon.

B. PRINCIPLES OF HOT-AIR BALLOONING

The average density of the heated air and associated combustion products is fairly close to the density of air alone at the equivalent temperatures. The air within the balloon is not uniformly hot, but is a circulating turbulent mixture of air in which strong temperature gradients exist. Nevertheless, considerable insight can be achieved by assuming an average value. It is possible, for example, to derive a specific lift as a func-

tion of temperature for any specified altitude. Whenever balloon performance is computed at a given altitude, it is generally assumed that environmental conditions at that altitude may be represented by the U.S. Standard Atmosphere, 1962. Figure 1 illustrates the variation of specific lift with temperature at sea level on a standard day with an ambient temperature of 59°F (15°C). The lifting force is quite sensitive to ambient temperature, and Fig. 2 illustrates the variation of specific lift with outside temperature, again at sea level, for a balloon hot-air temperature of 250°F (121°C). A temperature of 250°F ensures long envelope fabric life, and Fig. 1 shows that the specific lift is approximately 0.020 lb/ft³ (0.32 kg/m³) on a standard day at sea level. Specific lift is plotted as a function of altitude in Fig. 3, both for a constant balloon temperature of 250°F and for a constant temperature differential between balloon and air of 191°F (88°C).

Figure 3 shows one of the problems of achieving very high altitude flights for hot-air balloons--the specific lift decreases monotonically as altitude increases. It is reasonable to expect that hot-air systems will find utility in the upper reaches of the troposphere, but above the tropopause it seems unlikely that hot-air balloons will be used except as

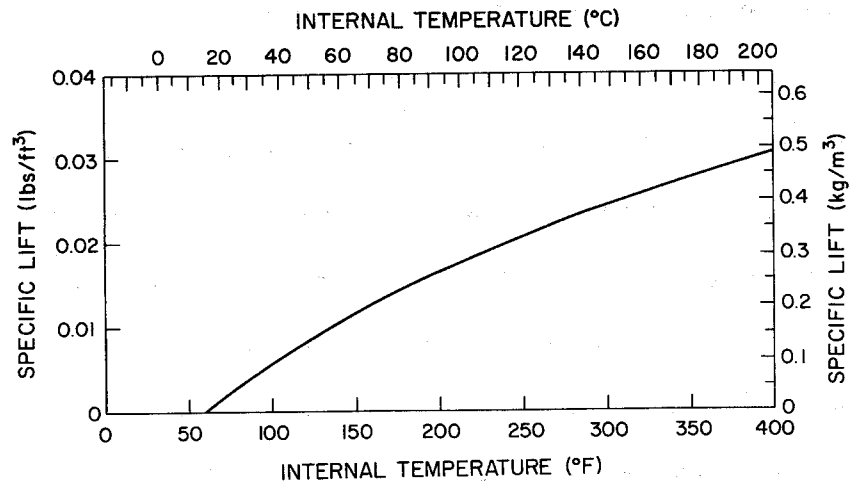


Fig. 1. Specific lift vs balloon internal temperature for a balloon operating at sea level in the U.S. Standard Atmosphere, 1962.

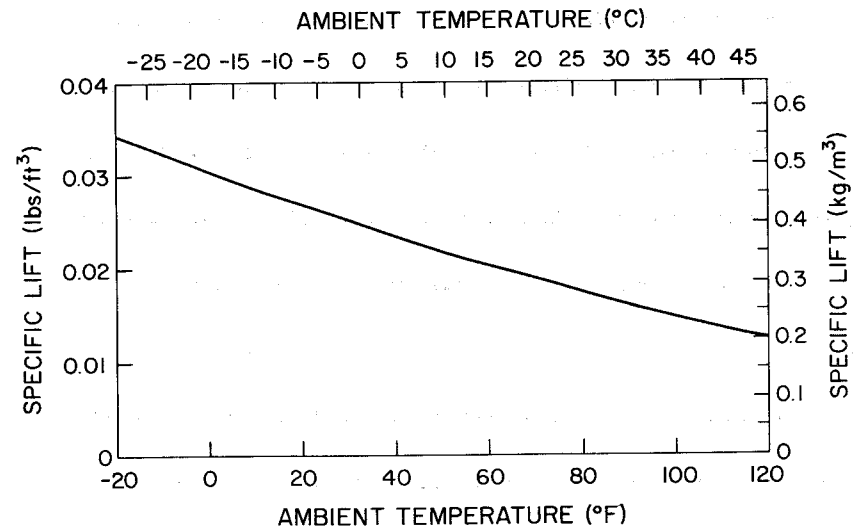


Fig. 2. Specific lift vs ambient temperature for a balloon with an internal gas temperature of 250°F (121°C) operating at a pressure of one atmosphere.

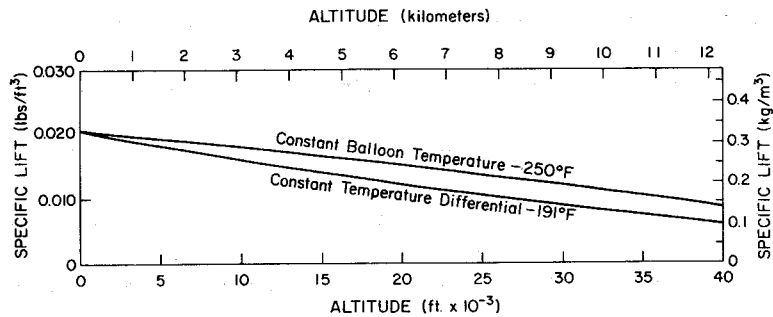


Fig. 3. Specific lift vs altitude for a balloon operating in the U.S.

Standard Atmosphere, 1962, with: 1) an average internal temperature of 250°F (121°C) and 2) an average internal temperature which differs by 191°F (88°C) from ambient air temperature.

decelerating devices that ultimately fall into the lower atmosphere.

The specific lift can be increased by operating at higher temperatures although the nature of the lift equation sets an upper limit even for infinite temperatures. Hot-air balloons normally operate in the neighborhood of 0.25 to 0.5 the theoretical maximum. Fabric durability at elevated temperatures is, of course, one of the paramount restraints on increasing lift by increasing temperature.

To determine the effects of flame temperature on fabric temperature, Raven Industries, Inc. instrumented a small balloon and obtained the results illustrated in Fig. 4. It can be seen that the temperature probe indicated a flow field that starts at the burner, rises to the crown of the balloon, and then descends down the sides. Along the streamlines the temperature gradually moderates, which is a fortuitous effect with regard to the fabric. In the experiment illustrated, the temperature near the flame was 240°F (116°C) above ambient, but at the crown it was only 140°F (60°C) above ambient.

An interesting outcome of the measurement was that the maximum skin temperature turned out to equal the temperature that would account for the

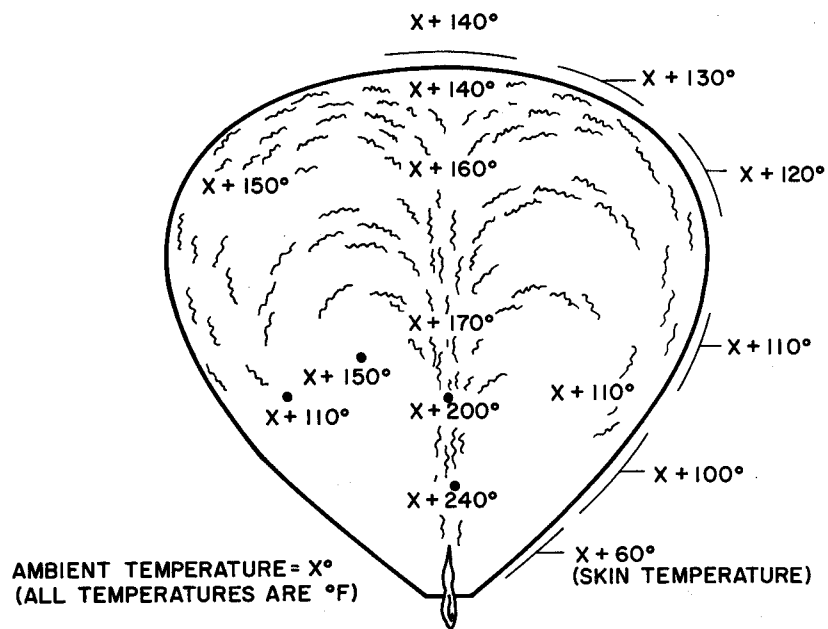


Fig. 4. Gas and skin temperatures as observed in static model hot-air experiment. Average temperature differential is 140°F .

measured lift. This immediately suggested that a temperature probe at the crown of the balloon be used to compute lift and also to warn if maximum temperatures approached unsafe values.

The use of a burner, as suggested by Fig. 4, causes ambient air to be entrained into the flow field. The air not only provides the oxygen for combustion of the fuel, but also serves to reduce the temperature. In addition to several other effects, the entrained air loosely couples the internal temperature to the outside temperature. There is, therefore, a tendency toward a constant temperature difference rather than a constant temperature.

At sea level a burner such as the one shown in Fig. 5 passes about 180% of the air required to sustain combustion. The excess air and the combustion products are ultimately exhausted by seepage through the fabric and the seams and by counterflow or ventilation through the base throat. A significant part of the thermal input can ultimately be lost in this fashion under some circumstances.

In practice a maximum operating temperature based upon the durability requirements of the envelope is established for a balloon. Then the sizes of balloon and the burner to accomplish the mission profile without exceed-

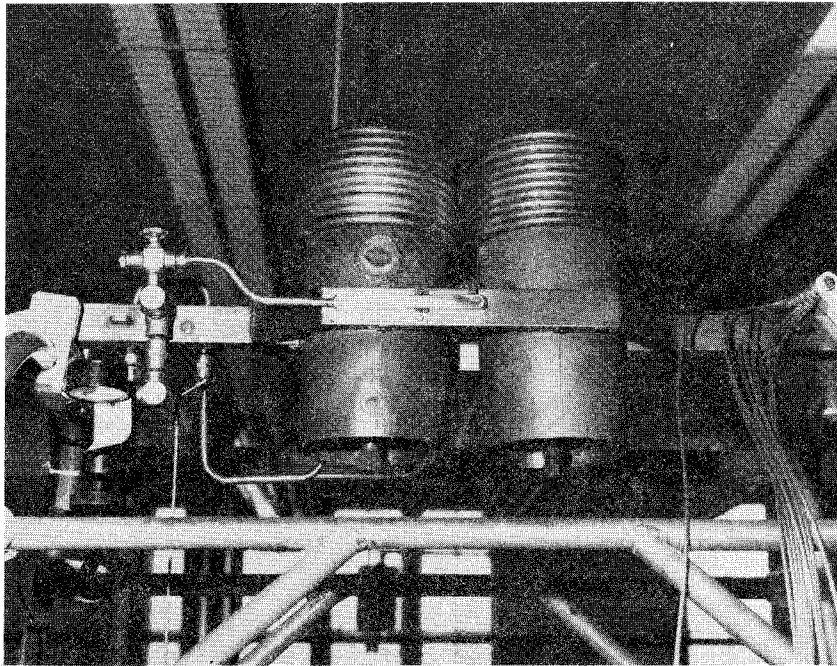


Fig. 5. Propane burner for a hot-air balloon.

ing that limit are established. For manned systems the limit is 250°F (121°C), and for short-lived unmanned systems it may be as high as about 350°F (177°C).

Nylon is the most frequently used fabric, although dacron is also used. Special high-temperature materials exist and are being considered for special applications as either full envelopes or as crown caps.

The polymeric fabrics, nylon and dacron, tend to soften with elevated temperatures. At the same time the percentage elongation under strain increases markedly and much of it is inelastic. At 484°F (251°C) these materials actually melt and, of course, their strength evaporates.

Recent improvements in the cross-linking of nylon and dacron molecules have resulted in the so-called high-tenacity forms which do not degrade in strength as rapidly as previous forms. High-tenacity nylon is most commonly used in hot-air balloons and some of its characteristics are included below.

Breaking tenacity	1.5 - 1.9 ($\times 10^{-2}$) lb/denier [6.7 - 8.4 ($\times 10^{-2}$) N/denier]
Breaking elongation	17-45%

The basic strength and temperature characteristics are not the only characteristics of interest. Other important factors include: 1) high strength-to-weight ratio at design temperature, 2) high strength-to-packed volume ratio, 3) minimal creep at elevated temperatures, 4) good crease resistance, 5) low thermal conduction, 6) low storage degradation, 7) moderate gas permeability, and 8) for repeated use, good scuff resistance.

Clearly the physical characteristics of the basic material are only part of the story. The way the fibers ultimately are formed into a fabric remains equally important. The choice of fabric or fabrics ultimately depends upon the mission to be accomplished. For medium-sized balloons (30 to 50 ft in diameter--9 to 15 m) the standard material is 1.6 oz/yd² (54 gr/m²) ripstop nylon which has been calendared (pressed with a hot roller to flatten the threads and reduce permeability). The physical properties of the fabric are:

Tensile strength	90 lb Warp and filling
Thread count	120/in.(47/cm) Warp and filling
Tear strength	6 lb (27 N) Warp and filling
Thread	30 denier High-tenacity nylon

A typical hot-air balloon is shown in Fig. 6. Since hot-air balloons tend to operate at low altitudes with large payload-to-balloon weight ratios, the design shape corresponds to a low sigma value.

Although the natural-shape balloon has no circumferential stresses when fully deployed, the manner in which hot-air balloons are used frequently introduces transient circumferential stresses. The balloon gores are sewn together in a simple lap seam that retains 75% of the parent fabric strength. Since the ventilation loss through the throat is comparatively large, it is not necessary to make the seams gas tight, which alleviates the production problem considerably.

The magnitude of the meridional loads normally exceeds the circumferential stresses considerably. For manned systems it is common practice to provide a design load factor of seven or more to ensure safe operation. Special care must be exercised in the way the load is introduced into the fabric and in the design of the balloon near the crown where stresses concentrate and the temperature is a maximum.

The rigging weight associated with the envelope accounts for some 10-20% increase over the bare envelope weight. The burner and fuel add additional



Fig. 6. Typical hot-air balloon in flight.

weight that subtracts from the lift available for carrying a payload.

Figure 7 illustrates the payload that can be carried by balloons of various diameters under one set of assumptions at sea level. Figure 8 shows the same information for a balloon operating at 20,000 ft (6 km).

The relationship between diameter, surface area, and volume is not simple for balloon shapes (see Section V). For the low altitude hot-air balloon, the following relationships apply: $\Sigma = -0.05$, $V = 0.125 \lambda^3$, $R = 0.3175 \lambda$, $A = 1.21 \lambda^2$, $H = 0.66 \lambda$, and $\theta = 95^\circ$, where V is volume, R is radius at the equator, H is height, A is area, θ is base cone angle, and λ is gore length.

To facilitate comparison, the relationships between diameter and volume, area, and gross lift are included in Figs. 9, 10, and 11. Figure 12 compares the envelope weight with balloon diameter. The envelope weight is purposely left somewhat indeterminate since for the larger balloons it depends upon design safety factors and the materials used.

The heat required to initiate and sustain flight may, in theory, be supplied from a wide variety of sources, including propane burners, modified liquid or solid fuel rocket motors, pyrotechnic devices, and nuclear power

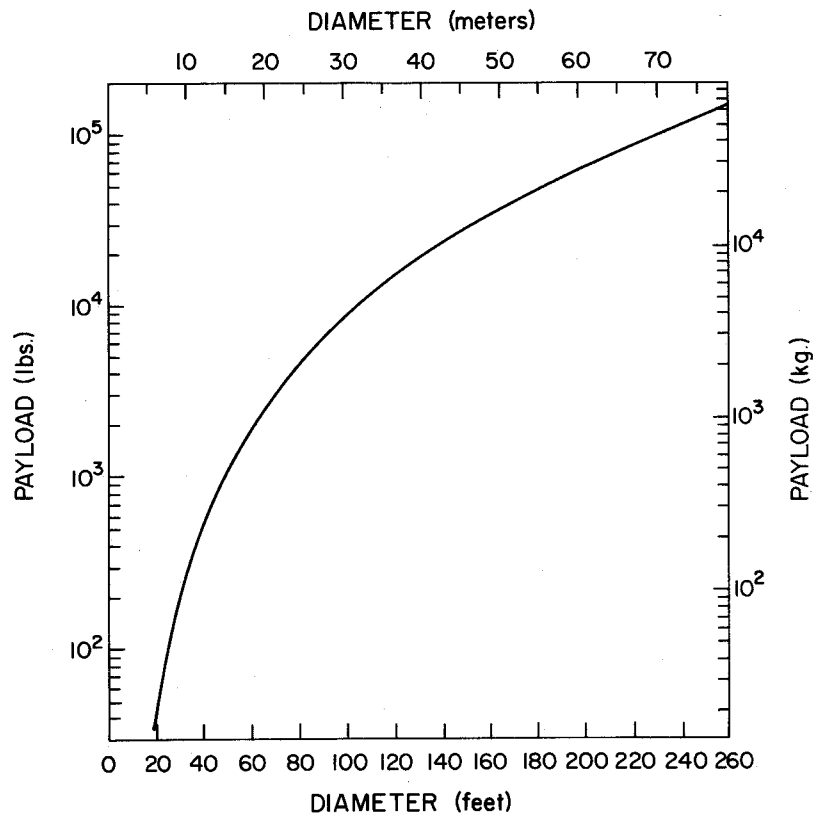


Fig. 7. Payload vs diameter for hot-air balloons at sea level. It is assumed that the envelope is a metalized material, that specialized, light-weight, stainless steel tanks are used, that rigging weight is 10% of envelope weight, that fuel is carried for one-hour flight at sea level, and that 50% of the fuel will be used for ascent. Internal temperature is 250°F (121°C).

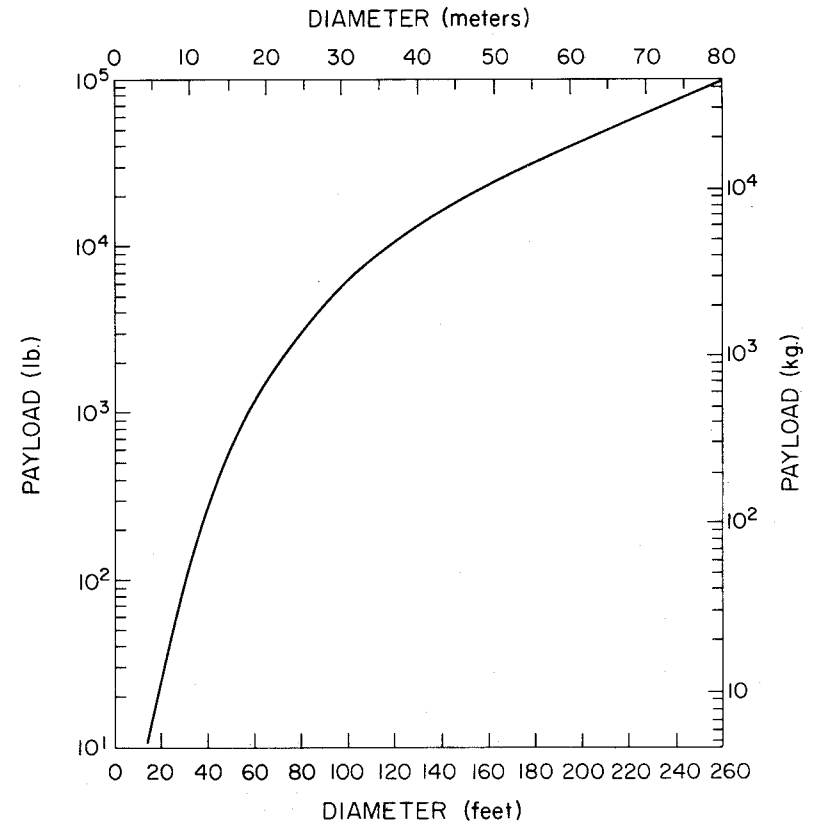


Fig. 8. Payload vs diameter for hot-air balloons at 20,000 ft (6 km).

See caption of Fig. 7 for balloon system characteristics.

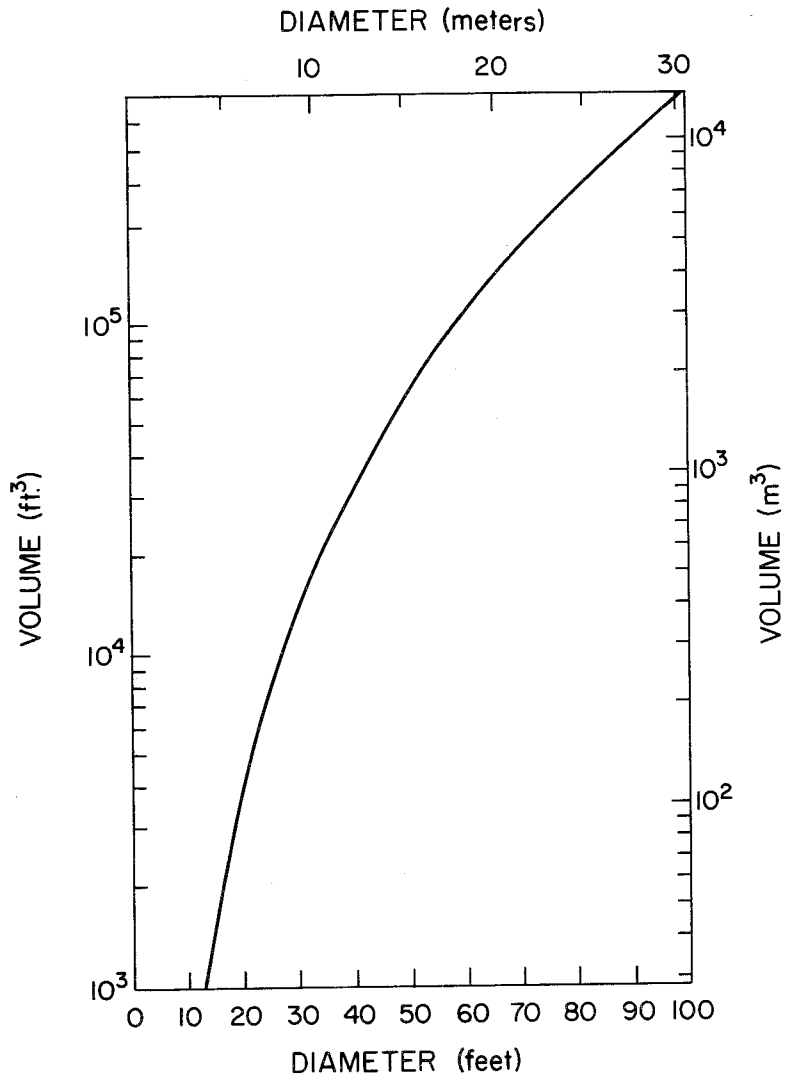


Fig. 9. Volume vs diameter for a natural shape hot-air balloon.

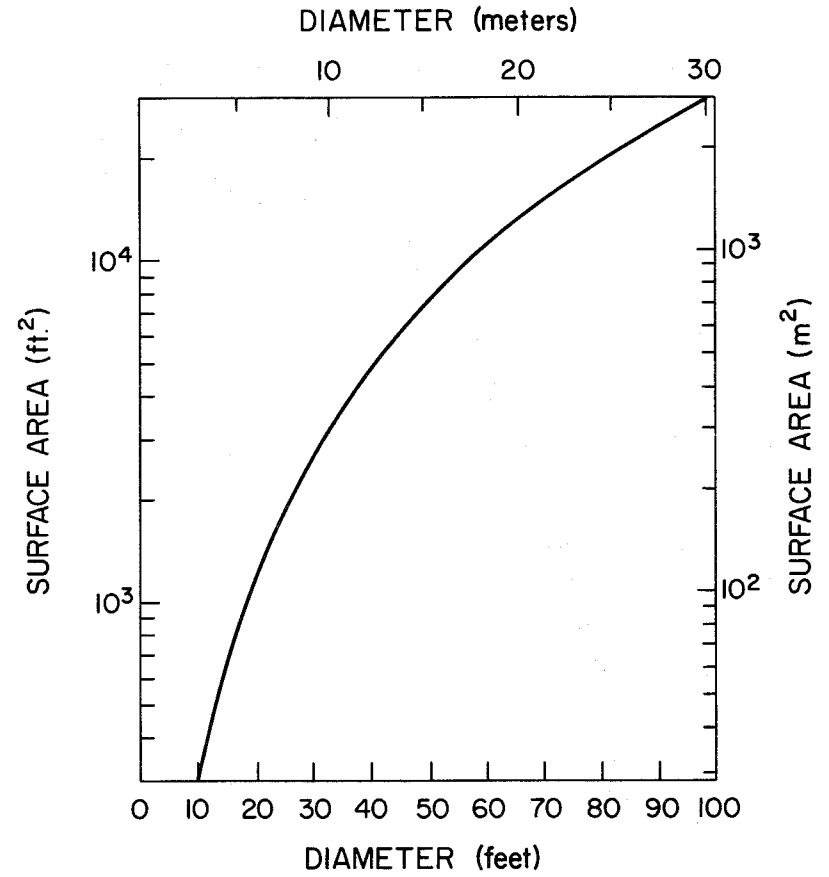


Fig. 10. Surface area vs diameter for a natural shape hot-air balloon.

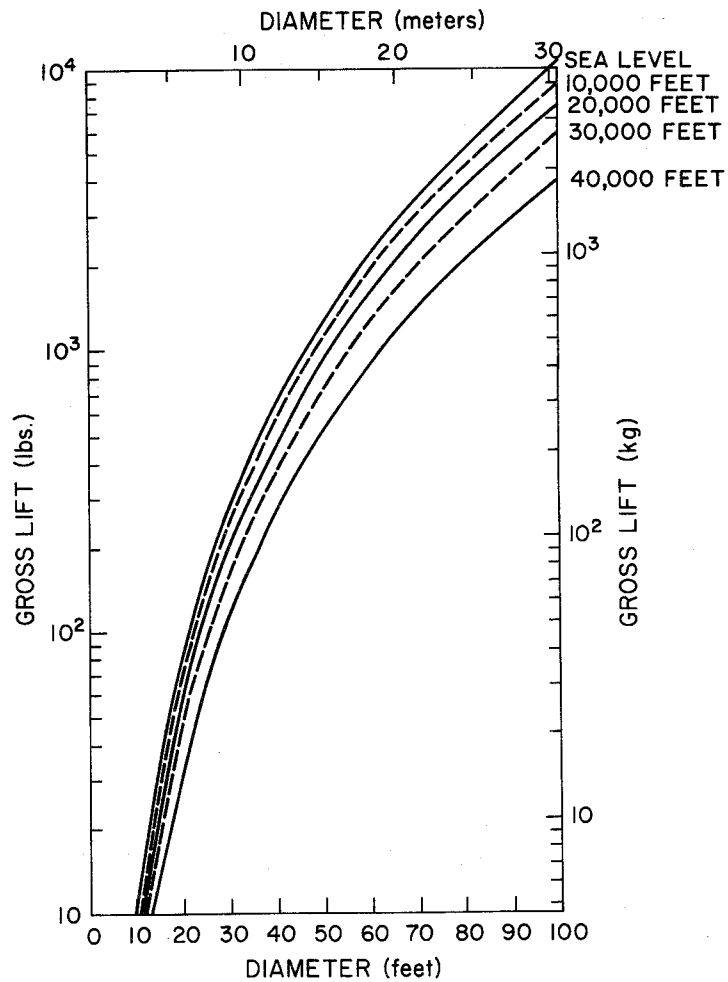


Fig. 11. Gross lift vs diameter for balloon flying in the Standard Atmosphere with an internal temperature of 250°F.

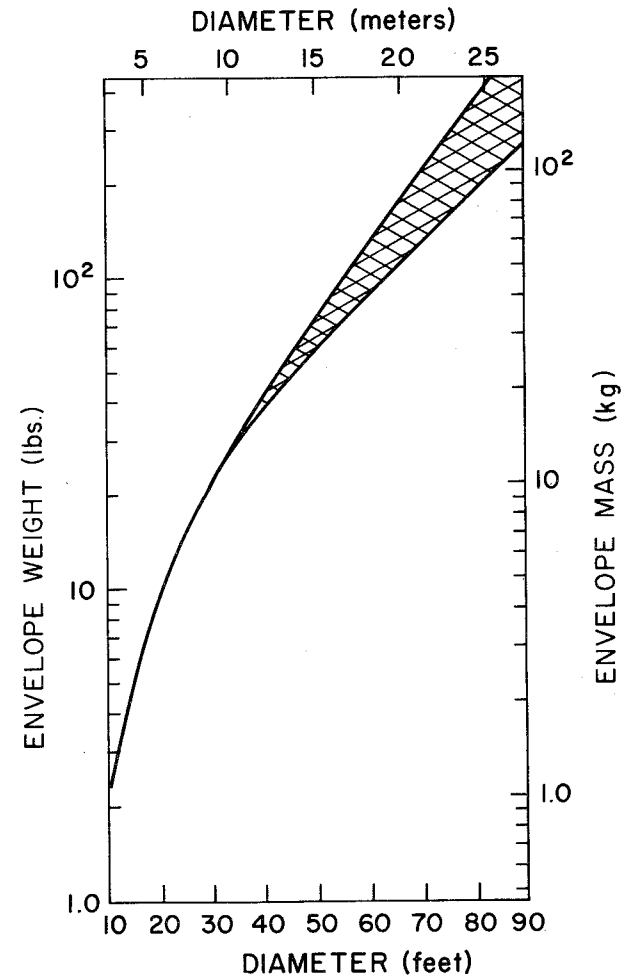


Fig. 12. Envelope weight vs diameter for a balloon made of available fabric. In flight at sea level in the U.S. Standard Atmosphere, 1962, with an internal temperature of 250°F; the safety factor is three.

supplies. Only propane burners and pyrotechnic devices have been extensively evaluated.

Propane has many desirable features. It is stored as a liquid but has a significant vapor pressure at normal temperatures, which alleviates the need for pumping mechanisms in many cases. At the same time the vapor pressure does not rise to excessive values in "hot" conditions. Figure 13 shows the vapor pressure of propane as a function of temperature. For normal usage, the U.S. Interstate Commerce Commission has established standards for propane tanks, which cause them to weigh approximately 75% as much as the propane in a full tank. Special purpose tanks can be made which achieve more nearly 45% of the full fuel weight. In all cases it is mandatory to provide a pressure relief valve to compensate for unanticipated thermal surges.

By far the most difficult aspect of hot-air balloon system design is the computation of fuel and burner requirements. Energy balance relationships of hot-air balloons are complex. They must account for thermal storage and compression of the air in the balloon, burner heat addition, heat transfer through the balloon fabric, ventilation heat losses, and variability of air temperature and pressure.

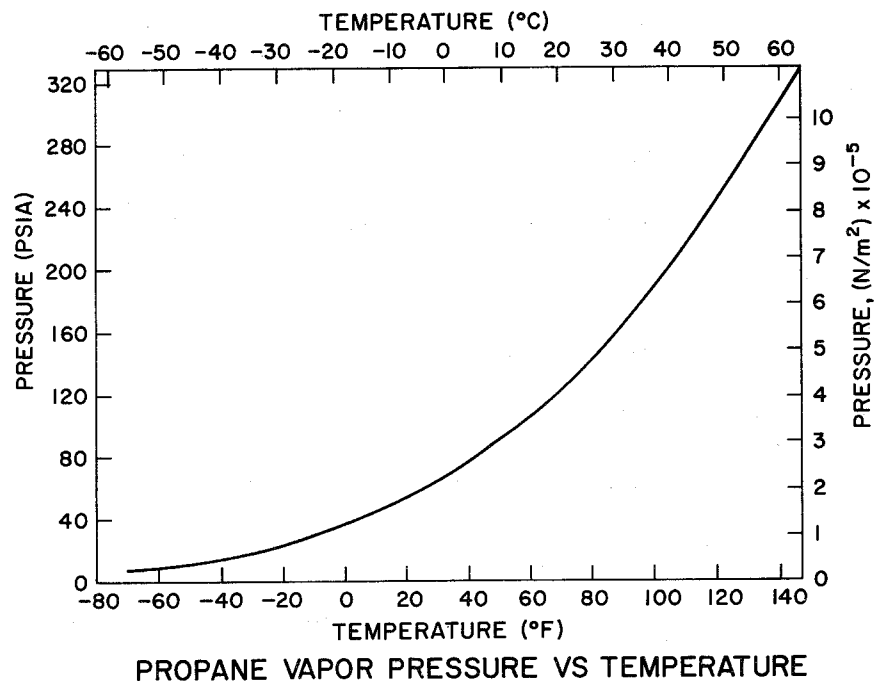


Fig. 13. Propane vapor pressure vs temperature.

Many of the effects--burner performance, for example--are further dependent upon altitude and velocities. The energy relationships may, however, be analyzed with a computer. By also solving the equations of motion, the entire flight performance of a hot-air system may be simulated with fair success. (See Section III.)

For many applications it is not necessary to determine performance with precision, since it will vary with atmospheric conditions, and the analysis may be simplified. Figure 14 serves as a guide for computing the hovering requirements for a balloon at sea level.

Considerably larger values may be needed for maneuvering or for initial heating. Rules of thumb indicate that initial heating may require 10 times as much heat as hovering. Maneuvering vertically requires about twice the heat rate of hovering.

Propane, with a density of 4.2 lb/gal (500 kg/m³), has a thermal output of approximately 20,000 BTU/lb (actually 21,560, but there are losses). A propane burner of the type shown in Fig. 6 is capable of producing 2 x 10⁶ BTU/hr (585 kw). The burners are designed to provide more than 1000 hr of service. The specific weight of burners (in lb of burner weight per

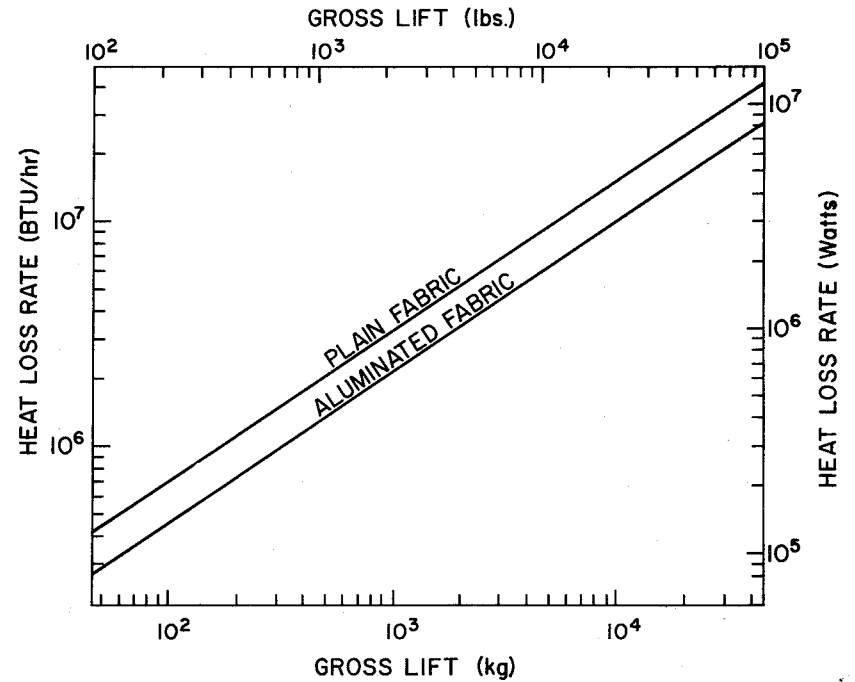


Fig. 14. Basic envelope heat loss rate vs gross lift for a balloon at sea level having an internal temperature of 250°F.

BTU/hr capacity) can be improved by cutting the life cycle, using more expensive materials, or using higher unit outputs.

C. FLIGHT LIMITATIONS AND CONTROLS

The modern hot-air balloon is an outgrowth of an effort to devise a manned flight vehicle that would be simple to operate, inexpensive, and capable of storage for long periods of time without degradation. Today most manned balloons are 50 ft (15 m) in diameter, although both smaller and larger versions do exist.

A balloon 50 ft in diameter having a volume of 61,000 ft³ (1700 m³) is a commonly used balloon. Though normally considered a two-man system, it is possible to carry three--a pilot and two passengers--at the lower altitudes. With conventional burners it has been flown to 24,000 ft (7.3 km), but this cannot be recommended.

The flight duration of a balloon depends heavily upon the amount of fuel carried. Typically, two 22-gal tanks of propane (83 kg) are enough for three to four hr of flight for a 50-ft balloon, depending upon the ambient temperature and the amount of maneuvering. As with aircraft, fuel reserve should always be maintained.

The propane burner is a relatively simple apparatus. As shown in Fig. 15 the fuel flows from the tanks through coils surrounding the burner barrel. The propane leaves the fuel tank as a liquid but is transformed to a gas as a result of heat passing from the barrel to the fuel line. Air is entrained through the lower opening in the burner barrel and serves to supply oxygen for combustion and to moderate the temperature of the combustion product.

The rate of flow of propane is governed by a needle valve that acts as a cruise control and is adjusted as needed during the flight. To provide maximum lift in emergencies, a by-pass valve and line permit the full burner capacity to be made available instantaneously.

A maneuvering vent in the envelope provides an additional means of controlling lift. The maneuvering vent illustrated in Fig. 16 is a feature available with hot-air balloons that is impractical for helium or hydrogen systems. Basically a controllable slit in the envelope, the maneuvering vent is possible as a result of the "zero circumferential stress" design. The vent is controlled by a line extending from the gondola and along the side of the balloon wall where it is split into a "Y" and then passed through a pulley and connected to each side of the vent. A simple pull from the

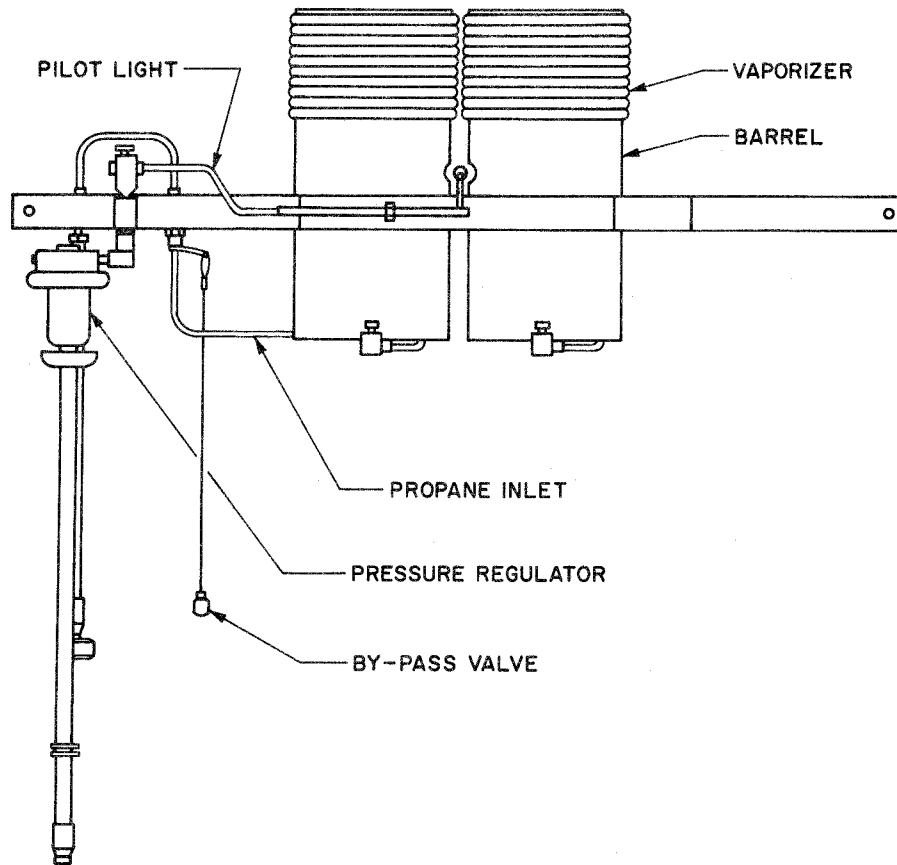


Fig. 15. Double propane burner.



Fig. 16. Inflated balloon with maneuvering vent open.

gondola opens the vent proportionally to the amount of line taken in.

A maneuvering vent in a balloon can be quite useful. Normally a balloon of the 50-ft class will take approximately a minute to respond sensibly to a change in thermal input. By spilling heated air through a maneuvering vent, almost instantaneous decrease in lift is possible. Precise altitude control, even at low levels, can be achieved by running the burner a little "high" while spilling the excess lift through a partially opened vent as needed for increasing or decreasing the effective lift.

Another interesting feature of the modern hot-air balloon is a cap which can be removed by a steady pull on a line (rip cord) from the gondola. In the Raven Industries, Inc. design, shown in Fig. 17, load tapes fastened along the gore lines cross over the top of the balloon where the top portion of the envelope has been eliminated. Then the cap is placed under the load tapes and secured at its edge with Velcro tape except for an 18-in. section, which is sewn. The Velcro keeps the cap in place; the load is taken up by the load tapes; and once on the ground, only a light steady tug with the rip cord is necessary to peel open the cap and spill the hot air. Reinstallation of the cap is made easy by the Velcro.

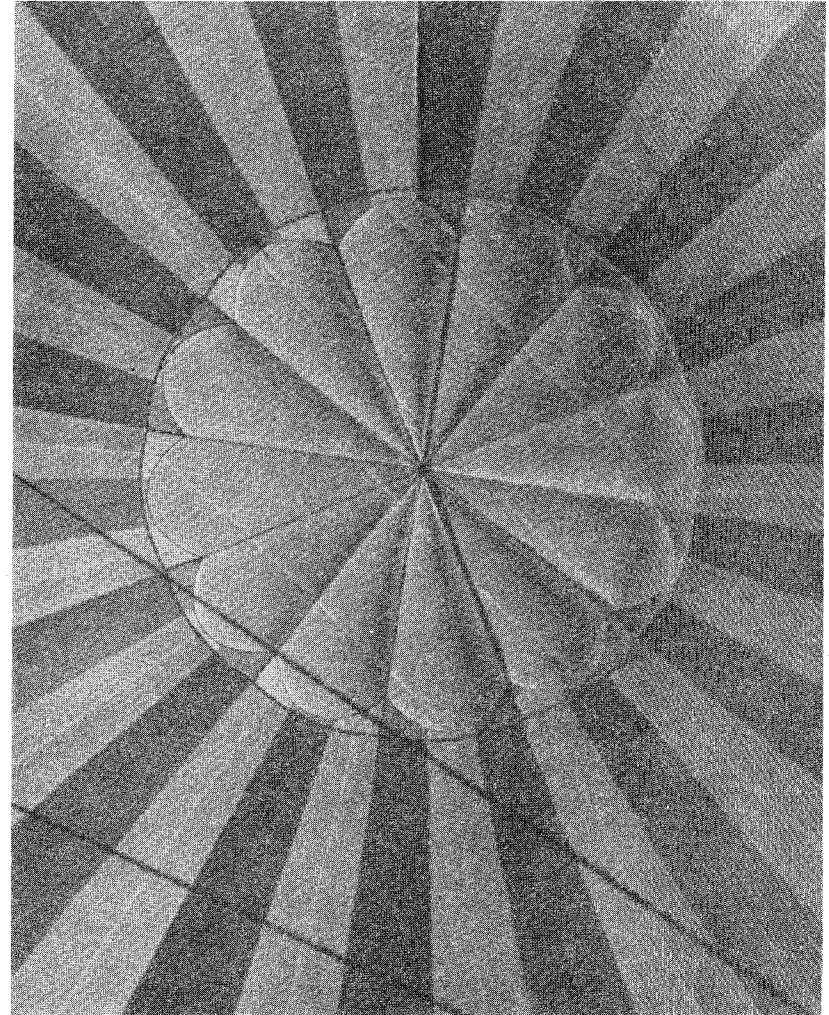


Fig. 17. View of the removable cap inside a hot-air balloon.

A cylindrical skirt is attached to the bottom of the balloon externally. At the attachment point this skirt has the same diameter as the balloon. The skirt is 6 ft long and 8 ft in diameter. The purpose of the skirt is to direct the hot gases into the interior of the balloon and divert horizontal wind gusts which might deflect the burner flame onto the main envelope. The skirt has a spring steel hoop at its base to maintain its circular shape.

Handling lines attached near the equator of the envelope are used to assist in inflation and launching of the balloon.

Instrumentation of hot-air balloons is relatively simple. An altimeter and a rate-of-climb meter are required. A fuel gage is indispensable. From a safety standpoint, the most important instrument is a thermocouple sewn near the crown of the balloon to indicate maximum envelope temperature.

D. APPLICATIONS

From a technical standpoint the upsurge in sport ballooning has provided a great deal of information on balloon performance that would not otherwise have become available at this time, and flight experience with hot-air balloons has led to a number of commercial and technical applications. For

example, pheasant populations have been checked in South Dakota by slowly and silently gliding low over fields. It has been possible to test and evaluate instrumentation for satellites on balloons in cases where the speed of airplanes and the vibration of helicopters have prohibited their use. Schools of fish have been studied from a hot-air balloon tethered above a ship.

More and more applications for tethered hot-air balloons are being found. A 60-ft (18 m) balloon is capable of carrying two or three technicians, plus oscilloscopes and auxiliary laboratory equipment for an hour. It is less expensive to use a balloon than to build a tower, and a tethered balloon may be moved from one site to another for subsequent tests without difficulty. Experience indicates that a 60-ft balloon is capable of such operations in winds up to 15mi/hr (~ 7 m/sec).

Both tethered balloons and ground launched free balloons have considerable historical precedence, and the movement of hot-air balloons into these fields is not surprising. What is somewhat startling is that the promise of air launched hot-air balloons is perhaps even greater. Air launched hot-air balloons offer the potential of causing a suitable payload to rise, to hover, or to descend slowly--more slowly than possible with a parachute or

other passive decelerators. With the addition of modest controls the hot-air balloon can accomplish all these modes on a programmed or adaptive basis.

The air launched hot-air balloon may be ejected from either aircraft or rockets. If the speed and altitude of injection are such as to provide an excessive dynamic pressure, it may be necessary to provide a primary decelerator, a drogue parachute, for example, to slow the system down. Below a specified dynamic pressure (30 lb/ft^2 [1450 N/m^2] in a system to be described) the balloon may be deployed. The balloon, when filled with air, serves as a secondary decelerator. Based upon cross sectional area, the cold balloon will have a drag coefficient of between 0.5 and 1.0 depending upon whether high drag is desired.* Thus, the cold balloon compares favorably with a standard parachute on area drag, although not on a weight basis. The important fact is that a cold balloon will provide a terminal descent rate comparable to that of a parachute in the event that the burner does not function or fuel should be exhausted.

*Experiments have shown that a "burble fence" on the balloon increases both stability and drag.

The balloon is somewhat more difficult to fill than a parachute--or rather takes a bit more sophistication. Common practice is to place a series of inflation scoops near the equator. The inflation scoops allow the top of the balloon to fill and stiffen the envelope to the point where the base throat may be opened (see Fig. 18). Then additional air is "rammed" into the balloon through the throat until the envelope is filled. Early air-launched balloons used throat inflation only, and problems were occasionally encountered. As the first air was ingested, a bubble developed at the throat of the envelope that tended to buffet and alternately open and close the throat as a result of instabilities in the air stream. The result was to permit the envelope to fall too far before inflation was complete and to burn the envelope if the burner was turned on.

In a normal sequence with inflation scoops, the inflation process is completed in a matter of seconds. When the cold inflation process has progressed sufficiently to hold the throat open, the burner may be turned on.

Computer studies have revealed considerable insight into the performance of air-filled balloons undergoing heating while falling. If, for example, the balloon is dropped at one altitude and the mission involves hovering

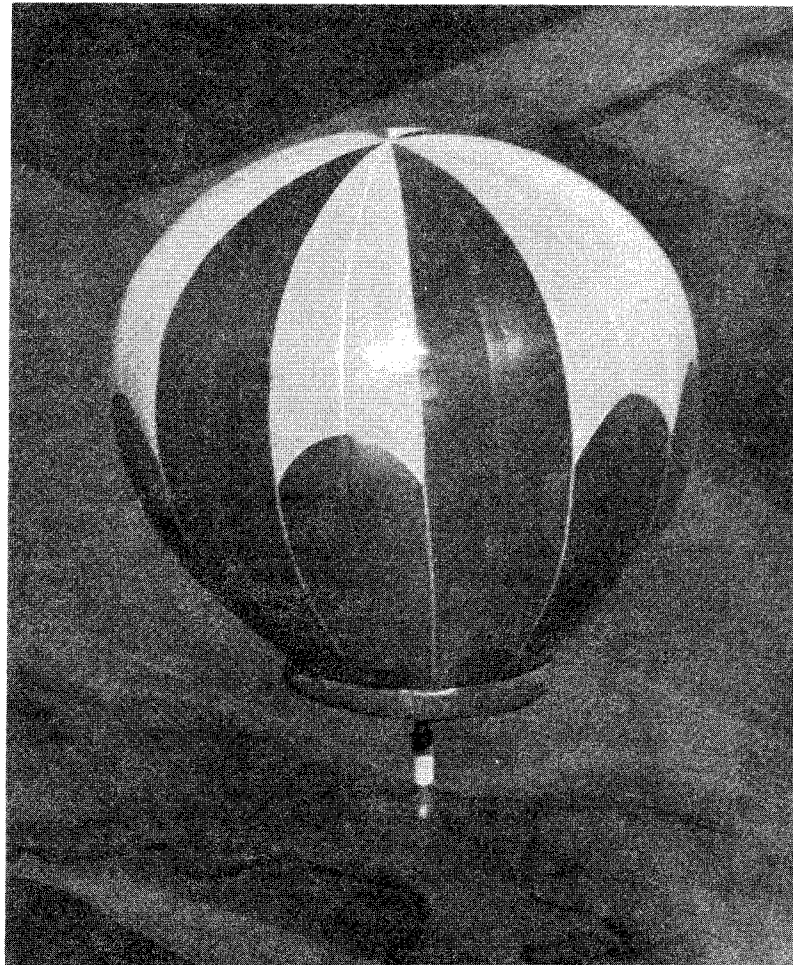


Fig. 18. An unmanned hot-air balloon. The white sectors are scoops which help the falling balloon to inflate before the burner is turned on. This balloon was dropped from an airplane.

at a lower altitude, there is an optimum heat generation profile. The optimum amount of heat at any instant is that which is just adequate to raise the volume of the balloon gas enough to compensate for the compression that occurs as a result of falling, plus heat losses due to conduction. In other words, the thermal input should be just that which results in no flow of air in or out of the balloon.

Since a variable heat generation profile is complex, a comparison has been made of the loss of efficiency that occurs for a fixed heat generation system. It turns out that there can be found an on-off fixed level heat generation profile that differs in fuel consumption from the optimum profile by a negligible amount. Analysis also shows that the distance that a balloon will fall during the heating period (assuming that the vertical motion just stops and the balloon hovers) will be one-third the distance that the balloon would free-fall in that same time. Finally, it has been determined that little is gained in beginning to heat a balloon at altitudes above 30,000 ft (9 km) since the percentage energy requirement is low at those altitudes.

Figure 19 illustrates the performance of a system which was designed to hover in the vicinity of 25,000 ft (7-8 km) regardless of the altitude de-

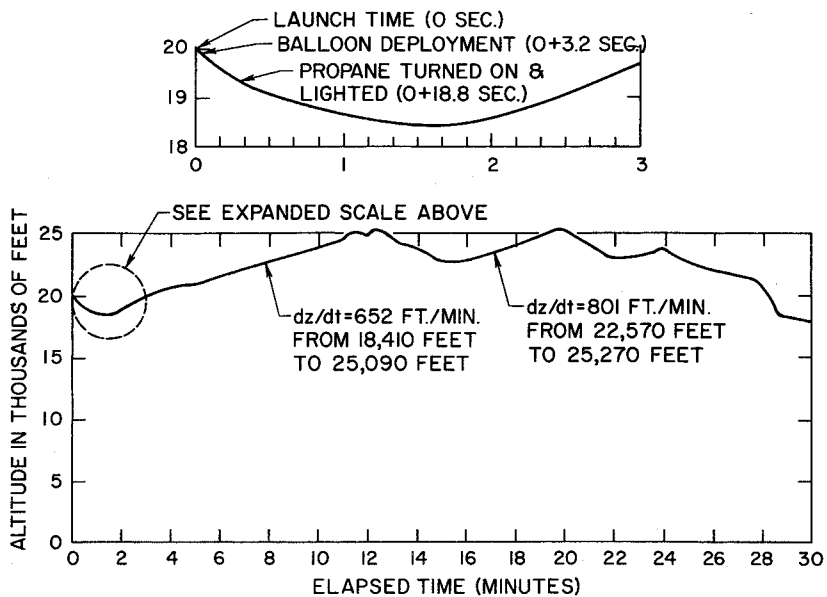


Fig. 19. Performance of a hovering hot-air balloon.

ployed. In this instance the balloon was deployed at 20,000 ft (6 km), descended to 18,600 ft (5.7 km) during initiation and then climbed to 25,000 ft (7.6 km). At that altitude the burner was turned off and the system settled to 22,500 ft (6.9 km), where reignition was accomplished.

In summary, the hot-air balloon provides an inexpensive way to carry a useful payload upward through as much as two-thirds of the atmosphere. It is easy to fly, capable of extended storage, and it can be moved from site to site in a small truck or trailer.

SECTION X

LIST OF SYMBOLS

PARACHUTES

by

Alvin L. Morris

List of Symbols. ii

List of Figures iv

A. INTRODUCTION 1

B. DESCRIPTION OF A PARACHUTE SYSTEM 1

C. PARACHUTE DESCENT. 5

1. A Simplified Descent Model 13

a. Phase 1 15

b. Phase 2 17

c. Phase 3 28

d. Phase 4 29

D. CONSIDERATIONS IN SELECTING A PARACHUTE 30

1. Parachute Size 32

2. Multiple Parachutes 40

3. Time of Descent 42

REFERENCES 44

<u>Symbol</u>	<u>Description</u>	<u>Dimensions</u>
A	cross-sectional area, usually the effective area of the inflated canopy	L^2
A'	nominal area, usually taken as the area of material in the canopy	L^2
B	subscript indentifying its symbol with the balloon system	
C	constant of integration	
C_D	drag coefficient (dimensionless)	
C'_D	pseudo drag coefficient, used with an area other than the effective area	
D	diameter of a canopy	L
D'	nominal diameter of a canopy, usually taken to be the diameter of a circle whose area is equal to the nominal area, A'	
d	symbol indicating differentiation of the variable following it	
g	acceleration due to gravity	LT^{-2}
H	height above sea level	L
m	mass of parachute system	M
m_v	virtual mass of an accelerating parachute system	M
N	number of parachutes used in a cluster	
n	exponent of 10 used to expand the scales of Figs. 6 and 7	

o	subscript identifying its symbol with the base or zero level	
Re	Reynolds number	
T	subscript used with v to indicate terminal or equilibrium velocity	
t	time	T
v	vertical velocity. Algebraic sign identifies its direction, (+) upward and (-) downward	LT^{-2}
v_T	terminal or equilibrium velocity	LT^{-2}
v_w	horizontal speed of surface wind	LT^{-2}

Greek letters

ρ	air density	ML^{-3}
π	3.14159	

List of Figures

Fig. 1	Parachute nomenclature	3
Fig. 2	Acceleration versus time for a parachute system for which terminal velocity is constant. Acceleration is in effect plotted as multiples of the acceleration of gravity and time as multiples of $(-v_T/g)$	20
Fig. 3	Acceleration traces of quick-opening and delayed-opening parachutes	23
Fig. 4	Descent velocity versus time for a parachute system for which terminal velocity is constant. Velocity is plotted as a multiple of v_T and time as a multiple of $(-v_T/g)$	26
Fig. 5	Loss of altitude versus time for a parachute system for which terminal velocity is constant. Height difference is in effect plotted in multiples of (v_T^2/g) and time in multiples of $(-v_T/g)$	27
Fig. 6	Sea level terminal velocity of a parachute as a function of parachute system mass and the product of parachute area and drag coefficient. Numbers on the abscissa and ordinate may be multiplied concurrently by any factor 10^n to cover all non-zero values	34

Fig. 7 Nominal diameter of a parachute as a function of area and drag coefficient. Numbers on the ordinate may be multiplied by 10^n if numbers on the abscissa are concurrently multiplied by 10^{2n} to cover all non-zero values 36

Fig. 8 Terminal velocity and time of descent as functions of sea level terminal velocity and altitude in the U.S. Standard Atmosphere, 1962 39

PARACHUTES

A. INTRODUCTION

Parachutes are used on most scientific balloon flights to lower the scientific payload upon termination of the ballooning phase of the flight. A parachute is also used as a safety device on virtually every balloon flight even though the balloon system is to be brought down intact by valving gas from it. This section discusses a highly simplified theory of parachute behavior during descent and explains procedures for selecting a parachute. For a more complete discussion of parachute theory and practice the reader is referred to the U.S. Air Force Technical Report cited as reference (1).

B. DESCRIPTION OF A PARACHUTE SYSTEM

A parachute consists of a woven textile or plastic canopy which is attached to the load by means of suspension lines, frequently called shroud lines. The canopy may have various forms, but is usually axially symmetric about the vertical axis, and may be made with or without holes in it. For some special purposes the canopy is made of ribbons.

Figure 1 schematically illustrates a descending parachute with attached load. Most features of parachutes used in scientific ballooning are shown, though variations may be found. A parachute with its payload and ancillary equipment will be termed a parachute system.

The suspension lines join the canopy at its outer periphery, or skirt. They are normally fastened to the skirt at the seams between gores, and they may or may not continue upward over the canopy to the vent on the top. Not all parachutes have vents, but, although the theory of parachute behavior is far from complete, it is generally believed that parachutes having an axially symmetric canopy benefit from the vent.

The porosity of the canopy material affects the performance of a parachute in several important ways. A highly porous canopy fills more slowly, is more stable, and has a lower drag coefficient than a less porous canopy. The effective porosity of a cloth is defined as the ratio of the average speed of air through the porous sheet to the free stream speed. A canopy can be made more porous than the cloth from which it is made by leaving open areas in it. Geometric porosity is defined as the ratio of the open area of a canopy's drag-producing surface to the total area of the drag-producing surface.

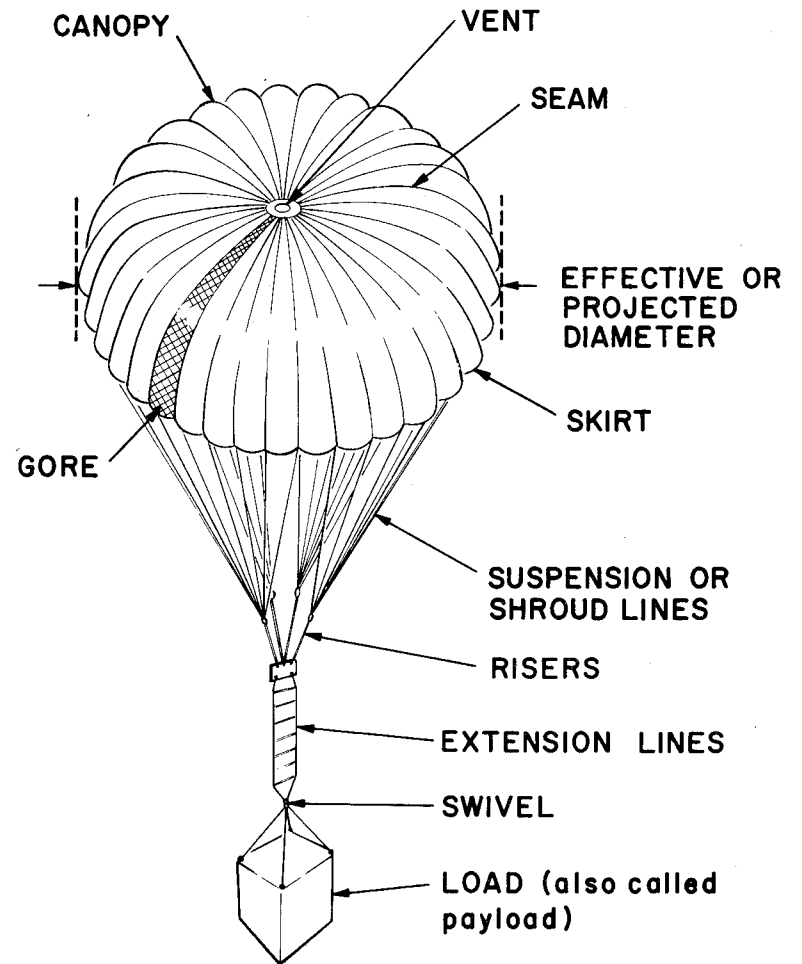


Fig. 1. Parachute nomenclature.

The payload may be fastened directly to the lower end of the risers, but if there is reason to suspend it lower, extension lines may be used. A prismatic, multipoint suspension system (see Fig. 1, Section VII) consisting of two or more cables is commonly used. If it is desirable that the payload be free to turn independently of the parachute, a swivel may be placed in the suspension system anywhere below the risers.

Parachutes are usually described by their nominal diameter, the diameter of a circle whose area is equal to the area of the drag-producing surface of the canopy. Thus the nominal diameter of a flat circular canopy is the diameter of the material in its flat form, whereas the effective diameter is the projected diameter of the inflated parachute as shown in Fig. 1. The latter is a function of the parachute's design and the load it is carrying.

Packed parachutes are used only occasionally in scientific ballooning. Instead, the parachute is fully deployed (extended) at all times, and inflation can start immediately upon separation from the balloon. The parachute frequently serves as a link in the suspension system between the

balloon and the payload. Or, it may be fully deployed throughout the flight but not carry the suspended load prior to flight termination. In the latter case, the parachute is carried parallel to the suspension system or up along the balloon, and is fastened at the top by a break-away device, frequently a light cord.

C. PARACHUTE DESCENT

Existing theory cannot describe the complete behavior of a parachute system in flight, but theory does give some insight into the behavior and provides the foundation for methods of selecting parachutes for given applications.

The equation of motion of a body through a still, fluid subject to the forces of gravity and fluid drag may be written

$$\frac{d(m_v v)}{dt} = -\frac{1}{2}C_D \rho A |v| v - mg \quad (1)$$

where m_v is the virtual mass of the moving body, v is its vertical velocity, C_D is a dimensionless drag coefficient, ρ is the density of the fluid, A is the cross-sectional area of the body normal to its direction of motion, m is the mass of the body, and g is the acceleration due to gravity.

Virtual mass is discussed in Section II.F. The virtual mass of a parachute system, when the canopy is filled, is approximately the mass of the system plus an added mass which is equal to 0.7 times the mass of a spherical volume of air having the density of the ambient air and a radius equal to the effective radius of a parachute canopy. The mass, m , of a descending parachute system is equal to the mass of the payload, the parachute, the suspension system, and all other attached objects. At the high altitudes (low densities) at which parachutes dropped from balloons are normally inflated, the added mass is small compared to the mass of the parachute system; therefore, the approximation $m = m_v$ will be used henceforth.

The coordinates and units discussed in Section II.C. will be used here. Thus, during descent, the vertical velocity causes a positive, or upward, acceleration, and the weight of the system (mg) causes it to accelerate negatively, or downward. Since the direction of the vector velocity is determined by its algebraic sign, vector notation is not used.

For a parachute, C_D is a function primarily of the shape and porosity of the canopy. It is weakly dependent on Reynolds number. If the fluid is

compressible and the motion causes appreciable compression, C_D is a function of Mach number also. However, unless a parachute system's descent velocity exceeds half the speed of sound, compressibility may be ignored. In practice, the drag coefficient is normally considered constant for a given parachute system throughout descent.

Air density is a function of altitude in the atmosphere. This functional relationship is discussed in detail in Section XI. . It is necessary to consider the variation of ρ with time in a descending parachute system, but some phases of the descent are of such short duration that during those phases ρ can be considered constant.

The cross-sectional area of the parachute system during descent is essentially the effective cross-sectional area of the parachute canopy since, by comparison, the payload contributes a negligible area. The canopy's area is dependent on the design and size of the parachute and on the load it bears. Prior to the start of inflation, A is negligible; after the canopy is inflated and a steady state descent is reached, A can be calculated from known conditions. While inflation is occurring, A may momentarily have a value from nearly zero to the area of the flat canopy.

The vertical velocity of a parachute system only is considered here since a still or motionless fluid has been specified. Equation (1) is valid in a moving fluid if v is defined as the relative vector velocity of the body through the fluid, but the magnitude of vertical motion of the atmosphere is small enough compared to the magnitude of the descent velocity of a parachute system that vertical atmospheric motions are neglected. If parachute descents were made in convective cells such as thunderstorms, the theory developed here would differ markedly from practice. An equation similar to Eq. (1) may also be used to calculate the horizontal motion of a parachute system in a moving atmosphere, but it is usually assumed that the parachute system moves horizontally at the speed of the wind system in which it is embedded. Until wind velocity as a function of time and position is known much more accurately than it is now, any refinement in currently used methods of calculating parachute drift does not appear to be warranted unless it also offers a cost advantage.

For convenience of discussion, a parachute descent may be divided into four phases: 1) the initiation of descent and deployment of the parachute,

2) inflation of the canopy and acceleration to terminal velocity, 3) steady state descent at terminal velocity, and 4) landing.

A parachute descent is initiated when the parachute system is separated from the balloon. A parachute is deployed when it is fully extended just before or even during inflation. Packed parachutes usually deploy before starting to inflate. Parachutes which are serving as a link in the suspension system (see Fig. 3, Section II) usually contract like a stretched spring upon separation from the balloon and then deploy again as inflation is starting.

During inflation, air rams into the open lower side of the canopy and fills it under slightly greater pressure than ambient air pressure. The adjustment of the canopy to the incoming air is rapid, as disclosed by cameras on the payload, but the canopy does undergo several oscillations about its equilibrium shape before it assumes that shape. Drag force develops rapidly as the canopy inflates. Parachutes are often referred to as decelerators, implying that they decrease the speed of the parachute system. In scientific ballooning use, a system frequently continues to

gain speed after the parachute is inflated. This will be discussed in greater detail later.

Terminal velocity (also called equilibrium velocity) is the velocity which a parachute system would have if it were descending without acceleration, i.e. if $dv/dt = 0$ or $v = \text{const.}$ Under conditions of terminal velocity and constant virtual mass, Eq. (1) becomes

$$\frac{1}{2}C_D\rho A|v_T|v_T = -mg \quad (2)$$

or

$$v_T = -\sqrt{\frac{2mg}{C_D\rho A}} = \text{const.} \quad (3)$$

Now for a parachute system in phase 3 descending in the atmosphere, m , C_D , and A may all be expected to remain constant, and g varies quite slowly. Air density, however, increases from near $4 \times 10^{-3} \text{ kg/m}^3$ at 40km to near 1.2 kg/m^3 at sea level. Therefore, v_T at 40km cannot be the same as v_T at sea level. If not, a parachute system must accelerate as it descends, and thus the condition for terminal velocity is not fulfilled. Although terminal velocity may never be achieved by a descending parachute system, the concept is still useful if the limitations are kept in mind. For example,

the descent velocity of a parachute system may be quite adequately computed by Eq. (3) for a thin stratum in the atmosphere using for ρ the mean density of the stratum. Also, by using many thin strata, time of descent from any given level to any lower level may be satisfactorily calculated. Finally, the concept of terminal velocity simplifies theoretical examination of parachute descent.

As a parachute system nears the surface, motions other than the vertical motion may become important. The most critical of these are drift and oscillation. An ideal landing is one in which the parachute system descends at a known rate in a perfectly vertical position without horizontal motion onto a readily accessible, unoccupied, firm surface. Manned parachute systems have been developed to the point where this sort of landing can generally be made. The man must, of course, plan ahead, making his descent only at times and in places where the parachute system controls are used within their limitations. To a lesser extent a parachute system can be controlled remotely. Although some experimental remote-control descents have been made, such systems are neither common nor well developed. Anyone planning a parachute drop from a balloon must anticipate that the landing

site cannot be selected precisely, that the system will be drifting horizontally at the time of impact, and that an oscillation of the system probably will cause the payload to be tilted at touchdown.

Proper planning and execution can make parachute descents safe and effective despite difficulties. Carefully designed buffer systems, such as a framework which yields progressively or honeycomb crush pads can be used to absorb the kinetic energy that the system has at the moment of impact. Forecasts by a competent meteorologist can prevent flights from being undertaken when low level winds at the landing site are likely to be excessive, and can provide descent drift vectors in the flight termination area. A drift vector is based on the winds anticipated at all levels through which the parachute system must descend, and it lets the flight controller on the scene estimate the landing site from the known position of the balloon system at the time of flight termination. Stable parachutes, i.e., parachutes which do not oscillate during descent, may also be used to increase the probability that the payload will land upright so that the landing buffer system will have an opportunity to function properly. Unfortunately, choosing a stable parachute may lead to other compromises, such as slow

opening or less certain opening, which may be unacceptable. Available data are inadequate to answer this question definitively.

1. A Simplified Descent Model

Equation (1) and the concept of terminal velocity provide a starting point for a simplified theoretical model of a parachute system descending in the atmosphere which simulates many of the features of a real descent. For a given parachute system at a level in the atmosphere where ρ and g are known, a value of v_T can be calculated using Eq. (3). Unless the parachute system has reached the steady state phase of its descent, the terminal velocity will not constitute a good approximation to the actual velocity. It may, however, be viewed as a value toward which the actual velocity tends, and it is a convenient single variable which may be substituted for a combination of others.

Substituting from Eq. (2) into Eq. (1) and rearranging gives

$$\frac{dv}{dt} = \frac{g}{v_T^2} (v^2 - v_T^2) \quad (4)$$

if it is assumed that $m_v = m = \text{const.}$ Equation (4) may also be written

$$\frac{dv}{v^2 - v_T^2} = \frac{g}{v_T^2} dt \quad (5)$$

Now although both g and v_T are functions of time during descent, they both change slowly. Let it be assumed that over a short time interval they may be treated as constants.

In phase 1 of the descent, the canopy is not inflated. Consequently, the cross-sectional area of the system is quite small. Air density will also be small, and although the drag coefficient may be relatively large, the magnitude of v_T will be large during phase 1. Assume further that the change from phase 1 to phase 2 is instantaneous--that is, the canopy snaps instantly from its deployed but uninflated state to a state of full inflation. This is not entirely in keeping with the actual behavior of a parachute, but, as will be shown later, it leads to conservative results from the design and planning point of view.

Throughout phases 2 and 3 the parachute remains essentially unchanged; therefore, A may be considered constant. The drag coefficient is a function of Reynolds number, Re , and therefore of the actual speed and dimensions of the parachute system, the air density, and air viscosity. For Reynolds numbers associated with a parachute system in phases 2 and 3, however, the dependence of C_D on Re is weak and the assumption of constant C_D is realistic.

Density is then essentially the only variable in v_T ; therefore, any time interval in which ρ does not change significantly will be short enough to justify the assumption that v_T is constant.

Integrating Eq. (5) once yields

$$-\frac{1}{v_T} \tanh^{-1} \frac{v}{v_T} = \frac{gt}{v_T^2} + C \quad \text{for } \frac{v}{v_T} < 1 \quad (6)$$

$$\text{or } -\frac{1}{v_T} \coth^{-1} \frac{v}{v_T} = \frac{gt}{v_T^2} + C \quad \text{for } \frac{v}{v_T} > 1 \quad (7)$$

$$\text{or } v = \text{const} = v_T \quad \text{for } \frac{v}{v_T} = 1 \quad (8)$$

a. Phase 1. Let $t = t_0 = 0$ be the time at which the parachute is separated from the balloon. At that time $v = v_B$ (velocity of the balloon); consequently, the constant of integration, C , in Eq. (6) is $(-1/v_T) \tanh^{-1}(v_B/v_T)$. Because v_B is frequently zero and is always small compared to v_T , the integration constant may be ignored in most descents. It will be considered negligible here in further discussions of phase 1. In phase 1, $(v/v_T) < 1$; therefore Eqs. (7) and (8) are not applicable.

Equation (6) may now be written

$$v = v_T \tanh \left(-\frac{gt}{v_T} \right) \quad (9)$$

Note that in the coordinate system in use here, $v_T < 0$. Thus the argument of the hyperbolic tangent is positive and grows linearly with time. As time increases, $\tanh(-gt/v_T)$ also increases, approaching but never reaching one. Similarly, v will approach but never reach v_T . This tendency of v to approach v_T as a limiting value is characteristic of the descent model used here. For practical purposes, $v = v_T$ and Eq. (6) degenerates into Eq. (8) when $(-gt/v_T)$ grows larger than three.

Substituting dH/dt for v in Eq. (9) and integrating yields

$$H = -\frac{v_T^2}{g} \ln \cosh\left(-\frac{gt}{v_T}\right) + C \quad (10)$$

where H is height and C is the constant of integration. When $t = t_0$,

$H = H_0$; therefore, $C = H_0$ and

$$H = H_0 - \frac{v_T^2}{g} \ln \cosh\left(-\frac{gt}{v_T}\right) \quad (11)$$

Differentiating Eq. (9) yields acceleration in terms of t as follows:

$$\frac{dv}{dt} = g \left[\tanh^2\left(-\frac{gt}{v_T}\right) - 1 \right] \quad (12)$$

Examination of Eq. (12) shows the acceleration to be made up of two parts, one of which is downward (negative) and one upward, and the upward accelera-

tion grows with time. The growth term can never quite reach one, although for practical purposes it will have done so when $(-gt/v_T)$ has reached 3.0. At that time acceleration will have ceased, and the descending system will have reached terminal velocity.

Equations (9), (11), and (12) contain a description of the motion of a parachute system starting from rest and descending without change of shape in a homogeneous atmosphere. If interest is restricted to a short time interval so that the stratum through which the system falls in that interval is thin, the restriction on homogeneity may be relaxed.

b. Phase 2. Equations (7) and (8) as well as Eq. (6) must be considered in a discussion of phase 2 because the magnitude of the downward velocity may be less than, equal to, or greater than the magnitude of v_T . The initial velocity in phase 2 in the descent model being used is equal to the final velocity in phase 1. This permits evaluation of the constants of integration in Eqs. (6) and (7). Thus for $t = t_1$ (the time of inflation of the canopy and the initiation of phase 2) $v = v_1$, and from Eqs. (6) and (7) respectively

$$C = -\frac{1}{v_T} \tanh^{-1} \frac{v_1}{v_T} - \frac{gt_1}{v_T^2}$$

$$C = -\frac{1}{v_T} \coth^{-1} \frac{v_1}{v_T} - \frac{gt_1}{v_T^2}$$

Substituting these in Eqs. (6) and (7) and solving for v yields

$$v = v_T \tanh \left[\tanh^{-1} \frac{v_1}{v_T} - \frac{g(t-t_1)}{v_T} \right] \quad \text{for } \frac{v_1}{v_T} < 1 \quad (13)$$

$$\text{and } v = v_T \coth \left[\coth^{-1} \frac{v_1}{v_T} - \frac{g(t-t_1)}{v_T} \right] \quad \text{for } \frac{v_1}{v_T} > 1 \quad (14)$$

Integrating Eqs. (13) and (14) gives

$$H = H_1 + \frac{v_T^2}{g} \left\{ \ln \cosh \tanh^{-1} \frac{v_1}{v_T} - \ln \cosh \left[\tanh^{-1} \frac{v_1}{v_T} - \frac{g(t-t_1)}{v_T} \right] \right\} \quad \text{for } \frac{v_1}{v_T} < 1 \quad (15)$$

$$H = H_1 + \frac{v_T^2}{g} \left\{ \ln \sinh \coth^{-1} \frac{v_1}{v_T} - \ln \sinh \left[\coth^{-1} \frac{v_1}{v_T} - \frac{g(t-t_1)}{v_T} \right] \right\} \quad \text{for } \frac{v_1}{v_T} > 1 \quad (16)$$

Similarly Eq. (8) may be integrated to give

$$H = H_1 - v_T(t-t_1) \quad \text{for } \frac{v_1}{v_T} = 1 \quad (17)$$

Differentiating Eqs. (13) and (14) provides the following expressions

for acceleration as functions of t :

$$\frac{dv}{dt} = g \left\{ \tanh^2 \left[\tanh^{-1} \frac{v_1}{v_T} - \frac{g(t-t_1)}{v_T} \right] - 1 \right\} \quad \text{for } \frac{v_1}{v_T} < 1 \quad (18)$$

$$\frac{dv}{dt} = g \left\{ \coth^2 \left[\coth^{-1} \frac{v_1}{v_T} - \frac{g(t-t_1)}{v_T} \right] - 1 \right\} \quad \text{for } \frac{v_1}{v_T} > 1 \quad (19)$$

Also, from the definition of v_T

$$\frac{dv}{dt} = 0 \quad \text{for } \frac{v_1}{v_T} = 1 \quad (20)$$

Equations (18) through (20) are plotted in dimensionless form in Fig. 2. Two distinctive features of the descent model are immediately obvious. First, the acceleration at time $t = t_1$ is very sensitive to the value of the ratio (v_1/v_T) . Thus for low acceleration the parachute should inflate when this ratio is small. In fact, if inflation occurs before the velocity of the system has reached the inflated terminal velocity, downward acceleration will continue until $v = v_T$. If inflation should occur just as

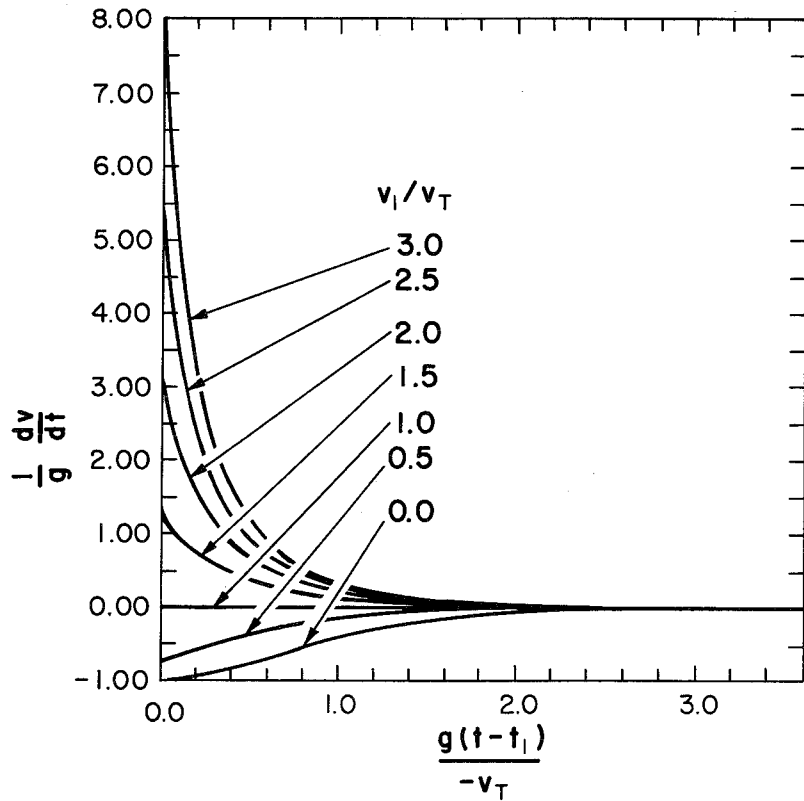


Fig. 2. Acceleration versus time for a parachute system for which terminal velocity is constant. Acceleration is in effect plotted as multiples of the acceleration of gravity and time as multiples of $(-v_T/g)$.

inflated terminal velocity is reached, acceleration will cease. If, on the other hand, inflation does not occur until the system velocity has exceeded the terminal velocity of the inflated system, an upward acceleration will immediately start to slow the descent. The magnitude of that acceleration is most easily determined from Eq. (4) written as follows:

$$\left(\frac{dv}{dt}\right)_1 = g \left[\left(\frac{v_1}{v_T}\right)^2 - 1 \right]$$

The subscript 1 is used to denote that the events are occurring at the instant of inflation, i.e., at $t = t_1$. If this equation is multiplied through by the mass of the system, it may be written

$$m \left(\frac{dv}{dt}\right)_1 = mg \left(\frac{v_1}{v_T}\right)^2 - mg$$

Thus the forces acting on the system are the upward drag and the downward weight. Since the drag is exerted almost wholly on the canopy of the parachute, the suspension system must be strong enough to withstand at least the force $mg(v_1/v_T)^2$. This force is called opening shock. In this model it is proportional to the square of the velocity at the time of inflation. Equation (9) shows that the system velocity increases in phase 1 as a func-

tion of time up to its uninflated terminal velocity, and since the uninflated terminal velocity can be several times as great as the inflated terminal velocity, early inflation will assure low opening shocks, while delayed inflation will cause large opening shocks. This is contrary to the experience of parachutists jumping from high-speed aircraft. Their initial speed through the air is generally greater than the magnitude of their terminal velocity without a parachute. Therefore, their speed starts to decrease immediately, and they realize a lower opening shock by waiting until they have reached the terminal velocity of their own body to "pop the chute."

The second distinctive feature of Fig. 2 is that regardless of the magnitude of the acceleration at the time of inflation, it has, for practical purposes, been reduced to zero after an elapsed time $(t-t_1) = -3v_T/g$.

Figure 3 shows time vs acceleration traces for two parachute systems descending according to this model. Since time is shown in the dimensionless form which involves v_T , the time scale changes at $t = t_1$. The symbols $v_{T,1}$ and $v_{T,2}$ are used for the terminal velocities in phases 1 and 2, respectively.

The curve for a system which does not open until $v = v_1 = 2v_{T,2}$ is the curve labeled 1,2,3,4,5,6. At point 1 the parachute is separated from

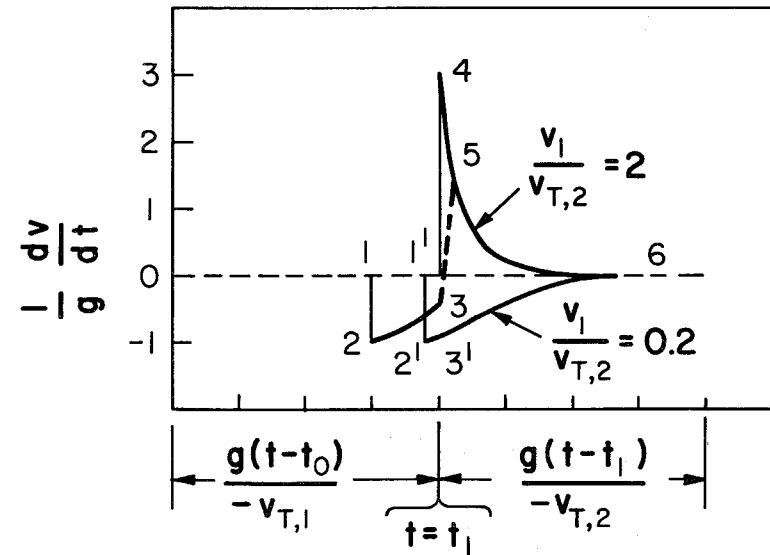


Fig. 3. Acceleration traces of quick-opening and delayed-opening parachutes.

the balloon. A downward acceleration of 1 g occurs immediately, as shown by point 2. The magnitude of that acceleration is then decreased slowly by the drag of the system with a deployed but uninflated parachute until at point 3 opening occurs instantaneously, and the acceleration changes to an upward acceleration of 3 g (point 4). This decays rapidly, reaching zero at point 6. More realistically, the parachute does not open instantaneously, and the change from a downward to an upward acceleration occurs over a small time increment along a path something like that shown from point 3 to point 5. This decreases the maximum acceleration the system will experience; therefore, the model used here is conservative from the design point of view. A more realistic model is discussed by Heinrich and Noreen (2), who have studied the forces on a parachute during the period of opening.

The curve labeled 1', 2', 3', 6 is representative of a parachute system whose parachute opens well before the system velocity has reached $v_{T,2}$. Its general characteristics have already been explained.

Opening accelerations as great as 16 g have been reported in parachute drops from balloons by Niccum and Aube (3), but 70% of the accelerations

they reported were under 4 g. The accelerometers used were mounted in such a way that they may have sensed large accelerations which were internal to the suspension system. Unfortunately, neither the time of opening nor the downward speed at the time of opening could be determined reliably from the data; therefore, attempts to check these data against other observations and against theory led to inconclusive results. These data point to the possibility of high opening accelerations, but the known areas of uncertainty in the measurements suggest that the values are too high so that they also are generally conservative for design purposes.

The graphs of Eqs. (8), (13), and (14) are shown in Fig. 4, also in dimensionless form. The curves of $(v_1/v_T) = \text{constant}$ on this graph resemble the curves in Fig. 2. The most significant feature is that regardless of the velocity at the time of inflation, within an elapsed time given by $(t-t_1) = -3v_T/g$, the descent velocity will have become very nearly equal to the terminal velocity.

Equations (15) through (17) are plotted in dimensionless form in Fig. 5. The curves show the rather obvious fact that a parachute system will

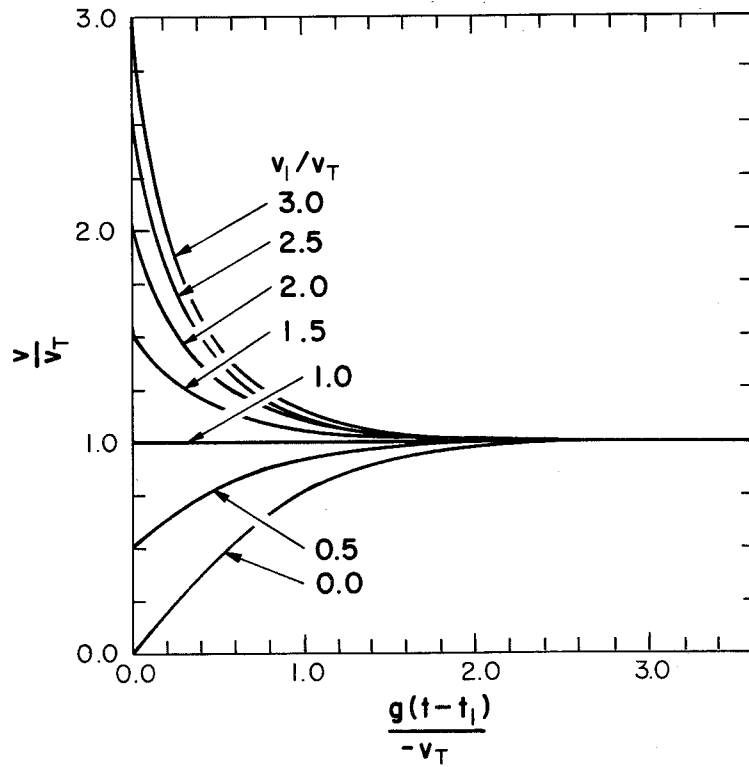


Fig. 4. Descent velocity vs time for a parachute system for which terminal velocity is constant. Velocity is plotted as a multiple of v_T and time as a multiple of $(-v_T/g)$.

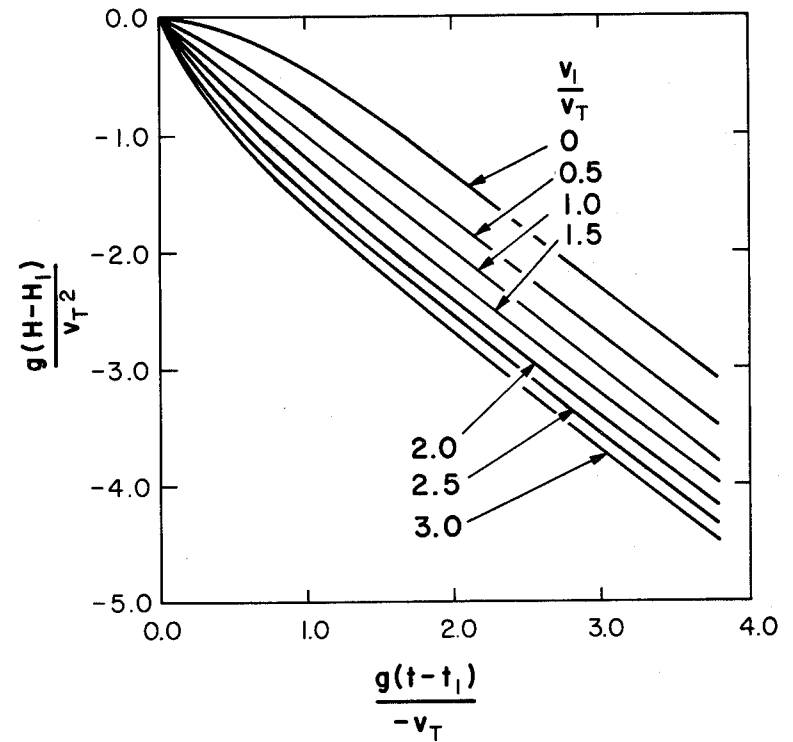


Fig. 5. Loss of altitude vs time for a parachute system for which terminal velocity is constant. Height difference is in effect plotted in multiples of (v_T^2/g) and time in multiples of $(-v_T/g)$.

have descended further in a given time if it had a high downward velocity at the time of inflation than if its velocity were low. After $-g(t-t_1)/v_T$ exceeds 3.0, however, the separation remains virtually constant.

The time period given by $(t_2-t_1) = -3v_T/g$ is the period required for a descending parachute system to accelerate from its opening velocity v_1 to its terminal velocity v_T . Time t_2 is then the time at which phase 2 ends and phase 3 begins. The change of v_T during phase 2, because of the change in air density, is large enough in descents from altitudes in excess of 30km that holding it constant may produce errors of up to 10% in the calculated distance traveled during phase 2. Such errors are rarely important, but they can be overcome by slicing the atmosphere into thin strata and using the mean value of the terminal velocity within each stratum to calculate descent data.

c. Phase 3. As soon as an inflated parachute system has reached terminal velocity, i.e. when $(t-t_1) = -3v_T/g$, it will enter phase 3. Equations (13) through (20) and Eq. (8) are valid for this phase of descent, but the smaller set consisting of Eqs. (8), (17), and (20) provides an

adequate description of the descent in phase 3 of this model. Because v_T is not constant throughout the deep atmospheric stratum through which a parachute system descends in phase 3, the equations must be applied through a number of thin strata with v_T calculated from Eq. (3) for each stratum.

d. Phase 4. The few seconds immediately preceding and following the actual landing of a parachute system are the most critical in the descent. Descent velocity is given adequately by Eq. (8) and hence by Eq. (3) if the system has passed through phase 2 before reaching the surface.

Any acceleration of the payload immediately prior to landing which is large enough to be important will be due to an oscillation of the system about the vertical. Such accelerations are internal to the parachute system; their principal consequence is to decrease the probability that the payload will land on its base, but motion of the payload because of them may cause the payload to have a velocity significantly different from the motion of the system as a whole.

Horizontal motion is quite important, and an appropriate balance between the horizontal and vertical velocity components is a consideration in selecting a parachute for a given job. From Eq. (3) it appears that large parachutes can be selected to produce a low vertical velocity and

assure a relatively soft landing. If winds exist near the surface, however, lower vertical velocities increase the probability that the system will drag on obstacles, such as power lines, trees, etc. during the final seconds of descent; this in turn increases the probability of damage to people and property, as well as to the payload. A large parachute also increases the likelihood that the payload will be dragged by the wind after landing. The drag force is given approximately by Eq. (2) written as

$$F = \frac{1}{2} C_D \rho A v_w^2, \text{ where } v_w \text{ is the speed of the surface wind.}$$

Separation of the parachute and payload upon landing would obviate the danger of dragging, but unless the separation mechanism were highly reliable, it could cause greater danger by causing premature separation.

D. CONSIDERATIONS IN SELECTING A PARACHUTE

To be satisfactory for scientific ballooning a parachute should be highly reliable, and it should prevent accelerations, including landing accelerations that are destructive to the payload. Choosing a parachute involves making compromises between conflicting demands, and because of incomplete knowledge of parachute behavior at high altitude, the selection of one type of parachute over another is often a matter of personal pref-

erence. This discussion is therefore limited to a brief summary of the questions usually considered in selecting a parachute and to aids which are general enough to be used with several types of parachutes.

The most important factors in selecting a parachute are those which are directly concerned with safety. At the very least, a parachute must open reliably and be strong enough to withstand any opening shocks and carry the weight of the payload in all conceivable situations; it must also be capable of slowing the entire system to an acceptable vertical velocity at landing. Other features may also be desirable, e.g., that the parachute not swing or spin during descent; but unless these can be provided without sacrificing the features which are essential to safety, they should not be considered.

Two types of parachutes have been used enough for scientific ballooning flights to be considered proven. One has a flat circular canopy with a vent in the center; the other has a canopy in the form of a cross with no vent. The flat circular canopy is known to open reliably and rapidly even at the high altitudes where it is used in scientific ballooning. It is commercially available in sizes up to 30 meters in diameter, and two or more

can be used together. Its terminal velocity can be predicted accurately when it is used within proper load limits. Its chief drawback is its tendency to oscillate more than is desirable during descent.

Parachutes with cross-shaped canopies have been used in scientific ballooning almost exclusively by the firm which manufactures them. Their use has been reported informally by a representative of the Office of Naval Research (4) for whom they have been flown. They have performed well in all respects and are less subject to oscillation than flat canopy parachutes. No load more massive than 365kg (800 lbs) has been flown on one, and no flight has been made which used two or more of them together. At present, anyone desiring parachute descent for a heavy load will find that the history of satisfactory descents with comparable loads is much more extensive for flat canopy parachutes than for any other type.

1. Parachute Size

To determine the parachute size required for a particular job, the mass of the payload and the permissible vertical velocity at impact must be known. The mass of the payload can usually be determined by simply weighing it, but the permissible vertical velocity at impact must normally

be based on a value judgment. If a payload is particularly sensitive to shock, a large parachute can be used. An oversized parachute is not likely to give greater protection than a smaller one, however, unless it is used when surface winds are lower. Therefore, using a larger parachute than is considered optimum for general safety will increase the time one must wait for satisfactory weather conditions. Added to the cost of waiting is the cost of purchasing and maintaining the larger parachute. Since most of the reasons underlying the determination of an acceptable vertical landing speed can only be stated qualitatively, no quantitative guide to choosing it is offered. Vertical speeds of 7 to 8 m/sec (~25 ft/sec) have been found to give results which are acceptable for most payloads.

A solution of Eq. (3) in SI units, using sea level values of g and ρ from the U.S. Standard Atmosphere, 1962, is shown in graphical form in Fig. 6. This graph is reproduced in a more usable size in Section XII, together with a similar graph in English units. On the first pass through this graph, the user does not ordinarily know parachute mass and must approximate it. The mass of the payload multiplied by 1.05 is an adequate first approximation of the total system mass. With values for the system mass and the

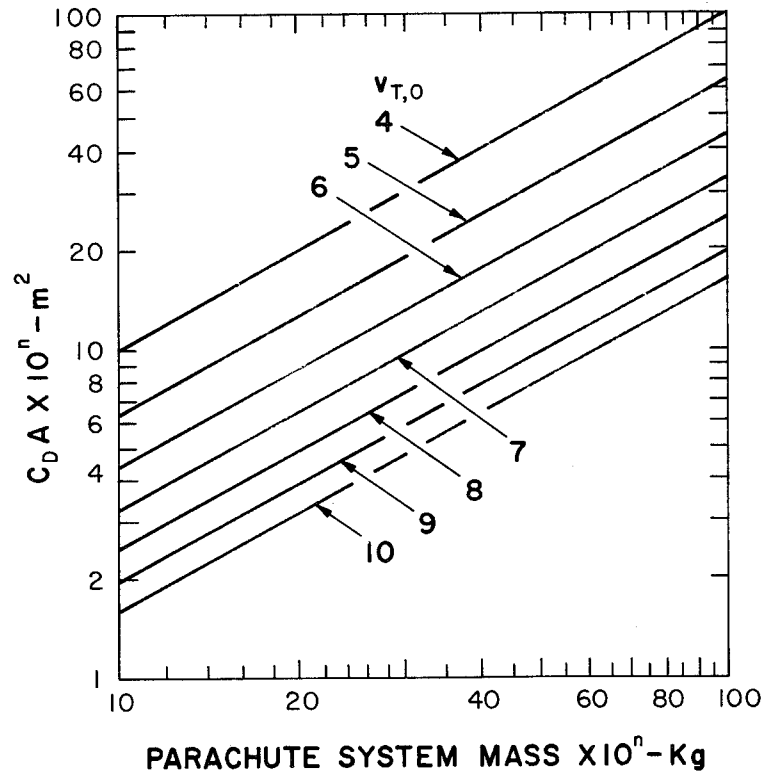


Fig. 6. Sea level terminal velocity of a parachute as a function of parachute system mass and the product of parachute area and drag coefficient. Numbers on the abscissa and ordinate may be multiplied concurrently by any factor 10^n to cover all non-zero values.

sea level terminal velocity, one may use the graph to determine a value of the product $C_D A$. Note that the numbers on the abscissa may be multiplied by a factor 10^n , where n may take any value, provided only that the numbers on the ordinate are also multiplied by the same factor. Thus, the graph can be used for any non-zero mass.

Having obtained a first approximation for $C_D A$ from Fig. 6, one may enter that value in Fig. 7 to obtain the diameter of a parachute if the value of C_D is known. Figure 7 is a graphical representation of the equation $C_D A = C_D' \pi (D/2)^2$; therefore, if the C_D for an inflated circular parachute is used, the value of D obtained from Fig. 7 will be the effective or projected diameter of the parachute (see Fig. 1). This value of D is not often of direct interest, however, because parachutes are described by the nominal diameter of the canopy. (See Section X.B.) To obtain the nominal diameter from Fig. 7, a pseudo drag coefficient must be used. Although the pseudo drag coefficient is usually determined experimentally, its significance can be readily explained.

Let C_D' and A' be the pseudo drag coefficient and the nominal area, respectively, of a parachute having an effective drag coefficient C_D and

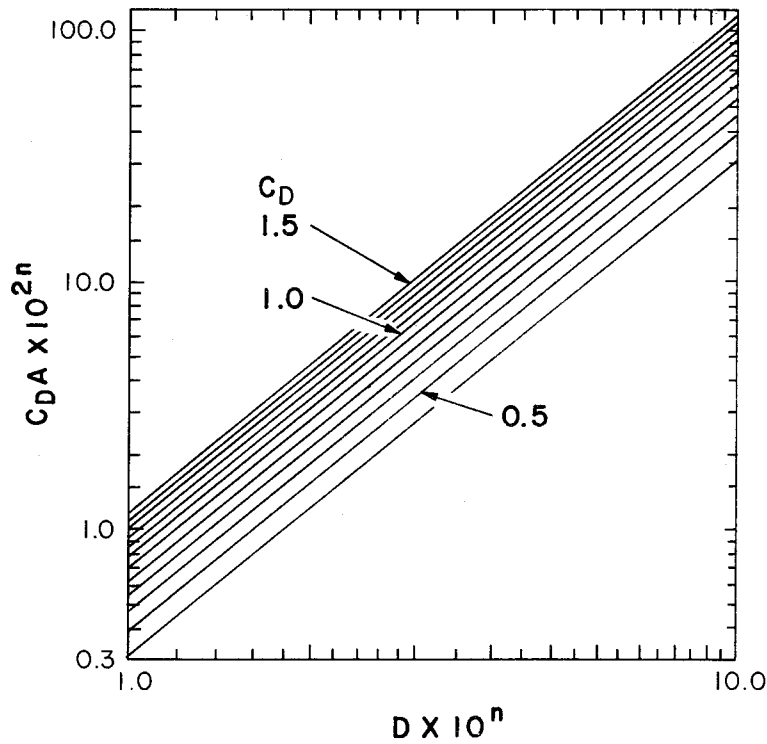


Fig. 7. Nominal diameter of a parachute as a function of area and drag coefficient. Numbers on the ordinate may be multiplied by 10^n if numbers on the abscissa are concurrently multiplied by 10^{2n} to cover all non-zero values.

effective area A so that $C_D' A' = C_D A$. Also let the nominal area be defined as the area of a circle of nominal diameter D' . Then if C_D' is defined so that $C_D A = C_D' \pi (D'/2)^2$ and its value is known, D' can be determined from Fig. 7. An excellent example of the use of the concept of pseudo drag coefficient is provided by the cross-shaped canopy. Rarely is its effective area or its drag coefficient known, but for one such parachute design, the product of the two is known to be given with acceptable accuracy by multiplying the area of a circle whose diameter is equal to the length of one of the cross members of the canopy by 0.55. Thus C_D' is 0.55 and D' is the length of the cross member for this particular parachute design.

Although parachutes can be manufactured in any size, it is more practical to manufacture them in certain discrete sizes, and it is rare that the size indicated by the selection process described thus far will agree precisely with one of the sizes commonly manufactured. Usually a scientific ballooning group will have parachutes of various sizes on hand, and a size can be selected which has a nominal diameter close to the first estimate of the required value. The known mass and the $C_D' A'$ of that parachute can then be used in conjunction with Fig. 6 to obtain the sea level terminal

velocity of the parachute system. If that velocity is too low or too high to be satisfactory, the data of the next smaller or the next larger parachute may be checked.

It is possible that the altitude of the anticipated landing site will be so far above sea level that the terminal velocity there will be significantly different from that at sea level. The curve in Fig. 8 labeled v_T provides a simple way to approximate the terminal velocity at any level up to 52km if the sea level terminal velocity is known. If $v_{T,0}$ is the sea level terminal velocity and v_T is the terminal velocity at any other level, then from Eq. (3)

$$v_T/v_{T,0} = \sqrt{\rho_0/\rho} \quad (21)$$

assuming that m , g , C_D , and A do not change with height. From Eq. (21) $v_T/v_{T,0}$ may readily be plotted as a function of ρ , and since ρ is a function of height in the atmosphere (see Section XI), $v_T/v_{T,0}$ may also be plotted as a function of height. That has been done in Fig. 8, using the relationship between ρ and H given in the U.S. Standard Atmosphere, 1962. Thus it is only approximate for the real atmosphere.

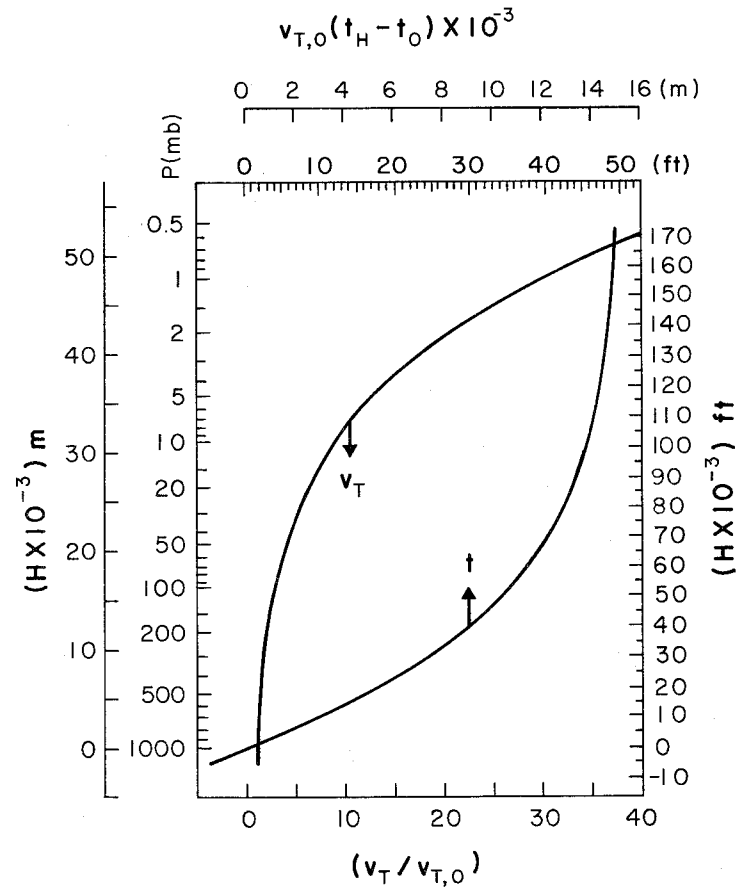


Fig. 8. Terminal velocity and time of descent as functions of sea level terminal velocity and altitude in the U.S. Standard Atmosphere, 1962.

It is apparent that the change of $v_T/v_{T,0}$ in the lowest 3km is not great enough to be resolved satisfactorily in Fig. 8. Yet it is that stratum in which almost all landings will occur. In it the linear relations $v_T/v_{T,0} = 1 + 5 \times 10^{-5}H$, where H is in meters above sea level, and $v_T/v_{T,0} = 1 + 1.52 \times 10^{-5}H$, where H is in feet, yield good approximations. Thus at 1 km (~3000 ft), v_T is 5% larger than at sea level, a difference which is nearly equal to the difference (error) which must be anticipated between the calculated and observed sea level terminal velocities. Nonetheless, the difference will occasionally justify using a larger parachute for a landing at a higher altitude than might be used at sea level.

2. Multiple Parachutes

It is sometimes convenient or necessary to use two or more parachutes to lower a load. Many low level, multiple parachute drops have been made; a few have been made successfully from balloon float altitudes. Thus it is known that drops using a cluster of parachutes are feasible, but the number of multiple parachutes flights on balloons to date has been too limited to warrant the degree of confidence that has been established for parachutes used singly.

The number and size of parachutes required to lower a load when more than one is needed may be determined by the procedure discussed above if 1) all parachutes used together are alike and the same size, 2) the drag coefficient of the cluster can be determined from the drag coefficient of one parachute used alone, and 3) the nominal area of a cluster of N parachutes is equal to the nominal area of a single one times N. Then one may enter Fig. 6 with 1.05 times the mass of the payload and the desired landing velocity (suitably corrected to sea level terminal velocity) to obtain $C_D A$. Dividing $C_D A$ by N and entering Fig. 7 with the quotient and C_D' for the cluster yields D' for one of the parachutes of the cluster. If there are N parachutes of nominal diameter D' available, the solution should be checked using the mass and C_D' data of the actual parachutes. If there are not N parachutes of diameter D' available, another value of N may be tried. When a satisfactory check is achieved using the data of available parachutes, the problem is solved.

The value of C_D' for a cluster of identical flat, circular, solid cloth canopy parachutes may be approximated by the equation $C_D'(\text{cluster}) = C_D'(\text{individual}) \times (0.95 - 0.3N)$ for $2 \leq N \leq 6$. Incidentally, a cluster of

flat canopy parachutes is more stable than a single one. The value of C_D' for a cluster of identical parachutes whose canopies have large geometric porosity (e.g. ribbon, ring slot, or cross-shaped parachutes) is nearly identical to the value of C_D' for one of the individual parachutes.

3. Time of Descent

Recalling that $v_T = (dH/dt)_T$, Eq. (21) may be written

$$\frac{dH}{dt} = v_{T,o} \sqrt{\frac{\rho_o}{\rho}} \quad (22)$$

where one of the T subscripts has been omitted for convenience. This may be integrated as follows:

$$v_{T,o}(t_H - t_o) = \rho_o^{-\frac{1}{2}} \int_0^H \rho^{\frac{1}{2}} dH \quad (23)$$

The integration indicated on the right side of Eq. (23) can be performed if ρ is a known function of H; integration in the Standard Atmosphere yields the curve labeled t in Fig. 8. A value of $v_{T,o}(t_H - t_o)$ may be determined from the curve if the altitude of a parachute system is known. That value divided by the sea level terminal velocity of the system is the time required for the system to descend to sea level. The time of descent between any two levels may also be determined; it is the difference between

the two $v_{T,o}(t_H - t_o)$ values divided by $v_{T,o}$. If the two levels are close together, however, a more accurate result may be obtained by dividing the thickness of the stratum by the mean velocity within the stratum as determined from the v_T curve.

A number of auxiliary scales have been placed on Fig. 8 to make it more versatile. The terminal velocity, v_T , obtained from the figure will be in the units in which $v_{T,o}$ is expressed. Since $v_{T,o}(t_H - t_o)$ is a length, scales are given in both meters and feet; the scale to be used must be compatible with the units in which $v_{T,o}$ is expressed. The resulting time units are easily determined: for example, if $v_{T,o}(t_H - t_o)$ is read in feet and $v_{T,o}$ is expressed in feet per minute, time will be determined in minutes.

REFERENCES

- (1) U.S. Air Force, 1963: Performance of and Design Criteria for Deployable Aerodynamic Decelerators, Technical Report No. ASD-TR-61-579 of the U.S. Air Force Flight Dynamics Laboratory, Research and Technology Div., Air Force Systems Command, Wright-Patterson AFB, Ohio.
- (2) Heinrich, H.G. and R. A. Noreen, 1969: Analysis of Parachute Opening Dynamics with Supporting Wind Tunnel Experiments. In Proc., Aerodynamic Decelerations Systems Conference of Sept. 23-25, 1968, Vol. I-- Technical Report No. 69-11, Defense Document Center, Cameron Station, Alexandria, Va.
- (3) Niccum, R. J. and A. E. Aube, 1968: Heavy Load Recovery from High Altitude Balloon Borne Platforms. In Proc., Aerodynamic Deceleration Systems Conference of Sept. 23-25, 1968, Vol II--Technical Report No. 69-11, Defense Document Center, Cameron Station, Alexandria, Va.
- (4) Cross, William F., CDR, USN, February 22, 1972: Personal communication.

THE ATMOSPHERE

by

Alvin L. Morris and Samuel B. Solot

List of Symbols	ii	a. <u>The quasi-biennial oscillation.</u>	49
List of Figures	v	b. <u>The semiannual oscillation.</u>	53
List of Tables	vii	4. <u>Middle Latitude Vertical Structure in the Free Atmosphere.</u>	56
A. INTRODUCTION	1	5. <u>Boundary Layer</u>	60
B. OPERATIONAL METEOROLOGICAL REQUIREMENTS	3	6. <u>Low-Level Jet</u>	64
1. <u>Inflation</u>	4	E. OTHER METEOROLOGICAL VARIABLES, DATA SOURCES.	69
2. <u>Launch</u>	6	F. FORECASTS	75
3. <u>Ascent</u>	13	G. OPERATIONAL PLANNING.	76
4. <u>Tracking and Float</u>	13	REFERENCES.	79
5. <u>Descent</u>	15		
6. <u>Landing and Recovery</u>	17		
C. THERMAL STRUCTURE OF THE ATMOSPHERE	18		
1. <u>Temperature and Density</u>	18		
a. <u>The hydrostatic relationship</u>	18		
b. <u>The U.S. Standard Atmosphere, 1962</u>	25		
c. <u>Supplementary atmospheres</u>	29		
d. <u>Mean thermal structure</u>	33		
2. <u>Thermal Radiation</u>	33		
D. CIRCULATION	35		
1. <u>Mean Zonal Structure</u>	35		
2. <u>Polar Wind Structure</u>	47		
3. <u>Equatorial Zonal Wind Structure</u>	48		

LIST OF SYMBOLS

<u>Symbol</u>	<u>Description</u>	<u>Dimensions</u>			
a_0, a_2	empirical constants having dimensions of wind shear	T^{-1}	T_b	temperature at the base of a stratum	θ
a_1, a_3	dimensionless empirical constants		T_o	standard sea-level temperature	θ
b	dimensionless empirical constant		\bar{v}	time averaged wind speed at level z	LT^{-1}
b	subscript to denote base of stratum		\bar{v}_1	time averaged wind speed at level z_1	LT^{-1}
D	empirical constant having dimensions of wind shear	T^{-1}	\bar{w}	magnitude of mean vector wind shear	T^{-1}
e	vapor pressure of gaseous water in the atmosphere	$ML^{-1}T^{-2}$	\bar{w}_e	magnitude of extreme wind shear vectors	T^{-1}
g	acceleration due to gravity	LT^{-2}	z	height	L
g_o	standard acceleration due to gravity	LT^{-2}	z_1	height at a level specified as level one (1)	L
H	geopotential height	L	<u>Greek letters</u>		
H_b	geopotential height of the base of a stratum	L	ρ	density	ML^{-3}
L'	vertical gradient of temperature (dT/dH)	θL^{-1}	ρ_b	densith at the base of a stratum	ML^{-3}
m	mass	M	σ_w	standard deviation of the magnitude of the vector wind shear	T^{-1}
m_i	mass of ith gas of a mixture of gases	M			
M	molecular weight	$M(M - mol)^{-1}$			
M_i	molecular weight of ith gas of a mixture of gases	$M(M - mol)^{-1}$			
p	pressure	$ML^{-1}T^{-2}$			
p_b	pressure at the base of a stratum	$ML^{-1}T^{-2}$			
p_o	standard sea-level pressure	$ML^{-1}T^{-2}$			
R	universal gas constant	$ML^2\theta^{-1}T^{-2}(M - mol)^{-1}$			
T	temperature	θ			

List of Figures

Fig. 1	Balloon during inflation. The gas bubble is restrained by a roller through which the balloon may move.	5	Fig. 11	Typical summer anticyclonic vortex in the upper stratosphere. See Fig. 10 for explanation of the isolines . . .	40
Fig. 2	Static launch	7	Fig. 12	Time-Height cross section of the mean monthly zonal winds in the southern U.S. stratosphere	42
Fig. 3	Dynamic launch	8	Fig. 13	Well developed wave in the winter westerlies. Note the variety of wind directions on each pressure surface and the differences which occur between the surfaces, i.e., essentially between 54 km (a) and 41 km (b). See Fig. 10 for explanation of the isolines	44
Fig. 4	Temperature as a function of geopotential height in the <u>U.S. Standard Atmosphere, 1962</u>	28	Fig. 14	Transition from a winter cyclonic circulation to a summer anticyclonic circulation. A small anticyclone has formed in the vicinity of the pole and is spreading equatorward. See Fig. 10 for an explanation of the isolines	46
Fig. 5	Temperature-Height profiles of the 30 ^o , 45 ^o , 60 ^o , and 75 ^o N January and mid-latitude spring/fall Supplementary Atmospheres	30	Fig. 15	Time-Height cross section of mean monthly zonal winds at Canton Island (1953--Aug. 1967) and at Gan/Maledive Islands (Sept. 1967--1970). From Kriester (11). Lines are isolines of wind speed in meters per second	50
Fig. 6	Temperature-Height profiles of the 30 ^o , 45 ^o , 60 ^o , and 75 ^o N July and 15 ^o N annual Supplementary Atmospheres.	31	Fig. 16	Amplitude of the quasi-biennial and semiannual, equatorial oscillations as functions of height. Also, time of occurrence of maximum west winds (phase) of the semiannual oscillation in months	51
Fig. 7	Percentage departure from standard of densities of certain supplemental atmospheres given in reference (2)	32	Fig. 17	Estimated variation of zonal wind with month and altitude at the equator. After Reed (9)	54
Fig. 8	Mean thermal structure of the atmosphere in summer and winter, after Palmén and Newton (5)	34	Fig. 18	Selected zonal wind profiles for the White Sands Missile Range, New Mexico	57
Fig. 9	Mean zonal wind in summer and winter, after Palmén and Newton (5)	36			
Fig. 10	Typical winter cyclonic vortex in the upper stratosphere. Winds flow along the height contours (solid lines). The speed is indicated by the feathers--each flag represents 50 knots, each bar 10 knots, and a half bar 5 knots. The dashed lines are isotherms of temperature in °C	39			

Fig. 19 Dimensionless wind profiles according to the power-law.
 The value of b may be estimated from the scale at the top if dT/dz is known add 0.1 to the value of b estimated from dT/dz if the terrain is rough or wooded 63

Fig. 20 Mean cross section of the wind associated with a low-level jet, from Bonner et al. (20). The solid lines are isotachs of the wind component parallel to the jet axis; dashed lines are isotachs of the normal component 65

Fig. 21 Average vertical wind shear (m/sec km) in a vertical cross section normal to the core of the jet, after Bonner et al. (20) 66

Fig. 22 Mean wind component along the jet axis at the 0.5-km level, after Bonner et al. (20). 67

List of Tables

Table 1 Defining temperature vs height relationships in the lowest 61 km of the U.S. Standard Atmosphere, 1962 . . . 27

THE ATMOSPHERE

A. INTRODUCTION

Balloon flight is possible only because the density of the atmosphere in which a balloon is embedded is equal to or greater than the density of the balloon system. Therefore, atmospheric density is vitally important to the success of ballooning. The engineer who must calculate lift tables is keenly aware of this (see Section IV). The engineer who must calculate heat exchange between the balloon system and the environment (Section III) is also interested in the density of the balloon's immediate environment. These people must consider the composition of the environment also, at least to the point of determining whether changes of composition are significant to them. To a large extent, however, scientific ballooning needs for density and composition data are adequately met by some sort of mean or standard atmosphere.

The U.S. Standard Atmosphere, 1962, (1) is a model atmosphere which has gained widespread acceptance. When the expression "Standard Atmosphere" is used in this section, it should be understood that the U.S. Standard Atmosphere, 1962, is being named. In the Standard Atmosphere temperature

and composition are defined as functions of height. A number of other useful properties can be derived from the defining properties.

To fulfill the need for atmospheric data at high and low latitudes and in the hot and cold seasons for which the Standard Atmosphere is not adequate, supplementary model atmospheres have been defined. The most generally accepted of these are described in U.S. Standard Atmosphere Supplements, 1966

(2). Each represents approximately the mean state of the real atmosphere at some season and latitude. Thus, they provide some information about the temporal and latitudinal variability of the real atmosphere.

Balloon flight personnel and meteorologists who must provide atmospheric information for balloon operations find that wind is the most critical atmospheric variable. There are others, e.g., cloudiness, which may affect operations, but most of them are not of such continuing concern as wind. Unfortunately, the range of variation of the wind is so great and wind data are so sparse at the high altitudes at which modern balloons are flown that reliable mean values are available only in a few locations. Idealized circulation models based on the wind data available must, therefore, be used with full appreciation of their limitations.

The task of forecasting the actual state of the atmosphere a few days or hours in advance of a balloon flight demands understanding of the behavior of the atmosphere and data from which to establish its state at some time before the forecast period. Large balloon systems fly higher than meteorological sounding balloons. Rocket soundings provide data at these levels in a few locations and on a quite limited schedule. Despite the difficulties, experienced forecasters can provide 24-hour wind forecasts which are accurate enough to be useful for flight operations, and they can provide planning data on winds weeks or months in advance.

In this section the most important properties of the atmosphere in its relationship to scientific ballooning are discussed. Also, forecast and planning problems are covered briefly to give the non-meteorologists an idea of the magnitude of the forecaster's task and to suggest to meteorologists who have not supported ballooning operations the requirements for this task. Equations and data which are useful to an engineer who needs information about the atmosphere for his work are also provided.

B. OPERATIONAL METEOROLOGICAL REQUIREMENTS

To simplify the discussion, a balloon flight will be arbitrarily divided

into the following stages: 1) inflation, 2) launch, 3) ascent, 4) tracking and float, 5) descent, and 6) landing and recovery.

1. Inflation

Figure 1 illustrates a balloon during inflation. Many variations of the technique shown in Fig. 1 are used. Most large balloons are now inflated through tubes leading into the balloon near the top. This permits the balloon to be restrained at some point near the top but below the entry point of the inflation tubes, so that not much of the balloon fabric is exposed to the wind as gas flows into the balloon.

Until enough gas has entered the balloon to lift the fabric enclosing it, the fabric-encased gas bubble is free to roll about on the ground in response to the slightest wind. Therefore, wind is a critical factor during the early minutes of inflation. Rapid inflation shortens the period of greatest danger, but no way has been found of eliminating it. The danger to a balloon during early inflation is a function of both wind speed and the toughness of the balloon fabric. Steady winds less than five m/sec are acceptable for inflations of thin polyethylene balloons used for high altitude flights. Light winds are rarely steady, and a strong gust a few

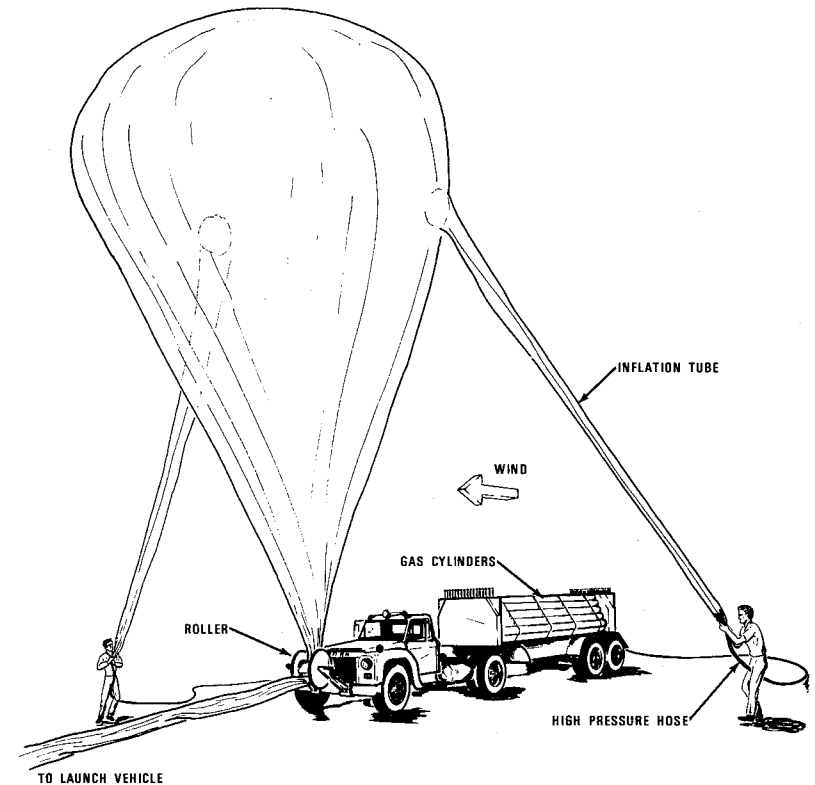


Fig. 1. Balloon during inflation. The gas bubble is restrained by a roller through which the balloon may move.

seconds in duration can destroy a balloon. Therefore, even lighter winds are preferred.

Occasionally balloons are inflated through a tube which enters the base. When this type of inflation is used, the balloon undergoes a much longer period during which it is not under control. Also, as the relatively small bubble rises and lifts the uninflated portion of the balloon, it is affected by the wind at levels up to 100 m. Therefore, the wind must be light (< 3 m/sec) through a deep stratum adjacent to the ground if this type of inflation is to be satisfactory.

Other factors are important during inflation, but none are as critical as the wind. Temperature extremes can cause discomfort to flight personnel, but they are not particularly limiting to the operation in other ways. Humidity is not a problem when the inflation gas is helium. If a flammable gas is used, however, low humidity may be more conducive to static discharges and so increase the hazard. Humidity can be controlled locally by sprinkling.

2. Launch

Two primary types of launch, static and dynamic, are used for large balloons. Figures 2 and 3 are illustrations of typical static and dynamic launches.

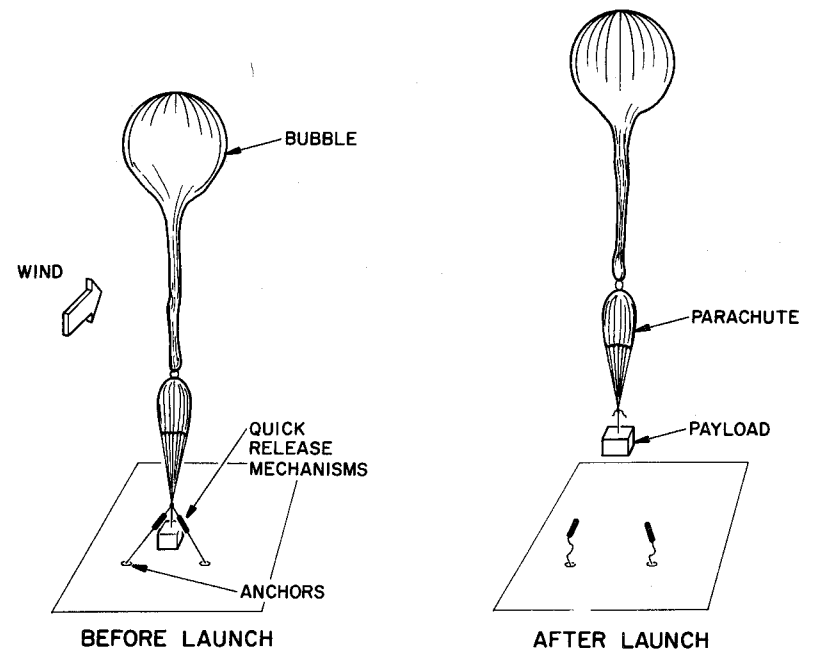


Fig. 2. Static launch.

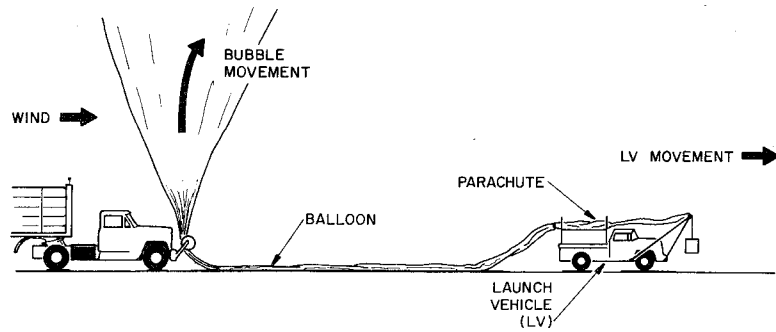


Fig. 3. Dynamic launch.

In the static launch, the balloon is allowed to stand erect over the payload immediately prior to launch. The payload is not moved until the balloon lifts it; then it moves in response to the free motion of the balloon. The meteorological factor that is most critical is the wind in the stratum immediately above the surface. Some of the larger balloon systems coming into use may stand 200 m (650 ft) high. Balloons standing erect in this manner have been known to form huge spinnaker-like sails. If this happens, the balloon will almost surely be destroyed, and the forces involved are quite sufficient to drag large vehicles or tear a payload apart. Thus, unless the winds are less than the design limits throughout a deep stratum adjacent to the surface, a static launch can rapidly change into a dynamic disaster. Design limits vary widely from system to system but few large systems have been designed to be launched in winds in excess of eight m/sec (~16 knots) at any level reached by the standing balloon system.

It is standard practice to choose a launch time when the diurnal winds are at their minimum. This consideration is especially important at tropical stations, subject to trade winds; at island and coastal stations, under the influence of land and sea breezes; and in deserts,

with intense diurnal heating and cooling. Instances may be found in all of the above cases where there is only a very short time span during the diurnal cycle when the surface wind speed has a significant probability of remaining below critical limits. As a general rule, unless the launch site is influenced by anomalous topographic effects, such as drainage winds from nearby slopes, the optimum time of launch is just before dawn, before the onset of diurnal heating.

A particularly damaging phenomenon known as the low-level jet is often widespread in the southern part of the United States during the summer months. The low-level jet is a nocturnal condition which usually begins near midnight and disappears near dawn. In a fully developed low-level jet, even a moderately small bubble may be difficult to launch. Thus, a paradox arises: if inflation is begun early enough for a safe launch, the balloon may be destroyed during inflation, but if inflation is delayed, it may be too late for a safe launch.

Dynamic launches are usually initiated while most of the balloon is lying on the ground, as shown in Fig. 3. Thus, before launch the balloon system is exposed only to the winds in a very shallow surface layer. The

first step in launch is to release the bubble at the launch spool. As soon as the balloon train is lifted off the ground by the rising bubble, the launch vehicle moves forward and to right or left, maneuvering the payload into a position which will be directly under the balloon bubble when the bubble has reached a height equal to the length of the balloon train. The payload is then released to be carried aloft. This type of launch can usually be accomplished if the maximum wind on the balloon at any level during launch does not exceed eight m/sec, but the actual limiting speed depends on the maneuverability of the launch vehicle, the space it has for maneuvering, and many other factors.

The launch depicted by Fig. 3 is called an upwind launch because the bubble is inflated and released from a position upwind of the launch vehicle. In another type, termed a downwind launch, the bubble is inflated and released downwind from the vehicle. After the bubble is released and has lifted the balloon train off the ground, the vehicle must move faster than the wind at the level of the bubble and overtake it. This type of launch requires that the vehicle be capable of greater speed than required during an upwind launch. It also requires more surface area in which to maneuver

the vehicle. In any dynamic launch, timing is important; it is perhaps less critical for a downwind than for an upwind launch. The wind on the balloon during this type of launch should normally not exceed eight m/sec.

Wind is the meteorological factor which is most restrictive in a physical sense at launch, and the wind through a stratum as deep as the length of the balloon train must be considered. Legal requirements may cause other meteorological variables to be restrictive also. For example, there may be a legal restriction against launching when the surface visibility is less than some specified value or when the balloon system must subsequently fly through a cloud layer. Falling rain or snow may create conditions which impose a legal restriction on launch, and either can make it more difficult. Snow on the ground or soft, muddy ground may also create a problem; therefore, a forecaster must be prepared to consider the possibility of precipitation as the flight date approaches. The possibility of lightning must be seriously considered also because many balloon systems have wires running from top to bottom. Usually, however, if lightning occurs, strong, gusty winds will also be probable.

3. Ascent

After launch, an ascending balloon system responds to its environment in a very complex way. Essentially, its horizontal speed is equal to the speed of the ambient air, but its rate of rise (ascent rate) is a function of the lapse rate of temperature in the atmosphere ($-dT/dH$) and the thermal environment (including radiation) of the balloon. The interaction of a balloon with its environment is described in some detail in Sections II and III.

As a balloon ascends through the tropopause it encounters extreme cold, and although most modern balloon materials can withstand quite low temperatures, a temperature below -80°C can cause problems. Cloud strata encountered during ascent may affect the radiation environment of the balloon enough to cause a dramatic change in its ascent rate. Cirrus clouds so thin that they are invisible, especially at night, may be significant. The distribution of moisture with height can give a clue to the existence of such clouds.

4. Tracking and Float

It may be desirable to track a balloon system for a variety of reasons.

Knowledge of the position of the system as a function of time may be essential to the scientist whose experiment is being flown. Legal restrictions may exist which require tracking, especially during ascent and descent while the balloon is moving vertically through space shared by airplanes.

During ascent, tracking may be done visually and electronically (radar, radio direction finding, etc.) from the launch site. Cloudiness and low visibility can severely limit visual tracking, but weather is not particularly restrictive to electronic tracking until the balloon nears the radio horizon. Then strata of differing reflective-index gradients may cause erratic radio transmission between the balloon system and the launch site.

As a balloon system moves away from the launch site, tracking may be done from a down-range station. Tracking away from the launch site is also frequently done by airplane. Automatic direction-finding equipment which is standard on many airplanes may be used to determine the location of a balloon system which includes a transmitter operating on an appropriate frequency. Visual fixes from an airplane are frequently possible even when visibility or cloudiness at low levels may prevent a balloon from being seen from the ground. An airplane thus constitutes an excellent, and nearly uni-

versal, tracking instrument for long balloon flights, and terminal and enroute flight weather for the airplane becomes more important to successful tracking than any meteorological element which may affect the balloon system directly, with the possible exception of the wind at balloon float level. In winter, in middle latitudes, balloon speed may exceed the speed of the tracking airplane.

5. Descent

A balloon-borne experiment may be returned to earth by the balloon itself or by parachute. A descending balloon system is affected by the atmosphere in much the same way as an ascending system. Therefore, the meteorological problems associated with descent are similar to those associated with ascent, except that they may be displaced many miles from the launch site and become critical many hours after launch. Thus, the forecaster must make a longer range (in time) forecast for descent than for ascent, for a site perhaps thousands of miles away from his base of operations.

Most balloon-borne payloads are returned to earth on a parachute. Section X describes the behavior of a descending parachute system. Its

descent rate depends on air density, and that is well enough defined in the Standard Atmosphere to enable one to calculate the descent rate quite accurately. Consequently, the descent vector, if it is assumed that the parachute system's horizontal velocity is equal to the velocity of the ambient air, can be calculated with an accuracy comparable to the accuracy with which the wind is known as a function of height. An accurate descent vector is particularly important in a parachute recovery, because operations personnel depend on it to enable them to start the descent when the balloon system is in an appropriate location to assure that the parachute will land in a safe, convenient spot.

Daytime parachute descents can often be followed to earth visually. Good visibility and clear skies enhance the probability of success. A payload containing a radio transmitter which can be tracked from an airplane can be followed to the ground even though it cannot be seen. This technique is used for night landings, and it may be used when low-level visibility is poor. A descent in the vicinity of a thunderstorm should be avoided if possible. Descending through any kind of convective cloud is also undesirable. Finally, it is important that winds near the surface

not be excessive. Designing and constructing a device to absorb the energy of horizontal motion safely and effectively is difficult, and if there is wind enough at the surface to drag a parachute system, a payload may be destroyed even after a satisfactory landing. Low-level winds in excess of eight m/sec are difficult to protect against in designing an energy absorber; also they are likely to drag a payload unless it is separated from the balloon or parachute upon landing. Winds less than three m/sec may be treated as zero wind in energy-absorber design, and such winds will not drag a payload after landing.

6. Landing and Recovery

One aspect of the landing was mentioned in the last paragraph, i.e., the dragging of the payload after landing. A balloon can form a much larger drag surface than a parachute. Therefore, immediately after a payload touches down with the balloon attached, the balloon should be deflated even if the surface winds are negligible.

The ideal landing area is a firm, unoccupied site which is readily accessible by truck. The immediate area should be free from trees, large bushes, etc. which might damage the payload or the parachute. The nearest

inhabitants should be close enough to provide assistance if needed, but far enough away that no question of danger to people or property will arise. The most important meteorological variables are surface and low-level winds; recent precipitation which may have left the surface soft, slick, or snow-covered; and precipitation anticipated during the few hours required to recover the payload. Low-level visibility and low clouds can also adversely affect recovery, because a ground crew must frequently be guided to a landing site by a low-flying airplane.

C. THERMAL STRUCTURE OF THE ATMOSPHERE

1. Temperature and Density

Taken together, the U.S. Standard Atmosphere, 1962, (1) and the Supplements (2) constitute a description of the whole atmosphere from which horizontal (latitudinal) and temporal variations may be coarsely determined. They are adequate for most scientific ballooning needs. The relationships between temperature, density, and height which are given in this section are applicable in the real and standard atmospheres unless otherwise noted.

a. The hydrostatic relationship. Although the atmosphere is in constant motion, the hydrostatic relationship is very nearly valid. A

more general relationship expressing the balance of vertical forces in a moving atmosphere is given by Haltiner and Martin (3). The hydrostatic equation may be stated

$$dp = -\rho g dz \quad (1)$$

where p is atmospheric pressure, g is the acceleration due to gravity, ρ is the air density, and z is height; p , g , and ρ are all functions of height, but the variation of g through the stratum in which balloons operate is not great. Equation (1) is, therefore, often written

$$dp = -g_0 \rho dH \quad (2)$$

where g_0 is a defined constant and H has the dimensions of height and is nearly equal to z . The acceleration of gravity at sea level at 45° is usually the value assigned to g_0 . If a height increment, ΔH , is determined by integrating Eq. (2) through an elevated atmospheric stratum bounded by pressure surfaces p_1 and p_2 where $g < g_0$, the value of ΔH will be less than the geometric distance between the pressure surfaces. To differentiate H from z , H is called geopotential height and is measured in geopotential meters or geopotential feet. At great height a geopotential meter is

longer than a physical meter; below sea level it may be shorter. Equation (2) is the hydrostatic equation which will be used for further development.

Air density under conditions found in the atmosphere may be expressed as a function of pressure and temperature by means of the equation of state for an ideal gas. Thus,

$$\rho = \frac{PM}{RT} \quad (3)$$

where M is the molecular weight of air, R is the universal gas constant, and T is the absolute temperature of the air. Since air is a mixture of gases, it has no single, true molecular weight, but for most purposes a molecular weight may be determined from Eq. (4)

$$M = \frac{m}{\sum (m_i/M_i)} \quad (4)$$

in which M_i is the molecular weight of the i th constituent which has a mass of m_i . The mass of the mixture is m . According to Glueckauf (4), the upper atmosphere, up to a height of at least 70 km, has the same composition as that of dry air found at the ground. Therefore, a single value of M for dry air suffices for almost all scientific ballooning needs. If a correction for water vapor, the most variable constituent, should be

deemed necessary, it may be made by multiplying the value of M for dry air by the factor $(1-0.379e/p)$ in which e is the vapor pressure of gaseous water in the atmosphere and p is atmospheric pressure.

Equations (2) and (3) may be combined to yield

$$\frac{dp}{p} = - \frac{Mg_0}{R} \frac{dH}{T} \quad (5)$$

This can be integrated if T can be expressed as a function of H. In the atmosphere T is often very nearly a linear function of height through deep layers, and it may not change with height through shallow layers. Both of these cases will be considered.

In a layer through which T varies linearly with H, one may write

$$T = T_b + L'(H - H_b) \quad (6)$$

where T_b is the temperature at the base of a stratum whose height is H_b and L' ($=dT/dH$) is the vertical gradient of temperature. The negative of L' is called the lapse rate by meteorologists. With Eq. (6) substituted into Eq. (5), the latter can be integrated as follows

$$\int_{p_b}^p \frac{dp}{p} = - \frac{Mg_0}{R} \int_{H_b}^H \frac{dH}{T_b + L'(H - H_b)}$$

to yield

$$p = p_b \left[1 + \frac{L'}{T_b} (H - H_b) \right]^{-\frac{Mg_o}{RL'}} \quad (7)$$

or

$$H = H_b + \frac{T_b}{L'} \left[\left(\frac{p_b}{p} \right)^{\frac{RL'}{Mg_o}} - 1 \right] \quad (8)$$

A layer through which T is constant may be integrated in the following

way

$$\int_{p_b}^p \frac{dp}{p} = - \frac{Mg_o}{RT_b} \int_{H_b}^H dH$$

to yield

$$p = p_b e^{-\frac{Mg_o}{RT_b} (H - H_b)} \quad (9)$$

or

$$H = H_b - \frac{RT_b}{Mg_o} \ln \frac{p}{p_b} \quad (10)$$

The notation employed in Eqs. (9) and (10) uses the temperature at the base of the layer. The mean temperature through a layer of thickness $(H - H_b)$ may be substituted for T_b in Eqs. (9) and (10) if it is known,

even though temperature changes with height in the layer. In thin layers, the mean temperature can readily be determined from a plot of T vs H, a practice which is widely used in meteorology. Similarly, a mean value of L' may be determined from a T vs H plot and used in Eqs. (7) and (8) although the actual T vs H curve may not be linear. Thus, Eqs. (7)-(10) are not as restricted in their application as the assumptions made in deriving them may suggest.

Starting from the equation of state and the hydrostatic equation, the relationship between density and height may also be derived. The derivation is shown here with a minimum of explanation. Taking the derivation of Eq. (3) yields

$$\frac{dp}{dH} = -\frac{M}{RT^2} \left(T \frac{dp}{dH} - p \frac{dT}{dH} \right)$$

In a layer in which $dT/dH (=L')$ is a constant not equal to zero, $T = T_b + L'(H - H_b)$, and

$$\frac{dp}{dH} = - \left(\frac{Mg_o}{RT} + \frac{pML'}{RT^2} \right) = - \frac{p}{T} \left(\frac{Mg_o}{R} + L' \right)$$

$$\int_b^p \frac{dp}{p} = - \left(\frac{Mg_o}{RL'} + 1 \right) \int_{H_b}^H \frac{d[T_b + L'(H - H_b)]}{T_b + L'(H - H_b)}$$

$$\rho = \rho_b \left[1 + \frac{L'}{T_b} (H - H_b) \right]^{-\left(\frac{Mg_o}{RL'} + 1\right)} \quad (11)$$

or

$$H = H_b + \frac{T_b}{L'} \left[\left(\frac{\rho}{\rho_b}\right)^{\frac{RL'}{Mg_o + RL'}} - 1 \right] \quad (12)$$

Similarly, in a layer in which $dT/dH = 0$,

$$\frac{d\rho}{dH} = -\frac{Mg_o \rho}{RT_b}$$

$$\int_{\rho_b}^{\rho} \frac{d\rho}{\rho} = -\frac{Mg_o}{RT_b} \int_{H_b}^H dH$$

$$\rho = \rho_b e^{-\frac{Mg_o}{RT_b} (H - H_b)} \quad (13)$$

or

$$H = H_b - \frac{RT_b}{Mg_o} \ln \frac{\rho}{\rho_b} \quad (14)$$

Note that the expression $\left[1 + (L'/T_b) (H - H_b) \right]$ is equal to T/T_b ;

therefore, it follows that Eq. (7) may be written

$$P = P_b \left(\frac{T}{T_b}\right)^{-\frac{Mg_o}{RL'}} \quad (15)$$

Also Eq. (11) may be written

$$\rho = \rho_b \left(\frac{T}{T_b}\right)^{-\left(\frac{Mg_o}{RL'} + 1\right)} \quad (16)$$

Finally, Eqs. (15) and (16) may be combined to give

$$\rho = \rho_b \left(\frac{P}{P_b}\right)^{\left(\frac{RL'}{Mg_o} + 1\right)} \quad (17)$$

Equations (15) through (17) are useful relationships between pressure,

temperature, and density in an atmospheric layer in which L' is constant

but not zero. If L' is zero, the relationship between pressure and density

is

$$\frac{P}{P_b} = \frac{\rho}{\rho_b} \quad (18)$$

and neither pressure nor density are functions of temperature within the

layer.

b. The U.S. Standard Atmosphere, 1962. The U.S. Standard Atmosphere,

1962, is defined up to 61 km as follows:

(1) The air is a dry gas, devoid of liquid water, water vapor, and dust, and it obeys the ideal gas law.

(2) The following defined and physical constants are applicable:

Sea level temperature-- $T_0 = 15^\circ\text{C} = 59^\circ\text{F} = 288.15^\circ\text{K} = 518.67^\circ\text{R}$

Sea level pressure-- $p_0 = 1013.25 \text{ mb} = 101325.0 \text{ N/m}^2 = 2116.22 \text{ lbf/ft}^2$

Sea level acceleration due to gravity-- $g_0 = 9.80665 \text{ m/sec}^2 =$
 32.1741 ft/sec^2

Molecular weight-- $M = 28.9644 \text{ kg/(kg - mol)}$

Universal gas constant-- $R = 8314.32 \text{ J/}^\circ\text{K(Kg - mol)} =$
 $1545.31 \text{ ft lbf/}^\circ\text{R(lb - mol)}$

(3) Temperature varies with geopotential height as shown in Table 1.

Pressure and density are also given at the base of each of the layers for convenience, but of these only the sea level pressure is a defined value.

Figure 4 is a plot of T vs H for the lowest 61 km of the U.S. Standard Atmosphere, 1962. Note that the curve is made up of a series of straight line segments; therefore, Eqs. (6) through (18) and the definition of the atmosphere given in (1) through (3) above may be used as appropriate to determine T, p, and ρ at any height H. More generally, given a value of T, p, or H, it is possible to determine uniquely the values of the other

Table 1

Defining Temperature vs Height Relationships in the Lowest 61 km
of the U.S. Standard Atmosphere, 1962.

Layer Height, Base and Top (gpm)*	Temperature at Base of Layer °K	Temperature Grad. in Layer °C	Temperature Grad. in Layer (°K/gpm)	Pressure at Base of Layer (mb)**	Density at Base of Layer (kg/m ³)
0-11,000	288.15	15.00	-0.0065	1013.25	1.2250
11,000-20,000	216.65	-56.50	0.00	226.320	0.36392
20,000-32,000	216.65	-56.50	+0.0010	54.749	0.088035
32,000-47,000	228.65	-44.50	+0.0028	8.680	0.013225
47,000-52,000	270.65	- 2.50	0.00	1.109	0.0014275
52,000-61,000	270.65	- 2.50	-0.0020	0.590	0.0007594

*The symbol gpm is the abbreviation for geopotential meter.

**One millibar (mb) is equal to 100 N/m^2 .

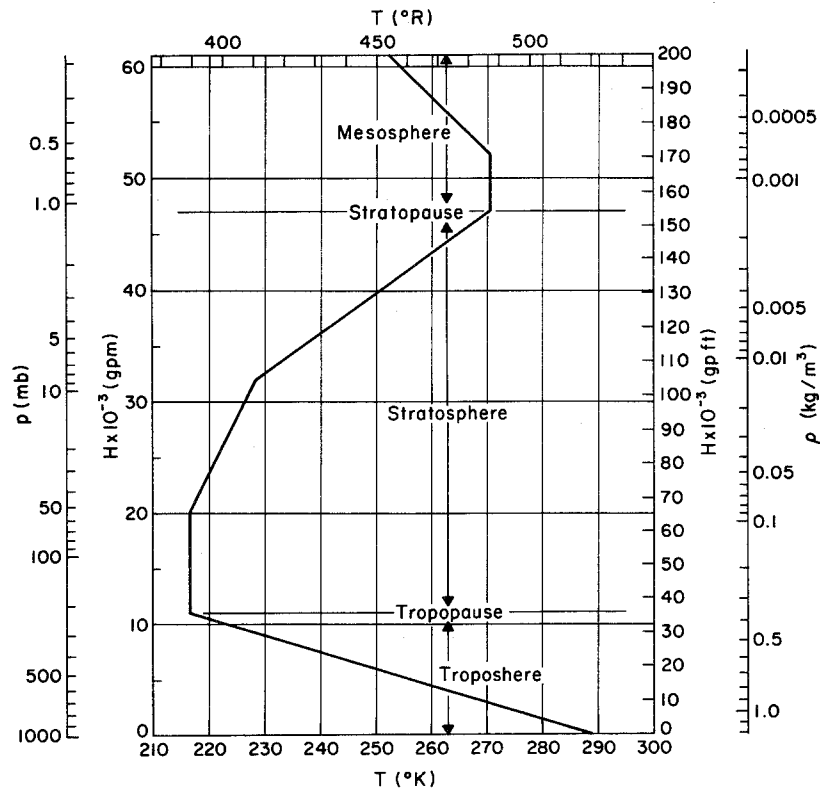


Fig. 4. Temperature as a function of geopotential height in the U.S. Standard Atmosphere, 1962.

two and T , but it is not usually possible to determine a unique value for any of the other variables if T alone is known. Auxiliary scales of p and ρ are shown along the ordinate of Fig. 4.

c. Supplementary atmospheres. Supplementary atmosphere temperature-height curves for several latitudes for January are given in Fig. 5. Similar curves for July are shown in Fig. 6. An annual curve for 15°N is also given in Fig. 6. Because of the small temporal variation of temperature in the tropics, the one curve is valid at any season. Also, the U.S. Standard Atmosphere, 1962, has been found to be a good approximation for the middle-latitude curves of spring and fall below 69 km. Supplementary atmospheres are not often used in scientific ballooning; if one is needed its precise definition may be found in reference (2).

Data, especially for balloon flight planning, can sometimes be obtained with sufficient accuracy from Figs. 5 or 6. If density is needed, Fig. 7 may be more convenient. Adapted from reference (2), it shows the percentage departure of density from the standard atmosphere as a function of height, season, and latitude. The variability in winter at high latitudes is so great that curves are given for warm and cold atmospheres as well as for the mean.

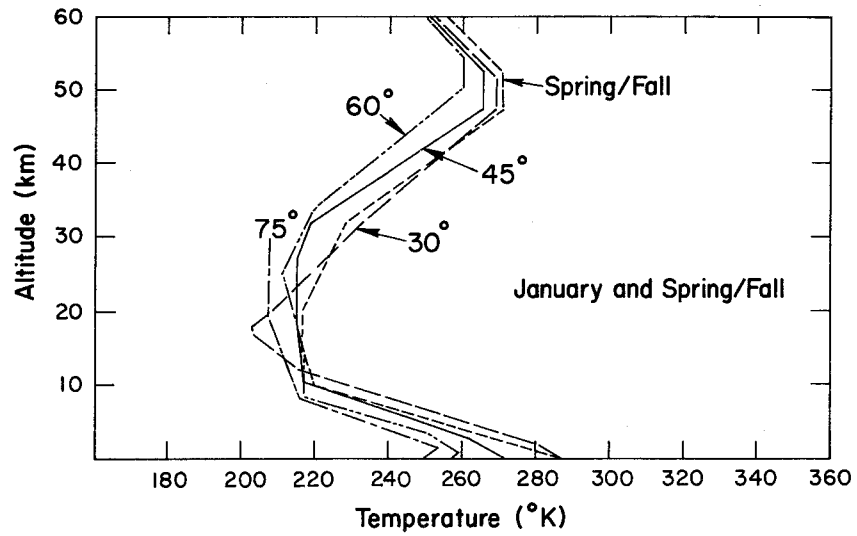


Fig. 5. Temperature-Height profiles of the 30°, 45°, 60°, and 75°N

January and mid-latitude spring/fall Supplementary Atmospheres.

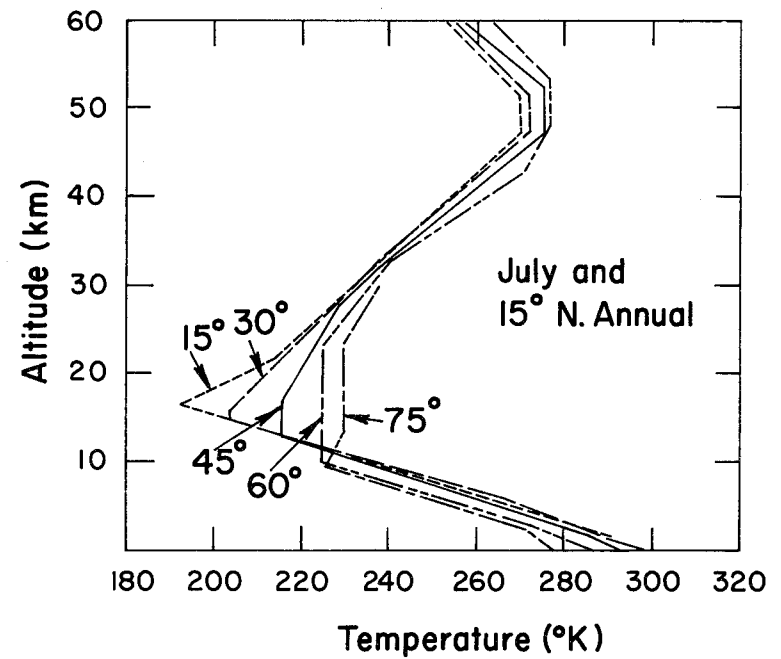


Fig. 6. Temperature-Height profiles of the 30°, 45°, 60°, and 75°N

July and 15°N annual Supplementary Atmospheres.

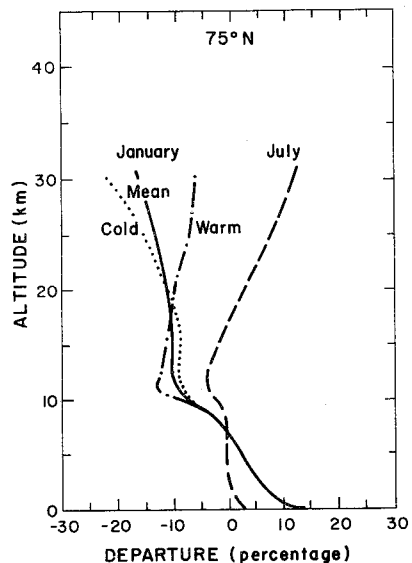
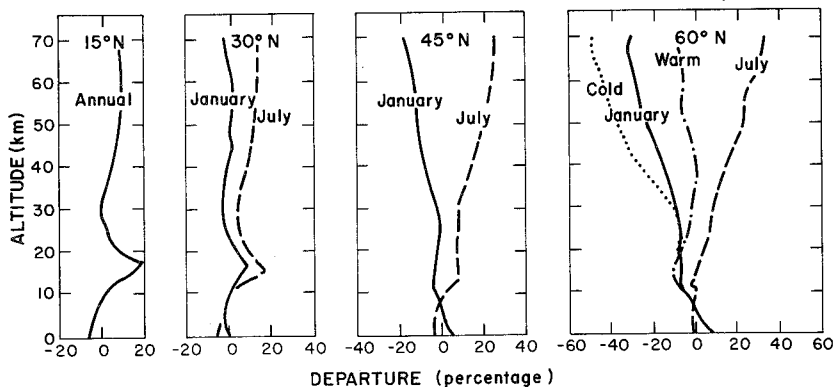


Fig. 7. Percentage departure from standard of densities of certain supplemental atmospheres given in reference (2).

d. Mean thermal structure. Mean temperature as a function of height and latitude for summer and winter is shown in Fig. 8 from Palmén and Newton (5). Because of the limited quantity and quality of high level data used to construct the figure, it will undoubtedly be found wrong in detail as additional, more reliable data become available. Nonetheless, the principal features of the temperature patterns depicted by the figure are believed to be essentially correct. Also, most of the data were observed in the Northern Hemisphere so that the chart shows the patterns of the Northern Hemisphere summer and winter. It may be interpreted, however, as a pattern of summer and winter hemisphere patterns shown concurrently.

2. Thermal Radiation

The atmosphere receives radiation from the sun and from earth, and it radiates to space. It is transparent to most of the solar radiation, but it absorbs enough radiant energy in several wave bands to affect its vertical temperature structure significantly. Much of Section III must necessarily be devoted to this subject; therefore, it is not discussed further here.

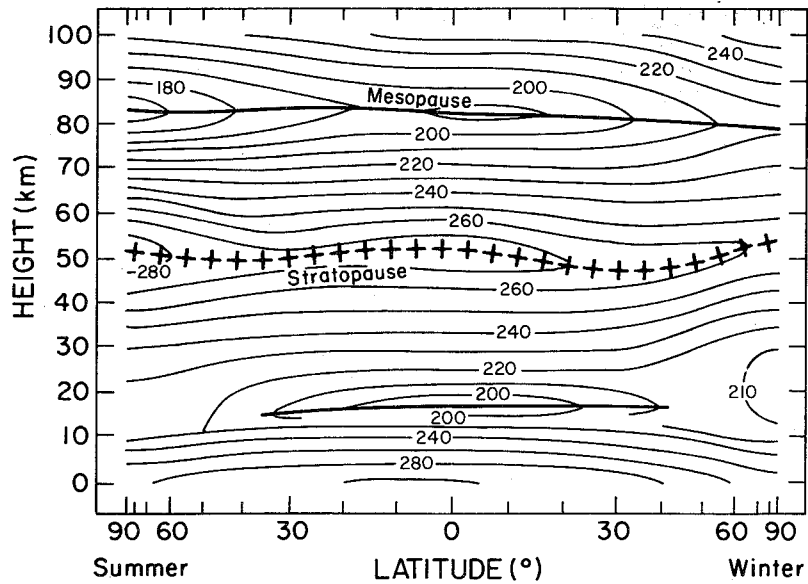


Fig. 8. Mean thermal structure of the atmosphere in summer and winter, after Palmen and Newton (5).

D. CIRCULATION

In the free atmosphere, especially at the high levels at which balloons fly, winds are nearly horizontal, and in the mean they are nearly zonal, i.e., they blow from either east or west. This makes it possible to describe the principal features of atmospheric circulation in terms of easterly (winds blowing from the east) and westerly winds only. However, for computing probable balloon trajectories, Solot and Darling (6), knowledge of the meridional (north-south) winds is also essential; therefore, although zonal winds receive most of the attention in this discussion of atmospheric circulation, it should be emphasized that meridional winds are highly important in balloon flight planning and operations.

1. Mean Zonal Structure

Figure 9 is a chart showing the mean zonal wind structure of the atmosphere as a function of height and latitude for the summer and winter seasons. It, like Fig. 8, is taken from Palmen and Newton (5), and it may also be interpreted as showing the winter and summer wind patterns in one hemisphere or the concurrent pattern in both hemispheres.

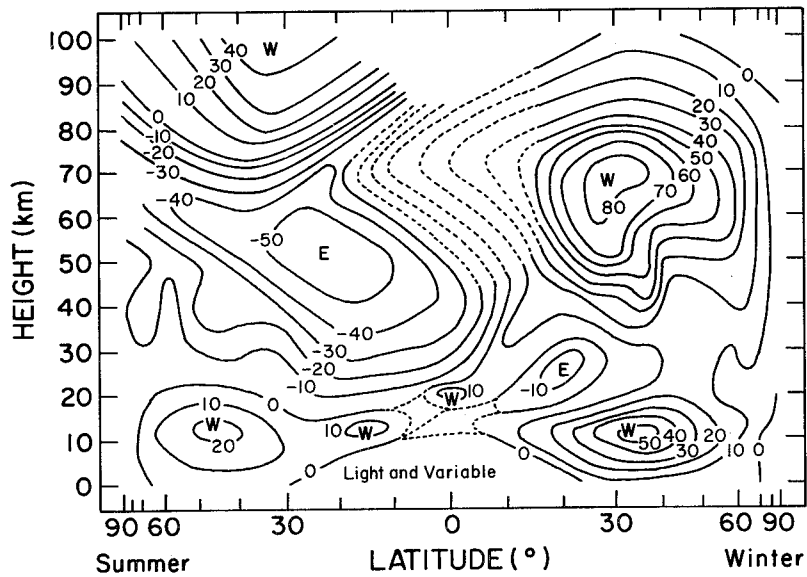


Fig. 9. Mean zonal wind in summer and winter, after Palmén and

Newton (5).

The patterns in Figs. 8 and 9 are not independent. Vertical wind shear is correlated closely with horizontal temperature gradient in the atmosphere. If the wind were geostrophic (horizontal, unaccelerated, frictionless flow) at all levels, the correlation between vertical wind shear and horizontal temperature gradient would be perfect. This correlation was kept in mind as the two charts were constructed so that the two patterns would be mutually consistent.

The most important features of Fig. 9 from the point of view of high altitude scientific ballooning are the stratum of low speed winds near 20 km, the strong westerlies which exist at higher levels in the winter hemisphere, and the easterlies which exist generally between 20 and 75 km in summer. It is also pertinent to note that westerlies exist at all levels below 20 km in the middle latitudes in both winter and summer. Neither polar nor tropical winds are explained well by Fig. 9. Both will be discussed separately later.

If west winds dominate the circulation of the middle latitude stratum between 20 and 75 km in winter and are replaced by east winds in the summer, there must be at least two transition periods when neither west nor east winds are strong.

It is useful, though vastly oversimplified, to view the winter stratospheric circulation as consisting of a cyclonic vortex centered near the pole. Figure 10, from reference (7), shows a typical winter flow pattern. There is no wind at the center of the vortex, and the wind at lower latitudes is westerly. Typically, the speed increases equatorward from the pole to a maximum at about 30° and then decreases from 30° to about 15° where it merges with an equatorial wind system.

Similarly, the summer circulation in the stratosphere may be viewed as an anticyclonic vortex centered near the pole (see Fig. 11). East winds increase in speed equatorward from the pole, reach a broad maximum in lower middle latitudes, and then decrease to $10 - 15^{\circ}$, where they merge with the equatorial system. The summer wind system in the stratosphere is perhaps the most stable current system in the atmosphere. After it becomes firmly established, it persists with remarkably little variation until the autumn transition, when it is replaced by the winter west wind system.

The autumn transition is one of the most predictable of the changes which the atmosphere undergoes. In the mean, it occurs at the time of the autumn equinox, usually starting at high altitude near the pole about a

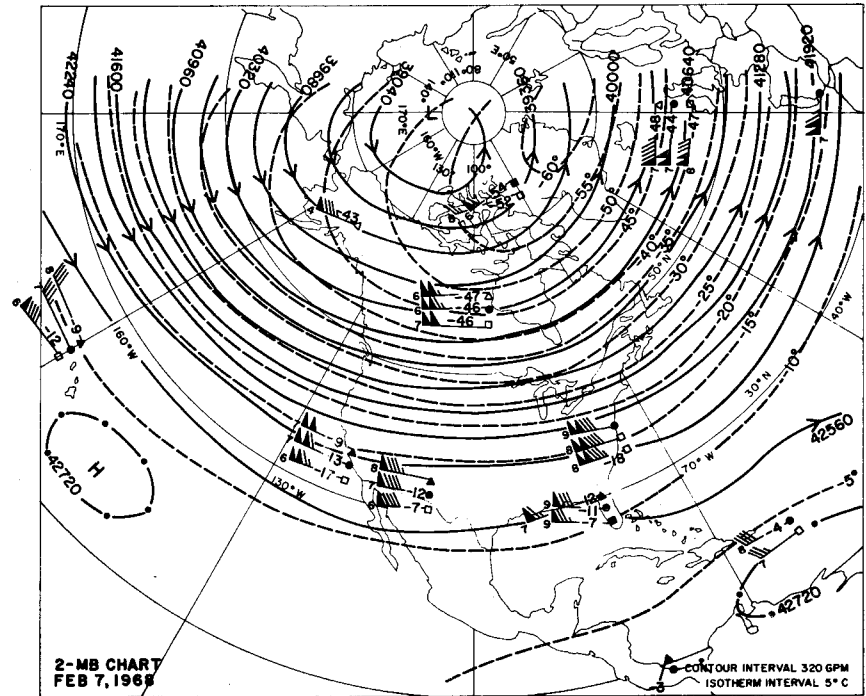


Fig. 10. Typical winter cyclonic vortex in the upper stratosphere.

Winds flow along the height contours (solid lines). The speed is indicated by the feathers--each flag represents 50 knots, each bar 10 knots, and a half bar 5 knots. The dashed lines are isotherms of temperature in $^{\circ}\text{C}$.

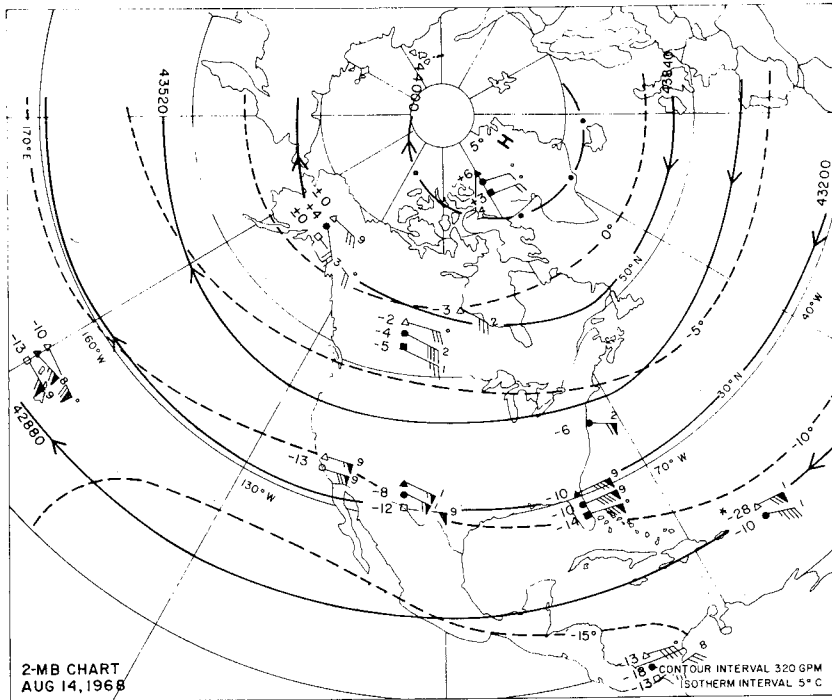


Fig. 11. Typical summer anticyclonic vortex in the upper stratosphere.

See Fig. 10 for explanation of the isolines.

month before the equinox. It then works its way downward and equatorward, and a month after the equinox, all winds poleward of 15° and above 30 km will be west winds. The downward and equatorward progression of the autumn transition is regular enough that its time of occurrence at one height and place is a good predictor of its time of occurrence at another. At any particular altitude and geographic location, light winds which are quite variable in direction may be expected to last about two weeks during the transition.

Figure 12 is a time cross section of stratospheric winds over the southern United States. It was derived from high level rawinsonde and rocket data from the southern United States, but it is believed to be representative of winds generally at 30° N. Mean zonal wind speed and the standard deviation of the zonal wind are given as functions of height and time of year. The isoline of zero wind speed may be interpreted as the wind reversal line. The zone on either side of the zero speed line in which the speed is less than one standard deviation gives a clue to the duration of light variable winds accompanying the transition.

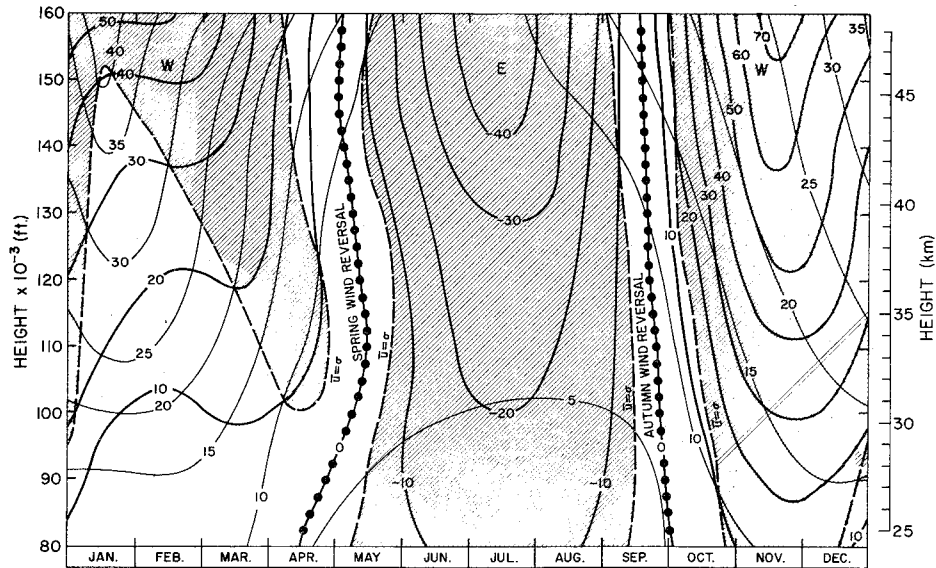


Fig. 12. Time-Height cross section of the mean monthly zonal winds in the southern U.S. stratosphere.

Winter winds in the stratosphere are much more variable than summer winds. After the autumn transition, the westerly flow becomes quite strong, usually reaching maximum speed in about two months. During the third month after transition, the mean zonal speed decreases but the variability increases. By the beginning of winter, a distinct wave pattern is likely to have formed on the westerly current, and during the winter these waves will occasionally grow so large that they dominate the circulation over a large part of the hemisphere. When this happens strong north, south, or even east winds may temporarily replace the usual west winds over large areas. Figure 13 shows how a typical well developed wave may distort the zonal winter wind system. Note that the only westerly winds over North America at 2 mb (~ 41 km) are found in the southwestern United States. Higher, at 0.4 mb (~ 54 km), the southern United States is experiencing west to southwest flow, but at Point Mugu, California, strong northeast winds are directly opposed to the southwest winds at 2 mb.

Occasionally, the polar cyclonic vortex will be almost entirely replaced in winter by an anticyclonic vortex. This occurs with dramatic suddenness, accompanied by a large increase in the high latitude, strato-

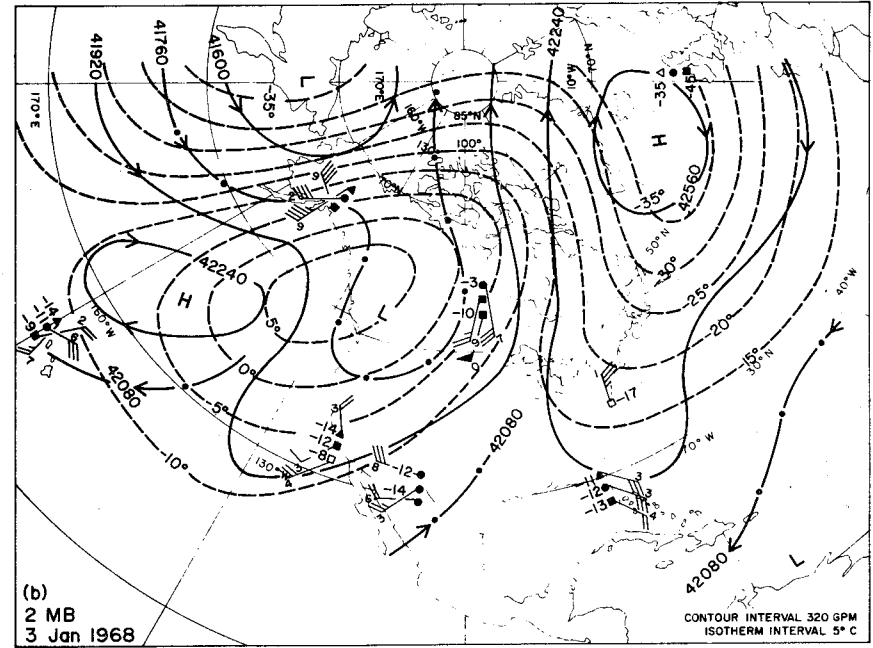
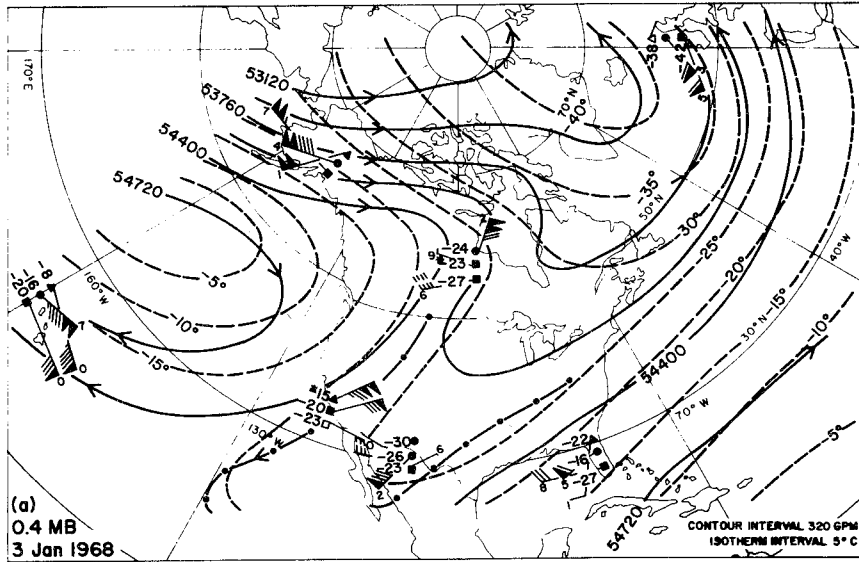


Fig. 13a. Well developed wave in the winter westerlies. Note the variety of wind directions on each pressure surface and the differences which occur between the surfaces, i.e., essentially between 54 km (a) and 41 km (b). See Fig. 10 for explanation of the isolines.

Figure 13b

spheric temperature; therefore, meteorologists often refer to the phenomenon as a sudden, stratospheric warming. Meteorologists who are forecasting for scientific balloon flights are more likely to think of it as a temporary wind reversal.

As winter wanes, the mean speed of the stratospheric wind system decreases. Temporary reversals often make it difficult to know when the summer easterlies have indeed begun. The true transition from the winter to the summer circulation pattern follows much the same pattern as the autumn transition. Westerlies give way to easterlies first at high altitude in polar latitudes. The northern hemisphere spring transition of 1968 at 43 km is shown by Fig. 14 shortly after it had started. A small vortex has already formed near the pole and is spreading southward. Westerly winds are still being observed in most of the United States. Nearly all observed winds are light, although the easterlies over Alaska are rapidly gaining speed.

The transition progresses downward and equatorward, requiring up to two months for completion. This transition occurs in middle latitudes roughly a month after the spring equinox. Neither its time of occurrence

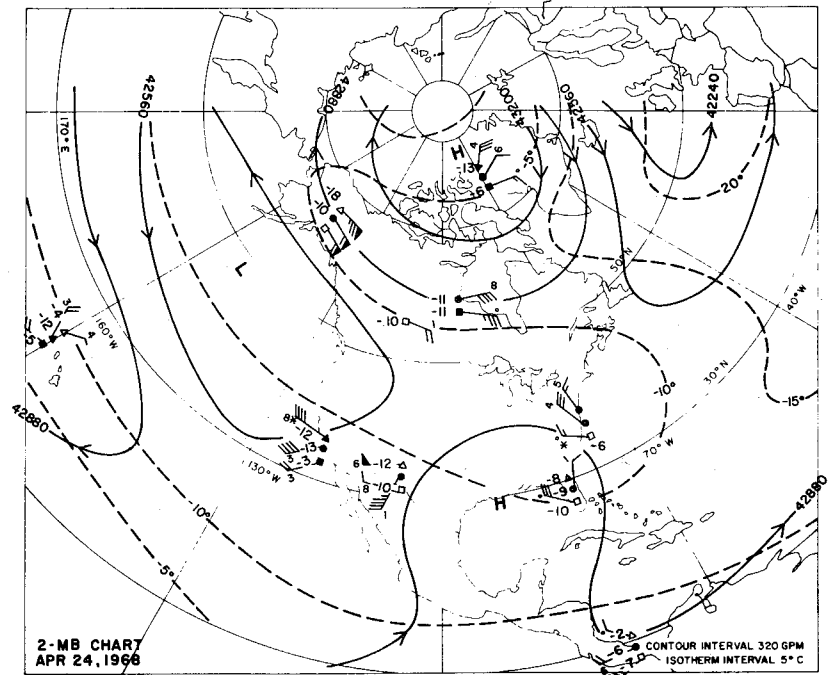


Fig. 14. Transition from a winter cyclonic circulation to a summer anticyclonic circulation. A small anticyclone has formed in the vicinity of the pole and is spreading equatorward. See Fig. 10 for an explanation of the isolines.

nor its rate of progression is as regular as the autumn reversal. Therefore, it is not as predictable.

The true wind reversals are highly important to scientific ballooning. Because of the light wind speeds in the stratosphere during the transition periods, balloons can fly for long periods without violating forbidden territory, e.g., over an ocean where recovery would be difficult or impossible. Often a balloon can fly up to 24 hours and remain above the radio horizon of the launch site. The temporary reversals of winter are sometimes accompanied by light winds over large areas. However, the winds associated with a well-developed wave in the stratospheric westerlies are likely to be strong. Except for flights of a few hours duration or flights which do not require payload recovery, attempts to take advantage of the light winds during temporary winter reversals of the normal stratospheric westerly circulation are not recommended. At such times the circulation is very unsteady and notoriously unpredictable.

2. Polar Wind Structure

The discussion of the mean zonal wind structure above included the polar regions, but some additional discussion is warranted. If the vortices

always remained centered at the poles, the winds there would always be zero. Further, the wind would never be strong in the vicinity of either pole. Note, however, that in none of the analyses shown (Figs. 10, 11, 13, and 14) is the center of the vortex at the pole. Winds at or near the poles are on the average lighter than at lower latitudes, but they can be strong, and they are highly variable in direction.

3. Equatorial Zonal Wind Structure

In the lower equatorial stratosphere, the principal wind system is a zonal current that alternates between east and west in an irregular fashion with a period which is usually a little more than two years. The oscillation is referred to as a 26-month or quasi-biennial oscillation by Reed (8). Higher in the stratosphere and in the lower mesosphere, equatorial winds oscillate from east to west in a semiannual cycle, Reed (9). In the middle stratosphere, where neither the quasi-biennial nor the semiannual cycle dominates, the variation of the wind with time is quite disorderly. Also, at a distance of $\sim 15^\circ$ from the equator in the lower stratosphere, the quasi-biennial oscillation has an amplitude about equal to the annual oscillation so evident in middle latitudes; therefore, the variation with time

of the wind structure there appears generally chaotic, Belmont and Dartt (10).

a. The quasi-biennial oscillation. Figure 15 from Kriester (11) shows the march of the quasi-biennial oscillation in the lower equatorial stratosphere from 1953 through 1970. Clearly, throughout most of the stratum from 20 to 30 km, west winds have alternated with east winds. Also, a directional regime (west or east) appears first at the top of the stratum and then progresses downward with the passage of time. Reed (8) has found that the downward speed of propagation is about 2 km per month above 30 km and 1 km per month below 30 km. By treating the oscillation at each level as a wave (making west wind speeds positive and east wind negative), Reed also found that the wave has its greatest amplitude at 24 km. Figure 16 shows the mean amplitude as a function of height.

At a given level in this stratum the wind appears to flow from the east for approximately a year and then from the west for a year. If one views the entire stratum from 18 to 35 km, however, both easterlies and westerlies will usually be flowing simultaneously, one above the other. When, roughly, the upper half of the stratum is dominated by west winds,

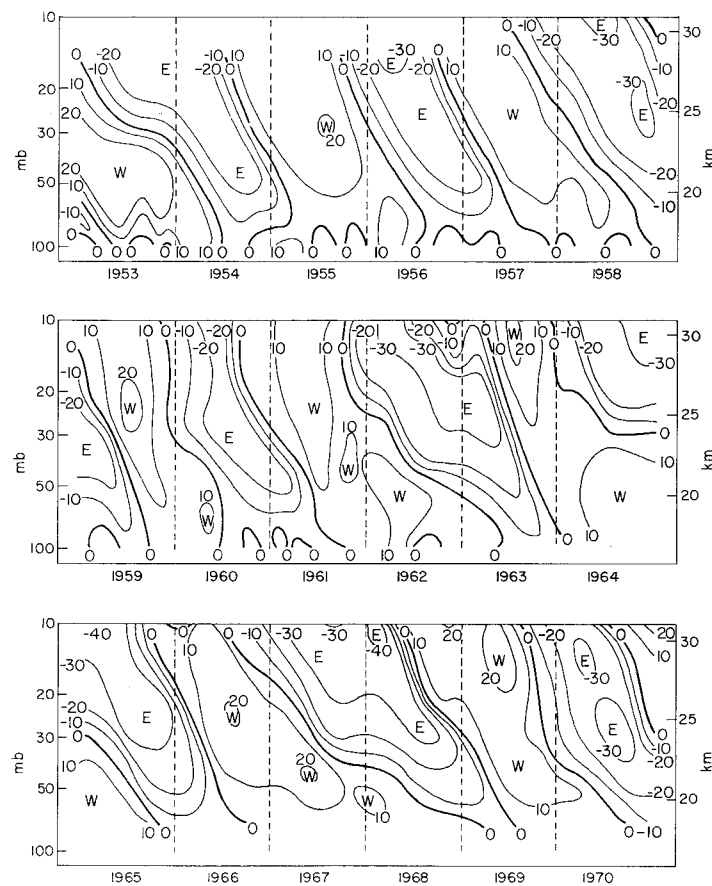


Fig. 15. Time-Height cross section of mean monthly zonal winds at Canton Island (1953--Aug. 1967) and at Gan/Malediv Islands (Sept. 1967--1970). From Kriester (11). Lines are isolines of wind speed in meters per second.

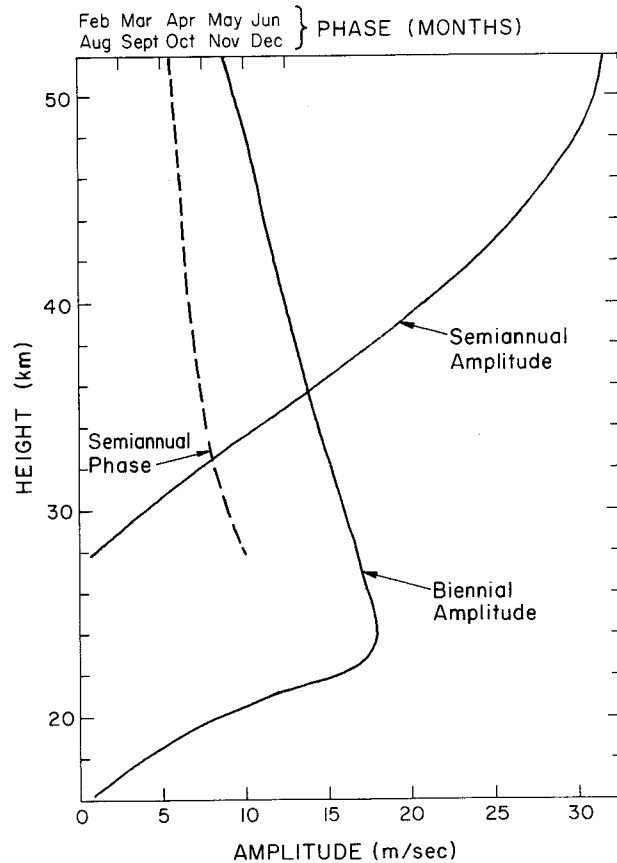


Fig. 16. Amplitude of the quasi-biennial and semiannual, equatorial oscillations as functions of height. Also, time of occurrence of maximum west winds (phase) of the semiannual oscillation in months.

weak east winds will appear at the top. These east winds will grow downward and gain strength in their lower reaches as they do so. When they have occupied about half of the stratum, weak west winds will appear above them. The east wind stratum, now sandwiched between two layers of westerlies, will continue to move downward, gaining strength until it reaches the vicinity of 24 km. Then it will lose strength as it moves on to lower levels until it disappears just above the tropopause. The westerly current which had formed above it will have a similar life cycle. Between the east and west currents is a thin stratum of light, variable winds.

One who wishes to fly a superpressure balloon on the surface of constant density (essentially constant height), will find that the wind can carry his balloon around the earth many times in one direction before it reverses. On the other hand, one who is flying large zero-pressure balloons may choose to take advantage of either an easterly or westerly current, or he may use controlled or uncontrolled (diurnal) height changes of the balloon system to fly alternately east and west. He may also attempt to fly in the low speed stratum between the east and west winds.

b. The semiannual oscillation. As shown by Fig. 16, the amplitude of the semiannual oscillation grows rapidly with increasing altitude above 28 km, reaching a maximum at about 52 km. The amplitude of the quasi-biennial oscillation decreases with height in this altitude range, and the two are equal in the vicinity of 35 km. From 30 to 40 km, the interference pattern of the two oscillations makes it difficult to identify either. Above 40 km the semiannual dominates.

Figure 17 shows Reed's (9) estimate of the variation of the equatorial zonal wind with month and height in the stratum in which the semiannual oscillation prevails. The quasi-biennial oscillation was filtered out of the data used to construct Fig. 17 so that the semiannual oscillation is apparent down to 30 km. The figure also suggests that above 64 km westerlies may prevail throughout the year; observation seems to confirm this.

Within the stratum from 35 to 64 km, the fully developed easterly flow in January and July is maximum in the layer between 45 and 50 km. However, the fully developed westerly flow maximum occurs somewhere above 64 km. In general, both east and west winds reach their maximum value at high altitudes sooner than at low altitudes. This is shown by both Figs.

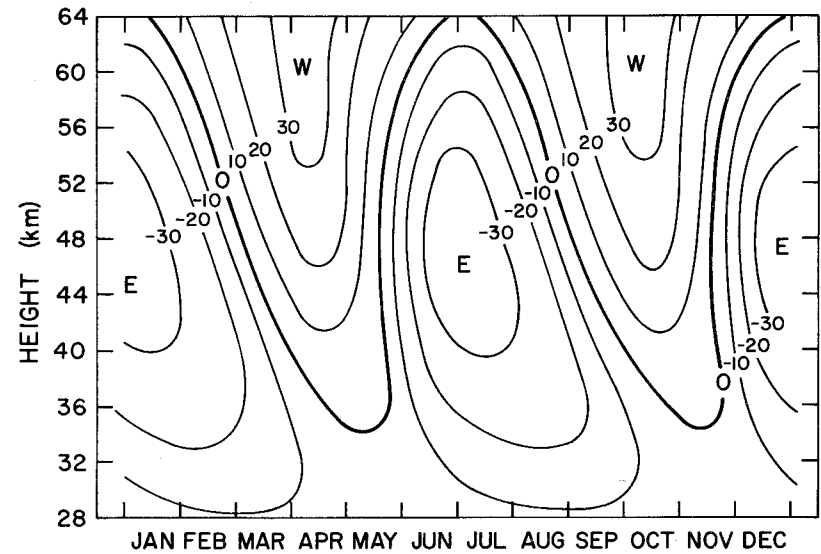


Fig. 17. Estimated variation of zonal wind with month and altitude at the equator. After Reed (9).

16 and 17. The semiannual phase curve in Fig. 16 shows that the time of maximum westerly flow occurs about two weeks after the equinoxes at 50 km and about a month after the equinoxes at 35 km.

Unlike the quasi-biennial oscillation below it, the semiannual oscillation fits into the annual oscillation to poleward in both the summer and winter hemispheres in a predictable way. Viewed most simply, the westerlies are an extension of the winter hemisphere west winds over the equator. Thus, following the spring equinox in the northern hemisphere, the equatorial, semiannual westerlies are part of the southern hemisphere, mesospheric, west wind system. Similarly, following the northern hemisphere fall equinox, the equatorial, semiannual westerlies are part of the northern hemisphere, mesospheric, west wind system.

The equatorial, semiannual easterlies may also be viewed as an extension of the summer hemisphere easterlies into equatorial regions. Indeed, Fig. 9 shows equatorial easterly winds from about 35 to 60 km as an extension of the summer hemisphere, high level easterlies. Reed (9) has some evidence to support the existence of a small easterly jet stream near 15° of latitude in the summer hemisphere, however. The existence of

such a jet will cause the easterly winds to increase in strength toward the pole on the summer hemisphere side of the equator, reach a maximum at about 15° , decrease to perhaps 20° , and then increase again as the summer, middle-latitude easterly wind maximum is approached.

4. Middle Latitude Vertical Structure in the Free Atmosphere

Some typical wind soundings for White Sands, New Mexico, are shown in Fig. 18. All of them show a stratum of relatively strong west winds in the vicinity of the tropopause, between 12 and 16 km. They also show a stratum of minimum wind speed near 20 km, but there the similarity ends. At higher levels the strong stratospheric westerlies are quite evident in the winter (Nov.) sounding, the summer easterlies are clearly shown in the summer (Aug.) sounding, and the light variable stratospheric winds so typical of the transition period are shown by the Sept. sounding. Note that the westerlies are established at high levels on 25 Sept.

The wind profiles shown in Fig. 18 are smoothed curves which show only the major features of the vertical profile. There are many perturbations having vertical dimensions of the order of one kilometer or less which are not measured by most sounding techniques. The profiles of Fig. 18

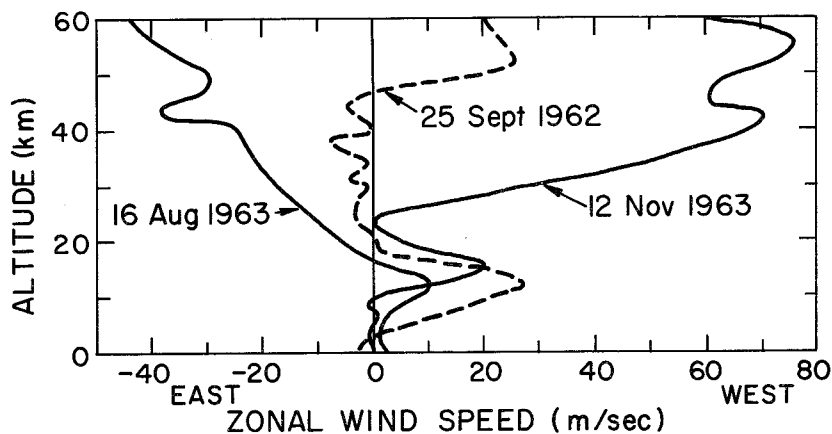


Fig. 18. Selected zonal wind profiles for the White Sands Missile

Range, New Mexico.

show that relatively strong vertical wind shear exists through deep layers above and below the wind maximum at 12 to 16 km. The shear is strongest just below and above the jet stream core where the speed is also greatest, and according to Endlich, et al. (12) in the mean the speed decays nearly linearly above and below the level of maximum speed, reaching a speed equal to one-half the maximum speed in a distance of about 5 km. Thus, the shear through a deep layer near the jet core is proportional to the wind speed at the jet core.

Both wind speed and shear are important in scientific ballooning.

Strong winds cause rapid movement of a balloon during ascent and may carry it beyond effective control from the launch site much sooner than is desirable. Strong wind shear has been suspected of causing balloon failure during ascent. (See Section II for a discussion of wind shear on an ascending balloon.) The flight of large balloon systems through strong jet streams should be avoided.

Shear in the free atmosphere has also been studied by Essenwanger (13) and (14), Weinstein, et al. (15), and Adelfang (16). Their studies included shear through thin layers and showed that very strong shear may

occur in thin strata. Essenwanger (13) proposed that the magnitude of the mean vector wind shear \bar{w} , may be expressed as a function of the height increment, ΔH , through which the shear occurs by means of an equation of the form

$$\bar{w} = a_0 (\Delta H)^{a_1} \quad (19)$$

where a_0 and a_1 are arbitrary constants. He also proposed that the standard deviation of the shear vector, σ_w , may be expressed in the following way

$$\sigma_w = a_2 (\Delta H)^{a_3} + D \quad (20)$$

where a_2 , a_3 , and D are all arbitrary constants.

Adelfang (16), using accurate wind data from the test ranges at Cape Kennedy, Florida, and Point Mugu, California, found that D may be considered negligible and that a_0 , a_1 , a_2 , and a_3 all vary with height and perhaps with season. Nonetheless, $a_0 = a_2$ and $a_1 = a_3$, approximately. This essential equality of the mean and the standard deviation is convenient because the extreme may then be taken as four times the mean, i.e., $(\bar{w} + 3\sigma_w)$. Doing so implies that the shear is normally distributed about the mean.

It is not, but estimates made in this way using Eq. (22) are well outside of the envelope of the data presented by Weinstein, et al. (15), and they are comparable in layers 200-1000 m thick with values estimated by a formula for extreme values given by Essenwanger (14).

The constants in Eqs. (21) and (22) are estimated from the 12-14 km region of Adelfang's (16) graphs. Equation (21) fits the mean data of Weinstein, et al. (15) relatively well. Equations (21) and (22) are believed to provide mean and extreme shear data, respectively, which are suitable for planning purposes for flights in middle latitudes.

$$\frac{\bar{w}}{\Delta H} = 0.12 (\Delta H)^{-0.4} \quad (21)$$

$$\frac{w_e}{\Delta H} = 0.48 (\Delta H)^{-0.4} \quad (22)$$

As written, Eqs. (21) and (22) yield values having the dimension of sec^{-1} , but it is more meaningful to think of shear in terms of (m/sec)/m or (ft/sec)/ft. As long as the length units in velocity are consistent with the length units in height, the equations are valid.

5. Boundary Layer

The wind structure in the lowest 200 meters above the surface is of great interest during inflation and launch. Discussions of the theory of the variation of wind with height near the surface may be found in Priestly (17) and Lumley and Panofsky(18). In general, the shape of the wind profile is a function of the roughness of the surface, the mean wind speed, and the change of temperature with height.

The wind speed profile that has the best theoretical foundation is a generalized profile which is logarithmic in height. A profile which fits observed data relatively well and is simple to use is called a power-law profile. It may be expressed by an equation of the form

$$\left(\frac{\bar{v}}{\bar{v}_1}\right) = \left(\frac{z}{z_1}\right)^b \quad (23)$$

in which \bar{v} and \bar{v}_1 are the mean winds (averaged over a short time from a few minutes to an hour) at heights z and z_1 above the surface, respectively;

b is a constant for each profile which may take values from 0 to 1.0

depending on the lapse rate of temperature through the stratum from the surface to level z and the roughness of the surface. If z_1 is the height above the surface of an anemometer at which \bar{v}_1 is measured, and if b is

known or can be estimated, the speed of the wind at any level z may be approximated from Eq. (23). Figure 19 is a graphical solution of Eq. (23). The scale at the top of the graph shows a relationship between b and dT/dz which is adapted from Frost (19). It is valid when the terrain is relatively level and vegetation is short. The value of b should be increased by about 0.1 to correct for wooded or rough terrain.

It must be emphasized that the power-law profile can provide only a rough approximation to the real wind profile. Ideally, the anemometer level z_1 should be as near as possible to the level of greatest interest. If winds are measured at two levels, b may be determined directly from Fig. 19, or it may be calculated since $b = \log(v_2/v_1)/\log(z_2/z_1)$. Normally, with one measurement near or above 10 m, the power-law approximation is useful through a stratum up to 200 m deep.

The value of b undergoes a readily discernible diurnal variation. This is associated with the static stability of the air in the boundary layer; hence, it is associated with changes in the value of dT/dz . Large values of dT/dz occur on clear nights when the mean wind speed is low. Low values occur at the time of maximum heating, usually in the early after-

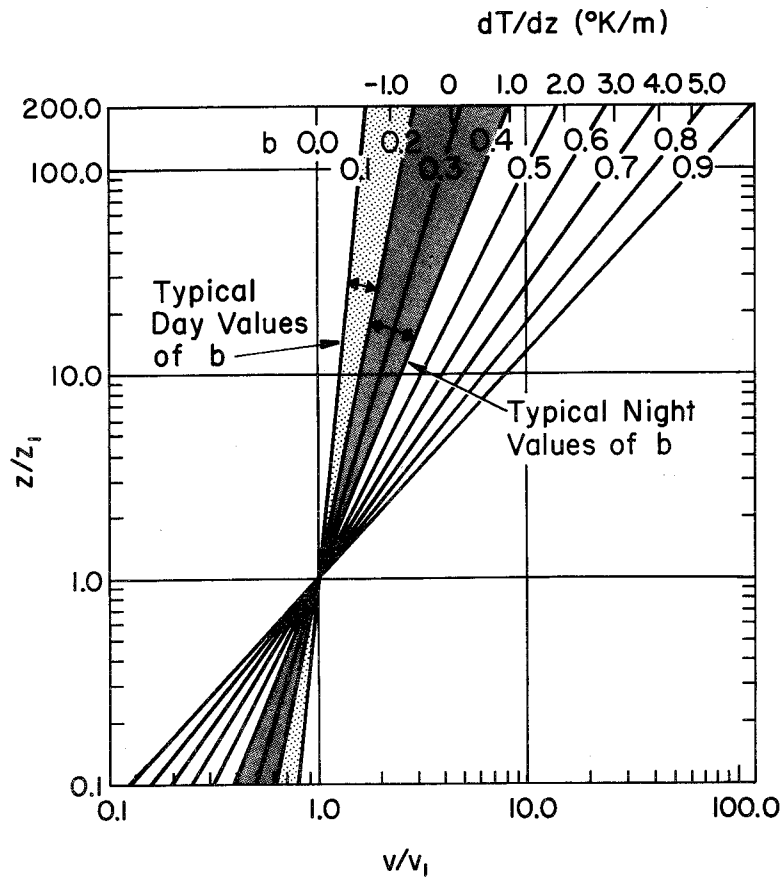


Fig. 19. Dimensionless wind profiles according to the power-law. The value of b may be estimated from the scale at the top if dT/dz is known; add 0.1 to the value of b estimated from dT/dz if the terrain is rough or wooded.

noon. The ranges of typical day and night values of b are indicated on

Fig. 19.

6. Low-Level Jet

A phenomenon which occurs commonly in the Great Plains area of the United States is called a low-level jet or nocturnal jet. Figure 20, from Bonner, et al. (20), is a mean cross section of the winds through the core of a well developed low-level jet. The section, taken normal to the axis of the jet, shows isotachs of wind along the axis and normal to it. Clearly, the wind vector is directed nearly parallel to the jet axis. The most remarkable feature of the jet is its diurnal variation. It appears at night and disappears early the following day.

Other features of the low-level jet which are shown by Fig. 20 are its very small vertical extent, the proximity of the core to the surface, and the strong vertical wind shear under the jet. The vertical wind shear about the jet core is shown more directly by Fig. 21. An important feature which is not obvious from Fig. 20 is the wafer-like character of the jet. Note that the 12 m/sec isotach encloses an area which is about 1.7 km thick and 650 km wide. Figure 22 shows it to be well over 1600 km long.

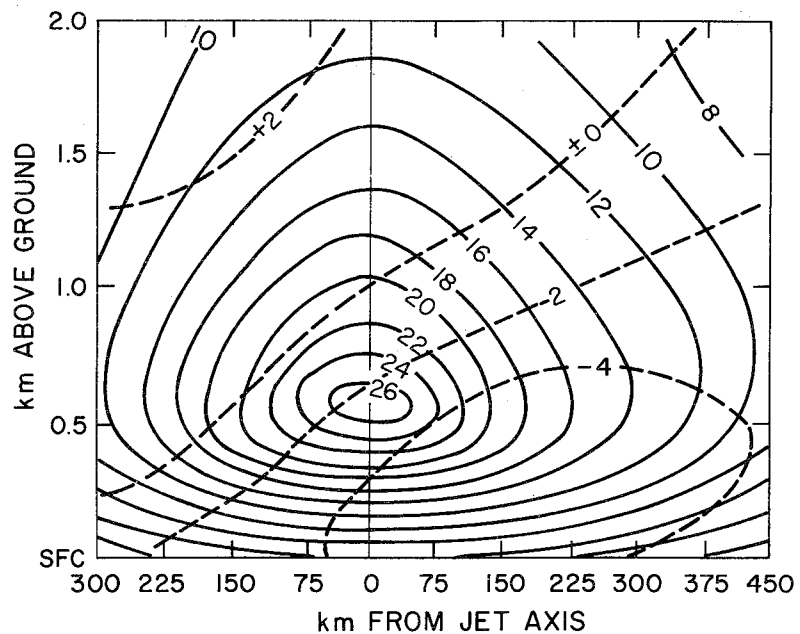


Fig. 20. Mean cross section of the wind associated with a low-level jet, from Bonner et al. (20). The solid lines are isotachs of the wind component parallel to the jet axis; dashed lines are isotachs of the normal component.

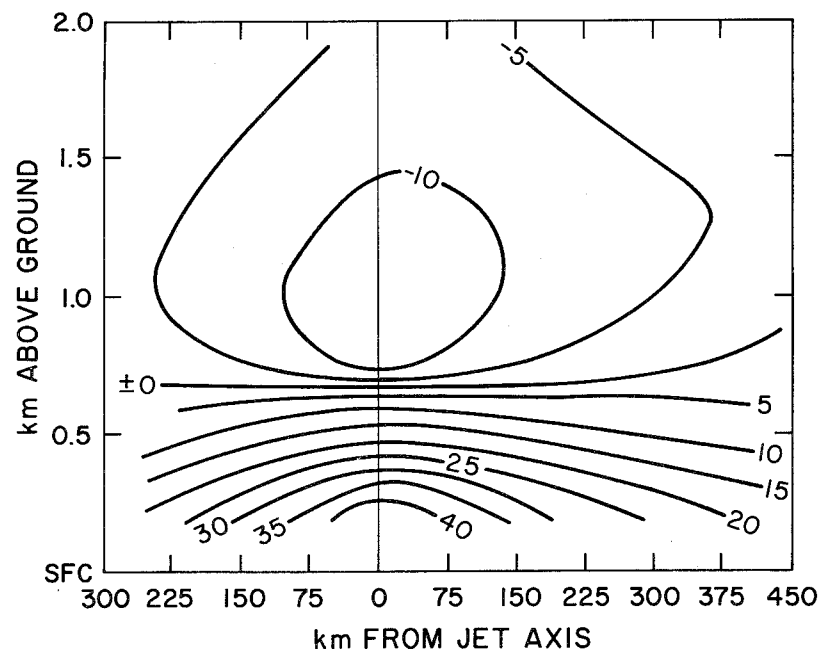


Fig. 21. Average vertical wind shear (m/sec km) in a vertical cross section normal to the core of the jet, after Bonner et al. (20).

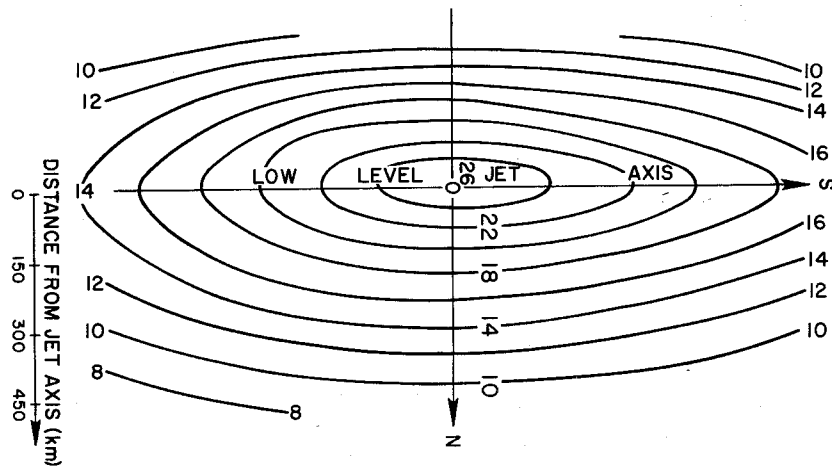


Fig. 22. Mean wind component along the jet axis at the 0.5-km level, after Bonner et al. (20).

The diurnal oscillation of the low-level jet is nearly opposite in phase to the surface wind oscillation. Winds at the level of the jet core reach maximum speed early in the morning (0000-0600 local standard time) and minimum speed in the afternoon. At the time of maximum development, the wind profile under the jet core is approximated satisfactorily for balloon flight planning by Eq. (23) if a value of 0.35 is used for b . The maximum wind shear under the jet core also falls within the values given by Eq. (22) for extreme shear in the free atmosphere.

The low-level jet appears to reach a high state of development in summer in the central Great Plains area of the United States, but diurnal wind variations at low levels which shared most of the features associated with the low-level jet were observed throughout most of the United States in July 1958 by Hering and Borden (21). Also, Rider and Armendariz (22) have reported many well-developed low-level jets in the valley between the Organ and San Andres mountains on one side and the Sacramento mountains on the other in New Mexico. Theory (which is inadequate to explain many features of the jet) and observation suggest that if the mean circulation in the lower troposphere is changing little from day to day in middle latitudes

in summer and if the hydrostatic stability of the boundary layer is undergoing marked diurnal changes, a phenomenon akin to the low-level jet should be expected.

E. OTHER METEOROLOGICAL VARIABLES, DATA SOURCES

The thermal structure of the whole atmosphere and its circulation have been described briefly in C and D of this section. To attempt to describe global cloudiness or visibility in a meaningful way is not feasible here. The same is true of most of the other atmospheric properties which may affect a scientific ballooning operation. However, once the proposed site for a balloon flight has been localized to a few areas, a competent meteorologist can usually find climatological data for those areas, from which he can answer most planning needs. Studying the climate of an area also gives a meteorologist a better perspective of day-to-day weather in the area and is helpful in making an operational forecast.

The following list of sources of data is not complete, but the sources listed do provide much valuable, summarized data useful to a meteorologist. Others may also find much of value in them, but they can be misleading if

they are not properly interpreted. General data summaries are listed first, and more specialized summaries are listed later.

Handbook of Geophysics, Rev. Edition. Published initially by the U.S. Air Force in 1957 and in revised form by The Macmillan Company in 1961, this volume is an excellent source of geophysical data. It also contains much explanatory material which helps the reader to understand and interpret the data.

U.S. Naval Weather Service World Wide Airfield Summaries. Most meteorological data in recent decades have been observed at airfields. These summaries provide that data in highly usable form. Volume I covers Southeast Asia; Vol. II--Part 1 and Part 2--the Middle East; Vol. III, the Far East; Vol. IV, Canada, Greenland, and Iceland; Vol. V, Australia and Antarctica; Vol. VI--Part 1 and 2--South America; Vol. VII, Central America; Vol. VIII--Parts 1 through 8--the United States. These summaries are available from the Federal Clearinghouse for Scientific and Technical Information, Springfield, Va. 22151.

U.S. Navy Marine Climatic Atlas of the World. This atlas in seven volumes provides highly useful summaries of weather information for all

the world's oceans. The volumes and the area covered by each are:

Vol. I, North Atlantic; Vol. II, North Pacific; Vol. III, Indian Ocean;

Vol. IV, South Atlantic; Vol. V, South Pacific; Vol. VI, Arctic; Vol.

VII, Antarctic. These may be obtained from the U.S. Navy Weather

Service Command MOIA, Washington Navy Yard, Bldg. 200, Washington,

D.C. 20390.

Climatic Atlas of the United States. This atlas, published by the U.S. Department of Commerce, contains many useful climatic charts of the United States. It is available from the U.S. Government Printing Office, Washington, D.C. 20401.

Selected Level Temperatures and Dew Points for the Northern Hemisphere. This is a collection of monthly mean Northern Hemisphere temperature and dew point charts for selected levels up to and including the 100-mb level. It is available from the U.S. Naval Weather Service Command MOIA, Washington Navy Yard, Bldg. 200, Washington, D.C. 20390.

Climate of the Upper Air, Part 1--Southern Hemisphere. Planned as a four-volume series, the first volume was published in September 1969. It contains monthly mean temperatures, dew points, and heights

at selected pressure levels up to and including the 100-mb level for some variables. Later volumes are to contain geostrophic wind data and meridional cross sections of temperature, dew point, and isobaric height.

Volume I may be obtained from U.S. Naval Weather Service Command MOIA, Washington Navy Yard, Bldg. 200, Washington, D.C. 20390.

Upper Wind Statistics Charts of the Northern Hemisphere.

Vol. I (850-, 700-, and 500-mb levels)

Vol. II (300-, 200-, and 100-mb levels)

These volumes show charts of wind vectors and vector standard deviations. This method of presentation concentrates information tremendously, but to recover the information, the user must have a good understanding of the basis and limitations of the data presentation technique. Instructions are provided.

These volumes may be obtained from U.S. Naval Weather Service Command MOIA, Washington Navy Yard, Bldg. 200, Washington, D.C. 20390.

Data Report Meteorological Rocket Network Firings. These reports contain data from the U.S. meteorological rocket network. Data are

shown in both graphical and tabular form. The reports, covering data for the fall of 1959 through December 1963, were prepared by the U.S. Army Electronics Research and Development Activity, White Sands Missile Range, New Mexico. The data of January 1964 through December 1968 were prepared by the World Data Center A for Meteorology, which is located at the National Climatic Center of the National Oceanic and Atmospheric Administration, Asheville, North Carolina 28801.

High Altitude Meteorological Data. Beginning with the January 1969 data, the World Data Center A for Meteorology started publishing monthly reports of all types of high altitude meteorological data, including U.S. and other rocket data. These reports are available from the Superintendent of Documents, Government Printing Office, Washington, D.C. 20402.

Exametnet Data Report Series Annual Reports. These annual reports contain data from the Experimental Inter-American Meteorological Rocket Network. Published by The National Aeronautics and Space Administration, they are available from the Clearinghouse for Federal Scientific and Technical Information, Springfield, Va. 22151.

Weekly Synoptic Analyses, 5-, 2-, and 0.4 Millibar Surfaces.

The Upper Air Branch of the U.S. National Meteorological Center, using data from the rocket network and rawinsonde data with elaborate extrapolation techniques, prepares weekly analyses at high levels which are a valuable source of information to a meteorologist who must support scientific ballooning operations. Unfortunately, the analyses are not available until months after the data are observed; therefore, they serve as a tool for learning about the behavior of the high atmosphere, but not as a forecasting tool. Inquiries about these reports may be addressed to The Upper Air Branch, National Meteorological Center, National Oceanic and Atmospheric Administration, Washington, D.C.

Special Data Summaries. The National Climatic Center of the National Oceanic and Atmospheric Administration at Asheville, North Carolina 28801, can provide special data summaries upon request. The cost of such a summary can be high, and a careful review of requirements with personnel at the Center is well worthwhile before a summary is ordered.

F. FORECASTS

A meteorologist can make a completely successful forecast for an operation only if he understands the operation well enough to know how it is sensitive to the weather, has adequate current meteorological data, and has a thorough understanding of the atmosphere and its behavior.

In B of this section an attempt has been made to show how balloon operations are affected by the weather. It can serve as a starting point for both the meteorologist and operations personnel when a balloon flight is being planned, but as flight techniques and requirements change, meteorological and support requirements will also change. Therefore, they should be reviewed before each flight. Having the meteorologist serve as an active member of the operations team throughout the flight planning and execution is one way to assure that he or she understands support requirements.

Most experienced airways forecasters who have been briefed on balloon flight requirements will be able to make adequate forecasts for launch and recovery operations. They will also be able to forecast for the operation of a tracking aircraft. These aspects of balloon flight operations occur in the lower troposphere where data are most available and where data analyses

are most carefully performed.

Only one who has devoted much study to the middle and upper stratosphere can analyze the extremely limited data at those levels and make an acceptable forecast from them. A local forecast office may be able to provide some high level data, but often it can do that only if special arrangements are made in advance. Also, the computation of ascent and descent vectors, although conceptually simple, is not a part of the service normally offered by a local forecast office. Furthermore, high level wind forecasts must be made before ascent and descent vectors can be computed. Consequently, this computation must be done by a specialist if it is to be done well.

G. OPERATIONAL PLANNING

It is important that an experienced balloon meteorologist be consulted before deciding on an operational plan for any but the most routine balloon flights. By fitting the requirements of the operation into the optimum atmospheric environment, a knowledgeable operations analyst can reduce the probability of failure and, indeed, make a close estimate of the feasibility of an operation. He can often suggest minor modifications of the original requirements which will improve the cost-effectiveness of the operation.

Because most scientific balloon flights are conducted in middle latitudes and a successful flight depends so much on the winds, the following rather specific thoughts are offered.

The stratospheric easterlies in summer are the scientific balloonists' best friend. They are the steadiest winds known, and during the season in which they blow, one can launch a balloon a considerable distance upwind from a target area (~ 120 km) with reasonable confidence that it will cross the target meridian in a given time and that the crossing will be practically over the target. The optimum months for such flights are July and August at latitude 35°N, somewhat earlier farther north, and later farther south, at any altitude above 25 km. Long-range flights, even round-the-world flights, can be planned with the aid of these winds with excellent prospects of recovery.

In the stratospheric westerlies in winter, transcontinental flights of up to three days' duration from United States west-coast sites, and one-or two-day-duration flights from sites farther east can be achieved. Winter ballooning in temperate latitudes is severely limited, however, by unfavorable surface weather. Also, west-coast sites, in particular, are inoperative

for several weeks during periods of circulation reversal. These winds, unlike the easterlies, are often characterized by waves of great amplitude so that tracking and recovery facilities must be very flexible.

The stratum of minimum winds found at about 20 km may be used to good advantage, especially in the spring and fall, for long duration flights of limited horizontal displacement. Experience has shown that although the vector mean wind may be zero, the scalar winds at these levels are never really zero, and they meander with a minimum speed of about 6 m/sec.

Hovering flights are also feasible in the early summer. In these flights, the balloon rises during the daytime to the edge of the easterlies and descends at night into the light westerlies below. Such flights require careful planning and coordination.

REFERENCES

- (1) U.S. Standard Atmosphere, 1962: U.S. Government Printing Office, Washington, D. C., pp. 278.
- (2) U.S. Standard Atmosphere Supplements, 1966: U.S. Government Printing Office, Washington, D. C., pp. 289.
- (3) Haltiner, George J. and Frank L. Martin, 1957: Dynamic and Physical Meteorology, McGraw-Hill, New York, p. 164.
- (4) Glueckauf, E., 1951: The Composition of Atmospheric Air, Compendium of Meteorology, edited by Thomas F. Malone, American Meteorological Society, Boston, Mass., p. 3.
- (5) Palmén, E. and C. W. Newton, 1969: Atmospheric Circulation Systems, Academic Press, New York and London, pp. 603.
- (6) Solot, Samuel B. and Eugene M. Darling, Jr., 1958: Theory of Large Scale Atmospheric Diffusion and its Application to Air Trajectories, Vols. I and II. Geophysical Research Paper No. 58, U.S. Air Force Cambridge Research Laboratory, Bedford, Mass.
- (7) Anonymous, 1971: Weekly Synoptic Analyses 5-, 2-, and 0.4-Millibar Surfaces for 1968, NOAA Technical Report NWS 14.
- (8) Reed, Richard J., 1965: The Present Status of the 26-Month Cycle, Bulletin of the American Meteorology Society, Vol. 46, No. 7, 374-387.
- (9) Reed, Richard J., 1966: Zonal Wind Behavior in the Equatorial Stratosphere and Lower Mesosphere, Journal of Geophysical Research, Vol. 71, No. 18, 4223-4233.

- (10) Belmont, A. D. and D. G. Dartt, 1966: The Non-Repeating Variations of the Observed Wind in the Equatorial Stratosphere, Tellus XVIII, 2, 381-390.
- (11) Kriester, Barbara, 1971: Large Scale Circulation Patterns of the Stratosphere. A paper presented at the SPARMO Colloquium on The Technology and Utilization of Stratospheric Balloons, Seattle, Wash., June 1971.
- (12) Endlich, R. M., S. B. Solot and H. A. Thur, 1955: The Mean Vertical Structure of the Jet Stream, Tellus 7, 308-313.
- (13) Essenwanger, O., 1963: On the Derivation of Frequency Distributions of Vector Wind Shear Values for Small Shear Intervals, Geofis. Pura. Appl. 56, 216-224.
- (14) Essenwanger, O., 1967: Comments on "Mesoscale Structure of 11-20 km Winds," Journal of Applied Meteorology, Vol. 6, No. 3, 591-593.
- (15) Weinstein, A. I., E. R. Reiter and J. R. Scoggins, 1966: Mesoscale Structure of 11-20 km Winds, Journal of Applied Meteorology, Vol. 5, No. 1, 49-57.
- (16) Adelfang, Stanley I., 1971: On the Relations Between Wind Shears over Various Altitude Intervals, Journal of Applied Meteorology, Vol. 10, No. 1, 156-159.
- (17) Priestly, C. H. B., 1959: Turbulent Transfer in the Lower Atmosphere, University of Chicago Press, Chicago, Ill.
- (18) Lumley, John L. and Hans A. Panofsky, 1964: The Structure of Atmospheric Turbulence, Interscience Publishers, New York, 99-118.
- (19) Frost, R., 1948: Atmospheric Turbulence, Quarterly Journal, Royal Meteorological Society, Vol. 74, 316-338.

- (20) Bonner, W. D., S. Esbensen and R. Greenberg, 1968: Kinematics of the Low-Level Jet, Journal of Applied Meteorology, Vol. 7, No. 3, 339-347.
- (21) Hering, Wayne S. and Thomas R. Borden, Jr., 1962: Diurnal Variations In the Summer Wind Field over the Central United States, Journal of the Atmospheric Sciences, Vol. 19, No. 1, 81-86.
- (22) Rider, Laurence J. and Manuel Armendariz, 1970: Nocturnal Maximum Winds in the Planetary Boundary Layer at WSMR, Tech. Report ECOM 5321, U.S. Army Electronics Command, Fort Monmouth, N.J.

SECTION XII

TABLES, GRAPHS, AND MISCELLANEOUS INFORMATION

by

Alvin L. Morris

List of Figures iii

List of Tables v

A. INTRODUCTION 1

B. CROSS SECTIONAL AREA OF A BALLOON 2

C. BALLOON ROTATION 6

D. BALLOON SYSTEM PENDULATION 9

1. Simple Pendulum 9

2. Compound Pendulum 14

3. Torsional Pendulum 16

 REFERENCES 21

E. GAS FLOW THROUGH AN ORIFICE 22

F. VERTICAL CUTOFF RIGIDITY 24

 REFERENCES. 26

G. LANDING ENERGY ABSORBERS 27

1. Landing Energy 27

2. Energy and Acceleration 27

3. Energy Absorbers 29

4. Horizontal Motion 40

 REFERENCES. 45

H. PARACHUTE COMPUTATIONAL AIDS 46

1. Selecting a Parachute 46

2. Terminal Velocity and Time of Descent 50

I. GAS MEASUREMENT AND INFLATION PROCEDURES 58

J. GAS DATA 78

1. Miscellaneous Gas Data 79

 REFERENCES 80

2. Gas Constant and Specific Heat Data for Selected Gases 81

 REFERENCES 89

3. Thermal Conductivity of Selected Gases 90

 REFERENCES 96

4. Viscosity of Selected Gases 97

 REFERENCES 103

5. Prandtl Number of Selected Gases 104

 REFERENCES 108

K. SPECIFIC LIFT OF HELIUM AND HYDROGEN AND PROPERTIES OF THE
 U.S. STANDARD ATMOSPHERE, 1962 109

 REFERENCES 119

L. BASIC NATURAL-SHAPE BALLOON PARAMETERS 120

M. BUOYANT EQUILIBRIUM DIAGRAMS 128

N. SUNRISE AND SUNSET 131

O. STAR CHARTS. 133

List of Figures

Fig. B-1	Area of a sphere-on-cone figure projected on a plane normal to the vector \vec{v}_r	3	Fig. H-1a	Sea level terminal velocity of a parachute system as a function of system mass and the product of parachute area and drag coefficient.	54
Fig. B-2	Sketch of a partially inflated balloon which has formed a spinnaker-like sail in a relative wind represented by the vector \vec{v}_r	5	Fig. H-1b	Sea level terminal velocity of a parachute system as a function of system weight and the product of parachute area and drag coefficient.	55
Fig. C-1	Rotation data for large balloon systems. For any point on a curve, rotation rates less than or equal to the abscissa value of the point were observed to occur with the percentage frequency of the ordinate value of the point	7	Fig. H-2	Diameter of a parachute as a function of area and drag coefficient. Diameter is nominal diameter if the pseudo drag coefficient is used. The following are typical pseudo drag coefficients: $C_D' = 0.75$ (design value often quoted for a flat, circular canopy), $C_D' = 0.85$ (empirical value used by NCAR for large flat, circular canopies), and $C_D' = 0.55$ (value quoted by Raven Industries, Inc. for their RAVEN PLUS $\text{\textcircled{R}}$ shape).	56
Fig. D-1	A sketch of a balloon system showing the nomenclature used in considering the system as a pendulum	10	Fig. H-3	Terminal velocity and time of descent as functions of sea level terminal velocity and altitude in the <u>U.S. Standard Atmosphere, 1962</u>	57
Fig. D-2	A balloon payload acting as a compound pendulum	15	Fig. I-1	Relationship between p_c , p_l , and p_f	65
Fig. D-3	Torsional pendulum model of a balloon system	17	Fig. M-1	Buoyant equilibrium diagram for helium	129
Fig. F-1	Vertical cutoff rigidity. The curves are isolines of vertical cutoff rigidity in gigavolts.	25	Fig. M-2	Buoyant equilibrium diagram for hydrogen	130
Fig. G-1	Typical stress-strain curve for paper honeycomb.	30	Fig. O-1	Northern Hemisphere star chart	135
Fig. G-2	Rod and die energy absorber	32	Fig. O-2	Southern Hemisphere star chart	136
Fig. G-3	Plan view (upper) and side view of a single layer of a crush pad made of sections of honeycomb between light, rigid plates.	39			
Fig. G-4	A multilayer honeycomb crush pad bound by vertical cables-- before and after landing	42			

List of Tables

Table G-1 Paper honeycomb strength data	38
Table I-1 Lift (kg/m^3) of gas contained in steel cylinders--helium . . .	66
Table I-2 Lift (lb/ft^3) of gas contained in steel cylinders--helium . . .	68
Table I-3 Lift (kg/m^3) of gas contained in steel cylinders--hydrogen . . .	72
Table I-4 Lift (lb/ft^3) of gas contained in steel cylinders--hydrogen . . .	74
Table J-1 Miscellaneous gas data.	85
Table J-2 Constants for the specific heat-temperature correlating equation.	86
Table J-3 Gas constant R in various systems of units	87
Table J-4 Value of C_p/R for select gases as a function of temperature . . .	88
Table J-5 Values of C_p/C_v for select gases as a function of temperature . . .	89
Table J-6 Values of n for select gases.	93
Table J-7 Values of k_o for selected gases	93
Table J-8 Thermal conductivity ratios for selected gases as a function of temperature.	95
Table J-9 Values of S for selected gases	99
Table J-10 Values of μ_o for selected gases	101
Table J-11 Values of μ/μ_o for selected gases as a function of temperature. . .	102
Table J-12 Constants for the Prandtl number-temperature correlating equation	106
Table J-13 Prandtl number for selected gases as a function of temperature. . .	107
Table K-1 Specific lift of helium and hydrogen and properties of the <u>U.S. Standard Atmosphere, 1962</u>	113
Table L-1 Balloon design parameters	122

TABLES, GRAPHS, AND MISCELLANEOUS INFORMATIONA. INTRODUCTION

This section contains information which is useful in the practice of scientific ballooning but was not deemed appropriate for inclusion in any of the other sections. Each topic is essentially complete and unrelated to the others in the section; the topics are arranged arbitrarily. Tables, figures, and equations are number sequentially within each principal sub-section with letter prefixes corresponding to the sub-section. Each sub-section lists its own literature references.

B. CROSS SECTIONAL AREA OF A BALLOON

The form of a tethered balloon and of a balloon in normal flight may be approximated by the sphere-on-cone shape shown in Fig. B-1. The radius r is the radius of a sphere whose volume is equal to the volume of the gas. The value of θ is controlled in a tethered balloon and is known. For a balloon in flight, θ may take a value as low as 15° when the balloon is only slightly inflated; when the balloon is fully inflated, it will be the nadir (base) angle of the balloon (see Sections V and XII.L).

The area A_D of a sphere-on-cone figure projected on a plane normal to the relative wind is

$$A_D/r^2 = \pi + \left[\sin \cos^{-1} \left(\frac{\sin \theta}{\sin b} \right) \right] \left[\left(\cot^2 \theta - 1 + \frac{\sin^2 \theta}{\sin^2 b} \right)^{\frac{1}{2}} \right. \\ \left. \sin \left(b - \tan^{-1} \frac{\tan^2 \theta}{\tan b} \right) + \frac{\sin \theta}{\sin b} \right] - \cos^{-1} \left(\frac{\sin \theta}{\sin b} \right) \quad (B-1)$$

where b is defined by Fig. B-1. When $b < \theta$, let $\sin \theta / \sin b = 1.0$.

A graph of this equation is also presented in Fig. B-1.

The equation

$$\frac{A_D}{r^2} = \pi + \left(\theta - \frac{\pi}{2} + \cot \theta \right) \sin b \quad (B-2)$$

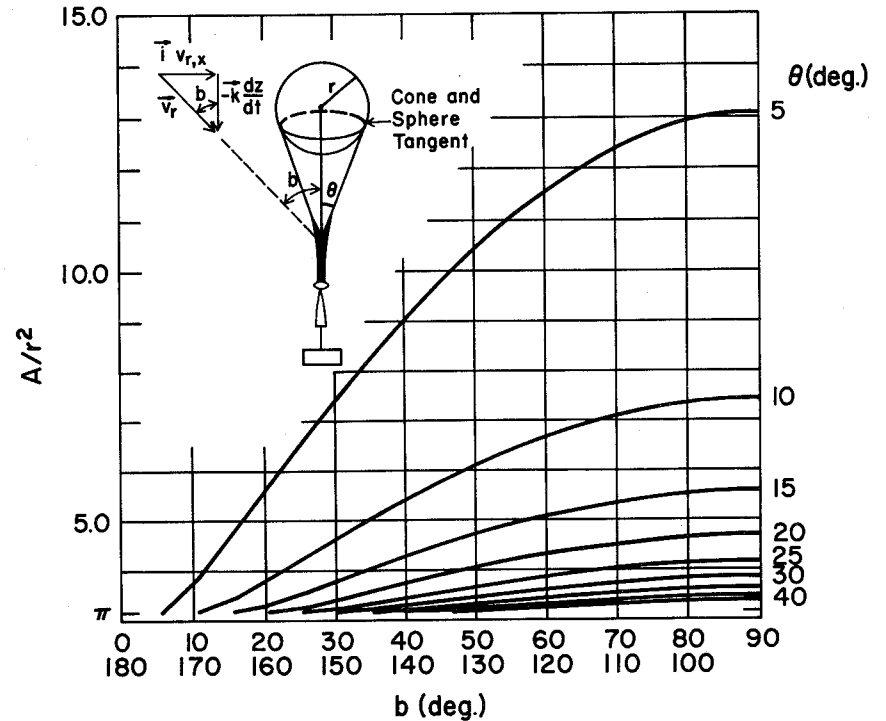


Fig. B-1. Area of a sphere-on-cone figure projected on a plane normal to the vector \vec{v}_r .

is much simpler, and for most ballooning calculations it provides an adequate means of approximating A_D .

A balloon which has formed a sail is shaped much like a hemispherical cup with the concave side facing into the wind. Figure B-2 depicts a balloon which has "sailed." The equation

$$A_D = 1.21 V_i^{2/3} \left(\frac{1 + \sin b}{2} \right) \quad (\text{B-3})$$

may be used to approximate A_D for such a balloon. In this case V_i is the nominal, fully-inflated volume of the balloon.

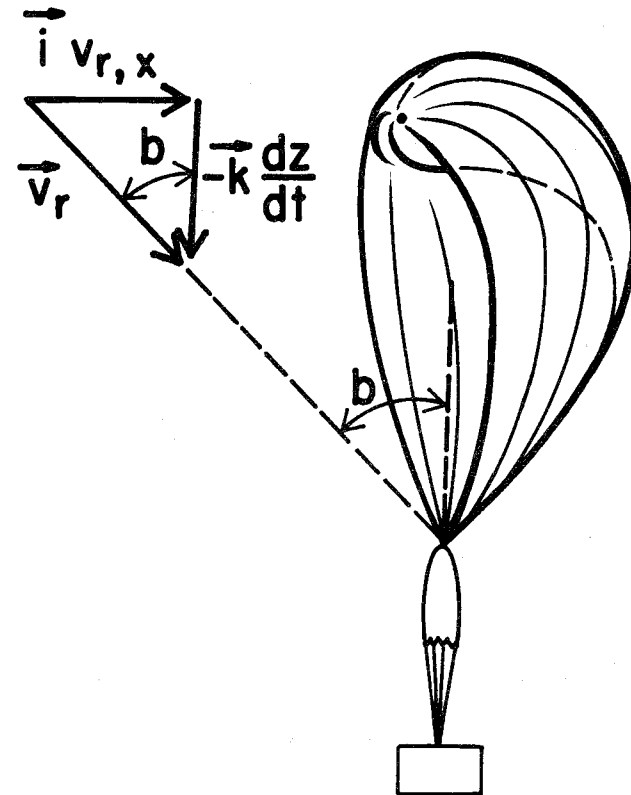


Fig. B-2. Sketch of a partially inflated balloon which has formed a spinnaker-like sail in a relative wind represented by the vector \vec{v}_r .

C. BALLOON ROTATION

A balloon is set in rotation about its vertical axis during ascent by the relative downward motion of the air past it. Even when a balloon is floating, it often oscillates up and down with a period of a few minutes (see Section II.I.4), and either this motion or the turbulent motion of the ambient air is enough to cause rotation.

Rotational data from five flights are summarized by the curve marked "FLOAT" in Fig. C-1. One balloon floated at 22 km, two at 37 km, one at 39 km, and one at 40 km. The data are not adequate to permit the rotation rate to be related quantitatively to float altitude, but they do suggest that balloons floating at greater heights rotate less than balloons at lower heights. The curve for floating balloons can be fitted quite well by the empirical equation

$$y = 100 \left(\tanh \frac{x}{22} \right)^{\frac{1}{2}} \quad (C-1)$$

where y is the percentage frequency of occurrence of rotation rates of x deg/min or less.

The curve marked "ASCENT" summarizes ascent rotational data up to 150 deg/min for three flights. All of the balloon systems rose to heights of 37

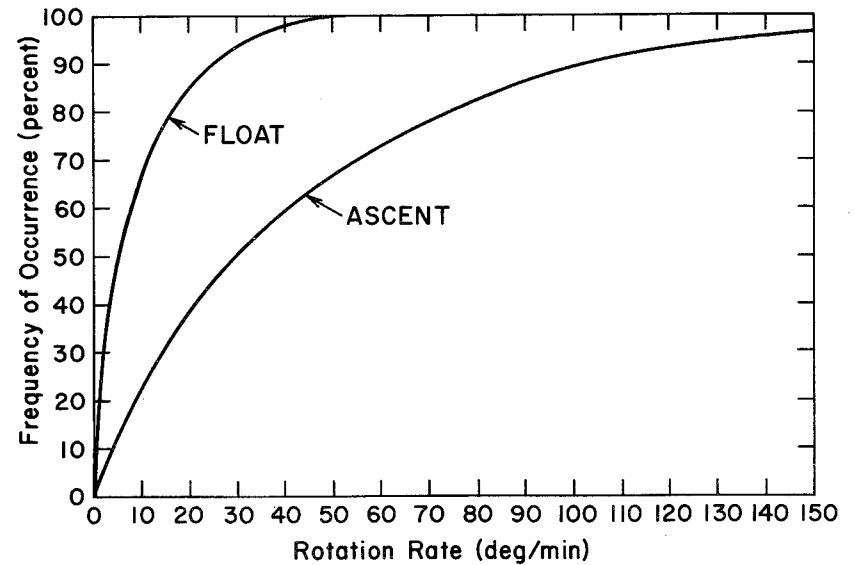


Fig. C-1. Rotation data for large balloon systems. For any point on a curve, rotation rates less than or equal to the abscissa value of the point were observed to occur with the percentage frequency of the ordinate value of the point.

km or more, and no systematic variation from flight to flight was noted.

The data are fitted well for all rotation rates by the empirical equation

$$y = 100 \left[\tanh \frac{x^2}{94(x+8)} \right]^{\frac{1}{2}} \quad (C-2)$$

The maximum angular acceleration observed on any of the flights was $2.5 \times 10^{-2} \text{ deg/sec}^2$, averaged over a two-minute period. This occurred during ascent when the vertical speed of the balloon was large and the moment of inertia of the system was relatively small.

D. BALLOON SYSTEM PENDULATION

1. Simple Pendulum

The longitudinal (vertical) axis of a large, fully-inflated balloon with a payload suspended from it is known to deviate very little from the vertical during flight. The balloon system is embedded in the air and moves with it; therefore, unless there is wind shear, turbulence, or wind acceleration in the atmosphere, there are no perturbing forces external to the balloon to act upon it. Internal forces which may be created in an effort to change the aspect of all or part of the payload may perturb the system.

Figure D-1 is a sketch of a balloon system which shows the nomenclature used here.

Perhaps the simplest pendulum model is one which treats the payload as a point mass at the end of a massless suspension system and the balloon as a rigid platform. This is the simple pendulum. Its period is $2\pi\sqrt{l/g}$; its angular frequency is $\sqrt{g/l}$.

A more realistic model considers the system to consist of a sphere which can turn about its center. At one point on the surface of the sphere, a massless line of length l is fastened. A point mass payload is secured to

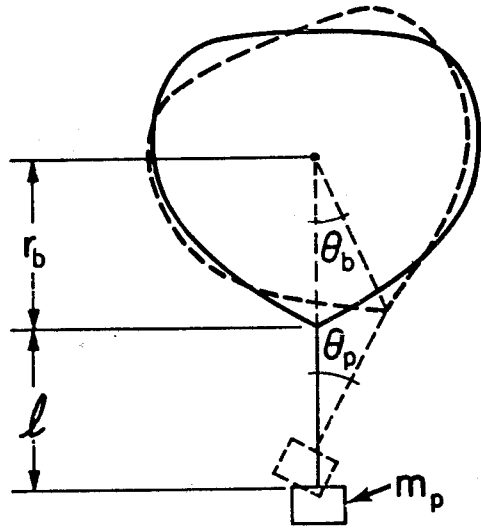


Fig. D-1. A sketch of a balloon system showing the nomenclature used in considering the system as a pendulum.

the other end of the line. The addition of a viscous force to dampen the motion of either the sphere or the payload or both adds still more realism.

A further simplification may be made by substituting a wheel for the balloon and restricting the motion to the plane of the wheel. The system is thus reduced to one having two degrees of freedom. Also, let the wheel's mass be uniformly distributed about its rim, its radius be given by the equation $4\pi r_B^3/3 = V_B$ (where V_B is the volume of gas in the balloon), and its moment of inertia be equal to that of the sphere. Since a fully-inflated balloon is approximately a sphere and since the moment of inertia of a thin shelled hollow sphere about an axis through its center is $2/3 mr^2$, while that of a wheel of the type assumed here is mr^2 , the mass of the wheel is taken as $2/3$ the mass of the balloon.

The equations of motion of the model for small displacements are

$$\left. \begin{aligned} \left(\frac{2}{3} m_B + m_p\right) r_B \ddot{\theta}_B + m_p l \ddot{\theta}_p + m_p g \theta_B &= 0 \\ r_b \ddot{\theta}_b + l \ddot{\theta}_p + g \theta_p &= 0 \end{aligned} \right\} \quad (D-1)$$

or if the motion of both the balloon and payload are viscously damped and

c_B and c_p are their respective damping coefficients

$$\left. \begin{aligned} \left(\frac{2}{3}m_B + m_p\right)r_B \ddot{\theta}_B + m_p l \ddot{\theta}_p + c_B r_B \dot{\theta}_B + m_p g \theta_B &= 0 \\ r_B \ddot{\theta}_B + l \ddot{\theta}_p + c_p l r_B \dot{\theta}_B + c_p l^2 \dot{\theta}_p + g \theta_p &= 0 \end{aligned} \right\} \text{(D-2)}$$

Either set of equations may be solved analytically. Both sets yield oscillatory solutions, and the frequency equation for each set is a quartic equation. The frequency equation for set (D-1) is quadratic in ω^2 where ω is the angular frequency, while the equation for set (D-2) is not. Therefore, the solution equations for set (D-1) are simpler and more amenable to intuitive understanding than those for set (D-2). They do, however, contain the principal features of the motion; consequently, they alone are given as set (D-3):

$$\left. \begin{aligned} \theta_B &= A_1 \sin(\omega_1 t + \psi_1) + A_2 \sin(\omega_2 t + \psi_2) \\ \theta_p &= B_1 \sin(\omega_1 t + \psi_1) + B_2 \sin(\omega_2 t + \psi_2) \end{aligned} \right\} \text{(D-3)}$$

in which

$$\omega^2 = \left(\frac{g}{l}\right) \frac{\left[\frac{2}{3}m_B r_B + m_p (r_B + l)\right] \pm \sqrt{\left[\frac{2}{3}m_B r_B + m_p (r_B + l)\right]^2 - \frac{8}{3}m_B m_p r_B l}}{\frac{4}{3}m_B r_B} \quad \text{(D-4)}$$

The frequency ω_1 is given when the (+) sign is used before the radical;

ω_2 is given when the (-) sign is used. Negative frequencies are not allowed.

If $m_B \gg m_p$ and r_B is not small compared to l , Eq. (D-4) reduces to approximately $\omega_1 = \sqrt{g/l}$ and $\omega_2 = 0$.

It can be shown that

$$\left. \begin{aligned} \frac{A_1}{B_1} &= \frac{-(l\omega_1^2 - g)}{r_B \omega_1^2} \\ \frac{A_2}{B_2} &= \frac{-(l\omega_2^2 - g)}{r_B \omega_2^2} \end{aligned} \right\} \text{(D-5)}$$

Therefore, if $\omega_1^2 = g/l$ and $\omega_2^2 = 0$, B_2 is zero and from set (D-3)

$$\theta_p = B_1 \sin\left(\sqrt{\frac{g}{l}} t + \psi_1\right)$$

which is the solution equation for a simple pendulum of length l . If

$r_B \approx l$, as it usually is in a scientific balloon system, m_B must be at

least two orders of magnitude larger than m_p for this approximation to be

reasonable. Since it rarely is, however, the simple pendulum model is not

a good one.

The values of B_1 and B_2 (or A_1 and A_2) and ψ_1 and ψ_2 must be determined from the initial conditions of the system. In large balloon systems, θ_p

rarely exceeds a few minutes of arc after the system has reached a steady state float condition.

2. Compound Pendulum

The payload may vibrate as a compound pendulum, and this vibration may be nearly independent of the pendulation of the entire balloon system. On the other hand, energy may be exchanged between the two modes of vibration. Figure D-2 illustrates a payload which cannot be suspended from its top. If a substantial portion of the mass is above the suspension point, the distance d from the suspension point to the center of gravity may be small. The equation of motion of such a system, if it is not damped, is

$$J \ddot{\theta} + m_p g d \sin \theta = 0 \quad (D-6)$$

where J is the moment of inertia of the payload about the axis of suspension, m_p is the payload mass, g is the acceleration due to gravity, and θ and d are defined in Fig. D-2. If θ is small so that $\sin \theta \approx \theta$, the solution of Eq. (D-6) is

$$\theta = C \sin (\omega t + \psi) \quad (D-7)$$

and

$$\omega = \sqrt{mgd/J} \quad (D-8)$$

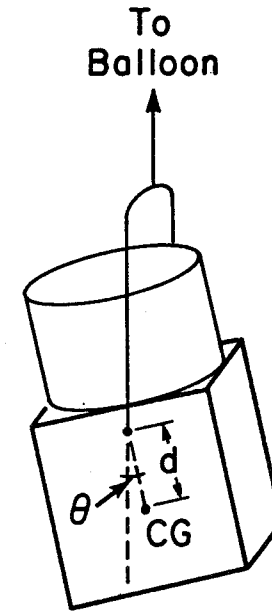


Fig. D-2. A balloon payload acting as a compound pendulum.

Assume that $t = 0$, $\theta = 0$, and $\dot{\theta} = \dot{\theta}_0$. With these initial conditions $\psi = 0$ and $C = \dot{\theta}_0 / \omega = \dot{\theta}_0 \sqrt{J/mgd}$. Since $J = md^2 + J_0$, where J_0 is the moment of inertia of the payload about its center of gravity, the ratio $J/d = md + J_0/d$ becomes very large as d becomes small. Thus, the amplitude C of any oscillation, and consequently the excursions θ , may become large if d is small. On the other hand, the torque required to change (e.g., stop) any motion is $J\ddot{\theta}$ or $(md^2 + J_0)\ddot{\theta}$ which becomes a minimum when the suspension point coincides with the center of gravity.

3. Torsional Pendulum

A balloon system may also act as a torsional pendulum which may be simulated by a horizontal wheel of radius r_B joined co-axially to a second wheel of radius r_p by the suspension system. In this model, r_B is the radius of the balloon from the equation $4\pi r_B^3/3 = V_B$ and r_p is the radius of gyration of the payload. Figure D-3 illustrates the model.

The suspension system usually consists of two or more lines separated by a small distance, and the spring constant K of such a system can be calculated from the relationship between torque and displacement given in Fig. 1 of Section VII. For a suspension system consisting of n identical

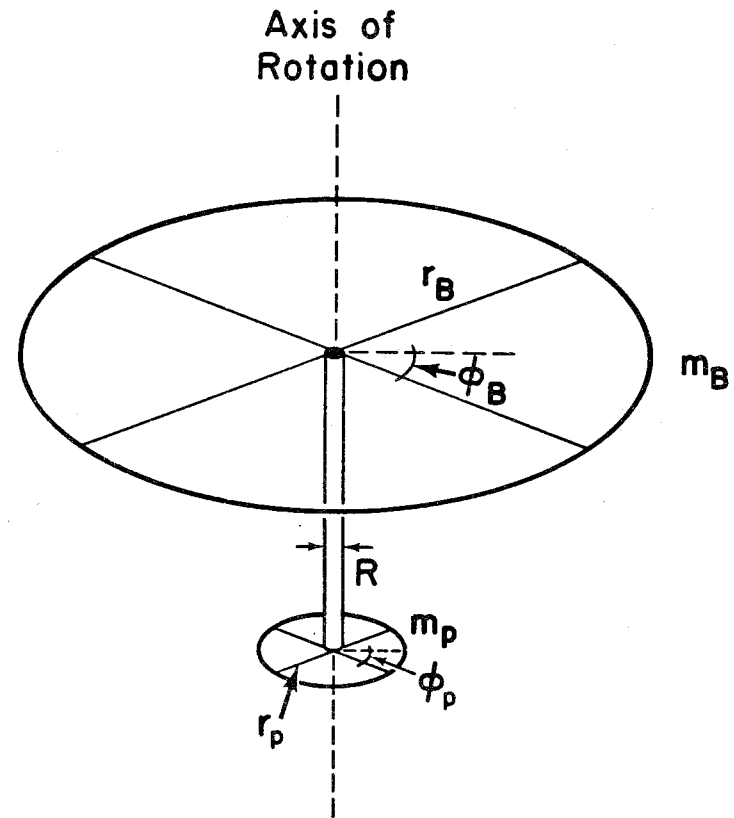


Fig. D-3. Torsional pendulum model of a balloon system.

prismoidal sections of radius R joined end to end,

$$K = \frac{-m_p g R^2}{l} \quad (D-9)$$

where l is the overall length of the suspension and the maximum twisting of any section is so small that $\sin \phi \approx \phi$ and $\cos \phi \approx 1.0$.

The equations of motion of the model are

$$\left. \begin{aligned} J_B \ddot{\phi}_B + \eta_B \dot{\phi}_B + K (\phi_B - \phi_P) &= 0 \\ J_P \ddot{\phi}_P + \eta_P \dot{\phi}_P + K (\phi_P - \phi_B) &= 0 \end{aligned} \right\} \quad (D-10)$$

where η_B and η_P are the torsional damping coefficients of the balloon and payload, respectively. The solution equations are

$$\left. \begin{aligned} \phi_B &= B_1 + f_2 B_2 e^{k_2 t} + C_1 e^{k_3 t} \sin(\omega t + \varphi_1) \\ \phi_P &= B_1 + B_2 e^{k_2 t} + C_2 e^{k_3 t} \sin(\omega t + \varphi_2) \end{aligned} \right\} \quad (D-11)$$

In scientific balloon systems the value of C_1 is normally so small that it may be equated to zero. Also, if the suspension system is not to become twisted, $f_2 \approx 1$. Therefore, the solution equations may be written

$$\left. \begin{aligned} \phi_B &= B_1 + B_2 e^{k_2 t} \\ \phi_P &= B_1 + B_2 e^{k_2 t} + C e^{k_3 t} \sin(\omega t + \varphi) \end{aligned} \right\} \quad (D-12)$$

The sum $(B_1 + B_2)$ is the value of ϕ_B at $t = 0$, and B_1 is the value of ϕ_B when translatory rotation has ceased. The total rotational translation which the balloon will undergo is therefore B_2 . Also the rate of rotation of the balloon at $t = 0$ is $B_2 k_2$.

The amplitude of the undamped oscillation of the payload is given by C .

The frequency of set (D-11) can be determined by solving the characteristic equation of the system. This involves solving a cubic equation and the expression is complicated. Morris and Stefan (1) have shown that the following simple expressions for ω , k_2 , and k_3 are adequate approximations for use in set (D-12):

$$\omega = \frac{R}{r_p} \sqrt{\frac{g}{l}} \quad (D-13)$$

$$k_2 = -\eta_B / J_B \quad (D-14)$$

$$k_3 = -\eta_P / 2J_P \quad (D-15)$$

Values for B_1 , B_2 , C and φ must be determined from initial conditions.

The value of η is a function of air density, air viscosity, and the radius of the balloon. The following equation has been found to give reasonable values of η_B for four flights for which rotation rates were measured:

$$\eta_B = 6 (\mu \rho)^{\frac{1}{2}} r_B^4 \quad (D-16)$$

The form of the equation was suggested by the work of Germeles et al. (2), but as used here, it is strictly an empirical equation. The numerical coefficient, which has the dimensions of $t^{-\frac{1}{2}}$, was determined from about a dozen instances where the rotation decayed monotonically with time. There was no way to assure that the decay rate was not speeded or impeded by relative air motion on the balloon. Therefore, values of η_B computed from the equation should be regarded as crude approximations. The air viscosity μ and the air density ρ may be determined from Tables J-11 and K-1, respectively, or from the U.S. Standard Atmosphere, 1962, (3).

The value of η_p is small for most scientific payloads, and the energy loss in the suspension system may be more effective in damping payload oscillations than energy loss to the atmosphere. Damping is observed, however, and $\eta_p \approx 10^{-3} \eta_B$ appears to give an order-of-magnitude approximation to η_p .

REFERENCES

- (1) Morris, Alvin L. and Karl H. Stefan, 1969: High Altitude Balloons as Scientific Platforms, unpublished NCAR paper presented at The American Society of Photogrammetry Symposium on Earth Observations from Balloons, 6 and 7 Feb. 1969, Washington, D.C.
- (2) Germeles, A. E., R. M. Lucas, E. R. Benton, 1963: Rotation of Balloons at Floating Altitudes. A. D. Little, Inc. Tech Rept. III to Office of Naval Research.
- (3) U.S. Standard Atmosphere, 1962: U.S. Government Printing Office, Washington, D.C., pp 278.

E. GAS FLOW THROUGH AN ORIFICE

Gas will flow through an orifice in a balloon with a speed v_g given by the equation

$$\frac{1}{2} \rho_g v_g^2 = p_g - p_a \quad (E-1)$$

where ρ_g is the density of the gas and p_g and p_a are the pressures of the gas and air, respectively.

Also

$$\frac{dV_g}{dt} = -A_e v_g = -A_e \sqrt{\frac{2(p_g - p_a)}{\rho_g}} \quad (E-2)$$

where dV_g/dt is the volume rate of gas flowing through the orifice and A_e is the effective area of the orifice. Normally, CA is substituted for A_e . In the product CA , A is a nominal area (πr^2 for a circular orifice) while C is an orifice coefficient which accounts for any obstructions that may exist in the orifice as well as for all deviations of the actual flow from the theoretical flow. The value of C must be determined empirically; it is rarely below 0.5 and it cannot exceed 1.0. The negative sign is used to indicate that when $(p_g - p_a) > 0$, the flow is a loss of gas by the balloon. The equations above are not valid if $(p_g - p_a) < 0$.

At an orifice on top of a balloon $(p_g - p_a) = g(\rho_a - \rho_g) D_g$ if D_g is the vertical distance from the zero-pressure level to the orifice. Assuming the gas bubble to be spherical and the zero-pressure level to be at its bottom makes D_g the diameter of the gas bubble. The mass of gas in such a bubble is $m_g = \pi \rho_g D_g^3/6$ and its volume is $V_g = \pi D_g^3/6$. Therefore, the volume rate of flow through an orifice at the top of a balloon may be written in the following forms:

$$\frac{dV_g}{dt} = -CA \sqrt{\frac{2g(\rho_a - \rho_g) D_g}{\rho_g}} \quad (E-3)$$

$$\frac{dV_g}{dt} = -1.58 CA \sqrt{g \left(\frac{\rho_a - \rho_g}{\rho_g} \right) V_g^{1/3}} \quad (E-4)$$

$$\frac{dV_g}{dt} = -1.58 CA \sqrt{g \left(\frac{\rho_a - \rho_g}{\rho_g} \right) \left(\frac{m_g}{\rho_g} \right)^{1/3}} \quad (E-5)$$

Also, if $p_g = p_a$ and $T_g = T_a$ for the purpose of computing density and $g = 9.8$

$$\frac{dV_g}{dt} = -12.3 CA \left(\frac{m_g}{\rho_g} \right)^{1/6} = -12.3 CA V_g^{1/6} \quad (E-6)$$

for helium, and

$$\frac{dV_g}{dt} = -18.1 CA \left(\frac{m_g}{\rho_g} \right)^{1/6} = -18.1 CA V_g^{1/6} \quad (E-7)$$

for hydrogen.

F. VERTICAL CUTOFF RIGIDITY

The vertical cutoff rigidity of a charged particle is defined as the lowest rigidity that particle can possess and still arrive at a specific point on the earth's surface from the zenith, Shea et al. (1). Only particles having a high rigidity can penetrate the earth's magnetic field near the geomagnetic equator, while particles with very low rigidity can penetrate the field at the geomagnetic poles. Figure F-1 is a world map of vertical cutoff rigidities based on charged particle trajectory calculations by Shea and Smart (2) for particles reaching a point 20 km above sea level from the zenith.

According to Haymes (3) cosmic rays are defined as those charged particles that reach the earth's magnetosphere with velocities greater than the solar wind velocity. Cosmic rays are then affected by the earth's magnetic field, and as shown by various studies, e.g., Kent and Pomerantz (4), cosmic ray intensity is highly correlated with the vertical cutoff rigidity. This effect of the magnetic field makes the earth useful as a charged particle energy analyzer. For some experiments high rigidity is preferred; for others, low rigidity will be necessary.

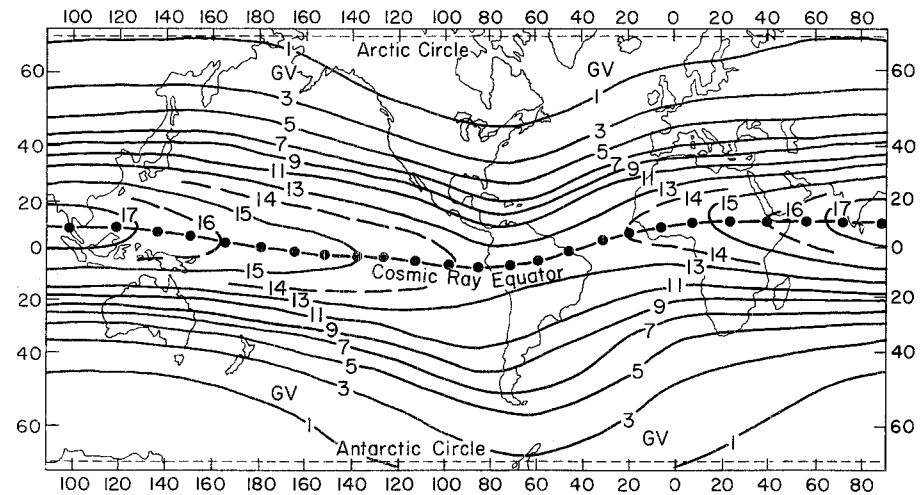


Fig. F-1. Vertical cutoff rigidity. The curves are isolines of vertical cutoff rigidity in gigavolts.

REFERENCES

- (1) Shea, M. A., D. F. Smart, K. G. McCracken, 1965: A Study of Vertical Cutoff Rigidities Using Sixth Degree Simulations of the Geomagnetic Field. Journal of Geophysical Res., Vol. 70, 4117-4130.
- (2) Shea, M. A. and D. F. Smart, 1967: Worldwide Trajectory-Derived Vertical Cutoff Rigidities and Their Application to Experimental Measurements. Journal of Geophysical Res., Vol. 72, 2021-2027.
- (3) Haymes, Robert C., 1971: Introduction to Space Science, John Wiley and Sons, Inc., New York, 369-400.
- (4) Kent, D. W. and M. A. Pomerantz, 1971: Cosmic Ray Intensity Variations in the Lower Atmosphere. Journal of Geophysical Res., Vol. 76, 1652-1661.

G. LANDING ENERGY ABSORBERS1. Landing Energy

If v_i is the vertical velocity of a parachute system at the time the payload touches earth, the energy due to vertical motion which must be dissipated in bringing the payload to a complete stop is $\frac{1}{2} mv_i^2$, where m is the mass of the payload. Likewise, if v_x is the horizontal motion of the payload, it will have a horizontal energy of $\frac{1}{2} mv_x^2$ which must be dissipated. Many types of energy absorbers have been suggested and several have been used in scientific ballooning. None have been entirely satisfactory. Only two will be discussed here, but the problems which are pointed out and much of the discussion will be applicable to others. The one which has been most widely used is a crush pad made from paper honeycomb.

2. Energy and Acceleration

If the acceleration which a payload experiences upon landing were not important, the energy could be absorbed by the gondola and landing surface directly. This would result, in most instances, in destruction or severe damage to the gondola and perhaps to the scientific and control equipment in the gondola. Therefore, it is desirable to limit the acceleration to

some preassigned maximum value while the kinetic energy of the payload is being dissipated.

The relationship $d^2 z/dt^2 = dv/dt = a$ may be integrated between limits as follows:

$$\int_{v_i}^{v_r} dv = \int_{t_i}^{t_r} a dt$$

to yield

$$v_i = - \int_{t_i}^{t_r} a dt = -\bar{a}t_r \quad (G-1)$$

where v_i is the velocity at the time of initial impact t_i , and $v_r = 0$ is the velocity at t_r , the time at which the kinetic energy has been expended. Also, \bar{a} is the average value of acceleration during the period $(t_r - t_i)$. Ideally the acceleration should be constant during that period, because if it is not, then at some time during the period a must be larger than \bar{a} .

Also, $d^2 z/dt^2 = a$ may be integrated twice with limits $z = z_i$, $v = v_i$ at $t = 0$, and $z = z_r$, $v = 0$ at $t = t_r$ to give

$$(z_i - z_r) = \frac{1}{2} \bar{a} t_r^2 \quad (G-2)$$

The height difference $(z_i - z_r)$ is the vertical distance the payload mass

travels from time of first impact with the earth until motion ceases.

If time is eliminated between Eqs. (G-1) and (G-2)

$$(z_i - z_r) = \frac{1}{2} \frac{v_i^2}{\bar{a}} \quad (G-3)$$

This, upon multiplying by m and rearranging, becomes

$$m\bar{a}(z_i - z_r) = \frac{1}{2} m v_i^2 \quad (G-4)$$

Thus, any braking device capable of exerting a force $m\bar{a}$ through a distance $(z_i - z_r)$ can completely dissipate the kinetic energy of mass m moving at a velocity v_i at the instant braking starts.

3. Energy Absorbers

Paper honeycomb is a light, inexpensive material which typically yields to a compressive force acting in a direction parallel to its tubes, as shown by the solid curve in Fig. G-1. The abscissa of Fig. G-1 is the ratio of the relative displacement of the two surfaces to the uncrushed thickness of the material. The ordinate is the ratio of the pressure required to crush the material to the nominal compressive strength. Compressive strength is defined here as the force which must be exerted per unit area to cause the material to yield. More important is the continuing

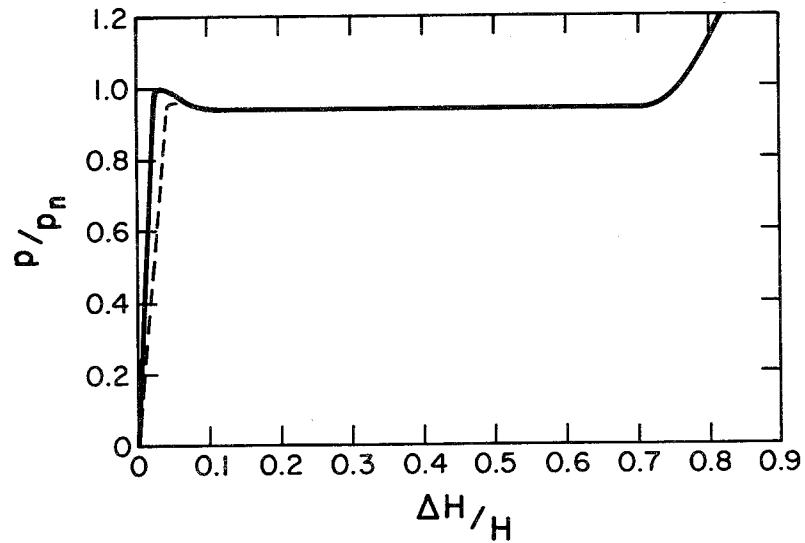


Fig. G-1. Typical stress-strain curve for paper honeycomb.

strength of the material after yield has started and before the cellular structure is so destroyed that the paper itself starts being compressed. If a sheet of paper honeycomb is precrushed, that is, crushed just enough to start the yield, its subsequent yield can be made nearly equal to its continuing strength. It will then have a nearly constant crush strength through about two-thirds of its thickness. The dashed line in Fig. G-1 is a typical stress-strain curve for precrushed paper honeycomb. The constant compressive strength which is a characteristic of good paper honeycomb makes it a good energy absorber.

A rod and die arrangement like that shown in Fig. G-2 may also be used as an energy absorber. The rod is drawn through the die when the drawing force becomes equal to the design actuating force of the rod and die combination. The stress-strain curve is almost identical to that for precrushed honeycomb except that if a uniform rod is used and the die slips off the end, the curve goes down abruptly instead of up when $\Delta H/H$ approaches one. Enlarging the rod near the end, however, will cause the curve to rise as the die approaches the end of the rod.

Consider a load of mass m which is supported on a light, rigid plate.

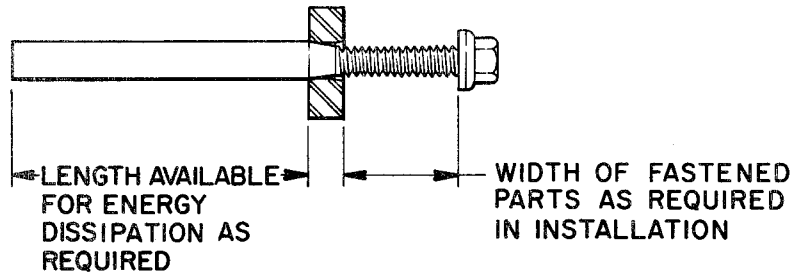


Fig. G-2. Rod and die energy absorber.

Assume that paper honeycomb is available which has a continuing crush pressure (strength) of p_c . Also assume that the maximum acceleration which can be tolerated by the load on landing is ng , where g is the acceleration due to gravity. Then the force required to produce that acceleration of the mass m is mng . That force can be supported by honeycomb having an area A , such that

$$p_c A = mng \quad (G-5)$$

If p_c is constant, then the acceleration ng may be expected to be constant.

From Eq. (G-5) the honeycomb area needed to produce an acceleration ng may be determined.

If the acceleration ng is substituted for \bar{a} in Eq. (G-3), the thickness $(z_i - z_r) = \Delta H$ of honeycomb which must be crushed may also be determined. Because p/p_n starts to grow rapidly for $\Delta H/H > 2/3$, the total thickness H of honeycomb needed is $1.5 \Delta H$. Therefore, Eq. (G-3) written in terms of H is

$$H = 0.75 \frac{v_i^2}{ng} \quad (G-6)$$

Equation (G-5) may be written

$$A = \frac{mg}{P_c} \quad (G-7)$$

Equations (G-6) and (G-7) permit one to calculate the area and thickness of paper honeycomb needed to absorb the energy of a load of mass m moving vertically downward at an initial speed v_i while accelerating the load at the rate ng .

It is interesting that the product AH is the volume of the energy absorber needed and that it is not a function of acceleration. This may be seen by multiplying Eqs. (G-6) and (G-7) together. The resulting equation is

$$Vol = HA = \frac{1.5}{P_c} \left(\frac{1}{2}mv_i^2 \right) \quad (G-8)$$

Equation (G-8) is written in such a way that the kinetic energy is readily identifiable. From Eq. (G-8) it is apparent that one can reduce the area and increase the thickness of a crush pad and not change the quantity of energy which it can absorb. On the other hand, reducing the area will reduce the acceleration during the energy absorption process according to Eq. (G-7). Therefore, subject to the requirement for adequate base area to give the

assemblage stability and the possible requirement to keep it short, a crush pad having a small horizontal area and great vertical depth is preferable to one having a large horizontal area and small vertical depth. An example is useful.

Example: A load of 1000 kg is expected to descend vertically at 7.5 m/sec upon a solid, hard-packed surface. Paper honeycomb which has a compressive strength of 5×10^4 N/m² is available in sheets 10 cm thick. How can a crush pad be designed to absorb the kinetic energy and avoid an acceleration of more than 15 g?

Solution: Using Eq. (G-6) and a slide rule,

$$H = 0.75 \times 7.5 \times 7.5 / (15 \times 9.8) = 0.29 \text{ m}$$

Using Eq. (G-7),

$$A = 10^3 \times 15 \times 9.8 / 5 \times 10^4 = 2.94 \text{ m}^2$$

Three layers of honeycomb formed into a square 1.71 m on a side would meet the requirements if they were mounted in such a way that the compressive forces were uniformly distributed over the surfaces. A larger area would cause an excessive acceleration throughout the energy absorption period. A crush pad having a smaller area and the same thickness would be

crushed completely before all the kinetic energy could be absorbed, and the acceleration would then exceed 15 g.

The volume of crush material required in this example is $2.94 \times 0.29 \text{ m}^3$. If a pad is made four layers or 0.4 m thick, the area can then be reduced to $2.94 \times 0.29/0.40 = 2.13 \text{ m}^2$. Entering this number in Eq. (G-7) yields

$$ng = \frac{2.3 \times 5 \times 10^4}{10^3} \approx 106$$

or $n = 10.8$

This is 28% below the allowable acceleration. Therefore, if an area of 2.13 m^2 provides an adequate base and the added layer of honeycomb does not cause a height problem, the same volume of material provides better protection to the payload in this configuration than in the first configuration. A larger area using four layers could be employed (up to 2.94 m^2) without causing acceleration to exceed 15 g. Doing so would waste material if the energy absorber worked perfectly, but it might provide some assurance of keeping acceleration within 15 g if the energy absorber were to fail to meet expectations.

Paper honeycomb is available in a number of strengths. Select data from one manufacturer are provided in Table 1. The strength of a specific type and sample of honeycomb which is to be used on a gondola should be obtained from the manufacturer or determined by experiment. Occasionally the area of a crush pad may be determined by the restrictions of the experiment on which it is to be used. If so, it will be necessary to select the strength to satisfy Eq. (G-7). For a given area, one may use a lower strength material than that which satisfies Eq. (G-7) if a greater thickness is employed.

If the area of material required according to Eq. (G-7) is smaller than the area desired for a crush pad, a pad may be built up as a multi-layer sandwich. Each layer should consist of two light, rigid plates between which the proper area of honeycomb is placed. The honeycomb should be dispersed symmetrically about the center of gravity of the load and bonded securely to the plates. Figure G-3 illustrates one layer of such a sandwich. Except for the top one, all plates may be made of very strong metal or paper-faced honeycomb or of plywood. The top one will normally be fastened to the gondola and will be made of metal.

Table G-1

Paper Honeycomb Strength Data

Verticel* Designation	Shear Strength**		Compression Strength	
	N/m ² x 10 ⁻⁴	lb/in. ²	N/m ² x 10 ⁻⁴	lb/in. ²
½" 40-50-15%	22.7	33.0	21.6	31.4
½" 60-80-20%	42.5	61.6	42.6	61.8
3/8" 40-50-15%	31.4	45.5	27.1	39.3
3/8" 60-80-20%	69	100	52.1	75.6
¼" 40-50-15%	78	113	71	103
¼" 60-60-20%	102	148	96	140
½" 30-30- 0%	--	--	4.8	7.0
½" 60-80- 0%	--	--	14.8	21.5
¼" 60-60- 0%	--	--	44.5	64.6

*Data courtesy The Verticel Co., Englewood, Colo. The designation numbers indicate the cell size, basis weight, and percent impregnation.

**The shearing forces were contained in parallel planes which cut the honeycomb normal to the axis of the tubes.

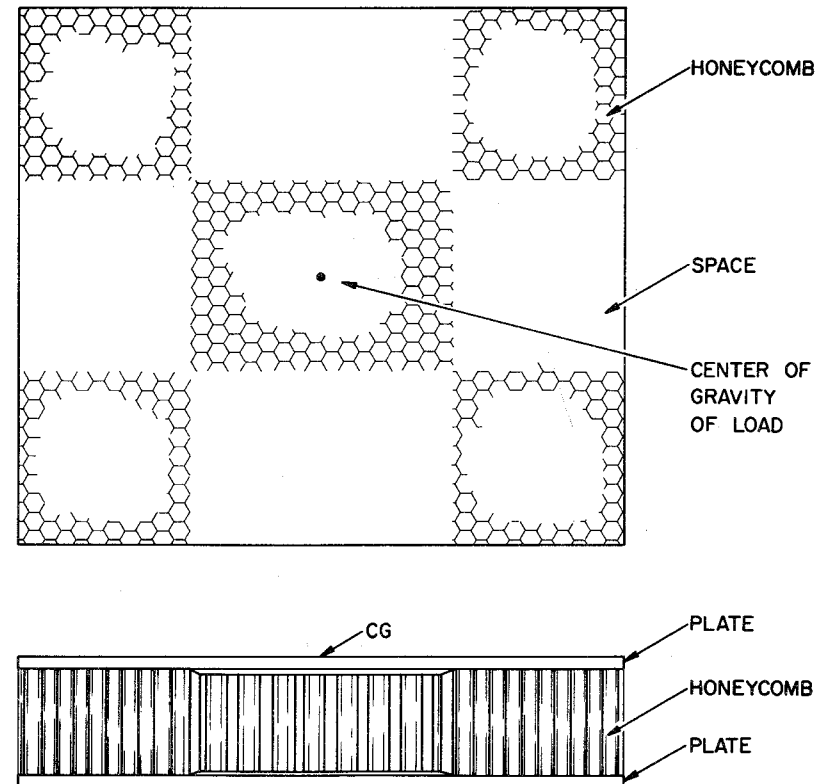


Fig. G-3. Plan view (upper) and side view of a single layer of a crush pad made of sections of honeycomb between light, rigid plates.

4. Horizontal Motion

When a descending system is drifting horizontally at the time of landing, the problem of absorbing the kinetic energy is vastly more complicated than when the motion is vertical. Present landing techniques do not allow the orientation of the impressed force relative to the gondola to be known in advance; therefore, an attempt must be made to make the crush pad absorb energy equally well regardless of the direction of relative horizontal motion. Further, the mechanism for absorbing the energy of horizontal motion must act independently of the mechanism for absorbing the energy of vertical motion, or the two must interact in a known way. Finally, regardless of how well the system is engineered to absorb the energy of a landing on a flat surface, design considerations are not likely to have been adequate if it lands on a steep slope or in a tree top.

The solution most often adopted is to use additional material, such as paper honeycomb, in exactly the same manner as it is used to absorb the energy of vertical motion. This relies on the shearing strength of the honeycomb to reduce the horizontal motion. Unfortunately, the stress-strain curve for the shearing motion involved does not contain a plateau like the

one which characterizes the stress-strain curve for compressive motion. Instead, stress builds nearly linearly until yield starts, and then it rapidly falls to zero as the material tears apart. The solution most often accepted is, therefore, not a good one. If enough area is added to assure that the crush pad has the strength to absorb the energy of horizontal motion without being torn away, resistance to vertical motion will be too large.

A crush pad may be made up as a multi-layered sandwich and made so that both the shear and compressive strengths of the layers increase from layer to layer, with the lowest layer being the weakest. This permits the weaker links in the chain of layers to be used, broken, and lost without losing the benefit of the crush pad. If the top layer were weakest, the entire crush pad might be torn away from the load without having slowed it appreciably. A difference of 3 to 5% in strength between successive layers is adequate.

As an alternative to losing the lower layers of a crush pad progressively, a crush pad may be bound together by bands, or sturdy top and bottom plates may be fastened together by cables as shown in Fig. G-4. Conceptually, this type of construction uses the shearing strength of the honeycomb to

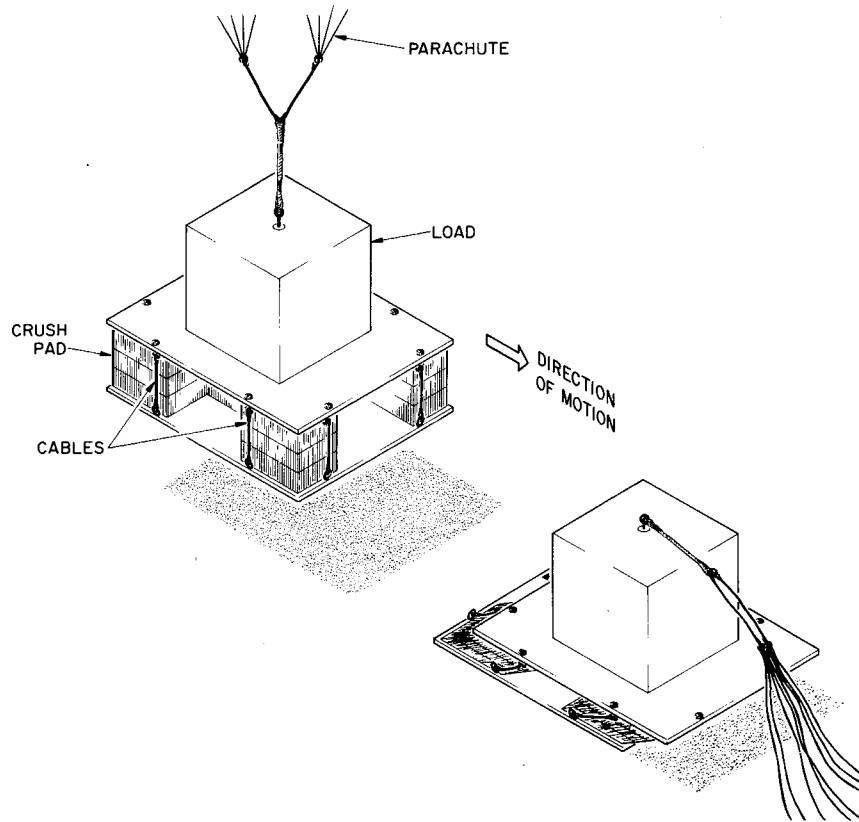


Fig. G-4. A multilayer honeycomb crush pad bound by vertical cables--
before and after landing.

absorb horizontal motion initially, but the cables prevent the paper from tearing apart as the displacement grows and converts horizontal motion into vertical motion. Thus, to a great extent, the horizontal and vertical energy are both absorbed in crushing the honeycomb, and appropriate adjustments to the thickness of the pad must be made. The honeycomb area should not be larger than the maximum allowable for a vertical descent, however, to provide for the contingency of no horizontal motion. The total area of the crush pad should be great enough to prevent the tipping moment caused by horizontal motion from overturning the gondola upon landing. If such a large base is not feasible, protective pads must be used to protect the gondola as it overturns.

Some crush pads were made and tested by Krog (1) in which paper honeycomb was added to the layers with its tubes oriented horizontally. He found that when honeycomb was subjected to shearing forces along its tubes, especially while also being compressed, it absorbed the energy of horizontal motion well and helped prevent the shearing motion from destroying the pad before it had accomplished its purpose. The compressive strength of honeycomb in a direction normal to the tubes is very low through most of its

thickness. Therefore, honeycomb with its tubes oriented parallel to the plates may be added to a sandwich without seriously affecting its reaction to vertical motion.

Practically, the problems of energy absorber design have been solved chiefly through a combination of inspiration (backed by efforts to make engineering approximations) and trial and error. A model energy absorber can readily be fabricated, loaded, and dropped from a truck in motion to simulate a landing. An accelerometer may be used to check the accelerations, and the crush pad may be inspected and its faults corrected. A natural inclination to correct a design by reinforcing the energy absorber to prevent it from being destroyed in such a test must be overcome. It is the load and not the energy absorber which is to be protected.

REFERENCES

- (1) Krog, D. L., 1972: Ball Brothers Research Corp., private communication.

H. PARACHUTE COMPUTATIONAL AIDS

1. Selecting a Parachute

To select a parachute for use with a balloon flight (see Section X for discussion):

- a. Determine m_p , the mass of the payload to be lowered by parachute. The masses of the scientific equipment, flight control equipment, and ballast are usually included.
- b. Multiply m_p by 1.05 to obtain a first approximation of the total parachute system mass m_s .
- c. Decide what vertical landing speed v_T will be acceptable at the altitude where the landing is anticipated. A speed of 7-8 m/sec (~25 ft/sec) is usually acceptable.
- d. From v_T determine $v_{T,o}$ -- the vertical speed the system would have at sea level. It may be approximated satisfactorily by the equation $v_{T,o} = v_T / (1 + 5 \times 10^{-5} H)$, where H is the height of the landing site above sea level in meters or by $v_{T,o} = v_T / (1 + 1.52 \times 10^{-5} H)$, where H is in feet.
- e. Enter Fig. H-1 with the value of m_s from step b and $v_{T,o}$ from step d and determine $C_D A$.

f. Using the value of $C_D A$ obtained in step e and the appropriate pseudo drag coefficient for the parachutes available, enter Fig. H-2 and determine an approximate value of the nominal diameter D' of a parachute. Some typical pseudo drag coefficients are given in the caption to Fig. H-2. Others may be provided by the parachute manufacturer.

g. If a parachute is available which has a nominal diameter near the value of D' determined in step f, use its actual mass, pseudo drag coefficient, and nominal diameter and proceed to step h. If no available parachute is large enough, proceed to step m.

h. Enter Fig. H-2 with the actual nominal diameter and pseudo drag coefficient and determine $C_D A$.

i. Using the $C_D A$ determined in step h and the actual mass of the parachute system (the payload mass including all initial ballast plus the actual mass of the parachute, extension lines, etc.) enter Fig. H-1 and determine $v_{T,o}$.

j. Convert $v_{T,o}$ to v_T using the equations $v_T = v_{T,o}(1 + 5 \times 10^{-5}H)$ for H in meters or $v_T = v_{T,o}(1 + 1.52 \times 10^{-5}H)$ for H in feet.

k. Repeat steps i and j except in step i use the parachute system mass without the ballast.

l. If the range of v_T determined in steps i through k is acceptable, the parachute selected in step g is tentatively acceptable. If v_T from either step j or step k is too large to be acceptable, start over at step g and select a larger parachute. If v_T from step j or k is too small, repeat step g and succeeding steps with a smaller parachute.

If a good selection of sizes is available so that the first parachute selected can have characteristics like those assumed in going through the first six steps, the first selection will probably be suitable. Rarely will it be necessary to go through steps g and h more than twice. If a large part of the initial payload is ballast, the difference in the vertical landing speeds with and without ballast may be so great that the two speeds cannot both be within the range of acceptability. If so, other measures will have to be taken, e.g., measures to assure that the ballast will be dropped in nearly any conceivable circumstance before landing. When a parachute has been tentatively selected on the basis of the steps outlined above, it is necessary to perform a check of the parachute itself to be assured that

it was designed to carry a load as large as the one to be flown and that it is in a good state of repair.

m. If the largest parachute available is not acceptable, consider using a cluster of several parachutes. As a first step in determining the number and size of parachutes, divide D' as determined from step f in turn by $\sqrt{2}$, $\sqrt{3}$, ... \sqrt{N} , where N is the number of identical parachutes which may conceivably be used in a cluster to lower the load. Two identical parachutes having diameter $D'/\sqrt{2}$ or three having diameter $D'/\sqrt{3}$ can be substituted for one having diameter D' if $C'_{D'}$ is the same for each of the parachutes in the cluster as for the entire cluster.

n. Select N identical parachutes, each having a nominal diameter near D'/\sqrt{N} . Multiply the nominal diameter of one of the parachutes by \sqrt{N} to determine the nominal diameter of the cluster. For example, if two 30-meter parachutes are to be used together, the nominal diameter of the cluster is $1.4 \times 30 = 42$ m.

o. If the N parachutes selected have flat, circular canopies, use the equation $C'_{D'} = (0.95 - 0.03N) C'_{D,i}$ to determine the value of $C'_{D'}$ for a cluster where $C'_{D,i}$ is the pseudo drag coefficient of each of the N identical

parachutes of the cluster. This equation is valid for values of N from 2 through 6. For canopies with large geometric porosity such as ribbon, ring slot, or cross-shaped parachutes use $C'_{D,i}$ as the value of $C'_{D'}$ for the cluster.

p. Using the product obtained in step n as a new nominal diameter and the value of $C'_{D'}$ for the cluster obtained in step o, enter step h and proceed through step k. Then proceed to step q.

q. If the range of v_T determined in step p is acceptable for the cluster of N parachutes tested, that cluster may be used; if not, other clusters should be tested via steps n through p until an acceptable cluster is found. Then each of the parachutes to be used in the cluster should be thoroughly checked for strength and state of repair. If a cluster of parachutes is to be used, each parachute should be capable of carrying the entire load at opening because they are not likely all to open simultaneously.

2. Terminal Velocity and Time of Descent

In Fig. H-3 the curve labeled v_T is a plot of $(v_T/v_{T,o})$ vs height in the U.S. Standard Atmosphere, 1962. At any level up to 52 km $(v_T/v_{T,o})$ may

be read from the graph and multiplied by $v_{T,o}$ as determined from either step i or k above to yield v_T at that level. Indeed, $v_{T,2}$ at any level 2 may be determined if $v_{T,1}$ at any other level is known. It is

$$v_{T,2} = \frac{v_{T,1} \left(\frac{v_T}{v_{T,o,2}} \right)}{\left(\frac{v_T}{v_{T,o,1}} \right)} \quad (H-1)$$

where $(v_T/v_{T,o})_2$ and $(v_T/v_{T,o})_1$ are values of $(v_T/v_{T,o})$ read from the graph at levels 2 and 1, respectively. Note the arrow on the v_T curve indicating that it is referred to the abscissa scale along the base of the chart. Height is given in meters on the left ordinate scale and in feet on the right ordinate scale. An equivalent pressure scale parallels the meter height scale.

The curve labeled t is referred to the abscissa scale at the top of the chart as indicated by the arrow. That scale is a plot of $v_{T,o}(t_H - t_o)$ which has the dimensions of length. The quantity $(t_H - t_o)$ is the time required for a parachute system to descend from level H to sea level in the U.S. Standard Atmosphere, 1962. It may be determined for any level by reading the value of $v_{T,o}(t_H - t_o)$ for that level and dividing it by $v_{T,o}$.

Also, the time to descend from any level 1 to any lower level 2 may be determined. It is

$$(t_1 - t_2) = \frac{[v_{T,o}(t_H - t_o)]_1 - [v_{T,o}(t_H - t_o)]_2}{v_{T,o}} \quad (H-2)$$

where $[v_{T,o}(t_H - t_o)]_1$ and $[v_{T,o}(t_H - t_o)]_2$ are read for levels 1 and 2, respectively. Through a thin stratum the two values may be nearly equal, and greater accuracy may be gained by estimating a mean value of v_T within the stratum from the v_T curve and dividing that value into the thickness of the stratum. The value of v_T at the middle of the stratum is a good estimate of the mean for layers up to 1 km thick. The units of time are determined by the units of v_T , and the units of v_T and length must be compatible. For example, if the thickness of a stratum is given in meters and v_T is given in m/sec, the ratio $\Delta H/v_T$ will yield time in seconds. Similarly, if $v_{T,o}(t_H - t_o)$ is read in feet and $v_{T,o}$ is in ft/min, the ratio will yield time in minutes.

Although descent speeds and times calculated with the aid of Fig. H-3 are strictly valid only in the U.S. Standard Atmosphere, 1962, they are good approximations to descent times in the real atmosphere. The following

empirical equations may be used in place of Fig. H-3. They fit the curves of Fig. H-3 better near the surface and in the stratosphere than near the tropopause.

$$\frac{v_T}{v_{T,o}} = e^{0.071 H} \quad \text{for } H \text{ in km} \quad (\text{H-3})$$

$$\frac{v_T}{v_{T,o}} = e^{0.0216 H} \quad \text{for } H \text{ in thousands of feet} \quad (\text{H-4})$$

$$v_{T,o}(t_H - t_o) = 15,450 (e^{-0.071 H} - 1) \quad \text{for } H \text{ in km} \quad (\text{H-5})$$

$$v_{T,o}(t_H - t_o) = 50,690 (e^{-0.0216 H} - 1) \quad \text{for } H \text{ in thousands of feet} \quad (\text{H-6})$$

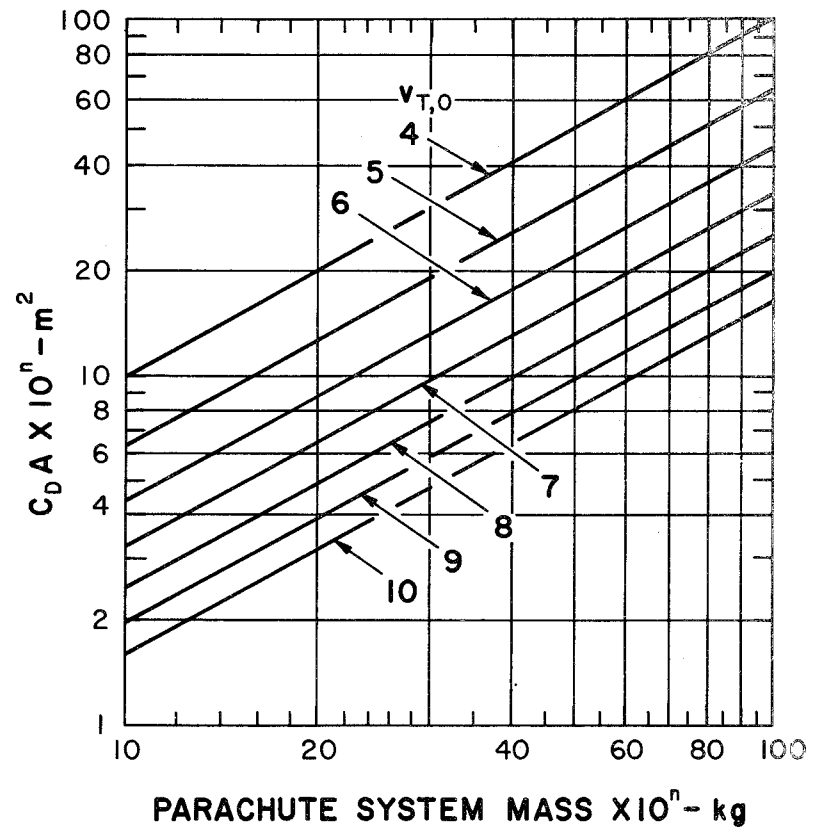


Fig. H-1a. Sea level terminal velocity of a parachute system as a function of system mass and the product of parachute area and drag coefficient.

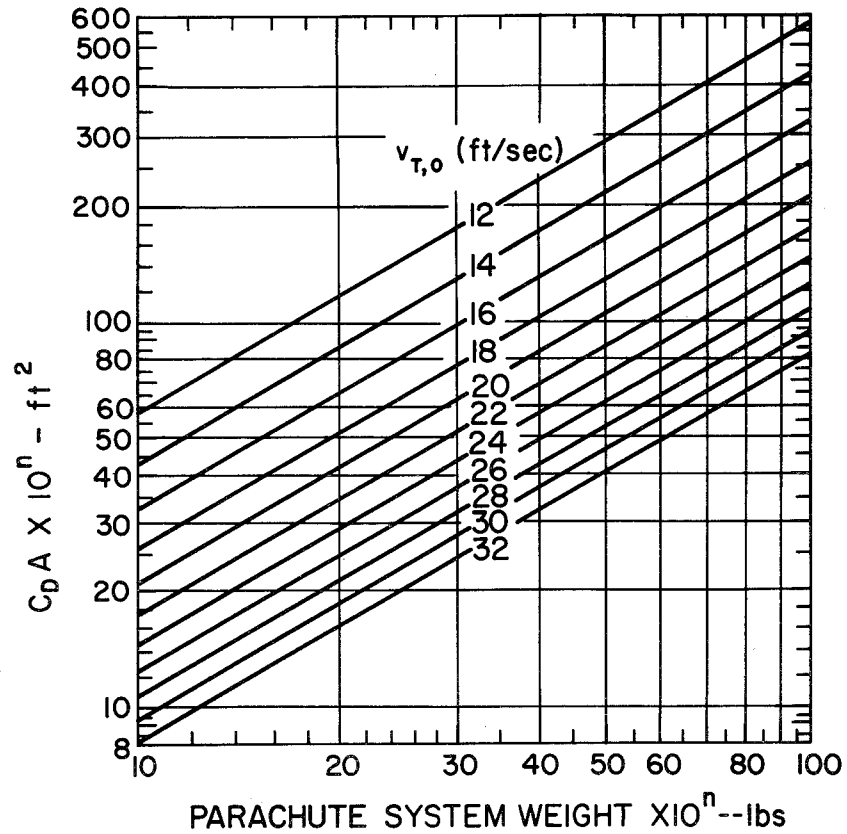


Fig. H-1b. Sea level terminal velocity of a parachute system as a function of system weight and the product of parachute area and drag coefficient.

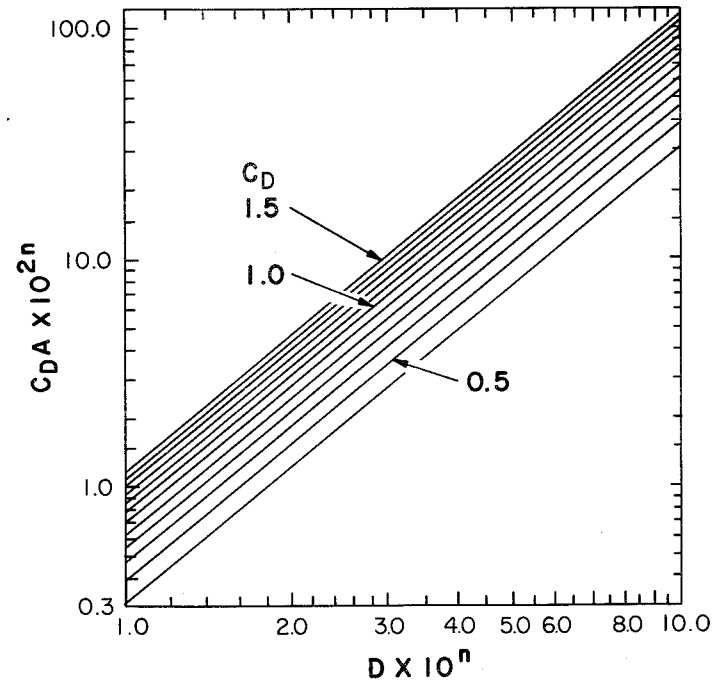


Fig. H-2. Diameter of a parachute as a function of area and drag

coefficient. Diameter is nominal diameter if the pseudo drag coefficient is used. The following are typical pseudo drag coefficients: $C_D' = 0.75$ (design value often quoted for a flat, circular canopy), $C_D' = 0.85$ (empirical value used by NCAR for large flat, circular canopies), and $C_D' = 0.55$ (value quoted by Raven Industries, Inc. for their RAVEN PLUS $\text{\textcircled{R}}$ shape).

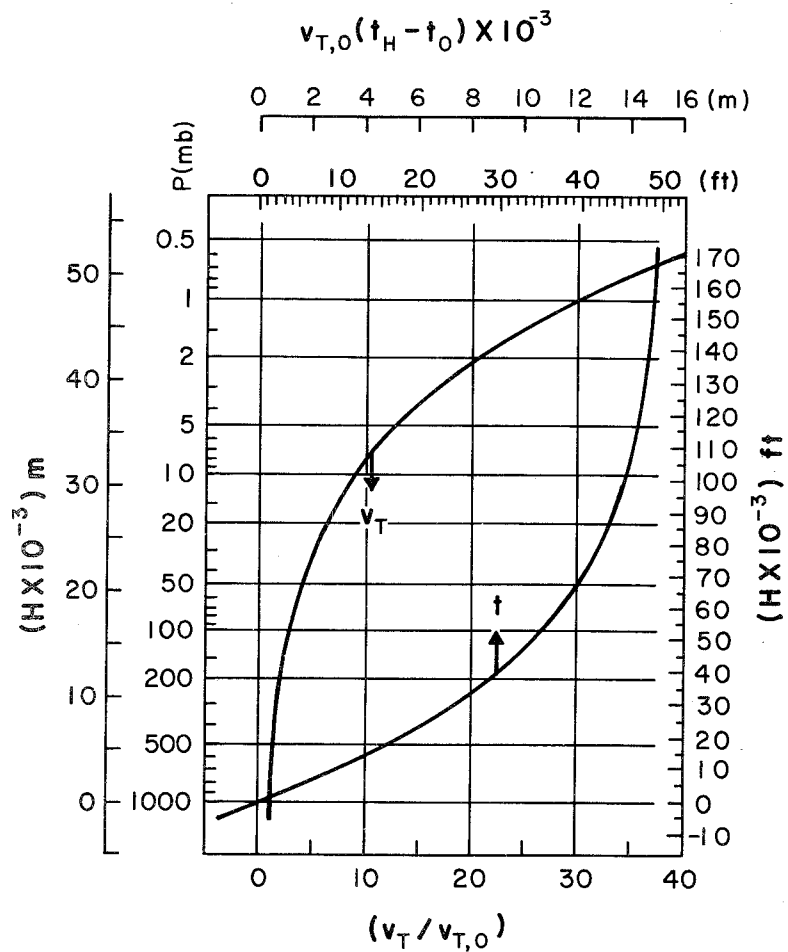


Fig. H-3. Terminal velocity and time of descent as functions of sea level terminal velocity and altitude in the U.S. Standard Atmosphere, 1962.

I. GAS MEASUREMENT AND INFLATION PROCEDURES

Figure I-1 and the tables of this section may be used to compute the lift of the helium or hydrogen contained in an array of cylindrical, steel containers if the total, nominal (water) volume of the array and the pressure and temperature of the gas are known. See Section IV for a discussion of lift gases and gas measurement. A procedure for using the tables and graph to inflate a balloon is given in the following steps:

1. At some time prior to the start of inflation, select enough cylinders of gas to assure that they contain more than the needed lift gas.
2. Arrange them so that the air can circulate freely through them, connect them with a manifold, and place a thermometer in contact with one of them. If a tube trailer like the one shown in Fig. 1 of Section IV is used, the cylinders will already be interconnected by a manifold.
3. At a time when ambient air temperature is not changing significantly with time (a few hours before sunrise is usually satisfactory) read the pressure and temperature. At that time the temperature of the thermometer should be a representative gas temperature. Pressure is always representative if the gas is not flowing and the gage is accurate and is tapped

gently prior to reading. If the temperature is taken during the day, shade the cylinders from the sun and ventilate them long enough prior to the reading to let them and the gas come into thermal equilibrium with the air.

4. Enter the appropriate table (helium or hydrogen in SI or English units) with the temperature and pressure from step 3 to determine the lift per unit of nominal volume of the array of cylinders. Linear interpolation may be used in these tables.

5. Multiply the tabular value obtained in step 4 by the nominal volume of the array to determine the total lift of the gas contained in the array. The nominal volume of each cylinder is usually stamped on it, frequently in cubic inches. To convert in.^3 to ft^3 multiply by 5.787×10^{-4} ; to convert in.^3 to m^3 multiply by 1.6387×10^{-6} . The water volume of the 2260-65# standard bottle is 1.57 ft^3 ($4.45 \times 10^{-2} \text{ m}^3$), on the average.

6. From the total lift contained in the array as determined in step 5 subtract the gross lift of the balloon system to be flown (the free lift plus the gross weight of the system not including the weight of the lift gas). The difference is the lift which should remain in the cylinder ar-

ray after inflation.

7. Divide the difference obtained in step 6 by the nominal volume of the array. This is the lift per unit nominal volume of the gas to be left in the array.

8. Enter the body of the appropriate table with the quotient obtained from step 7 and the temperature obtained in step 3 and obtain a pressure.

9. If the gage pressure obtained from step 8 is not less than $1.5 \times 10^5 \text{ N/m}^2$ (20 psi), the array contains enough gas to provide the required lift without draining the cylinders, and one may proceed to step

10. If the gage pressure obtained in step 8 is less than $1.5 \times 10^5 \text{ N/m}^2$, add additional cylinders and repeat steps 3 through 9 using the new nominal volume, pressure, and temperature of the array. Some prefer to use enough cylinders to leave the post-inflation gage pressure much higher than $1.5 \times 10^5 \text{ N/m}^2$. This assures relatively high flow rates throughout inflation. Others prefer to use just enough cylinders so that all except one must be drained. The latter technique provides greater accuracy of measurement at the expense of longer inflation time. When an array of cylinders has

been finally selected and interconnected by a manifold, all valves should be closed to prevent loss of gas.

10. A short time prior to the start of inflation, open all cylinders of the array selected in step 9 and let the pressure equalize in the array.

Read the initial pressure p_i .

11. Enter the appropriate table with the lift per unit nominal volume determined in step 4 for the final array chosen in step 9 and the pressure determined in step 10, and determine the mean gas temperature. This is a value of temperature taken from the table, not a value measured by thermometer. If post inflation pressure is to be left relatively high in all cylinders, proceed to step 12. If all cylinders except one are to be drained, proceed to step 12a.

12. Using the temperature determined in step 11 and the lift per unit nominal volume which should remain in the array after inflation from step 7, enter the appropriate table and determine the pressure. This is the first estimate of the pressure at which the gas flow should be cut off to end inflation; let it be designated p_f .

13. Divide p_f from step 12 by p_i from step 10; use the quotient and

Fig. I-1 to obtain the ratio p_c/p_f .

14. Multiply p_c/p_f obtained in step 13 by p_f from step 12 to obtain p_c . This is the pressure which the gas in the array should have immediately after the correct amount of lift gas has been removed.

15. When, during inflation, the pressure gage reads the value p_c determined in step 14, cut off the gas flow at the main valve. Let the pressure stabilize and read it. It will be higher than p_c ; call it $p_{c,1}$.

16. Take the difference ($p_{c,1} - p_c$) and subtract it from p_c to obtain $p_{c,2}$.

17. Open the valve again and let the flow continue until the pressure on the gage reads $p_{c,2}$. Close the valve and let the pressure stabilize; it should read very nearly p_c . If it is still slightly higher than p_c , another short burst of flow may be necessary. If it is slightly less than p_c , slightly more gas will have been added to the balloon than was desired. The difference is well within the indeterminacy of the method.

18. Shut off all valves and disconnect all hoses from the balloon.

12a. If all cylinders except one are to be drained during inflation, select the cylinder which is not to be drained. Close its valve and note

its nominal volume.

13a. Subtract the nominal volume of the closed cylinder from the nominal volume of the array as finally determined in step 9. This yields the nominal volume of the cylinders to be drained.

14a. Using the mean temperature of the gas determined in step 11 and a gage pressure of $1.5 \times 10^5 \text{ N/m}^2$, enter the appropriate table and determine the lift per unit nominal volume of the gas to be left in the array.

15a. Subtract the value obtained in step 14a from the value obtained in step 4 and multiply the difference by the nominal volume of the array to be drained from step 13a. This yields the usable lift in the array to be drained.

16a. Subtract the usable lift obtained in step 15a from the gross lift of the balloon system to be flown (used in step 6). The difference is the lift that must be taken from the cylinder which is closed off.

17a. Multiply the lift per unit nominal volume obtained in step 4 by the nominal volume of the cylinder which is closed off. This is the lift contained in that cylinder.

18a. Subtract the lift which must be taken from the cylinder (from step

16a) from the lift contained in the cylinder as determined in step 17a.

This yields the lift to be left in the one cylinder at the end of inflation.

19a. Using the mean temperature of the gas determined in step 11 and the lift to be left in the cylinder from step 18a, enter the appropriate table and determine the final pressure p_f .

20a. Divide p_f from step 19a by p_i from step 10; use the quotient and Fig. I-1 to obtain the ratio p_c/p_f .

21a. Multiply the ratio p_c/p_f obtained in step 20a by p_f from step 19a to obtain p_c . This is the pressure at which gas flow should be cut off in the final cylinder to obtain proper inflation. After the gas in the array (not including the cylinder closed in step 12a) has been allowed to flow into the balloon until the gage pressure has reached $1.5 \times 10^5 \text{ N/m}^2$, all cylinders of the array should be closed off. The one final cylinder is then opened and gas is allowed to flow from it until the pressure reaches the value p_c determined in step 21a above. Then the procedure outlined in steps 15 through 18 should be followed to complete the inflation. Steps 15 through 18 are less critical when only one cylinder is in use at the end than when several are in use. Also it is not necessary to follow that procedure when the final gage pressure is as low as $1.5 \times 10^5 \text{ N/m}^2$.

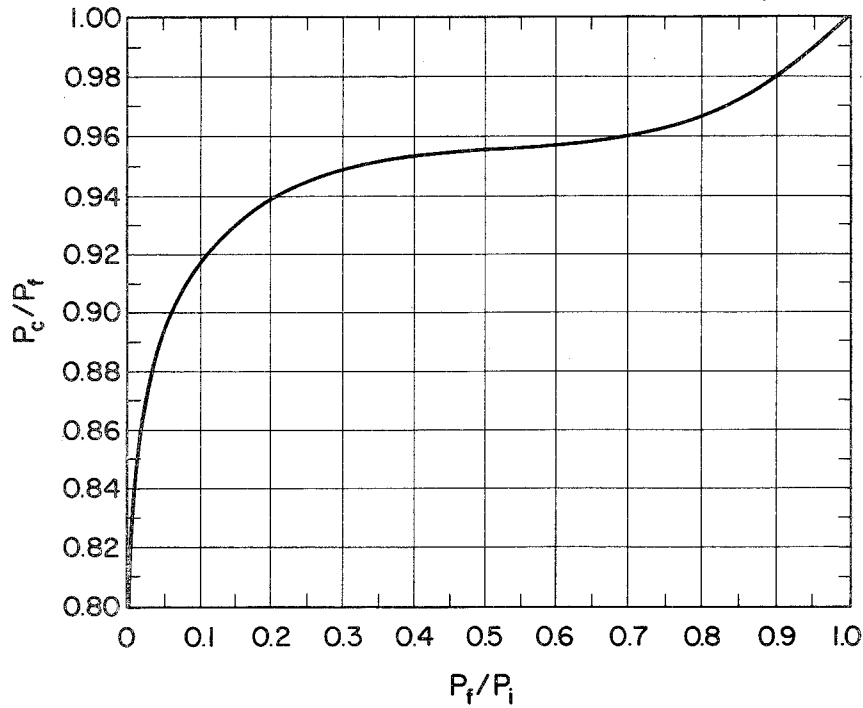


Fig. I-1. Relationship between P_c , P_i , and P_f .

Helium--SI Units

Table I-1

Lift (kg/m^3) of Gas Contained in Steel Cylinders

G.Press. ($\times 10^6$) (N/m^2)	Temperature ($^{\circ}\text{C}$)							
	-25	-20	-15	-10	-5	0	5	10
0.0	1.2235	1.1995	1.1765	1.1544	1.1330	1.1125	1.0927	1.0736
5.0	7.2405	7.0991	6.9633	6.8326	6.7067	6.5855	6.4686	6.3558
10.0	13.224	12.966	12.719	12.481	12.252	12.031	11.818	11.612
15.0	19.174	18.801	18.444	18.099	17.768	17.448	17.140	16.843
20.0	25.090	24.605	24.138	23.688	23.256	22.839	22.437	22.048
25.0	30.974	30.376	29.802	29.248	28.715	28.202	27.707	27.229
30.0	36.826	36.117	35.435	34.779	34.147	33.538	32.951	32.384
35.0	42.645	41.827	41.039	40.282	39.552	38.848	38.170	37.515
40.0	48.433	47.506	46.614	45.756	44.929	44.132	43.363	42.621
45.0	54.189	53.154	52.159	51.202	50.279	49.390	48.531	47.703
50.0	59.914	58.773	57.676	56.620	55.602	54.621	53.675	52.761
55.0	65.608	64.362	63.164	62.010	60.899	59.827	58.793	57.795
60.0	71.271	69.922	68.623	67.373	66.169	65.008	63.888	62.806
65.0	76.904	75.452	74.055	72.710	71.413	70.163	68.957	67.793
70.0	82.507	80.953	79.458	78.019	76.632	75.294	74.003	72.756
75.0	88.080	86.426	84.834	83.302	81.824	80.400	79.025	77.697
80.0	93.624	91.870	90.183	88.558	86.992	85.481	84.023	82.615
85.0	99.138	97.286	95.504	93.788	92.134	90.538	88.998	87.511
90.0	104.62	102.67	100.80	98.992	97.251	95.571	93.950	92.383
95.0	110.08	108.04	106.07	104.17	102.34	100.58	98.878	97.234
100.0	115.51	113.37	111.31	109.32	107.41	105.57	103.78	102.06
105.0	120.91	118.68	116.52	114.45	112.45	110.53	108.67	106.87
110.0	126.28	123.95	121.71	119.56	117.47	115.47	113.53	111.65
115.0	131.63	129.21	126.88	124.63	122.47	120.38	118.37	116.42
120.0	136.94	134.43	132.02	129.69	127.44	125.28	123.18	121.16
125.0	142.23	139.63	137.13	134.72	132.39	130.15	127.98	125.88
130.0	147.50	144.81	142.22	139.72	137.32	134.99	132.75	130.58
135.0	152.74	149.96	147.28	144.70	142.22	139.82	137.50	135.26
140.0	157.95	155.08	152.32	149.66	147.10	144.62	142.23	139.92
145.0	163.13	160.18	157.34	154.60	151.95	149.40	146.96	144.56
150.0	168.29	165.25	162.33	159.51	156.79	154.16	151.63	149.18
155.0	173.42	170.30	167.29	164.40	161.60	158.90	156.29	153.77
160.0	178.53	175.32	172.24	169.26	166.39	163.62	160.94	158.35
165.0	183.61	180.32	177.16	174.10	171.16	168.31	165.57	162.91
170.0	188.67	185.30	182.05	178.92	175.90	172.99	170.17	167.45
175.0	193.70	190.25	186.93	183.72	180.63	177.64	174.76	171.97
180.0	198.71	195.19	191.78	188.50	185.33	182.28	179.32	176.47
185.0	203.69	200.08	196.60	193.25	190.01	186.89	183.87	180.95
190.0	208.65	204.95	201.41	197.98	194.68	191.48	188.39	185.41
195.0	213.59	209.82	206.19	202.69	199.32	196.05	192.90	189.85
200.0	218.50	214.66	210.95	207.38	203.94	200.61	197.39	194.28
205.0	223.39	219.47	215.69	212.05	208.54	205.14	201.86	198.69
210.0	228.25	224.26	220.41	216.70	213.11	209.65	206.31	203.07
215.0	233.10	229.03	225.11	221.32	217.67	214.15	210.74	207.44
220.0	237.92	233.77	229.78	225.93	222.21	218.62	215.15	211.79
225.0	242.71	238.50	234.43	230.51	226.73	223.08	219.54	216.12
230.0	247.49	243.20	239.07	235.08	231.23	227.51	223.92	220.44
235.0	252.24	247.88	243.68	239.62	235.71	231.93	228.27	224.74
240.0	256.97	252.54	248.27	244.15	240.17	236.33	232.61	229.02
245.0	261.68	257.18	252.84	248.65	244.61	240.71	236.93	233.28

Helium--SI Units

Table I-1

Lift (kg/m³) of Gas Contained in Steel Cylinders

G. Press. (x10 ⁵) (N/m ²)	Temperature (°C)							
	15	20	25	30	35	40	45	50
0.0	1.0552	1.0374	1.0201	1.0035	.98739	.97179	.95669	.94206
5.0	6.2469	6.1418	6.0401	5.9418	5.8467	5.7546	5.6653	5.5789
10.0	11.414	11.222	11.037	10.858	10.684	10.516	10.354	10.196
15.0	16.556	16.279	16.011	15.751	15.503	15.257	15.022	14.794
20.0	21.674	21.312	20.962	20.623	20.295	19.978	19.671	19.372
25.0	26.767	26.321	25.890	25.473	25.069	24.678	24.299	23.932
30.0	31.837	31.308	30.796	30.301	29.822	29.358	28.908	28.472
35.0	36.882	36.271	35.680	35.108	34.554	34.018	33.498	32.994
40.0	41.904	41.212	40.542	39.893	39.266	38.658	38.068	37.497
45.0	46.903	46.130	45.382	44.658	43.957	43.278	42.619	41.981
50.0	51.878	51.025	50.200	49.401	48.628	47.878	47.152	46.447
55.0	56.831	55.898	54.997	54.124	53.278	52.459	51.665	50.895
60.0	61.760	60.750	59.772	58.826	57.909	57.021	56.160	55.325
65.0	66.667	65.579	64.527	63.507	62.520	61.564	60.636	59.736
70.0	71.552	70.387	69.260	68.169	67.112	66.088	65.094	64.130
75.0	76.414	75.173	73.973	72.810	71.684	70.593	69.534	68.507
80.0	81.254	79.938	78.665	77.432	76.237	75.079	73.956	72.866
85.0	86.073	84.682	83.336	82.033	80.771	79.547	78.359	77.207
90.0	90.869	89.405	87.988	86.615	85.285	83.996	82.745	81.531
95.0	95.645	94.107	92.619	91.178	89.781	88.427	87.114	85.838
100.0	100.40	98.789	97.231	95.721	94.259	92.840	91.464	90.129
105.0	105.13	103.45	101.82	100.25	98.717	97.236	95.798	94.402
110.0	109.84	108.09	106.39	104.75	103.16	101.61	100.11	98.658
115.0	114.53	112.71	110.95	109.24	107.58	105.97	104.41	102.90
120.0	119.20	117.31	115.48	113.71	111.98	110.32	108.70	107.12
125.0	123.85	121.89	119.99	118.15	116.37	114.64	112.96	111.33
130.0	128.48	126.45	124.49	122.59	120.74	118.95	117.21	115.52
135.0	133.09	131.00	128.97	127.00	125.09	123.24	121.44	119.70
140.0	137.68	135.52	133.42	131.39	129.42	127.51	125.66	123.85
145.0	142.25	140.02	137.86	135.77	133.74	131.77	129.86	128.00
150.0	146.80	144.51	142.28	140.13	138.04	136.01	134.04	132.13
155.0	151.33	148.97	146.69	144.47	142.32	140.23	138.21	136.24
160.0	155.85	153.42	151.07	148.79	146.58	144.44	142.36	140.33
165.0	160.34	157.85	155.44	153.10	150.83	148.63	146.49	144.41
170.0	164.81	162.26	159.79	157.39	155.06	152.81	150.61	148.48
175.0	169.27	166.65	164.12	161.66	159.28	156.96	154.72	152.53
180.0	173.70	171.03	168.43	165.92	163.48	161.11	158.80	156.57
185.0	178.12	175.38	172.73	170.16	167.66	165.23	162.88	160.59
190.0	182.52	179.72	177.11	174.38	171.82	169.34	166.94	164.59
195.0	186.90	184.04	181.27	178.58	175.97	173.44	170.98	168.59
200.0	191.26	188.34	185.51	182.77	180.11	177.52	175.01	172.56
205.0	195.61	192.63	189.74	186.94	184.23	181.59	179.02	176.53
210.0	199.94	196.90	193.96	191.10	188.33	185.64	183.02	180.47
215.0	204.24	201.15	198.15	195.24	192.41	189.67	187.00	184.41
220.0	208.54	205.38	202.33	199.36	196.49	193.69	190.97	188.33
225.0	212.81	209.60	206.49	203.47	200.54	197.69	194.93	192.23
230.0	217.07	213.80	210.64	207.57	204.58	201.68	198.87	196.13
235.0	221.31	217.99	214.77	211.64	208.61	205.66	202.79	200.00
240.0	225.53	222.16	218.88	215.70	212.62	209.62	206.70	203.87
245.0	229.74	226.31	222.98	219.75	216.61	213.57	210.60	207.72

Helium--Eng. Units

Table I-2

Lift (lb/ft³) of Gas Contained in Steel Cylinders

Gage Press. (lb/in. ²)	Temperature (°F)					
	0	10	20	30	40	50
0	.07424	.07268	.07118	.06974	.06836	.06703
50	.32616	.31929	.31271	.30640	.30034	.29451
100	.57712	.56499	.55337	.54222	.53152	.52123
150	.82714	.80980	.79317	.77722	.76190	.74718
200	1.0762	1.0537	1.0321	1.0114	.99150	.97238
250	1.3244	1.2967	1.2702	1.2447	1.2203	1.1968
300	1.5716	1.5388	1.5074	1.4773	1.4483	1.4205
350	1.8179	1.7801	1.7438	1.7090	1.6756	1.6435
400	2.0633	2.0205	1.9794	1.9399	1.9021	1.8657
450	2.3078	2.2600	2.2141	2.1701	2.1278	2.0871
500	2.5514	2.4986	2.4480	2.3994	2.3527	2.3079
550	2.7942	2.7364	2.6811	2.6280	2.5769	2.5279
600	3.0360	2.9734	2.9134	2.8557	2.8004	2.7472
650	3.2769	3.2095	3.1448	3.0827	3.0231	2.9658
700	3.5170	3.4447	3.3755	3.3089	3.2451	3.1836
750	3.7562	3.6792	3.6053	3.5344	3.4663	3.4008
800	3.9945	3.9127	3.8343	3.7591	3.6868	3.6172
850	4.2320	4.1455	4.0626	3.9830	3.9065	3.8330
900	4.4686	4.3775	4.2901	4.2062	4.1255	4.0480
950	4.7043	4.6086	4.5168	4.4286	4.3439	4.2624
1000	4.9393	4.8389	4.7427	4.6503	4.5615	4.4760
1050	5.1733	5.0685	4.9678	4.8712	4.7783	4.6890
1100	5.4066	5.2972	5.1922	5.0914	4.9945	4.9013
1150	5.6390	5.5251	5.4158	5.3109	5.2100	5.1129
1200	5.8706	5.7522	5.6387	5.5296	5.4248	5.3239
1250	6.1014	5.9786	5.8608	5.7476	5.6388	5.5342
1300	6.3314	6.2042	6.0821	5.9649	5.8522	5.7438
1350	6.5605	6.4290	6.3028	6.1815	6.0649	5.9527
1400	6.7889	6.6530	6.5226	6.3974	6.2769	6.1610
1450	7.0165	6.8763	6.7418	6.6125	6.4883	6.3687
1500	7.2433	7.0988	6.9602	6.8270	6.6989	6.5757
1550	7.4693	7.3206	7.1779	7.0408	6.9089	6.7821
1600	7.6945	7.5416	7.3948	7.2538	7.1183	6.9878
1650	7.9189	7.7618	7.6111	7.4662	7.3269	7.1928
1700	8.1426	7.9814	7.8266	7.6779	7.5349	7.3973
1750	8.3655	8.2002	8.0415	7.8890	7.7423	7.6011
1800	8.5876	8.4182	8.2556	8.0993	7.9490	7.8043
1850	8.8090	8.6355	8.4690	8.3090	8.1550	8.0069
1900	9.0296	8.8521	8.6817	8.5180	8.3605	8.2088
1950	9.2495	9.0680	8.8938	8.7263	8.5652	8.4101

Helium--Eng. Units

Table I-2

Lift (lb/ft³) of Gas Contained in Steel Cylinders

Gage Press. (lb/in. ²)	Temperature (°F)					
	60	70	80	90	100	110
0	.06575	.06452	.06334	.06220	.06110	.06004
50	.28891	.28352	.27834	.27333	.26851	.26386
100	.51134	.50182	.49265	.48381	.47529	.46707
150	.73303	.71941	.70629	.69364	.68145	.66968
200	.95399	.93630	.91925	.90282	.88697	.87168
250	1.1742	1.1525	1.1315	1.1114	1.0919	1.0731
300	1.3938	1.3680	1.3432	1.3192	1.2962	1.2739
350	1.6126	1.5828	1.5541	1.5265	1.4998	1.4741
400	1.8306	1.7969	1.7644	1.7331	1.7029	1.6737
450	2.0480	2.0104	1.9741	1.9391	1.9054	1.8728
500	2.2647	2.2231	2.1831	2.1445	2.1072	2.0712
550	2.4807	2.4352	2.3915	2.3492	2.3085	2.2691
600	2.6960	2.6467	2.5992	2.5534	2.5091	2.4664
650	2.9106	2.8575	2.8062	2.7569	2.7092	2.6632
700	3.1245	3.0676	3.0127	2.9598	2.9087	2.8593
750	3.3377	3.2770	3.2185	3.1620	3.1076	3.0549
800	3.5503	3.4858	3.4237	3.3637	3.3059	3.2500
850	3.7622	3.6940	3.6282	3.5648	3.5036	3.4445
900	3.9734	3.9015	3.8322	3.7653	3.7007	3.6384
950	4.1839	4.1083	4.0355	3.9652	3.8973	3.8318
1000	4.3938	4.3146	4.2382	4.1645	4.0933	4.0246
1050	4.6030	4.5202	4.4403	4.3632	4.2888	4.2169
1100	4.8116	4.7251	4.6418	4.5613	4.4836	4.4086
1150	5.0195	4.9295	4.8426	4.7589	4.6780	4.5998
1200	5.2268	5.1332	5.0429	4.9558	4.8717	4.7904
1250	5.4334	5.3363	5.2426	5.1522	5.0649	4.9805
1300	5.6394	5.5387	5.4417	5.3480	5.2576	5.1701
1350	5.8447	5.7406	5.6402	5.5433	5.4497	5.3592
1400	6.0494	5.9419	5.8381	5.7380	5.6412	5.5477
1450	6.2535	6.1425	6.0355	5.9321	5.8322	5.7357
1500	6.4570	6.3426	6.2322	6.1256	6.0227	5.9232
1550	6.6598	6.5420	6.4284	6.3187	6.2126	6.1101
1600	6.8621	6.7409	6.6240	6.5111	6.4020	6.2966
1650	7.0637	6.9392	6.8190	6.7030	6.5909	6.4825
1700	7.2647	7.1368	7.0135	6.8944	6.7793	6.6680
1750	7.4651	7.3339	7.2074	7.0852	6.9671	6.8529
1800	7.6649	7.5305	7.4007	7.2755	7.1544	7.0373
1850	7.8641	7.7264	7.5935	7.4652	7.3412	7.2212
1900	8.0627	7.9218	7.7857	7.6544	7.5274	7.4046
1950	8.2607	8.1165	7.9774	7.8431	7.7132	7.5876

Helium--Eng. Units

Table I-2

Lift (lb/ft³) of Gas Contained in Steel Cylinders

Gage Press. (lb/in. ²)	Temperature (°F)					
	0	10	20	30	40	50
2000	9.4686	9.2832	9.1051	8.9340	8.7694	8.6100
2050	9.6870	9.4976	9.3158	9.1410	8.9729	8.8110
2100	9.9047	9.7114	9.5258	9.3474	9.1757	9.0105
2150	10.122	9.9245	9.7351	9.5531	9.3780	9.2094
2200	10.338	10.137	9.9438	9.7582	9.5796	9.4077
2250	10.553	10.348	10.152	9.9626	9.7806	9.6054
2300	10.768	10.559	10.359	10.166	9.9810	9.8025
2350	10.982	10.770	10.566	10.370	10.181	9.9990
2400	11.195	10.979	10.772	10.572	10.380	10.195
2450	11.408	11.188	10.977	10.774	10.579	10.390
2500	11.620	11.397	11.182	10.975	10.777	10.585
2550	11.831	11.604	11.386	11.176	10.974	10.779
2600	12.042	11.811	11.589	11.376	11.171	10.973
2650	12.252	12.017	11.792	11.575	11.367	11.166
2700	12.461	12.223	11.994	11.774	11.563	11.359
2750	12.669	12.428	12.196	11.972	11.758	11.550
2800	12.877	12.632	12.397	12.170	11.952	11.742
2850	13.084	12.836	12.597	12.367	12.146	11.933
2900	13.291	13.039	12.797	12.564	12.339	12.123
2950	13.497	13.241	12.996	12.759	12.532	12.313
3000	13.702	13.443	13.194	12.955	12.724	12.502
3050	13.907	13.644	13.392	13.149	12.916	12.690
3100	14.110	13.845	13.589	13.343	13.107	12.879
3150	14.314	14.044	13.786	13.537	13.297	13.066
3200	14.516	14.244	13.982	13.730	13.487	13.253
3250	14.718	14.442	14.177	13.922	13.676	13.440
3300	14.919	14.640	14.372	14.114	13.865	13.626
3350	15.120	14.838	14.566	14.305	14.054	13.811
3400	15.320	15.035	14.760	14.496	14.241	13.996
3450	15.520	15.231	14.953	14.686	14.429	14.180

Helium--Eng. Units

Table I-2

Lift (lb/ft³) of Gas Contained in Steel Cylinders

Gage Press. (lb/in. ²)	Temperature (°F)					
	60	70	80	90	100	110
2000	8.4581	8.3108	8.1686	8.0312	7.8984	7.7700
2050	8.6549	8.5044	8.3591	8.2188	8.0832	7.9519
2100	8.8512	8.6975	8.5492	8.4059	8.2674	8.1334
2150	9.0468	8.8900	8.7387	8.5925	8.4511	8.3143
2200	9.2419	9.0820	8.9277	8.7785	8.6343	8.4948
2250	9.4364	9.2735	9.1161	8.9641	8.8171	8.6748
2300	9.6304	9.4643	9.3040	9.1491	8.9993	8.8544
2350	9.8238	9.6547	9.4914	9.3336	9.1810	9.0334
2400	10.017	9.8444	9.6782	9.5176	9.3623	9.2120
2450	10.209	10.034	9.8646	9.7011	9.5431	9.3901
2500	10.401	10.222	10.050	9.8841	9.7234	9.5677
2550	10.592	10.411	10.236	10.067	9.9032	9.7449
2600	10.782	10.598	10.420	10.249	10.082	9.9216
2650	10.972	10.785	10.605	10.430	10.261	10.098
2700	11.162	10.972	10.789	10.611	10.440	10.274
2750	11.351	11.158	10.972	10.792	10.618	10.449
2800	11.539	11.344	11.155	10.972	10.795	10.624
2850	11.727	11.529	11.337	11.151	10.972	10.798
2900	11.914	11.713	11.519	11.331	11.149	10.972
2950	12.101	11.897	11.700	11.509	11.325	11.146
3000	12.288	12.081	11.881	11.687	11.500	11.319
3050	12.473	12.264	12.061	11.865	11.675	11.492
3100	12.659	12.446	12.241	12.042	11.850	11.664
3150	12.843	12.628	12.420	12.219	12.024	11.836
3200	13.027	12.810	12.599	12.395	12.198	12.007
3250	13.211	12.991	12.777	12.571	12.371	12.178
3300	13.394	13.171	12.955	12.746	12.544	12.348
3350	13.577	13.351	13.133	12.921	12.717	12.518
3400	13.759	13.531	13.310	13.096	12.889	12.688
3450	13.941	13.710	13.486	13.270	13.060	12.857

Hydrogen--SI Units

Table I-3

Lift (kg/m³) of Gas Contained in Steel Cylinders

G. Press. (x10 ⁶) (N/m ²)	Temperature (°C)							
	-25	-20	-15	-10	-5	0	5	10
0.	1.3216	1.2957	1.2708	1.2469	1.2238	1.2017	1.1803	1.1596
5.	7.8184	7.6655	7.5185	7.3772	7.2411	7.1100	6.9836	6.8617
10.	14.274	13.996	13.728	13.470	13.222	12.983	12.752	12.530
15.	20.689	20.286	19.898	19.525	19.166	18.820	18.487	18.165
20.	27.064	26.537	26.030	25.543	25.074	24.622	24.187	23.766
25.	33.397	32.747	32.123	31.523	30.945	30.389	29.852	29.335
30.	39.689	38.919	38.178	37.466	36.781	36.120	35.484	34.869
35.	45.941	45.050	44.195	43.372	42.580	41.816	41.081	40.371
40.	52.151	51.142	50.173	49.240	48.343	47.478	46.644	45.843
45.	58.321	57.195	56.113	55.072	54.070	53.104	52.174	51.276
50.	64.450	63.208	62.014	60.866	59.761	58.696	57.669	56.679
55.	70.539	69.182	67.878	66.624	65.416	64.253	63.131	62.049
60.	76.587	75.117	73.704	72.344	71.036	69.775	68.560	67.387
65.	82.595	81.013	79.492	78.029	76.620	75.263	73.955	72.693
70.	88.563	86.869	85.242	83.677	82.169	80.717	79.317	77.966
75.	94.490	92.687	90.955	89.288	87.683	86.137	84.646	83.208
80.	100.376	98.467	96.630	94.863	93.162	91.523	89.943	88.418
85.	106.225	104.208	102.269	100.403	98.606	96.875	95.206	93.596
90.	112.034	109.911	107.870	105.906	104.016	102.194	100.437	98.742
95.	117.802	115.575	113.434	111.374	109.391	107.479	105.636	103.857
100.	123.532	121.202	118.962	116.807	114.732	112.731	110.803	108.941
105.	129.222	126.791	124.454	122.204	120.038	117.951	115.937	113.994
110.	134.874	132.343	129.909	127.567	125.311	123.137	121.040	119.016
115.	140.487	137.857	135.328	132.894	130.550	128.291	126.111	124.008
120.	146.062	143.334	140.711	138.187	135.756	133.412	131.151	128.969
125.	151.598	148.775	146.059	143.445	140.928	138.501	136.160	133.900
130.	157.097	154.178	151.371	148.670	146.067	143.558	141.137	138.800
135.	162.558	159.546	156.649	153.860	151.173	148.583	146.084	143.671
140.	167.981	164.877	161.891	159.016	156.247	153.577	151.000	148.513
145.	173.367	170.172	167.099	164.139	161.288	158.539	155.886	153.324
150.	178.716	175.432	172.272	169.229	166.297	163.470	160.742	158.107
155.	184.029	180.656	177.411	174.286	171.274	168.370	165.567	162.861
160.	189.305	185.845	182.515	179.309	176.220	173.239	170.363	167.585
165.	194.545	190.999	187.587	184.301	181.133	178.078	175.129	172.281
170.	199.749	196.118	192.624	189.259	186.016	182.887	179.866	176.949
175.	204.917	201.203	197.629	194.186	190.867	187.665	184.574	181.588
180.	210.050	206.254	202.600	199.081	195.687	192.414	189.253	186.200
185.	215.148	211.271	207.539	203.944	200.477	197.133	193.903	190.783
190.	220.211	216.254	212.445	208.775	205.237	201.822	198.525	195.339
195.	225.239	221.204	217.319	213.576	209.966	206.482	203.118	199.867
200.	230.234	226.121	222.161	218.345	214.665	211.114	207.684	204.369
205.	235.194	231.005	226.971	223.084	219.335	215.716	212.221	208.843
210.	240.120	235.856	231.750	227.793	223.975	220.290	216.731	213.290
215.	245.013	240.676	236.498	232.471	228.586	224.836	221.213	217.711
220.	249.873	245.463	241.214	237.119	233.168	229.354	225.668	222.106
225.	254.700	250.218	245.900	241.737	237.721	233.843	230.097	226.474
230.	259.495	254.942	250.556	246.327	242.246	238.306	234.498	230.817
235.	264.257	259.634	255.181	250.886	246.742	242.740	238.873	235.133
240.	268.987	264.296	259.776	255.417	251.211	247.148	243.221	239.424
245.	273.685	268.927	264.342	259.919	255.651	251.528	247.544	243.690

Hydrogen--SI Units

Table I-3

Lift (kg/m³) of Gas Contained in Steel Cylinders

G. Press. ($\times 10^6$) (N/m ²)	Temperature (°C)							
	15	20	25	30	35	40	45	50
0.	1.1397	1.1205	1.1019	1.0839	1.0665	1.0496	1.0333	1.0175
5.	6.7440	6.6303	6.5204	6.4142	6.3114	6.2119	6.1155	6.0221
10.	12.316	12.108	11.908	11.714	11.527	11.346	11.170	11.000
15.	17.854	17.555	17.265	16.984	16.713	16.451	16.196	15.950
20.	23.361	22.969	22.591	22.225	21.870	21.527	21.195	20.873
25.	28.835	28.352	27.886	27.435	26.998	26.576	26.167	25.770
30.	34.277	33.704	33.151	32.615	32.098	31.596	31.111	30.640
35.	39.686	39.024	38.385	37.766	37.168	36.588	36.027	35.483
40.	45.064	44.314	43.589	42.888	42.210	41.553	40.917	40.300
45.	50.409	49.572	48.763	47.988	47.223	46.490	45.779	45.091
50.	55.723	54.799	53.906	53.043	52.208	51.399	50.615	49.855
55.	61.005	59.996	59.020	58.077	57.164	56.280	55.424	54.594
60.	66.255	65.162	64.105	63.082	62.093	61.134	60.206	59.306
65.	71.474	70.297	69.159	68.058	66.993	65.962	64.962	63.993
70.	76.662	75.402	74.184	73.006	71.866	70.762	69.692	68.655
75.	81.819	80.477	79.180	77.925	76.711	75.535	74.395	73.290
80.	86.945	85.522	84.147	82.816	81.528	80.281	79.073	77.901
85.	92.040	90.538	89.085	87.679	86.319	85.001	83.724	82.486
90.	97.105	95.523	93.994	92.514	91.082	89.694	88.350	87.047
95.	102.139	100.479	98.874	97.321	95.818	94.362	92.951	91.582
100.	107.143	105.406	103.726	102.100	100.527	99.003	97.525	96.093
105.	112.117	110.303	108.549	106.852	105.209	103.618	102.075	100.579
110.	117.061	115.172	113.345	111.577	109.865	108.207	106.600	105.041
115.	121.976	120.012	118.112	116.274	114.495	112.771	111.100	109.479
120.	126.861	124.823	122.852	120.945	119.098	117.309	115.575	113.893
125.	131.716	129.606	127.564	125.589	123.676	121.822	120.025	118.282
130.	136.543	134.360	132.249	130.206	128.227	126.310	124.451	122.648
135.	141.340	139.087	136.907	134.796	132.753	130.773	128.853	126.991
140.	146.109	143.785	141.537	139.361	137.253	135.211	133.231	131.310
145.	150.849	148.456	146.140	143.899	141.728	139.624	137.584	135.605
150.	155.561	153.099	150.717	148.411	146.178	144.013	141.914	139.878
155.	160.245	157.715	155.268	152.898	150.603	148.378	146.220	144.127
160.	164.900	162.304	159.792	157.359	155.003	152.718	150.503	148.354
165.	169.528	166.866	164.290	161.795	159.378	157.035	154.762	152.558
170.	174.129	171.401	168.761	166.205	163.729	161.328	158.999	156.739
175.	178.702	175.910	173.208	170.591	168.055	165.597	163.212	160.898
180.	183.248	180.392	177.628	174.951	172.357	169.842	167.403	165.035
185.	187.766	184.848	182.023	179.287	176.636	174.065	171.571	169.150
190.	192.259	189.278	186.393	183.598	180.890	178.264	175.716	173.243
195.	196.724	193.683	190.738	187.886	185.121	182.440	179.839	177.314
200.	201.163	198.061	195.058	192.149	189.328	186.593	183.940	181.364
205.	205.576	202.415	199.353	196.388	193.513	190.724	188.019	185.392
210.	209.963	206.743	203.624	200.603	197.674	194.833	192.076	189.399
215.	214.324	211.046	207.871	204.794	201.812	198.919	196.111	193.385
220.	218.660	215.324	212.093	208.963	205.927	202.983	200.125	197.350
225.	222.970	219.578	216.292	213.107	210.020	207.025	204.117	201.294
230.	227.255	223.807	220.467	217.229	214.090	211.045	208.088	205.217
235.	231.515	228.012	224.615	221.328	218.138	215.043	212.038	209.120
240.	235.750	232.192	228.746	225.405	222.164	219.020	215.968	213.003
245.	239.961	236.349	232.850	229.453	226.168	222.976	219.876	216.865

Hydrogen--Eng. Units

Table I-4

Lift (lb/ft³) of Gas Contained in Steel Cylinders

Gage Press. (lb/in. ²)	Temperature (°F)					
	0	10	20	30	40	50
0	.08021	.07851	.07689	.07534	.07384	.07241
50	.35226	.34484	.33772	.33090	.32434	.31805
100	.62316	.61003	.59746	.58539	.57381	.56269
150	.89289	.87410	.85610	.83883	.82226	.80634
200	1.1615	1.1370	1.1136	1.0912	1.0697	1.0490
250	1.4289	1.3989	1.3701	1.3425	1.3161	1.2906
300	1.6951	1.6595	1.6255	1.5928	1.5614	1.5313
350	1.9602	1.9191	1.8798	1.8420	1.8058	1.7710
400	2.2241	2.1775	2.1329	2.0902	2.0491	2.0097
450	2.4868	2.4349	2.3851	2.3373	2.2914	2.2474
500	2.7484	2.6911	2.6361	2.5833	2.5327	2.4841
550	3.0089	2.9461	2.8860	2.8284	2.7730	2.7199
600	3.2681	3.2001	3.1349	3.0723	3.0123	2.9546
650	3.5263	3.4529	3.3827	3.3153	3.2506	3.1884
700	3.7833	3.7047	3.6294	3.5572	3.4878	3.4212
750	4.0391	3.9553	3.8750	3.7980	3.7241	3.6531
800	4.2938	4.2048	4.1196	4.0378	3.9594	3.8840
850	4.5473	4.4532	4.3631	4.2766	4.1936	4.1139
900	4.7997	4.7005	4.6055	4.5144	4.4269	4.3429
950	5.0509	4.9467	4.8469	4.7511	4.6592	4.5709
1000	5.3010	5.1918	5.0872	4.9869	4.8905	4.7979
1050	5.5500	5.4359	5.3265	5.2216	5.1208	5.0240
1100	5.7979	5.6788	5.5647	5.4552	5.3501	5.2492
1150	6.0446	5.9206	5.8019	5.6879	5.5785	5.4734
1200	6.2902	6.1614	6.0380	5.9196	5.8059	5.6966
1250	6.5346	6.4011	6.2731	6.1502	6.0323	5.9190
1300	6.7780	6.6397	6.5071	6.3799	6.2578	6.1404
1350	7.0202	6.8772	6.7401	6.6086	6.4822	6.3608
1400	7.2614	7.1137	6.9721	6.8362	6.7058	6.5804
1450	7.5014	7.3491	7.2030	7.0629	6.9283	6.7990
1500	7.7403	7.5834	7.4329	7.2886	7.1499	7.0167
1550	7.9782	7.8167	7.6619	7.5133	7.3706	7.2335
1600	8.2149	8.0489	7.8897	7.7370	7.5903	7.4493
1650	8.4506	8.2801	8.1166	7.9598	7.8091	7.6643
1700	8.6851	8.5102	8.3425	8.1816	8.0270	7.8783
1750	8.9186	8.7393	8.5674	8.4024	8.2439	8.0915
1800	9.1510	8.9674	8.7913	8.6222	8.4599	8.3038
1850	9.3823	9.1944	9.0141	8.8411	8.6749	8.5151
1900	9.6126	9.4204	9.2360	9.0591	8.8891	8.7256
1950	9.8418	9.6454	9.4569	9.2761	9.1023	8.9352

Hydrogen--Eng. Units

Table I-4

Lift (lb/ft³) of Gas Contained in Steel Cylinders

Gage Press. (lb/in. ²)	Temperature (°F)					
	60	70	80	90	100	110
0	.07103	.06970	.06842	.06719	.06600	.06486
50	.31200	.30617	.30056	.29516	.28995	.28492
100	.55199	.54170	.53179	.52224	.51303	.50415
150	.79103	.77629	.76211	.74844	.73526	.72254
200	1.0291	1.0100	.99152	.97376	.95663	.94010
250	1.2662	1.2427	1.2200	1.1982	1.1771	1.1568
300	1.5023	1.4745	1.4476	1.4218	1.3968	1.3727
350	1.7375	1.7053	1.6743	1.6444	1.6156	1.5878
400	1.9718	1.9353	1.9001	1.8663	1.8336	1.8021
450	2.2050	2.1643	2.1250	2.0872	2.0507	2.0155
500	2.4374	2.3924	2.3493	2.3073	2.2670	2.2282
550	2.6687	2.6195	2.5722	2.5265	2.4825	2.4400
600	2.8992	2.8458	2.7944	2.7449	2.6971	2.6510
650	3.1286	3.0711	3.0157	2.9624	2.9109	2.8612
700	3.3572	3.2956	3.2362	3.1790	3.1238	3.0706
750	3.5848	3.5191	3.4558	3.3948	3.3359	3.2792
800	3.8115	3.7417	3.6745	3.6097	3.5472	3.4870
850	4.0372	3.9634	3.8923	3.8238	3.7577	3.6940
900	4.2620	4.1842	4.1093	4.0371	3.9674	3.9002
950	4.4859	4.4041	4.3254	4.2495	4.1762	4.1056
1000	4.7089	4.6232	4.5406	4.4610	4.3843	4.3102
1050	4.9309	4.8413	4.7550	4.6718	4.5915	4.5140
1100	5.1520	5.0585	4.9685	4.8817	4.7979	4.7171
1150	5.3722	5.2749	5.1811	5.0908	5.0036	4.9194
1200	5.5916	5.4904	5.3930	5.2990	5.2084	5.1209
1250	5.8099	5.7050	5.6039	5.5064	5.4124	5.3216
1300	6.0274	5.9187	5.8140	5.7131	5.6156	5.5216
1350	6.2440	6.1316	6.0233	5.9189	5.8181	5.7208
1400	6.4597	6.3436	6.2317	6.1238	6.0197	5.9193
1450	6.6745	6.5547	6.4393	6.3280	6.2206	6.1169
1500	6.8885	6.7650	6.6461	6.5314	6.4207	6.3139
1550	7.1015	6.9744	6.8520	6.7340	6.6200	6.5100
1600	7.3137	7.1830	7.0571	6.9357	6.8186	6.7055
1650	7.5249	7.3907	7.2614	7.1367	7.0164	6.9001
1700	7.7353	7.5976	7.4649	7.3369	7.2134	7.0941
1750	7.9449	7.8036	7.6676	7.5363	7.4096	7.2873
1800	8.1535	8.0088	7.8694	7.7349	7.6051	7.4798
1850	8.3613	8.2132	8.0704	7.9328	7.7998	7.6715
1900	8.5683	8.4167	8.2707	8.1298	7.9938	7.8625
1950	8.7744	8.6195	8.4701	8.3261	8.1871	8.0528

Hydrogen--Eng. Units

Table I-4

Lift (lb/ft³) of Gas Contained in Steel Cylinders

Gage Press. (lb/in. ²)	Temperature (°F)					
	0	10	20	30	40	50
2000	10.070	9.8693	9.6769	9.4921	9.3146	9.1439
2050	10.297	10.092	9.8958	9.7072	9.5260	9.3517
2100	10.523	10.314	10.114	9.9214	9.7365	9.5587
2150	10.748	10.535	10.331	10.135	9.9461	9.7648
2200	10.972	10.755	10.547	10.347	10.155	9.9700
2250	11.195	10.974	10.762	10.558	10.363	10.174
2300	11.417	11.192	10.976	10.769	10.570	10.378
2350	11.638	11.409	11.189	10.978	10.776	10.581
2400	11.858	11.625	11.402	11.187	10.981	10.782
2450	12.077	11.840	11.613	11.395	11.185	10.983
2500	12.294	12.054	11.823	11.602	11.389	11.184
2550	12.511	12.267	12.033	11.808	11.591	11.383
2600	12.727	12.479	12.241	12.013	11.793	11.581
2650	12.942	12.690	12.449	12.217	11.994	11.779
2700	13.156	12.901	12.656	12.420	12.194	11.976
2750	13.369	13.110	12.861	12.622	12.393	12.172
2800	13.581	13.318	13.066	12.824	12.591	12.367
2850	13.792	13.526	13.270	13.025	12.789	12.561
2900	14.002	13.732	13.473	13.224	12.985	12.755
2950	14.211	13.938	13.675	13.423	13.181	12.948
3000	14.419	14.142	13.877	13.621	13.376	13.140
3050	14.626	14.346	14.077	13.819	13.570	13.331
3100	14.832	14.549	14.277	14.015	13.764	13.521
3150	15.037	14.751	14.475	14.211	13.956	13.711
3200	15.242	14.952	14.673	14.405	14.148	13.900
3250	15.445	15.152	14.870	14.599	14.339	14.088
3300	15.647	15.351	15.066	14.792	14.529	14.275
3350	15.849	15.549	15.261	14.985	14.718	14.462
3400	16.050	15.747	15.456	15.176	14.907	14.647
3450	16.249	15.943	15.649	15.367	15.094	14.832

Hydrogen--Eng. Units

Table I-4

Lift (lb/ft³) of Gas Contained in Steel Cylinders

Gage Press. (lb/in. ²)	Temperature (°F)					
	60	70	80	90	100	110
2000	8.9796	8.8213	8.6688	8.5216	8.3795	8.2423
2050	9.1840	9.0224	8.8666	8.7164	8.5713	8.4311
2100	9.3875	9.2227	9.0637	8.9103	8.7623	8.6193
2150	9.5903	9.4221	9.2600	9.1036	8.9526	8.8067
2200	9.7921	9.6207	9.4555	9.2960	9.1421	8.9934
2250	9.9932	9.8186	9.6502	9.4878	9.3309	9.1794
2300	10.193	10.016	9.8442	9.6787	9.5190	9.3646
2350	10.393	10.212	10.037	9.8689	9.7063	9.5492
2400	10.591	10.407	10.230	10.058	9.8930	9.7331
2450	10.789	10.602	10.421	10.247	10.079	9.9163
2500	10.986	10.796	10.612	10.435	10.264	10.099
2550	11.182	10.989	10.802	10.622	10.449	10.281
2600	11.378	11.181	10.992	10.809	10.632	10.462
2650	11.572	11.373	11.180	10.995	10.816	10.642
2700	11.766	11.564	11.368	11.180	10.998	10.822
2750	11.959	11.754	11.556	11.364	11.180	11.001
2800	12.151	11.943	11.742	11.548	11.361	11.180
2850	12.342	12.131	11.928	11.731	11.541	11.357
2900	12.533	12.319	12.113	11.913	11.721	11.534
2950	12.723	12.506	12.297	12.095	11.900	11.711
3000	12.912	12.692	12.480	12.276	12.078	11.887
3050	13.100	12.878	12.663	12.456	12.256	12.062
3100	13.288	13.063	12.845	12.635	12.433	12.236
3150	13.475	13.247	13.027	12.814	12.609	12.410
3200	13.661	13.430	13.207	12.992	12.784	12.583
3250	13.846	13.612	13.387	13.170	12.959	12.756
3300	14.030	13.794	13.566	13.346	13.134	12.928
3350	14.214	13.975	13.745	13.523	13.307	13.099
3400	14.397	14.156	13.923	13.698	13.480	13.270
3450	14.579	14.336	14.100	13.873	13.653	13.440

J. GAS DATA

Gas data which are of frequent use in scientific ballooning are given here. To keep the tables brief and yet provide the data in several of the more commonly used unit systems, the data are given in dimensionless form in some of the tables. For example, the ratio C_p/R is given in Table J-4, and values of R are given in six systems of units in Table J-3. The two tables contain more information than six tables of C_p values alone would contain, but to determine a value of C_p , it is necessary to select a number from each of the two tables and multiply them together.

Specific heat, thermal conductivity, viscosity, and the Prandtl number of the gases listed here all vary significantly with temperature but not with pressure in the range likely to be encountered in scientific ballooning. This variation is shown by the tables, but in many cases equations are more convenient than tables. Therefore, equations which correlate specific heat, etc., with temperature are given wherever possible. Since the equations are empirical, care should be taken not to use them for calculations outside of the range of validity specified in the description of the tables.

For convenience, references to data sources are given immediately following each table.

1. Miscellaneous Gas Data

Table J-1 lists useful gas data in both SI and English units. Some tabular entries have been shortened through multiplication by a factor 10^n . When this has been done, the multiplying factor is shown in the "Units" column. For example, all values of density given in lbm/ft^3 have been multiplied by 10^2 , and it is necessary to divide by 10^2 to recover the correct value. Thus, the density of dry air is $8.07 \div 10^2 = 0.0807 \text{ lbm/ft}^3$.

REFERENCES

- (1) Kaye, G.W.C. and T. H. Laby, 1966: Tables of Physical and Chemical Constants, John Wiley and Sons, Inc., New York.
- (2) Reid, Robert C. and Thomas K. Sherwood, 1966: The Properties of Gases and Liquids, 2nd ed., McGraw Hill Book Co., New York.
- (3) Weast, Robert C. and Samuel M. Selby, 1967-1968: Handbook of Chemistry and Physics, 48th ed., The Chemical Rubber Co., Cleveland, Ohio.

2. Gas Constant and Specific Heat Data for Selected Gases

The specific heat of all of the gases listed here is nearly independent of pressure under the pressure and temperature conditions they are likely to be subjected to in the atmosphere. Specific heat does vary with temperature in most of the gases, although helium is an exception, and the variation in nitrogen and air is not great. Also, if ammonia should reach the temperature of its normal boiling point (238.9°K) at a pressure near one atmosphere, its specific heat may be expected to be a strong function of both pressure and temperature.

Specific heat can be correlated with temperature for the gases listed over the range given in Table J-4 with deviations of less than 5% by means of an equation of the type

$$\frac{C_p}{R} = a + b \times 10^{-2}T + c \times 10^{-6}T^2 \quad (\text{J-1})$$

where C_p is the specific heat at constant pressure, R is the gas constant, and a , b , and c are arbitrary constants, chosen to give an adequate fit to the data. The fit is precise at $T = 273.15^\circ\text{K}$. The specific heat at constant volume C_v and the ratio C_p/C_v are both of frequent interest. For an

ideal gas $C_p - C_v = R$ or $C_v/R = (C_p/R) - 1$ and $C_p/C_v = (C_p/R)/[(C_p/R) - 1]$.

Table J-2 provides values of the constants a , b , and c , which may be used with the correlating equation to calculate C_p/R . Table J-3 lists values of R in several of the more commonly used systems of units. In Table J-4 are found values of C_p/R for each of the gases for the temperature range over which the correlating equation may be safely used. Finally, Table J-5 gives values of C_p/C_v .

From the entries in Tables J-3 and J-4 it is easy to determine either C_p or C_v in any of the systems of units given in Table J-3. To calculate C_p , multiply together appropriate entries from the two tables; to determine C_v , multiply the entry from Table J-3 by the entry from Table J-4 less one, that is, $C_v = R [(C_p/R) - 1]$.

For many purposes in scientific ballooning, an average value of specific heat may be satisfactory even though changes of temperature occur. The specific heats of air and nitrogen, for example, undergo such slight changes below 300°K that a constant value is often adequate, and the specific heat of helium is essentially constant to 50°K or lower.

The specific heat data for the mixture of hydrogen and nitrogen were

computed from the data for the component gases by the method recommended by Reid and Sherwood (1).

Example: Determine the specific heat at constant volume (C_v) at 250°K of the mixture of gases which results from the decomposition of ammonia and write an equation expressing C_v as a function of absolute temperature. The specific heat is desired in cal/gm°K.

Solution: When ammonia is decomposed into nitrogen and hydrogen, the mixture is essentially 3/4 hydrogen and 1/4 nitrogen by volume. Thus, from the column headed $3H_2 + N_2$ in Table J-3 the desired value of R is 0.23338 cal/gm°K. From Table J-4, C_p/R at $T = 250^\circ\text{K}$ is found to be 3.419. Then, to slide rule accuracy,

$$C_v = 0.23 (3.42 - 1) = 0.56 \text{ cal/gm}^\circ\text{K}$$

Alternatively, from Table J-2, a , b , and c are seen to be 2.72, 0.419, and -5.54, respectively. Substituting these and R into the correlating equation yields

$$\begin{aligned} C_v &= 0.233 (1.72 + 0.419 \times 10^{-2}T - 5.54 \times 10^{-6}T^2) \\ &= 0.56 \text{ cal/gm}^\circ\text{K} \end{aligned}$$

Note that 1.0 was subtracted from the value of a to change the equation

from an equation in C_p to one in C_v .

Table J-1

Miscellaneous Gas Data

	Units	Dry Air	Helium	Hydrogen	Nitrogen	Ammonia	Decomp. Ammonia	Methane	Oxygen
Chemical Formula	--	*	He	H ₂	N ₂	NH ₃	3H ₂ +N ₂	CH ₄	O ₂
Molecular Wt. (M)	kg/kg-Mol lb/lb-Mol	28.964	4.0026	2.0159	28.013	17.031	8.515	16.043	32.000
Gas Constant (R/M)	J/kg-Mol ^o K ft lb/lb-Mol ^o R	287.06 53.36	2077.2 386.1	4124.4 766.6	296.80 55.17	488.19 90.74	976.43 181.5	518.25 96.33	259.82 48.29
Density 273.15 ^o K, 101325 N/m ² 491.67 ^o R, 14.696 lbf/in ²	kg/m ³ lbm/ft ³ (x10 ³)	1.292 8.07	0.1786 1.11	0.0899 0.561	1.250 7.80	0.760 4.74	0.380 2.37	0.716 4.47	1.428 8.91
Density 288.15 ^o K, 101325 N/m ² 518.67 ^o R, 14.696 lbf/in ²	kg/m ³ lbm/ft ³ (x10 ³)	1.225 7.65	0.1693 1.057	0.0853 0.532	1.185 7.40	0.720 4.49	0.360 2.25	0.679 4.24	1.353 8.45
Density of Liquid at Normal Boiling Point	kg/m ³ lbm/ft ³	--	128 7.99	71.5 4.46	811 50.6	682 42.6	--	426 26.6	1090 68.0
Normal Boiling Point at 101325 N/m ² 14.696 lbf/in ²	^o K ^o R	78.8 141.8	4.21 7.58	20.4 36.7	87.4 157.3	239.6 431.3	--	111.6 200.9	90.2 162.4
Latent Heat of Vaporization at B.P.	J/kg (x10 ³) BTU/lbm	--	20.3 8.73	448 193	199 85.6	1370 589	--	510 219	213 91.6
Flammable limits in air	% by volume	--	--	4-75	--	15-28	7-73	5.3-14	--
Critical Temp	^o K ^o R	132.5 238.5	5.25 9.45	33.3 59.9	126.2 227.2	405.4 729.7	--	190.6 343.1	154.8 278.6
Critical Pressure	N/m ² (x10 ⁶) lbf/in ² (x10 ²)	3.77 5.47	0.229 0.332	1.297 1.88	3.39 4.92	11.30 16.4	--	4.62 6.70	5.08 7.37
Critical Density	kg/m ³ lbm/ft ³	312 19.5	69.3 4.33	31.0 1.94	311 19.4	235 14.7	--	162 10.1	410 25.6
Critical Volume	m ³ /kg-Mol ft ³ /lb-Mol	0.090 1.44	0.058 0.93	0.065 1.04	0.090 1.44	0.072 1.15	--	0.099 1.59	0.078 1.25
Critical Compressibility	--	0.318	0.307	0.304	0.291	0.243	--	0.288	0.308

*Dry air is a mixture of nitrogen (78.084% by volume), oxygen (20.950%), argon (0.934%), carbon dioxide (0.031%), and traces of other gases.

Table J-2

Constants for the Specific Heat-Temperature Correlating Equation

	Air	Helium	Hydrogen	Nitrogen	Ammonia	Mixture 3H ₂ +N ₂	Methane
a	3.54	2.50	2.463	3.503	2.93	2.72	2.10
b	-0.0438	0.	0.562	-0.00335	0.45	0.419	0.735
c	1.06	0.	-7.45	+0.112	-0.03	-5.54	-0.039
*Source	(1)(5)	(4)	(2)	(1)(3)	(1)	(1)(2)(3)	(1)(3)

*The numbers refer to the references which follow Table J-5.

Table J-3

Gas Constant R in Various Systems of Units

	Air	Helium	Hydrogen	Nitrogen	Ammonia	Mixture 3H ₂ +N ₂	Methane
J/(kg-Mol) ^o K	8314.3	8314.3	8314.3	8314.3	8314.3	8314.3	8314.3
J/kg K	287.06	2077.2	4124.4	296.80	488.19	976.43	518.25
*Cal/(g-Mol) ^o K	1.9872	1.9872	1.9872	1.9872	1.9872	1.9872	1.9872
Cal/g K	0.06861	0.49648	0.98576	0.07094	0.11668	0.23338	0.12387
BTU/(lb-Mol) ^o R	1.9859	1.9859	1.9859	1.9859	1.9859	1.9859	1.9859
BTU/lb R	0.06856	0.49615	0.98512	0.07089	0.11661	0.23322	0.12379

*The calories used here are gram calories.

Table J-4

Values of C_p/R for Select Gases as a Function of Temperature

Temp °K	Air	Helium	Hydrogen	Nitrogen	Ammonia	Mixture 3H ₂ +N ₂	Methane	Temp °R
150	3.501	2.501	3.138	3.500	--	3.222	3.202	270
160	3.500	2.501	3.171	3.500	--	3.246	3.275	288
170	3.499	2.501	3.203	3.500	--	3.270	3.348	306
180	3.498	2.501	3.233	3.501	--	3.293	3.422	324
190	3.498	2.501	3.261	3.501	--	3.314	3.495	342
200	3.497	2.501	3.289	3.501	--	3.334	3.568	360
210	3.497	2.501	3.314	3.501	--	3.354	3.642	378
220	3.498	2.501	3.338	3.501	--	3.372	3.715	396
230	3.498	2.501	3.361	3.501	--	3.389	3.788	414
240	3.498	2.501	3.382	3.501	--	3.405	3.861	432
250	3.499	2.501	3.402	3.502	4.059	3.419	3.935	450
260	3.500	2.501	3.420	3.502	4.104	3.433	4.008	468
270	3.502	2.501	3.437	3.502	4.149	3.446	4.081	486
280	3.503	2.501	3.452	3.502	4.194	3.457	4.155	504
290	3.505	2.501	3.466	3.503	4.240	3.467	4.228	522
300	3.506	2.501	3.478	3.503	4.285	3.477	4.301	540
310	3.509	2.501	3.488	3.503	4.330	3.485	4.374	558
320	3.511	2.501	3.498	3.504	4.375	3.492	4.447	576
330	3.513	2.501	3.505	3.504	4.420	3.498	4.521	594
340	3.516	2.501	3.512	3.504	4.465	3.503	4.594	612
350	3.519	2.501	3.517	3.505	4.510	3.506	4.667	630

Table J-5

Values of C_p/C_v for Select Gases as a Function of Temperature

Temp °K	Air	Helium	Hydrogen	Nitrogen	Ammonia	Mixture 3H ₂ +N ₂	Methane	Temp °R
150	1.400	1.666	1.468	1.400	--	1.450	1.454	270
160	1.400	1.666	1.461	1.400	--	1.445	1.440	288
170	1.400	1.666	1.454	1.400	--	1.441	1.426	306
180	1.400	1.666	1.448	1.400	--	1.436	1.413	324
190	1.400	1.666	1.442	1.400	--	1.432	1.401	342
200	1.400	1.666	1.437	1.400	--	1.428	1.389	360
210	1.400	1.666	1.432	1.400	--	1.425	1.379	378
220	1.400	1.666	1.428	1.400	--	1.422	1.368	396
230	1.400	1.666	1.424	1.400	--	1.419	1.359	414
240	1.400	1.666	1.420	1.400	--	1.416	1.349	432
250	1.400	1.666	1.416	1.400	1.327	1.413	1.341	450
260	1.400	1.666	1.413	1.400	1.322	1.411	1.332	468
270	1.400	1.666	1.410	1.400	1.318	1.409	1.325	486
280	1.400	1.666	1.408	1.400	1.313	1.407	1.317	504
290	1.399	1.666	1.406	1.400	1.309	1.405	1.310	522
300	1.399	1.666	1.404	1.400	1.304	1.404	1.303	540
310	1.399	1.666	1.402	1.399	1.300	1.402	1.296	558
320	1.398	1.666	1.400	1.399	1.296	1.401	1.290	576
330	1.398	1.666	1.399	1.399	1.292	1.400	1.284	594
340	1.397	1.666	1.398	1.399	1.289	1.400	1.278	612
350	1.397	1.666	1.397	1.399	1.285	1.399	1.273	630

REFERENCES

- (1) Reid, Robert C. and Thomas K. Sherwood, 1966: The Properties of Gases and Liquids, Second Edition, McGraw-Hill, New York, 169-196, 300-370.
- (2) Woolley, Harold W., Russell B. Scott, and F. G. Brickwedde, 1948: Compilation of Thermal Properties of Hydrogen in Its Various Isotopic and Ortho-Para Modifications, NBS Research Paper RP 1932, Vol. 4.
- (3) Rossini, Frederick D., Kenneth S. Pitzer, William J. Taylor, Joan P. Ebert, John E. Kilpatrick, Charles W. Beckett, Mary G. Williams, and Helene G. Werner, 1947: Selected Values of Properties of Hydrocarbons, NBS Circular C461.
- (4) Kropschot, R. H., B. W. Birmingham, and D. B. Mann, 1968: Technology of Liquid Helium, NBS Monograph 111, Supt. of Documents, U.S. Govt. Printing Office, Wash. D.C., 33-53.
- (5) Kreith, Frank, 1967: Principles of Heat Transfer, International Textbook Company, Scranton, Pa., 595.

3. Thermal Conductivity of Selected Gases

The thermal conductivity of most gases at pressures ranging from about 75 N/m² (~ one mm of H_g) to several atmospheres is only very slightly dependent on pressure. It is dependent on temperature, however, and increases with increased temperature. Tsederberg (1) suggests that over a range of temperature from 273°K to 775°K, thermal conductivity and temperature data are correlated well for many uses by means of the following equation:

$$\frac{k}{k_0} = \left(\frac{T}{T_0}\right)^n \quad (J-2)$$

where k_0 is the thermal conductivity at temperature T_0 and n is a constant which must be determined for each gas. Tsederberg (1) also lists a number of gases and gives values of the constants n and k_0 at $T_0 = 273^\circ\text{K}$ for them. Tables J-6 and J-7 provide similar data for a few gases which are most likely to be of concern to scientific ballooning. In Table J-7 values of k_0 are given in several of the more commonly used systems of units.

The constants listed in Tables J-6 and J-7 do not always agree with those given by Tsederberg. In scientific ballooning, interest is more

often focused on temperatures below 300°K than on higher temperatures. Therefore, an effort was made to find experimental data in the range $150^{\circ} - 350^{\circ}\text{K}$ and to fit the correlation equation to those data. Within that range of temperature, except for the mixture of hydrogen and nitrogen, the correlation equation with the constants given in Tables J-6 and J-7 fits the data to within 5%. Extrapolations beyond that temperature range should not be attempted unless comparison can be made between some of the extrapolated values and reliable data to assure that extrapolation is valid. Although Tseiderberg listed a value of k_0 for the mixture of hydrogen and nitrogen, it was necessary to calculate values at other temperatures to compute n . These calculations employed the technique of Brokaw described in Reid and Sherwood (2). The accuracy of the data for the mixture is therefore less certain than for the other gases.

Table J-8 was computed from the correlating equation using the constant n given in Table J-6. Tables J-7 and J-8 together provide a means of quickly obtaining thermal conductivity in any of the more commonly used systems of units for the selected gases. Note that each value of k_0 has been multiplied by the factor given in the units column prior to listing it

in Table J-7; therefore, the correct value of k_0 is the tabular entry divided by that factor.

Example: Determine the value of thermal conductivity in $\text{BTU}/\text{ft hr}^{\circ}\text{R}$ for hydrogen at 380°R and write an equation for the thermal conductivity of hydrogen as a function of temperature in degrees Rankine.

Solution: Since 380°R is not given directly in Table J-8, interpolation yields a value of 0.803 for k/k_0 . The accuracy of the table does not warrant retaining the third place number to the right of the decimal. From Table J-7, k_0 is found to be 9.72×10^{-2} , and $9.72 \times 10^{-2} \times 0.80$ yields $7.8 \times 10^{-2} \text{ BTU}/\text{ft hr}^{\circ}\text{R}$.

From Table J-6, n for hydrogen is found to be 0.85. Using that value and k_0 , the desired equation is found to be

$$k = 9.72 \times 10^{-2} \left(\frac{T}{491.67} \right)^{0.85}$$

Table J-6

Values of n for Selected Gases

	Air	Helium	Hydrogen	Nitrogen	Ammonia	Mixture 3H ₂ +N ₂	Methane
n	0.90	0.70	0.85	0.80	1.53	0.84	1.33

Table J-7

Values of k₀ for Selected Gases
 k₀ is the value of k at T = 273.15°K (491.67°R)

	Air	Helium	Hydrogen	Nitrogen	Ammonia	Mixture 3H ₂ +N ₂	Methane
Watts/m ² K (×10 ³)	2.41	14.40	16.82	2.42	2.10	9.8	3.07
Cal/cm sec ² K (×10 ⁵)	5.77	34.4	40.18	5.78	5.03	23.4	7.33
k Cal/m hr ² K (×10 ⁵)	2.08	12.38	14.46	2.08	1.81	8.4	2.64
BTU/ft hr ² R (×10 ³)	1.40	8.32	9.72	1.40	1.22	5.7	1.77
*Source	(1)(6)	(4)(5)	(1)(6)	(1)(5)	(1)	(1)	(1)(5)

*The numbers refer to the references which follow Table J-8.

Table J-8

Thermal Conductivity Ratios (k/k₀) for Selected Gases as a
 Function of Temperature

Temp °K	Air	Helium	Hydrogen	Nitrogen	Ammonia	Mixture 3H ₂ +N ₂	Methane	Temp °R
150	.612	.657	.601	.619	--	.604	.451	270
160	.645	.688	.635	.652	--	.638	.491	288
170	.678	.718	.668	.684	--	.671	.532	306
180	.710	.747	.702	.716	--	.704	.574	324
190	.743	.776	.735	.748	--	.737	.617	342
200	.774	.804	.767	.779	--	.770	.661	360
210	.806	.832	.800	.810	--	.802	.705	378
220	.837	.859	.832	.841	--	.834	.750	396
230	.868	.887	.864	.871	--	.866	.796	414
240	.899	.913	.896	.902	--	.897	.842	432
250	.930	.940	.927	.932	.873	.928	.889	450
260	.960	.966	.959	.961	.927	.959	.936	468
270	.991	.992	.990	.991	.982	.990	.985	486
280	1.021	1.017	1.021	1.020	1.039	1.021	1.033	504
290	1.050	1.043	1.052	1.049	1.096	1.052	1.083	522
300	1.080	1.068	1.083	1.078	1.154	1.082	1.133	540
310	1.109	1.093	1.114	1.107	1.214	1.112	1.183	558
320	1.139	1.117	1.144	1.135	1.274	1.142	1.234	576
330	1.168	1.142	1.174	1.163	1.335	1.172	1.286	594
340	1.197	1.166	1.205	1.191	1.398	1.202	1.338	612
350	1.225	1.190	1.235	1.219	1.461	1.232	1.391	630

REFERENCES

- (1) Tsederberg, N. V., 1965: The Thermal Conductivity of Gases and Liquids, The MIT Press, Cambridge, Mass., 88-97 and 144-165.
- (2) Reid, Robert C. and Thomas K. Sherwood, 1966: The Properties of Liquids and Gases, 2nd ed., McGraw-Hill, New York, 456-519.
- (3) The U.S. Standard Atmosphere, 1962, U.S. Govt. Printing Office, Washington, D.C., 1 and 91.
- (4) Kropschot, R. H., B. W. Birmingham, D. B. Mann, Editors, 1968: Technology of Liquid Helium, NBS Monograph 111, U.S. Govt. Printing Office, Washington, D.C., 50-51.
- (5) Ho, C. Y. and R. E. Taylor, 1969: Thermal Conductivity, Proceedings of the Eighth Conference, Plenum Press, New York, 76, 119, 125, 229.
- (6) Hilsenrath, Joseph, Charles W. Beckett, William S. Benedict, Lilla Fano, Harold J. Hoge, Joseph F. Masi, Ralph L. Nuttall, Yeram S. Touloukian, Harold W. Woolley, 1955: Tables of Thermal Properties of Gases, NBS Circular 564, U.S. Govt. Printing Office, Washington, D.C., 269 and 285.

4. Viscosity of Selected Gases

The dynamic viscosity of gases at low pressure (two atmospheres or less) is very nearly independent of pressure, but it is a function of temperature, and the viscosity increases with temperature. For most of the gases listed here, the two-constant Sutherland equation has been shown to be a highly reliable equation for correlating viscosity-temperature data.

It is

$$\mu = bT^{1.5} / (S + T) \quad (J-4)$$

where b and S are arbitrary constants which may be determined by any satisfactory curve fitting technique. The equation, in the form

$$\frac{\mu}{\mu_0} = \left(\frac{T}{273.15} \right)^{1.5} \frac{S + 273.15}{S + T} \quad (J-5)$$

in which T must be entered in degrees Kelvin, was used to compute the data of Table J-11 for all gases except hydrogen and helium. The value of S is given in Table J-9.

The hydrogen and helium data were computed using the following equations:

$$\text{Hydrogen} \quad \frac{\mu}{\mu_0} = 460 \left(\frac{T}{273.15} \right)^{1.5} \frac{T + 650.4}{(T + 19.6)(T + 1176)} \quad (J-6)$$

$$\text{Helium} \quad \frac{\mu}{\mu_0} = \left(\frac{T}{273.15} \right)^{0.647} \quad (\text{J-7})$$

Within the temperature range used in Table J-11, the tabulated values and the equations yield viscosity data which rarely differ more than 5% from the data used to determine the constants. Viscosity values for the mixture of hydrogen and nitrogen were computed using the Wilke method for estimating the viscosity of gas mixtures as described in Reid and Sherwood (1), and the Sutherland equation was fitted to the estimated data. Errors may be as large as 10%. The equations for hydrogen and helium may be used for values of T as low as 30°K without excessive error.

Kinematic viscosity η may be determined from μ if the gas density is known since $\eta = \mu/\rho$.

Example: Determine the viscosity of ammonia in lbf sec/ft² at T = 450°R. Also write an equation which may be used in a computer program to compute the viscosity in lbf sec/ft² using T in degrees Rankine.

Solution: The value of μ/μ_0 for ammonia at 450°R is selected directly from Table J-11. It is 0.898. The value of μ_0 for ammonia from Table J-10 is 1.881×10^{-7} lbf sec/ft². Their product is 1.69×10^{-7} lbf sec/ft².

Note that each value of μ_0 given in Table J-10 has been multiplied by the

factor (10⁷ in this example) which is shown in the units column. Therefore, the tabular entry must be divided by this factor.

The desired equation is

$$\mu = 1.881 \times 10^{-7} \left(\frac{5/9 T}{273.15} \right)^{1.5} \frac{670 + 273.15}{670 + 5/9 T}$$

where S = 670 is determined from Table J-9 and $5/9 T(^{\circ}\text{R}) = T(^{\circ}\text{K})$.

Table J-9

Values of S for Selected Gases

	Air	Helium	Hydrogen	Nitrogen	Ammonia	Mixture 3H ₂ +N ₂	Methane
S	110.4	--	--	100.1	670	98.9	93.5

Table J-10

Values of μ_0 for Selected Gases
 $\mu_0 = \mu$ when $T = 273.15^\circ\text{K}$

	Mixture						
	Air	Helium	Hydrogen	Nitrogen	Ammonia	$3\text{H}_2 + \text{N}_2$	Methane
kg/m sec ($\times 10^6$)	1.716	1.895	0.841	1.652	0.900	1.43	1.089
*poise ($\times 10^4$)	1.716	1.895	0.841	1.652	0.900	1.43	1.089
lbm/ft sec ($\times 10^5$)	1.153	1.273	0.565	1.110	0.605	0.96	0.732
lbm/ft hr ($\times 10^7$)	4.152	4.586	2.035	3.998	2.178	3.46	2.635
lbf sec/ft ² ($\times 10^7$)	3.586	3.961	1.758	3.453	1.881	2.99	2.276
slug/ft hr ($\times 10^4$)	12.90	14.25	6.324	12.42	6.768	10.75	8.189
**Source	(2)(5)	(3)	(4)(5)	(5)	(1)	(1)	(1)

*1 poise = 1 dyne sec/cm² = 1 gm/cm sec = 0.1 kg/m sec.

**The numbers refer to the reference which follow Table J-11.

Table J-11

Values of μ/μ_0 for Selected Gases as a Function of Temperature

Temp °K	Air	Helium	Hydrogen	Nitrogen	Ammonia	Mixture $3\text{H}_2 + \text{N}_2$	Methane	Temp °R
150	.599	.679	.666	.631	--	.642	.613	270
160	.635	.707	.696	.666	--	.676	.648	288
170	.671	.736	.726	.699	--	.709	.683	306
180	.706	.764	.755	.732	--	.740	.717	324
190	.740	.791	.783	.763	--	.771	.750	342
200	.773	.817	.811	.794	--	.801	.783	360
210	.806	.844	.838	.824	--	.830	.814	378
220	.838	.869	.865	.854	--	.859	.845	396
230	.870	.895	.892	.882	--	.886	.876	414
240	.901	.920	.918	.911	--	.914	.905	432
250	.931	.944	.943	.938	.898	.940	.934	450
260	.961	.969	.969	.965	.942	.966	.963	468
270	.990	.993	.994	.992	.986	.992	.991	486
280	1.019	1.016	1.018	1.018	1.030	1.017	1.019	504
290	1.047	1.039	1.043	1.043	1.075	1.042	1.046	522
300	1.075	1.063	1.067	1.068	1.119	1.066	1.072	540
310	1.102	1.085	1.091	1.093	1.163	1.089	1.098	558
320	1.129	1.108	1.114	1.117	1.208	1.113	1.124	576
330	1.155	1.130	1.137	1.141	1.252	1.136	1.150	594
340	1.181	1.152	1.161	1.164	1.297	1.158	1.174	612
350	1.207	1.174	1.183	1.187	1.341	1.180	1.199	630

REFERENCES

- (1) Reid, Robert C. and Thomas K. Sherwood, 1966: The Properties of Gases and Liquids, 2nd ed., McGraw-Hill, New York, 395-455.
- (2) The U.S. Standard Atmosphere, 1962, U.S. Govt. Printing Office, Washington, D.C., 14.
- (3) Kropschot, R. H., B. W. Birmingham, D. B. Mann, Editors, 1968: Technology of Liquid Helium, NBS Monograph 111, U.S. Govt. Printing Office, Washington, D.C., 50.
- (4) Woolley, Harold W., Russell B. Scott, F. G. Brickwedde, 1948: Compilation of Thermal Properties of Hydrogen in its Various Isotopic and Ortho-Para Modifications, NBS Research Paper, RP 1932, Vol. 41, 446-447.
- (5) Hilsenrath, Joseph, Charles W. Beckett, William S. Benedict, Lilla Fano, Harold J. Hoge, Joseph F. Masi, Ralph L. Nuttall, Yeram S. Touloukian, Harold W. Woolley, 1955: Tables of Thermal Properties of Gases, NBS Circular 564, U.S. Govt. Printing Office, Washington, D.C.

5. Prandtl Number of Selected Gases

The Prandtl number is frequently used in heat transfer correlations. Because it is a dimensionless number which is determined by the characteristics of the fluid and not by the heat transfer application, it can be tabulated for each fluid. The equations

$$\text{Pr} = \frac{C_p \mu}{k} \quad \text{and} \quad \text{Pr} = \frac{C_p \mu}{kM} \quad (\text{J-8})$$

define the Prandtl number Pr. In the first equation the specific heat C_p must be expressed in terms of energy per unit of mass per degree, while in the second it must be expressed in terms of energy per mol per degree. The variable μ is the dynamic viscosity, k is the thermal conductivity, and M is the molecular weight. Since all of these variables except M are functions of temperature only (or nearly so) at pressures equal to or less than one atmosphere, Pr is also a function of temperature. In fact, Pr can readily be computed from the data in the tables of sub-sections J.2, J.3, and J.4, and a correlating equation for Pr may be derived from the correlating equations given in those sub-sections.

For the gases listed here in the range of temperatures mostlikely to

be encountered in ballooning, Pr is nearly constant, and for many engineering applications an average value is adequate. For those applications which require greater precision, the following equation has been found to correlate Pr well with temperature for the gases listed here.

$$Pr = a + b \times 10^{-4}T \quad (J-9)$$

Table J-12 lists values of a and b for each gas. Temperature must be entered in °K. The equation yields values of Pr which differ from the data used to derive them by not more than 3% over the temperature range shown in Table J-13 for each gas.

Table J-13 gives values of Pr as a function of temperature for several gases. These values were computed by means of the correlating equation given above.

Table J-12

Constants for the Prandtl Number-Temperature Correlating Equation

	Air	Helium	Hydrogen	Nitrogen	Ammonia	Mixture 3H ₂ + N ₂	Methane
a	0.804	0.729	0.744	0.821	0.889	0.501	0.837
b	-3.25	-1.60	-1.25	-3.64	-0.71	-0.53	-2.90
*Source	(1)	(2)	(1)	(1)	**	**	**

*The numbers refer to the references which follow Table J-13.

**These constants are based on values of Pr computed from the data of subsections J.2, J.3, and J.4. The low values of Pr for the mixture of hydrogen and nitrogen have been verified in a study by Colburn and Coghlan (3).

Table J-13

Prandtl Numbers for Selected Gases as a Function of Temperature

Temp °K	Air	Helium	Hydrogen	Nitrogen	Ammonia	Mixture 3H ₂ +N ₂	Methane	Temp °R
150	.755	.705	.725	.766	--	.493	.793	270
160	.752	.703	.724	.763	--	.493	.791	288
170	.749	.702	.723	.759	--	.492	.788	306
180	.745	.700	.721	.755	--	.491	.785	324
190	.742	.699	.720	.752	--	.491	.782	342
200	.739	.697	.719	.748	--	.490	.779	360
210	.736	.695	.718	.745	--	.490	.776	378
220	.732	.694	.716	.741	--	.489	.773	396
230	.729	.692	.715	.737	--	.489	.770	414
240	.726	.691	.714	.734	--	.488	.767	432
250	.723	.689	.713	.730	.871	.488	.764	450
260	.719	.687	.711	.726	.871	.487	.762	468
270	.716	.686	.710	.723	.870	.487	.759	486
280	.713	.684	.709	.719	.869	.486	.756	504
290	.710	.683	.708	.715	.868	.486	.753	522
300	.706	.681	.706	.712	.868	.485	.750	540
310	.703	.679	.705	.708	.867	.485	.747	558
320	.700	.678	.704	.705	.866	.484	.744	576
330	.697	.676	.703	.701	.866	.484	.741	594
340	.693	.675	.701	.697	.865	.483	.738	612
350	.690	.673	.700	.694	.864	.482	.735	630

REFERENCES

- (1) Hilsenrath, Joseph, Charles W. Beckett, William S. Benedict, Lilla Fano, Harold J. Hoge, Joseph F. Masi, Ralph L. Nuttall, Yeram S. Touloukian, Harold W. Woolley, 1955: Tables of Thermal Properties of Gases, NBS Circular 564, U.S. Govt. Printing Office, Washington, D.C., 14-74, 254-368.
- (2) Kropschot, R. H., B. W. Birmingham, D. B. Mann, Editors, 1968: Technology of Liquid Helium, NBS Monograph 111, U.S. Govt. Printing Office, Washington, D.C., 35-53.
- (3) Colburn, A. P. and C. A. Coghlan, 1941: Trans. ASME, 63:561.

K. SPECIFIC LIFT OF HELIUM AND HYDROGEN AND PROPERTIES OF THE U.S. STANDARD

ATMOSPHERE, 1962

Table K-1 is an abridged version of a table contained in an NCAR Technical Note by Warren et al. (1). The basis for calculating the specific lift of a gas in the atmosphere is given in Section IV, and a discussion of the atmosphere, including the U.S. Standard Atmosphere, 1962, may be found in Section XI.

Although the original table has been reduced for inclusion here, linear interpolation is permissible throughout the abridged table. The variables presented in columns 6-10 are valid in any atmosphere in which the mixture of atmospheric gases has the same molecular weight as air, and in which both the pressure-to-temperature ratio in the lift gas and the atmosphere equal the tabulated value. Since gas and air pressure are very nearly equal in zero-pressure balloons during flight, the air and gas temperature must also be nearly equal if the tabulated specific lift values (columns 8-10) are to be valid. An error caused by a difference in temperature between the air and gas is not usually serious from the point of view of the balloon designer or the scientist, but flight operations

personnel must keep such differences in mind. See Sections II and III for a discussion of the consequences of differing gas and air temperatures during flight.

Columns 1 and 3 through 5 are derived directly from the definition of the U.S. Standard Atmosphere, 1962. Column 2 is calculated from an empirical equation derived by Morris (2). The equation is

$$m_n = 10 p_n (1.03751 - 5.27 \times 10^{-3} \log_{10} p_n) \quad (K-1)$$

where p_n is atmospheric pressure in mb at level n in the atmosphere and m_n is the total mass of air in kg in a one m^2 column extending from level n upward through the balance of the atmosphere. A similar equation,

$$p_n = m_n / (1.03757 - 5.27 \times 10^{-3} \log_{10} m_n)$$

in which m_n is given in gm/cm^2 and p_n is in mb, may be used to convert from the usual integrated mass units to pressure.

The following examples illustrate the use of this table:

1. Determine the altitude at which a balloon system having a gross mass m_G of 2721 kg and a volume V of $10^6 m^3$ will float when the balloon is inflated with helium.

Solution: The mass per unit volume (specific lift) which must be supported by the balloon is $m_G/V = m$. Note that m_G is the gross mass of the balloon system excluding the mass of the enclosed lift gas but including the mass of the balloon; m is then $2.721 \times 10^{-3} \text{ kg/m}^3$. Column 9 of the table lists values of $2.8360\text{E-}03$ (2.8360×10^{-3}) and $2.5812\text{E-}03$, corresponding to air densities of $3.2909\text{E-}03$ and $2.9952\text{E-}03$, respectively. Linear interpolation yields a density of 3.1574×10^{-3} corresponding to the specific lift of 2.721×10^{-3} , and the balloon system will float in the atmosphere at the level at which the air density is $3.1574 \times 10^{-3} \text{ kg/m}^3$. If density is known as a function of height, the height at which the balloon will float may be determined. If density is not known as a function of height in the real atmosphere, the height in a model atmosphere can serve as an approximation to the height in the real atmosphere. In this example the height in the U.S. Standard Atmosphere, 1962, is found in column 3 by interpolation to be 41,367 m.

2. Determine the volume of a helium-filled balloon required to support a gross mass of 6000 lb at a height of 135,600 ft in the U.S. Standard Atmosphere, 1962.

Solution: From the definition of specific lift, $V = m_G/m$; from column 10, interpolation yields $m = 1.7057 \times 10^{-4} \text{ lbs/ft}^3$ at 135,600 ft. Then $V = 6000/1.7057 \times 10^{-4}$, or approximately $35.2 \times 10^6 \text{ ft}^3$.

3. Another method of determining volume is to multiply the gas expansion factor for the desired height by the product of the gross mass and the volume of gas required to support a unit mass at sea level.

Solution: From column 7, the gas expansion is found to be 386.8; from Table 2 of Section IV, or by taking the reciprocal of the specific lift at sea level, the volume of helium required to lift a mass of one pound is found to be 15.17. Then $V = 6000 \times 15.17 \times 386.8 = 35.2 \times 10^6 \text{ ft}^3$.

4. A parachute has been selected to lower a payload, and the entire system will have a descent velocity of 22 ft/sec at sea level in the U.S. Standard Atmosphere, 1962. Compute its terminal descent velocity at 2.4 mb in that standard atmosphere.

Solution: Equation (21) of Section X, $v_T = v_{T,0} \sqrt{\rho_0/\rho}$, may be used in this case. The ratio of densities may be determined from the table by division, but the gas expansion factor found in column 7 is that ratio. Thus, $v_T = 22 \sqrt{372.2} = 424 \text{ ft/sec}$.

Table K-1

Specific Lift of Helium and Hydrogen and Properties of the U.S. Standard Atmosphere, 1962									
(1)	(2)	(3)	(4)	(5)	(6)	(7)	(8)	(9)	(10)
p Press. (mb)	Integrated Air Mass (kg/m ²)	H Geopot. Alt. (m)	H Alt. (ft)	T Temp. (°C)	ρ Density (kg/m ³)	Gas Ex- pansion	Lift H ₂ Pure (kg/m ³)	Lift He Grade A (kg/m ³)	Lift He Grade A (lb/ft ³)
1050	1.073E+04	-302	-989	16.96	1.2609E+00	.972	1.1731E+00	1.0866E+00	6.7832E-02
1040	1.062E+04	-220	-723	16.43	1.2511E+00	.979	1.1640E+00	1.0782E+00	6.7308E-02
1030	1.052E+04	-139	-454	15.90	1.2414E+00	.987	1.1550E+00	1.0698E+00	6.6784E-02
1020	1.042E+04	-56	-184	15.36	1.2316E+00	.995	1.1459E+00	1.0614E+00	6.6258E-02
1010	1.032E+04	27	89	14.82	1.2218E+00	1.003	1.1368E+00	1.0529E+00	6.5732E-02
1000	1.022E+04	111	364	14.28	1.2120E+00	1.011	1.1277E+00	1.0445E+00	6.5204E-02
990	1.012E+04	195	641	13.73	1.2022E+00	1.019	1.1185E+00	1.0360E+00	6.4676E-02
980	1.001E+04	281	920	13.18	1.1923E+00	1.027	1.1094E+00	1.0275E+00	6.4146E-02
970	9.911E+03	366	1202	12.62	1.1825E+00	1.036	1.1002E+00	1.0190E+00	6.3616E-02
960	9.809E+03	453	1486	12.06	1.1726E+00	1.045	1.0910E+00	1.0105E+00	6.3084E-02
950	9.707E+03	540	1773	11.49	1.1627E+00	1.054	1.0818E+00	1.0020E+00	6.2551E-02
940	9.605E+03	628	2062	10.92	1.1528E+00	1.063	1.0725E+00	9.9343E-01	6.2018E-02
930	9.503E+03	717	2353	10.34	1.1428E+00	1.072	1.0633E+00	9.8486E-01	6.1483E-02
920	9.401E+03	807	2647	9.76	1.1329E+00	1.081	1.0540E+00	9.7628E-01	6.0947E-02
910	9.299E+03	897	2944	9.17	1.1229E+00	1.091	1.0447E+00	9.6768E-01	6.0420E-02
900	9.197E+03	989	3243	8.57	1.1129E+00	1.101	1.0354E+00	9.5906E-01	5.9872E-02
890	9.096E+03	1081	3545	7.98	1.1029E+00	1.111	1.0261E+00	9.5042E-01	5.9333E-02
880	8.994E+03	1173	3850	7.37	1.0928E+00	1.121	1.0168E+00	9.4176E-01	5.8792E-02
870	8.892E+03	1267	4157	6.76	1.0828E+00	1.131	1.0074E+00	9.3309E-01	5.8251E-02
860	8.790E+03	1362	4468	6.15	1.0727E+00	1.142	9.9802E-01	9.2439E-01	5.7708E-02
850	8.688E+03	1457	4781	5.53	1.0626E+00	1.153	9.8861E-01	9.1568E-01	5.7164E-02
840	8.586E+03	1554	5098	4.90	1.0524E+00	1.164	9.7918E-01	9.0695E-01	5.6619E-02
830	8.484E+03	1651	5417	4.27	1.0423E+00	1.175	9.6973E-01	8.9820E-01	5.6073E-02
820	8.382E+03	1749	5740	3.63	1.0321E+00	1.187	9.6026E-01	8.8942E-01	5.5525E-02
810	8.280E+03	1849	6065	2.98	1.0219E+00	1.199	9.5077E-01	8.8063E-01	5.4976E-02

113

Table K-1

Specific Lift of Helium and Hydrogen and Properties of the U.S. Standard Atmosphere, 1962									
(1)	(2)	(3)	(4)	(5)	(6)	(7)	(8)	(9)	(10)
p Press. (mb)	Integrated Air Mass (kg/m ²)	H Geopot. Alt. (m)	H Alt. (ft)	T Temp. (°C)	ρ Density (kg/m ³)	Gas Ex- pansion	Lift H ₂ Pure (kg/m ³)	Lift He Grade A (kg/m ³)	Lift He Grade A (lb/ft ³)
800	8.178E+03	1949	6394	2.33	1.0117E+00	1.211	9.4125E-01	8.7182E-01	5.4426E-02
790	8.076E+03	2050	6727	1.67	1.0014E+00	1.223	9.3171E-01	8.6298E-01	5.3874E-02
780	7.974E+03	2153	7063	1.01	9.9113E-01	1.236	9.2215E-01	8.5413E-01	5.3321E-02
770	7.872E+03	2256	7402	.34	9.8083E-01	1.249	9.1256E-01	8.4525E-01	5.2767E-02
760	7.770E+03	2361	7745	-.34	9.7050E-01	1.262	9.0296E-01	8.3635E-01	5.2211E-02
750	7.668E+03	2466	8091	-1.03	9.6015E-01	1.276	8.9332E-01	8.2743E-01	5.1654E-02
740	7.566E+03	2573	8442	-1.72	9.4977E-01	1.290	8.8367E-01	8.1848E-01	5.1096E-02
730	7.464E+03	2681	8796	-2.43	9.3936E-01	1.304	8.7398E-01	8.0951E-01	5.0536E-02
720	7.362E+03	2790	9154	-3.14	9.2893E-01	1.319	8.6428E-01	8.0052E-01	4.9975E-02
710	7.260E+03	2901	9516	-3.85	9.1847E-01	1.334	8.5454E-01	7.9151E-01	4.9412E-02
700	7.158E+03	3012	9882	-4.58	9.0798E-01	1.349	8.4479E-01	7.8247E-01	4.8848E-02
690	7.056E+03	3125	10253	-5.31	8.9746E-01	1.365	8.3500E-01	7.7340E-01	4.8282E-02
680	6.954E+03	3239	10628	-6.06	8.8692E-01	1.381	8.2519E-01	7.6432E-01	4.7715E-02
670	6.852E+03	3355	11008	-6.81	8.7634E-01	1.398	8.1535E-01	7.5520E-01	4.7146E-02
660	6.749E+03	3472	11392	-7.57	8.6573E-01	1.415	8.0548E-01	7.4606E-01	4.6575E-02
650	6.647E+03	3591	11780	-8.34	8.5510E-01	1.433	7.9558E-01	7.3689E-01	4.6003E-02
640	6.545E+03	3711	12174	-9.12	8.4443E-01	1.451	7.8566E-01	7.2770E-01	4.5429E-02
630	6.443E+03	3832	12573	-9.91	8.3373E-01	1.469	7.7570E-01	7.1848E-01	4.4853E-02
620	6.341E+03	3955	12977	-10.71	8.2300E-01	1.488	7.6572E-01	7.0923E-01	4.4276E-02
610	6.239E+03	4080	13386	-11.52	8.1223E-01	1.508	7.5570E-01	6.9996E-01	4.3697E-02
600	6.137E+03	4206	13801	-12.34	8.0143E-01	1.529	7.4565E-01	6.9065E-01	4.3116E-02
590	6.035E+03	4335	14221	-13.17	7.9060E-01	1.549	7.3557E-01	6.8131E-01	4.2533E-02
580	5.933E+03	4464	14647	-14.02	7.7973E-01	1.571	7.2546E-01	6.7195E-01	4.1948E-02
570	5.831E+03	4596	15079	-14.87	7.6883E-01	1.593	7.1532E-01	6.6255E-01	4.1362E-02
560	5.729E+03	4730	15517	-15.74	7.5789E-01	1.616	7.0514E-01	6.5312E-01	4.0773E-02

114

Table K-1

Specific Lift of Helium and Hydrogen and Properties of the U.S. Standard Atmosphere, 1962

(1)	(2)	(3)		(4)	(5)	(6)	(7)	(8)	(9)	(10)
p Press. (mb)	Integrated Air Mass (kg/m ²)	H Geopot. Alt. (m) (ft)		T Temp. (°C)	ρ Density (kg/m ³)	Gas Ex- pansion	Lift H ₂ Pure (kg/m ³)	Lift He Grade A (kg/m ³)	Lift He Grade A (lb/ft ³)	
550	5.627E+03	4865	15962	-16.62	7.4691E-01	1.640	6.9493E-01	6.4366E-01	4.0183E-02	
540	5.525E+03	5003	16413	-17.52	7.3590E-01	1.665	6.8468E-01	6.3417E-01	3.9590E-02	
530	5.423E+03	5142	16871	-18.43	7.2484E-01	1.690	6.7439E-01	6.2464E-01	3.8995E-02	
520	5.321E+03	5284	17336	-19.35	7.1375E-01	1.716	6.6407E-01	6.1508E-01	3.8398E-02	
510	5.219E+03	5428	17809	-20.28	7.0261E-01	1.743	6.5371E-01	6.0549E-01	3.7799E-02	
500	5.116E+03	5574	18289	-21.23	6.9144E-01	1.772	6.4331E-01	5.9586E-01	3.7198E-02	
490	5.014E+03	5723	18777	-22.20	6.8022E-01	1.801	6.3287E-01	5.8619E-01	3.6595E-02	
480	4.912E+03	5874	19273	-23.18	6.6895E-01	1.831	6.2239E-01	5.7648E-01	3.5989E-02	
470	4.810E+03	6028	19777	-24.18	6.5765E-01	1.863	6.1187E-01	5.6674E-01	3.5380E-02	
460	4.708E+03	6184	20290	-25.20	6.4629E-01	1.895	6.0131E-01	5.5695E-01	3.4769E-02	
450	4.606E+03	6344	20812	-26.23	6.3489E-01	1.929	5.9070E-01	5.4713E-01	3.4156E-02	
440	4.504E+03	6506	21344	-27.29	6.2344E-01	1.965	5.8005E-01	5.3726E-01	3.3540E-02	
430	4.402E+03	6671	21886	-28.36	6.1195E-01	2.002	5.6935E-01	5.2735E-01	3.2922E-02	
420	4.299E+03	6839	22438	-29.45	6.0040E-01	2.040	5.5861E-01	5.1740E-01	3.2300E-02	
410	4.197E+03	7011	23000	-30.57	5.8879E-01	2.081	5.4781E-01	5.0740E-01	3.1676E-02	
400	4.095E+03	7185	23574	-31.71	5.7714E-01	2.123	5.3697E-01	4.9736E-01	3.1049E-02	
390	3.993E+03	7364	24160	-32.87	5.6543E-01	2.167	5.2607E-01	4.8727E-01	3.0419E-02	
380	3.891E+03	7546	24758	-34.05	5.5366E-01	2.213	5.1512E-01	4.7712E-01	2.9786E-02	
370	3.789E+03	7732	25369	-35.26	5.4183E-01	2.261	5.0412E-01	4.6693E-01	2.9150E-02	
360	3.687E+03	7923	25993	-36.50	5.2994E-01	2.312	4.9306E-01	4.5669E-01	2.8510E-02	
350	3.584E+03	8117	26631	-37.76	5.1799E-01	2.365	4.8194E-01	4.4639E-01	2.7867E-02	
340	3.482E+03	8316	27285	-39.06	5.0597E-01	2.421	4.7076E-01	4.3603E-01	2.7221E-02	
330	3.380E+03	8520	27954	-40.38	4.9389E-01	2.480	4.5951E-01	4.2562E-01	2.6570E-02	
320	3.278E+03	8729	28640	-41.74	4.8174E-01	2.543	4.4821E-01	4.1514E-01	2.5917E-02	
310	3.176E+03	8944	29343	-43.14	4.6951E-01	2.609	4.3683E-01	4.0461E-01	2.5259E-02	

115

Table K-1

Specific Lift of Helium and Hydrogen and Properties of the U.S. Standard Atmosphere, 1962

(1)	(2)	(3)		(4)	(5)	(6)	(7)	(8)	(9)	(10)
p Press. (mb)	Integrated Air Mass (kg/m ²)	H Geopot. Alt. (m) (ft)		T Temp. (°C)	ρ Density (kg/m ³)	Gas Ex- pansion	Lift H ₂ Pure (kg/m ³)	Lift He Grade A (kg/m ³)	Lift He Grade A (lb/ft ³)	
300	3.073E+03	9164	30065	-44.57	4.5721E-01	2.679	4.2538E-01	3.9401E-01	2.4597E-02	
290	2.971E+03	9390	30807	-46.04	4.4483E-01	2.754	4.1387E-01	3.8334E-01	2.3931E-02	
280	2.869E+03	9623	31570	-47.55	4.3236E-01	2.833	4.0227E-01	3.7260E-01	2.3261E-02	
270	2.767E+03	9862	32355	-49.10	4.1982E-01	2.918	3.9060E-01	3.6179E-01	2.2586E-02	
260	2.664E+03	10109	33164	-50.71	4.0718E-01	3.008	3.7884E-01	3.5090E-01	2.1906E-02	
250	2.562E+03	10363	33999	-52.36	3.9445E-01	3.106	3.6700E-01	3.3993E-01	2.1221E-02	
240	2.460E+03	10626	34861	-54.07	3.8163E-01	3.210	3.5507E-01	3.2887E-01	2.0531E-02	
230	2.358E+03	10898	35753	-55.83	3.6870E-01	3.322	3.4304E-01	3.1773E-01	1.9836E-02	
220	2.255E+03	11180	36679	-56.50	3.5575E-01	3.463	3.2913E-01	3.0485E-01	1.9031E-02	
210	2.153E+03	11475	37646	-56.50	3.3767E-01	3.628	3.1417E-01	2.9100E-01	1.8166E-02	
200	2.051E+03	11784	38662	-56.50	3.2159E-01	3.809	2.9921E-01	2.7714E-01	1.7301E-02	
190	1.948E+03	12109	39729	-56.50	3.0552E-01	4.010	2.8425E-01	2.6328E-01	1.6436E-02	
180	1.846E+03	12452	40854	-56.50	2.8944E-01	4.232	2.6929E-01	2.4943E-01	1.5571E-02	
170	1.744E+03	12815	42043	-56.50	2.7336E-01	4.481	2.5433E-01	2.3557E-01	1.4706E-02	
160	1.641E+03	13199	43304	-56.50	2.5728E-01	4.761	2.3937E-01	2.2171E-01	1.3841E-02	
150	1.539E+03	13608	44647	-56.50	2.4120E-01	5.079	2.2441E-01	2.0785E-01	1.2976E-02	
140	1.437E+03	14046	46082	-56.50	2.2512E-01	5.442	2.0945E-01	1.9400E-01	1.2111E-02	
130	1.334E+03	14516	47624	-56.50	2.0904E-01	5.860	1.9449E-01	1.8014E-01	1.1246E-02	
120	1.232E+03	15024	49290	-56.50	1.9296E-01	6.349	1.7953E-01	1.6628E-01	1.0381E-02	
110	1.129E+03	15575	51100	-56.50	1.7688E-01	6.926	1.6457E-01	1.5243E-01	9.5157E-03	
100	1.027E+03	16180	53083	-56.50	1.6080E-01	7.618	1.4961E-01	1.3857E-01	8.6506E-03	
95	9.757E+02	16505	54150	-56.50	1.5276E-01	8.019	1.4213E-01	1.3164E-01	8.2181E-03	
90	9.245E+02	16848	55275	-56.50	1.4472E-01	8.465	1.3465E-01	1.2471E-01	7.7856E-03	
85	8.732E+02	17210	56464	-56.50	1.3668E-01	8.963	1.2716E-01	1.1778E-01	7.3530E-03	
80	8.220E+02	17595	57726	-56.50	1.2864E-01	9.523	1.1968E-01	1.1086E-01	6.9205E-03	

116

Table K-1

Specific Lift of Helium and Hydrogen and Properties of the U.S. Standard Atmosphere, 1962									
(1)	(2)	(3)	(4)	(5)	(6)	(7)	(8)	(9)	(10)
p Press. (mb)	Integrated Air Mass (kg/m ²)	H Geopot. Alt. (m)	H Alt. (ft)	T Temp. (°C)	ρ Density (kg/m ³)	Gas Ex- pansion	Lift H ₂ Pure (kg/m ³)	Lift He Grade A (kg/m ³)	Lift He Grade A (lb/ft ³)
75	7.707E+02	18004	59069	-56.50	1.2060E-01	10.158	1.1220E-01	1.0393E-01	6.4880E-03
70	7.195E+02	18442	60504	-56.50	1.1256E-01	10.883	1.0472E-01	9.6999E-02	6.0554E-03
65	6.682E+02	18912	62046	-56.50	1.0452E-01	11.720	9.7244E-02	9.0070E-02	5.6229E-03
60	6.169E+02	19419	63711	-56.50	9.6478E-02	12.697	8.9763E-02	8.3142E-02	5.1904E-03
55	5.656E+02	19971	65522	-56.50	8.8439E-02	13.851	8.2283E-02	7.6213E-02	4.7578E-03
50	5.143E+02	20576	67507	-55.92	8.0185E-02	15.277	7.4605E-02	6.9101E-02	4.3138E-03
45	4.630E+02	21247	69708	-55.25	7.1945E-02	17.027	6.6937E-02	6.2000E-02	3.8705E-03
40	4.116E+02	22000	72177	-54.50	6.3731E-02	19.221	5.9295E-02	5.4921E-02	3.4286E-03
35	3.603E+02	22856	74987	-53.64	5.5547E-02	22.053	5.1681E-02	4.7868E-02	2.9883E-03
30	3.089E+02	23849	78244	-52.65	4.7397E-02	25.845	4.4098E-02	4.0845E-02	2.5499E-03
29	2.986E+02	24068	78962	-52.43	4.5772E-02	26.763	4.2586E-02	3.9445E-02	2.4625E-03
28	2.884E+02	24294	79706	-52.21	4.4148E-02	27.747	4.1075E-02	3.8045E-02	2.3751E-03
27	2.781E+02	24530	80478	-51.97	4.2526E-02	28.806	3.9566E-02	3.6648E-02	2.2878E-03
26	2.678E+02	24774	81280	-51.73	4.0906E-02	29.947	3.8059E-02	3.5251E-02	2.2007E-03
25	2.575E+02	25029	82115	-51.47	3.9287E-02	31.180	3.6553E-02	3.3857E-02	2.1136E-03
24	2.473E+02	25294	82984	-51.21	3.7671E-02	32.518	3.5049E-02	3.2464E-02	2.0266E-03
23	2.370E+02	25570	83892	-50.93	3.6056E-02	33.975	3.3547E-02	3.1072E-02	1.9398E-03
22	2.267E+02	25860	84841	-50.64	3.4444E-02	35.565	3.2047E-02	2.9683E-02	1.8530E-03
21	2.164E+02	26163	85836	-50.34	3.2833E-02	37.309	3.0548E-02	2.8295E-02	1.7664E-03
20	2.061E+02	26481	86881	-50.02	3.1225E-02	39.231	2.9052E-02	2.6909E-02	1.6799E-03
19	1.958E+02	26816	87981	-49.68	2.9620E-02	41.358	2.7558E-02	2.5525E-02	1.5935E-03
18	1.856E+02	27170	89142	-49.33	2.8016E-02	43.725	2.6066E-02	2.4144E-02	1.5072E-03
17	1.753E+02	27545	90371	-48.95	2.6416E-02	46.374	2.4577E-02	2.2764E-02	1.4211E-03
16	1.650E+02	27943	91678	-48.56	2.4818E-02	49.360	2.3090E-02	2.1387E-02	1.3351E-03

117

Table K-1

Specific Lift of Helium and Hydrogen and Properties of the U.S. Standard Atmosphere, 1962									
(1)	(2)	(3)	(4)	(5)	(6)	(7)	(8)	(9)	(10)
p Press. (mb)	Integrated Air Mass (kg/m ²)	H Geopot. Alt. (m)	H Alt. (ft)	T Temp. (°C)	ρ Density (kg/m ³)	Gas Ex- pansion	Lift H ₂ Pure (kg/m ³)	Lift He Grade A (kg/m ³)	Lift He Grade A (lb/ft ³)
15	1.547E+02	28368	93071	-48.13	2.3223E-02	52.750	2.1606E-02	2.0012E-02	1.2493E-03
14	1.444E+02	28823	94564	-47.68	2.1631E-02	56.632	2.0125E-02	1.8641E-02	1.1637E-03
13	1.341E+02	29313	96170	-47.19	2.0042E-02	61.121	1.8647E-02	1.7272E-02	1.0782E-03
12	1.238E+02	29843	97909	-46.66	1.8457E-02	66.370	1.7173E-02	1.5906E-02	9.9296E-04
11	1.135E+02	30420	99804	-46.08	1.6876E-02	72.588	1.5701E-02	1.4543E-02	9.0790E-04
10.0	1.032E+02	31055	101885	-45.45	1.5299E-02	80.07	1.4234E-02	1.3184E-02	8.2307E-04
9.5	9.807E+01	31397	103008	-45.10	1.4512E-02	84.41	1.3502E-02	1.2506E-02	7.8074E-04
9.0	9.292E+01	31758	104193	-44.74	1.3727E-02	89.24	1.2771E-02	1.1829E-02	7.3848E-04
8.5	8.777E+01	32141	105448	-44.11	1.2928E-02	94.75	1.2028E-02	1.1141E-02	6.9552E-04
8.0	8.262E+01	32548	106785	-42.97	1.2107E-02	101.18	1.1265E-02	1.0434E-02	6.5136E-04
7.5	7.747E+01	32984	108215	-41.74	1.1291E-02	108.50	1.0505E-02	9.7301E-03	6.0743E-04
7.0	7.231E+01	33453	109753	-40.43	1.0479E-02	116.90	9.7494E-03	9.0302E-03	5.6374E-04
6.5	6.716E+01	33959	111414	-39.01	9.6713E-03	126.66	8.9982E-03	8.3344E-03	5.2030E-04
6.0	6.200E+01	34509	113220	-37.47	8.8690E-03	138.12	8.2517E-03	7.6430E-03	4.7714E-04
5.5	5.685E+01	35112	115196	-35.79	8.0721E-03	151.76	7.5103E-03	6.9563E-03	4.3427E-04
5.00	5.169E+01	35777	117377	-33.93	7.2812E-03	168.2	6.7744E-03	6.2747E-03	3.9172E-04
4.80	4.963E+01	36063	118317	-33.12	6.9666E-03	175.8	6.4817E-03	6.0036E-03	3.7479E-04
4.60	4.756E+01	36362	119299	-32.29	6.6531E-03	184.1	6.1900E-03	5.7334E-03	3.5792E-04
4.40	4.550E+01	36676	120329	-31.41	6.3407E-03	193.2	5.8994E-03	5.4642E-03	3.4112E-04
4.20	4.344E+01	37006	121411	-30.48	6.0294E-03	203.2	5.6098E-03	5.1960E-03	3.2437E-04
4.00	4.137E+01	37353	122551	-29.51	5.7194E-03	214.2	5.3213E-03	4.9288E-03	3.0769E-04
3.80	3.931E+01	37720	123753	-28.48	5.4106E-03	226.4	5.0340E-03	4.6627E-03	2.9108E-04
3.60	3.724E+01	38108	125027	-27.40	5.1032E-03	240.0	4.7480E-03	4.3978E-03	2.7454E-04
3.40	3.518E+01	38520	126379	-26.24	4.7972E-03	255.4	4.4633E-03	4.1340E-03	2.5808E-04
3.20	3.312E+01	38959	127820	-25.01	4.4926E-03	272.7	4.1799E-03	3.8716E-03	2.4169E-04

118a

Table K-1

Specific Lift of Helium and Hydrogen and Properties of the U.S. Standard Atmosphere, 1962									
(1)	(2)	(3)	(4)	(5)	(6)	(7)	(8)	(9)	(10)
p Press. (mb)	Integrated Air Mass (kg/m ²)	H Geopot. Alt. (m)	H Alt. (ft)	T Temp. (°C)	ρ Density (kg/m ³)	Gas Ex- pansion	Lift H ₂ Pure (kg/m ³)	Lift He Grade A (kg/m ³)	Lift He Grade A (lb/ft ³)
3.00	3.105E+01	39429	129362	-23.70	4.1896E-03	292.4	3.8980E-03	3.6104E-03	2.2539E-04
2.80	2.898E+01	39935	131019	-22.28	3.8882E-03	315.1	3.6176E-03	3.3507E-03	2.0918E-04
2.60	2.692E+01	40481	132810	-20.75	3.5886E-03	341.4	3.3389E-03	3.0926E-03	1.9306E-04
2.40	2.485E+01	41074	134757	-19.09	3.2909E-03	372.2	3.0619E-03	2.8360E-03	1.7705E-04
2.20	2.279E+01	41723	136887	-17.28	2.9952E-03	409.0	2.7868E-03	2.5812E-03	1.6114E-04
2.00	2.072E+01	42440	139238	-15.27	2.7018E-03	453.4	2.5137E-03	2.3283E-03	1.4535E-04
1.80	1.865E+01	43239	141859	-13.03	2.4107E-03	508.2	2.2429E-03	2.0774E-03	1.2969E-04
1.60	1.658E+01	44140	144815	-10.51	2.1222E-03	577.2	1.9745E-03	1.8289E-03	1.1417E-04
1.40	1.451E+01	45172	148202	-7.62	1.8367E-03	666.9	1.7089E-03	1.5828E-03	9.8814E-05
1.20	1.245E+01	46378	152158	-4.24	1.5546E-03	788.0	1.4464E-03	1.3397E-03	8.3634E-05
1.00	1.038E+01	47820	156890	-2.50	1.2872E-03	951.7	1.1976E-03	1.1092E-03	6.9247E-05
.90	9.340E+00	48655	159629	-2.50	1.1584E-03	1057.5	1.0778E-03	9.9830E-04	6.2322E-05
.80	8.304E+00	49588	162690	-2.50	1.0297E-03	1189.6	9.5805E-04	8.8738E-04	5.5397E-05
.70	7.268E+00	50646	166161	-2.50	9.0101E-04	1359.6	8.3830E-04	7.7646E-04	4.8473E-05
.60	6.232E+00	51867	170167	-2.50	7.7229E-04	1586.2	7.1854E-04	6.6553E-04	4.1548E-05
.50	5.195E+00	53305	174885	-5.11	6.4984E-04	1885.1	6.0461E-04	5.6001E-04	3.4960E-05
.40	4.158E+00	55044	180592	-8.59	5.2671E-04	2325.8	4.9005E-04	4.5390E-04	2.8336E-05
.30	3.121E+00	57254	187840	-13.01	4.0174E-04	3049.2	3.7378E-04	3.4621E-04	2.1613E-05
.20	2.082E+00	60305	197850	-19.11	2.7426E-04	4466.5	2.5517E-04	2.3635E-04	1.4755E-05
.10	1.043E+00	65281	214176	-37.62	1.4791E-04	8282.1	1.3762E-04	1.2746E-04	7.9573E-06

REFERENCES

- (1) Warren, J.C., J. H. Smalley, A. L. Morris, 1971: Aerostatic Lift of Helium and Hydrogen in the Atmosphere. NCAR-TN/TA-69, National Center for Atmospheric Research, Boulder, Colo., 79 pp.
- (2) Morris, Alvin L., 1970: Atmospheric Mass above Balloon Payloads, Facilities for Atmospheric Research. 14, Sept. 1970. National Center for Atmospheric Research, Boulder, Colo., 21-24.

L. BASIC NATURAL-SHAPE BALLOON PARAMETERS

The principles of balloon design are discussed in detail in Section V, and the history of the development of the natural-shape balloon is reviewed in Section I. For nearly two decades a set of "Sigma Tables" was an indispensable tool of the balloon designer, and, although digital computers now enable a design engineer to by-pass the tables, many uses are still found for them. Table L-1, which was computed by Smalley (the author of Section V) is valid for zero-pressure, fully tailored balloons carrying the full payload at the nadir. All parameters are non-dimensional except the angle, which is in degrees. Lengths have been non-dimensionalized by dividing by λ , forces by dividing by P. Examples of the use of the table are given in Section V.

Terms used in the table are defined as follows:

$$\text{SIGMA} = (2 \pi)^{1/3} (w/b \lambda)$$

where w is film weight per unit area, b is specific buoyancy of lifting gas, λ is $(P/b)^{1/3}$, and P is total payload (located at nadir).

GORE STA.--curvilinear coordinate measured from nadir.

RADIUS--Radial coordinate measured horizontally from axis of rotation.

HEIGHT--Height coordinate measured vertically from nadir.

ANGLE--angle of tangent to curve measured with respect to the axis of rotation.

FILM LOAD--totalized meridional film stress.

PARTIAL AREA--area of balloon below the gore station.

PARTIAL VOLUME--volume of balloon below the gore station.

$$A/S^{*2} = A/S^2 = (\text{total area})/(\text{total gore length})^2$$

$$V/S^{*3} = V/S^3 = (\text{total volume})/(\text{total gore length})^3$$

Note: A constant gore station increment has been used for each SIGMA value. The RADIUS and HEIGHT are given, however, at the level where RADIUS is maximum, i.e., where ANGLE is zero.

TABLE 1
 (continued)

BASE ANGLE = 54.39144 SIGMA = 0.10						
GOPE STA.	RADIUS	HEIGHT	ANGLE	FILM LOAD	---PARTIAL---	---
					AREA	VOLUME
0.00000	0.00000	0.00000	50.149	1.56056	0.00000	0.00000
.03999	.03062	.02556	50.146	1.56056	.00384	.00003
.07978	.06124	.05110	50.130	1.56056	.01535	.00020
.11960	.09185	.07671	50.034	1.56056	.03453	.00068
.15955	.12242	.10232	49.995	1.56056	.06138	.00161
.19944	.15295	.12800	49.849	1.56056	.09589	.00314
.23933	.18339	.15374	49.630	1.56056	.13804	.00544
.27922	.21371	.17964	49.325	1.56056	.18781	.00866
.31911	.24388	.20579	48.918	1.56056	.24515	.01296
.35899	.27383	.23212	48.396	1.56056	.31003	.01851
.39888	.30351	.25878	47.744	1.56056	.38239	.02550
.43877	.33285	.28580	46.946	1.56056	.46214	.03410
.47866	.36177	.31327	45.988	1.56056	.54919	.04452
.51855	.39019	.34126	44.855	1.56056	.64343	.05696
.55843	.41801	.36985	43.533	1.56056	.74472	.07164
.59832	.44510	.39912	42.005	1.56056	.85290	.08878
.63821	.47135	.42915	40.258	1.56056	.96776	.10861
.67810	.49660	.46002	38.278	1.56056	1.08908	.13135
.71799	.52071	.49180	36.050	1.56056	1.21659	.15720
.75788	.54349	.52454	33.561	1.56056	1.34997	.18634
.79776	.56474	.55825	30.800	1.56056	1.48888	.21892
.83765	.58426	.59307	27.755	1.56056	1.63291	.25502
.87754	.60182	.62888	24.420	1.56056	1.78158	.29462
.91743	.61716	.66569	20.789	1.56056	1.93438	.33761
.95732	.63005	.70344	16.859	1.56056	2.09073	.38376
.99721	.64021	.74203	12.634	1.56056	2.24997	.43267
1.03709	.64741	.78122	8.121	1.56056	2.41139	.48378
1.07698	.65141	.82090	3.332	1.56056	2.57422	.53640
1.11687	.65218	.86077	0.000	1.56056	2.73762	.59064
1.15676	.65199	.90053	-5.986	1.56056	2.90073	.64255
1.19665	.64925	.93983	-12.456	1.56056	3.06261	.69406
1.23653	.63176	.97830	-18.080	1.56056	3.22234	.74315
1.27642	.61751	1.01553	-23.313	1.56056	3.37897	.78885
1.31631	.59959	1.05115	-29.003	1.56056	3.53156	.83035
1.35620	.57817	1.08478	-35.393	1.56056	3.67922	.86703
1.39609	.55348	1.11603	-41.126	1.56056	3.82104	.89957
1.43598	.52580	1.14476	-46.742	1.56056	3.95640	.92489
1.47586	.49549	1.17070	-52.185	1.56056	4.08443	.94616
1.51575	.46291	1.19368	-57.400	1.56056	4.20454	.96277
1.55564	.42841	1.21368	-62.338	1.56056	4.31630	.97529
1.59553	.39236	1.23074	-66.955	1.56056	4.41919	.98435
1.63542	.35511	1.24495	-71.213	1.56056	4.51288	.99026
1.67530	.31693	1.25649	-75.081	1.56056	4.59711	.99473
1.71519	.27810	1.26557	-78.534	1.56056	4.67168	.99728
1.75508	.23881	1.27244	-81.553	1.56056	4.73646	.99873
1.79497	.19923	1.27739	-84.123	1.56056	4.79136	.99949
1.83486	.15948	1.28071	-86.234	1.56056	4.83631	.99983
1.87475	.11965	1.28273	-87.880	1.56056	4.87123	.99999
1.91463	.07977	1.28377	-89.057	1.56056	4.89623	.99999
1.95452	.03989	1.28415	-89.764	1.56056	4.91128	1.00000
1.99441	-.00000	1.28421	-90.000	1.56056	4.91628	1.00000

A/S**2 = 1.23597 V/S**3 = .12605 HEIGHT = 0.00000

TABLE 1

BASE ANGLE = 54.39144 SIGMA = 0.10						
GOPE STA.	RADIUS	HEIGHT	ANGLE	FILM LOAD	---PARTIAL---	---
					AREA	VOLUME
0.00000	0.00000	0.00000	54.391	1.71749	0.00000	0.00000
.04309	.03363	.02809	54.382	1.71764	.06974	.00063
.08618	.06705	.05620	54.342	1.71809	.01837	.00026
.12927	.10505	.08753	54.257	1.71834	.04267	.00087
.17236	.13999	.10455	54.111	1.71983	.07585	.00207
.21545	.17486	.14288	53.867	1.72125	.11847	.00405
.25855	.20960	.16130	53.571	1.72292	.17052	.00762
.30164	.24418	.17708	53.140	1.72491	.23196	.01119
.34473	.27854	.20308	52.938	1.72722	.30273	.01678
.38782	.31262	.22945	51.910	1.72987	.38276	.02403
.43091	.34635	.25627	51.067	1.73288	.47198	.03319
.47400	.37963	.28364	50.054	1.73627	.57027	.04453
.51709	.41238	.31164	49.856	1.74034	.67750	.05834
.56018	.44449	.34037	47.457	1.74424	.79352	.07493
.60327	.47584	.36994	45.844	1.74837	.91813	.09462
.64636	.50628	.40044	44.002	1.75288	1.05110	.11775
.68946	.53565	.43197	41.917	1.75957	1.19218	.14465
.73255	.56379	.46460	39.576	1.76568	1.34104	.17568
.77564	.59049	.49842	36.968	1.77233	1.49734	.21105
.81873	.61554	.53347	34.304	1.77953	1.66064	.25116
.86182	.63870	.56980	30.915	1.78729	1.83043	.29608
.90491	.65973	.60740	27.457	1.79560	2.00630	.34592
.94800	.67835	.64626	23.706	1.80446	2.18750	.40060
.99109	.69429	.68628	19.666	1.81382	2.37339	.45988
1.03418	.70726	.72736	15.342	1.82360	2.56319	.52331
1.07727	.71700	.76933	10.746	1.83382	2.75607	.59203
1.12036	.72325	.81195	5.894	1.84420	2.95113	.66572
1.16346	.72578	.85495	.868	1.85487	3.14737	.73070
1.20655	.72583	.89613	0.000			
1.24964	.72441	.89801	-4.484	1.86550	3.34378	.80188
1.29273	.71951	.94074	-9.948	1.87601	3.53928	.87188
1.33582	.70351	.98275	-15.545	1.88623	3.73275	.93928
1.37891	.68593	1.02363	-21.232	1.89602	3.92311	1.00276
1.42200	.66783	1.06295	-26.963	1.90523	4.10924	1.06116
1.46509	.64929	1.10002	-32.686	1.91373	4.29080	1.11355
1.50818	.63189	1.13537	-38.352	1.92142	4.46463	1.15935
1.55127	.60355	1.16781	-43.911	1.92825	4.63195	1.19830
1.59437	.57224	1.19739	-49.312	1.93418	4.79118	1.23043
1.63746	.53833	1.22395	-54.505	1.93920	4.94158	1.25627
1.68055	.50220	1.24741	-59.460	1.94336	5.08249	1.27627
1.72364	.46423	1.26776	-64.124	1.94672	5.21335	1.29124
1.76673	.42477	1.28506	-68.468	1.94934	5.33373	1.30202
1.80982	.38416	1.29944	-72.462	1.95132	5.44326	1.30944
1.85291	.34268	1.31110	-76.082	1.95277	5.54167	1.31431
1.89600	.30058	1.32025	-79.308	1.95377	5.62827	1.31731
1.93909	.25806	1.32718	-82.125	1.95444	5.70440	1.31902
1.98218	.21526	1.33216	-84.522	1.95484	5.76848	1.31991
2.02528	.17230	1.33551	-86.490	1.95506	5.82095	1.32031
2.06837	.12926	1.33755	-88.024	1.95517	5.86177	1.32046
2.11146	.08618	1.33859	-89.122	1.95521	5.89093	1.32050
2.15455	.04309	1.33895	-89.780	1.95522	5.90843	1.32051
2.19764	-.00000	1.33903	-90.000	1.95522	5.91427	1.32051

A/S**2 = 1.27406 V/S**3 = .13203 HEIGHT = .32051

Table L-1

BASE ANGLE = 58.88617 SIGMA = .20						
GORE STA.	RADIUS	HEIGHT	ANGLE	FILM LOAD	-----PARTIAL----- AREA	-----VOLUME
0.00000	0.00000	0.00000	58.886	1.93521	0.00000	0.00000
.04701	.04024	.02430	58.867	1.93554	.00594	.00004
.09402	.08047	.04862	58.798	1.93654	.02377	.00033
.14103	.12065	.07302	58.663	1.93821	.05347	.00112
.18803	.16076	.09754	58.444	1.94056	.09504	.00265
.23504	.20075	.12224	58.125	1.94361	.14843	.00520
.28205	.24058	.14721	57.689	1.94736	.21361	.00903
.32906	.28019	.17253	57.121	1.95185	.29052	.01444
.37607	.31951	.19828	56.403	1.95711	.37910	.02173
.42308	.35847	.22459	55.521	1.96318	.47923	.03124
.47009	.39698	.25155	54.458	1.97012	.59081	.04334
.51709	.43494	.27928	53.199	1.97798	.71369	.05844
.56410	.47222	.30791	51.728	1.98683	.84768	.07697
.61111	.50870	.33755	50.033	1.99673	.99256	.09940
.65812	.54422	.36834	48.097	2.00777	1.14809	.12623
.70513	.57862	.40038	45.909	2.02003	1.31394	.15800
.75214	.61168	.43379	43.457	2.03357	1.48976	.19521
.79915	.64321	.46866	40.731	2.04848	1.67513	.23838
.84615	.67295	.50505	37.723	2.06480	1.86955	.28795
.89316	.70064	.54303	34.427	2.08257	2.07245	.34428
.94017	.72600	.58260	30.841	2.10180	2.28320	.40759
.98718	.74874	.62374	26.967	2.12246	2.50106	.47792
1.03419	.76893	.66636	22.809	2.14449	2.72521	.55506
1.08120	.78508	.71035	18.379	2.16777	2.95474	.63892
1.12821	.79808	.75551	13.699	2.19213	3.18863	.72750
1.17521	.80724	.80161	8.760	2.21733	3.42580	.82087
1.22222	.81232	.84832	3.617	2.24311	3.66509	.91719
1.26923	.81334	.88837	0.000	2.26912	3.90524	1.01478
1.31624	.81311	.89531	-1.711	2.29502	4.14498	1.11174
1.36325	.80948	.94216	-7.190	2.32042	4.38298	1.20614
1.41026	.80133	.98844	-12.783	2.34493	4.61790	1.29610
1.45727	.78869	1.03369	-18.449	2.36820	4.84844	1.37990
1.50428	.77162	1.07747	-24.145	2.38991	5.07330	1.45617
1.55128	.75030	1.11935	-29.828	2.40980	5.29126	1.52389
1.59829	.72495	1.15891	-35.452	2.42767	5.50118	1.58251
1.64530	.69587	1.19583	-40.973	2.44341	5.70200	1.63191
1.69231	.66342	1.22981	-46.350	2.45699	5.89279	1.67240
1.73932	.62798	1.26067	-51.541	2.46845	6.07271	1.70462
1.78633	.58994	1.28826	-56.509	2.47788	6.24106	1.72945
1.83334	.54973	1.31254	-61.224	2.48545	6.39725	1.74795
1.88034	.50766	1.33355	-65.642	2.49136	6.54081	1.76121
1.92735	.46417	1.35136	-69.748	2.49581	6.67134	1.77033
1.97436	.41955	1.36615	-73.515	2.49906	6.78857	1.77628
2.02137	.37410	1.37812	-76.923	2.50131	6.89227	1.77994
2.06838	.32805	1.38751	-79.958	2.50279	6.98241	1.78204
2.11539	.28158	1.39461	-82.605	2.50369	7.05859	1.78312
2.16240	.23485	1.40315	-84.856	2.50419	7.12103	1.78361
2.20941	.18797	1.40315	-86.704	2.50442	7.16962	1.78380
2.25641	.14101	1.40523	-88.145	2.50451	7.20433	1.78384
2.30342	.09402	1.40630	-89.175	2.50453	7.22515	1.78385
2.35043	.04701	1.40670	-89.794	2.50453	7.23210	1.78385
A/S**2 = 1.30909	V/S**3 = .13738	WEIGHT = .78385				

Table L-1

BASE ANGLE = 63.46893 SIGMA = .30						
GORE STA.	RADIUS	HEIGHT	ANGLE	FILM LOAD	-----PARTIAL----- AREA	-----VOLUME
0.00000	0.00000	0.00000	63.469	2.23872	0.00000	0.00000
.05176	.04630	.02313	63.438	2.23927	.00753	.00005
.10351	.09258	.04631	63.333	2.24092	.03011	.00042
.15527	.13879	.06961	63.137	2.24367	.06774	.00141
.20703	.18491	.09311	62.833	2.24756	.12037	.00336
.25879	.23107	.11691	62.403	2.25261	.18798	.00660
.31054	.27662	.14110	61.830	2.25889	.27051	.01152
.36230	.32210	.16582	61.099	2.26645	.36787	.01849
.41406	.36722	.19117	60.193	2.27538	.47997	.02798
.46582	.41189	.21732	59.096	2.28579	.60666	.04046
.51757	.45600	.24439	57.792	2.29779	.74780	.05651
.56933	.49943	.27254	56.266	2.31153	.90317	.07672
.62109	.54203	.30193	54.564	2.32717	1.07254	.10179
.67285	.58365	.33200	52.492	2.34487	1.25960	.13246
.72460	.62408	.36500	50.218	2.36481	1.45201	.16951
.77636	.66312	.39898	47.671	2.38715	1.66135	.21378
.82812	.70052	.43474	44.841	2.42108	1.88313	.26607
.87987	.73602	.47240	41.723	2.43972	2.11677	.32718
.93163	.76931	.51202	38.313	2.47019	2.36160	.39776
.98339	.80008	.55363	34.612	2.50356	2.61686	.47833
1.03515	.82799	.59720	30.622	2.53981	2.88166	.56913
1.08690	.85269	.64267	26.354	2.57886	3.15504	.67010
1.13866	.87383	.68990	21.820	2.62053	3.43587	.78078
1.19042	.89106	.73869	17.037	2.66452	3.72295	.90124
1.24218	.90406	.78877	12.029	2.71146	4.01496	1.02710
1.29393	.91254	.83981	6.821	2.75784	4.31046	1.15950
1.34569	.91628	.89141	1.446	2.80606	4.60796	1.29518
1.39745	.91646	.90510	0.000	2.85447	4.90588	1.43155
1.44920	.91511	.94314	-4.064	2.90234	5.20261	1.56591
1.50096	.90893	.99450	-9.671	2.94897	5.49651	1.69552
1.55272	.89773	1.04901	-15.338	2.99366	5.78596	1.81786
1.60448	.88159	1.09917	-21.025	3.03579	6.06937	1.93079
1.65623	.86366	1.14148	-26.692	3.07481	6.34524	2.03262
1.70799	.83518	1.18651	-32.300	3.11032	6.61211	2.12226
1.75975	.80546	1.22886	-37.810	3.14203	6.86868	2.19924
1.81151	.77185	1.26819	-43.185	3.16981	7.11375	2.26365
1.86326	.73475	1.30426	-48.390	3.19365	7.34624	2.31610
1.91502	.69459	1.33689	-53.391	3.21367	7.55223	2.35761
1.96678	.65180	1.36597	-58.158	3.23010	7.73939	2.38945
2.01854	.60680	1.39151	-62.662	3.24325	7.90969	2.41309
2.07029	.55998	1.41354	-66.880	3.25348	8.13396	2.42998
2.12205	.51171	1.43224	-70.788	3.26119	8.29239	2.44156
2.17381	.46233	1.44767	-74.369	3.26679	8.43659	2.44912
2.22556	.41211	1.46018	-77.604	3.27067	8.56036	2.45376
2.27732	.36130	1.46999	-80.483	3.27322	8.66954	2.45641
2.32908	.31008	1.47740	-82.993	3.27478	8.76201	2.45778
2.38084	.25860	1.48273	-85.126	3.27564	8.83771	2.45840
2.43259	.20697	1.48631	-86.877	3.27604	8.89661	2.45863
2.48435	.15526	1.48848	-88.242	3.27620	8.93869	2.45870
2.53611	.10351	1.48960	-89.219	3.27623	8.96394	2.45871
2.58787	.05176	1.49001	-89.805	3.27623	8.97235	2.45871
A/S**2 = 1.33975	V/S**3 = .14187	WEIGHT = 1.45871				

Table L-1

BASE ANGLE = 67.91954 SIGMA = .40						
GORE STA.	RADIUS	HEIGHT	ANGLE	FILM LOAD	---PARTIAL--- AREA	---PARTIAL--- VOLUME
0.00000	0.00000	0.00000	67.920	2.66022	0.00000	0.00000
.05741	.05319	.02159	67.875	2.66101	.00999	.00066
.11482	.10635	.04328	67.730	2.66336	.03837	.00051
.17223	.15943	.06514	67.467	2.66732	.08631	.00174
.22964	.21239	.08732	67.069	2.67294	.15338	.00417
.28705	.26516	.10995	66.519	2.68030	.23951	.00824
.34446	.31767	.13312	65.861	2.68951	.34464	.01445
.40187	.36986	.15705	64.898	2.70072	.46865	.02336
.45928	.42161	.18188	63.795	2.71411	.61141	.03561
.51669	.47284	.20781	62.476	2.72991	.77275	.05194
.57409	.52339	.23501	60.926	2.74837	.95245	.07318
.63150	.57313	.26367	59.130	2.76979	1.15024	.10029
.68891	.62188	.29398	57.075	2.79447	1.36580	.13435
.74632	.66944	.32614	54.749	2.82276	1.59874	.17692
.80373	.71556	.36031	52.146	2.85501	1.84858	.22808
.86114	.75999	.39666	49.240	2.89155	2.11477	.29032
.91855	.80243	.43531	46.045	2.93270	2.39663	.36453
.97596	.84253	.47638	42.552	2.97873	2.69380	.45191
1.03337	.87995	.51940	38.763	3.02981	3.00443	.55345
1.09078	.91429	.56590	34.684	3.08603	3.32783	.66986
1.14819	.94515	.61429	30.327	3.14734	3.66331	.80140
1.20560	.97213	.66495	25.717	3.21351	4.00923	.94780
1.26301	.99483	.71766	20.844	3.28416	4.36812	1.10813
1.32042	1.01287	.77214	15.764	3.35868	4.72637	1.28076
1.37783	1.02592	.82803	10.495	3.43631	5.09423	1.46338
1.43524	1.03370	.88488	5.069	3.51609	5.46586	1.65298
1.49265	1.03601	.94223	-.479	3.59695	5.83931	1.84607
1.55006	1.03603	.93730	0.000	3.67770	6.21259	2.03881
1.60747	1.02378	1.05620	-11.800	3.75712	6.58366	2.22728
1.66488	1.00927	1.11172	-17.499	3.83403	6.95050	2.40769
1.72228	.98932	1.16553	-23.176	3.90730	7.31112	2.57667
1.77969	.96417	1.21711	-28.793	3.97596	7.66360	2.73144
1.83710	.93413	1.26601	-34.318	4.03921	8.00612	2.87003
1.89451	.89957	1.31183	-39.716	4.09645	8.33697	2.99115
1.95192	.86091	1.35424	-44.958	4.14734	8.65460	3.09455
2.00933	.81860	1.39301	-50.012	4.19171	8.95762	3.18059
2.06674	.77309	1.42799	-54.853	4.22966	9.24478	3.25032
2.12415	.72486	1.45910	-59.454	4.26143	9.51502	3.30528
2.18156	.67435	1.48636	-63.792	4.28743	9.76744	3.34730
2.23897	.62198	1.50985	-67.846	4.30819	10.00129	3.37840
2.29638	.56813	1.52971	-71.598	4.32432	10.21598	3.40058
2.35379	.51314	1.54617	-75.031	4.33646	10.41102	3.41576
2.41120	.45730	1.55946	-78.132	4.34526	10.58607	3.42565
2.46861	.40085	1.56988	-80.889	4.35137	10.74086	3.43172
2.52602	.34398	1.57775	-83.292	4.35538	10.87520	3.43518
2.58343	.28686	1.58341	-85.335	4.35782	10.98898	3.43698
2.64084	.22958	1.58721	-87.011	4.35917	11.08213	3.43779
2.69825	.17221	1.58952	-88.318	4.35981	11.15460	3.43809
2.75566	.11482	1.59071	-89.252	4.36005	11.20637	3.43819
2.81306	.05741	1.59114	-89.813	4.36010	11.23743	3.43819
2.87047	-.00000	1.59121	-90.000	4.36011	11.24778	3.43819

A/S**2 = 1.36508 V/S**3 = .14537 WEIGHT = 2.42819

Table L-1

BASE ANGLE = 72.01204 SIGMA = .50						
GORE STA.	RADIUS	HEIGHT	ANGLE	FILM LOAD	---PARTIAL--- AREA	---PARTIAL--- VOLUME
0.00000	0.00000	0.00000	72.012	3.23816	0.00000	0.00000
.06396	.06083	.01977	71.953	3.23919	.01222	.00008
.12792	.12162	.03968	71.767	3.24228	.04889	.00062
.19188	.18232	.05985	71.435	3.24750	.10997	.00210
.25584	.24287	.08046	70.942	3.25497	.19542	.00505
.31980	.30321	.10168	70.273	3.26484	.30516	.01005
.38376	.36326	.12371	69.411	3.27734	.43910	.01777
.44772	.42294	.14674	68.342	3.29277	.59710	.02898
.51168	.48212	.17100	67.048	3.31147	.77899	.04463
.57564	.54069	.19670	65.517	3.33387	.98455	.06581
.63960	.59849	.22409	63.733	3.36045	1.21350	.09378
.70356	.65535	.25340	61.682	3.39175	1.46549	.13004
.76752	.71104	.28486	59.351	3.42826	1.74011	.17625
.83148	.76531	.31869	56.731	3.47090	2.03684	.23427
.89544	.81789	.35510	53.812	3.52001	2.35544	.30666
.95940	.86845	.39428	50.590	3.57628	2.69399	.39369
1.02336	.91660	.43636	47.062	3.64026	3.05278	.49915
1.08732	.96196	.48144	43.231	3.71240	3.43038	.62427
1.15128	1.00408	.52957	39.105	3.79238	3.82557	.77054
1.21524	1.04249	.58069	34.696	3.88209	4.23696	.93890
1.27920	1.07674	.63469	30.022	3.97956	4.66297	1.12959
1.34316	1.10635	.69127	25.106	4.08493	5.10182	1.34195
1.40712	1.13088	.75042	19.974	4.19744	5.55157	1.57431
1.47108	1.14992	.81146	14.657	4.31601	6.01009	1.82393
1.53504	1.16314	.87402	9.187	4.43924	6.47510	2.08705
1.59900	1.17027	.93756	3.600	4.56551	6.94421	2.35911
1.66296	1.17155	.97823	0.000	4.69299	7.41492	2.63453
1.72692	1.17113	1.00149	-2.070	4.82279	7.88471	2.90798
1.79088	1.16564	1.02519	-7.786	4.95977	8.35102	3.17374
1.85484	1.15383	1.03803	-13.513	5.09389	8.81133	3.42658
1.91880	1.13581	1.03938	-19.219	5.22352	9.26318	3.66196
2.00000	1.11181	1.02484	-24.868	5.34829	9.70424	3.87629
2.08112	1.08213	1.00527	-30.431	5.46737	10.13228	4.06712
2.16224	1.04710	1.00000	-35.877	5.57986	10.54528	4.23313
2.24336	1.00731	1.00881	-41.179	5.68489	10.94137	4.37417
2.32448	.96338	1.04499	-46.319	5.78226	11.31888	4.49106
2.40560	.91497	1.09712	-51.242	5.87229	11.67637	4.58547
2.48672	.86349	1.16505	-55.956	5.95496	12.01257	4.65965
2.56784	.80914	1.24873	-60.427	6.02921	12.32643	4.71625
2.64896	.75238	1.33921	-64.637	6.09486	12.61708	4.75804
2.73008	.69368	1.43658	-68.567	6.15181	12.88380	4.78782
2.81120	.63343	1.54052	-72.201	6.20000	13.12607	4.80316
2.89232	.57198	1.65027	-75.524	6.23929	13.34345	4.81411
2.97344	.50965	1.76710	-78.524	6.26929	13.53564	4.82141
3.05456	.44669	1.88833	-81.190	6.29000	13.70244	4.82533
3.13568	.38329	1.99681	-83.514	6.30125	13.84477	4.82617
3.21680	.31962	1.70291	-85.489	6.30375	13.96336	4.82567
3.29792	.25579	1.70701	-87.110	6.30625	14.05829	4.82386
3.37904	.19188	1.70949	-88.373	6.30625	14.13055	4.82141
3.46016	.12792	1.71077	-89.277	6.30375	14.18000	4.81817
3.54128	.06396	1.71104	-89.919	6.30000	14.20625	4.81386
3.62240	-.00000	1.71131	-90.000	6.29625	14.21875	4.80816

A/S**2 = 1.38484 V/S**3 = .14790 WEIGHT = 3.85818

M. BUOYANT EQUILIBRIUM DIAGRAMS

A floating balloon is in a precarious state of equilibrium, and a slight decrease in the ratio of gas to air temperature or a slight loss of gas will cause it to accelerate downward unless corrective measures are taken. Figures M-1 and M-2 provide graphical solutions to the equation of buoyant equilibrium for balloons inflated with helium and hydrogen, respectively. The theory upon which these diagrams are based and some examples of their use are given in Section II.I.4.a.

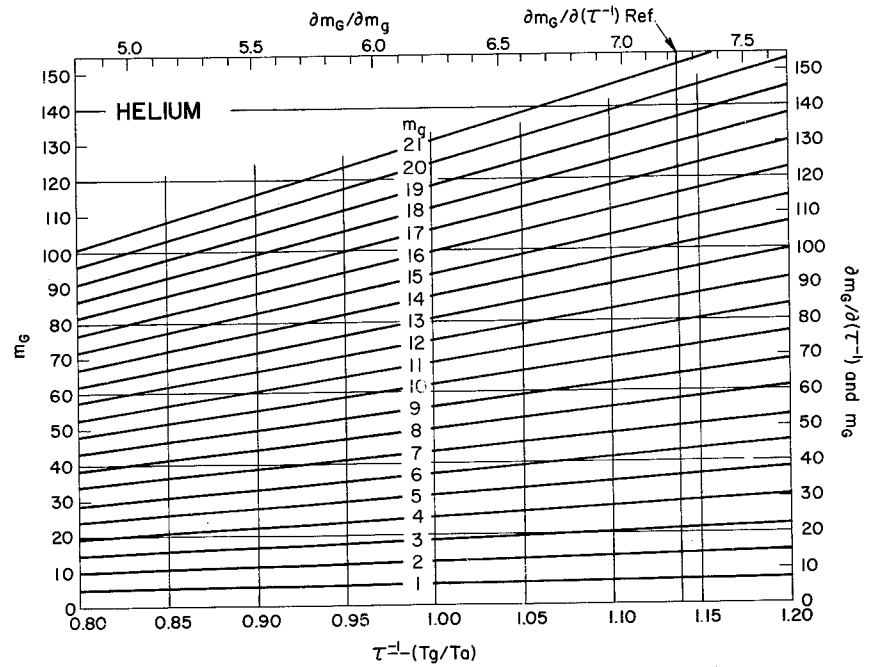


Fig. M-1. Buoyant equilibrium diagram for helium.

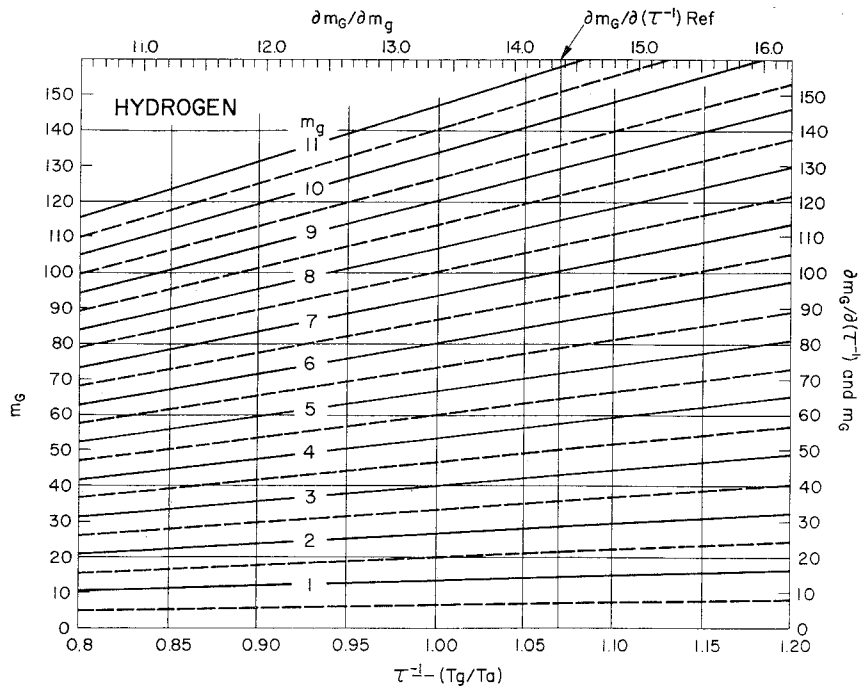


Fig. M-2. Buoyant equilibrium diagram for hydrogen.

N. SUNRISE AND SUNSET

The times of sunrise and sunset, both at the ground and on a floating balloon, are often important. If a nautical almanac is available, it is a relatively simple matter to determine sunrise and sunset at the surface. If it is more convenient, however, the local hour angle of sunrise and sunset at the surface may be approximated by the formula

$$(\text{LHA})_S = \cos^{-1} \left[\frac{-0.01 - \sin \lambda_1 \sin \delta_s}{\cos \lambda_1 \cos \delta_s} \right] \quad (\text{N-1})$$

in which λ_1 is the latitude of the observer and δ_s is the solar declination. Both λ_1 and δ_s are positive north of the equator and negative south of the equator. The formula includes a coarse correction for the apparent diameter of the sun and atmospheric refraction. The $(\text{LHA})_S$ in degrees divided by 15 is the time in hours by which the sunrise precedes true solar noon or the sunset follows true solar noon.

Similarly, the formula

$$(\text{LHA})_B = \cos^{-1} \left[\frac{-\sqrt{\frac{2H}{r}} - 0.016 - \sin \lambda_1 \sin \delta_s}{\cos \lambda_1 \cos \delta_s} \right] \quad (\text{N-2})$$

gives approximately the local hour angle of sunrise or sunset on a balloon

floating at height H where r is the radius of the earth; H and r must be expressed in the same length units.

The time difference in minutes between sunrise (or sunset) at the surface and sunrise (or sunset) at a floating balloon is

$$\Delta t = 4 [(LHA)_B - (LHA)_S] \quad (N-3)$$

if the LHA values are determined in degrees.

The value of δ_s is a function of time; it is given approximately by the formula

$$\delta_s = - 23.45 \cos \frac{360}{365} (n + 10) \quad (N-4)$$

in which n is the number of the day in the year counting 1 January as n = 1, 2 January as n = 2, etc. to 31 December = 365.

0. STAR CHARTS

The appearance of the brighter stars in the sky at any hour of the night and any time of the year may be visualized by referring to Figs. 0-1 and 0-2. These star charts may also be used to determine the approximate positions (declination and local hour angle) of any of the charted stars, day or night.

A star chart provides the most direct visual simulation of the star pattern when it is "set" against the sky. To set a chart for midnight, hold it directly overhead facing downward so that it can be read and turn it until an imaginary line drawn from the time of year on the outer ring through the pole on the chart points toward the earth's pole. The star pattern on the chart will then correspond to the midnight star pattern in the heavens at the observer's location at the time of year for which the chart was set.

An observer at a Northern Hemisphere site where there are no obstructions on the horizon should be able to see stars on the northern horizon which are below Polaris at a co-latitude equal numerically to his latitude. He should see stars on the southern horizon which are at a southern latitude

equal to his co-latitude. The stars on his eastern and western horizon will be directly over the equator, and their local hour angle will be 90° , i.e., they will pass over his meridian in six hours. By using these four points, the horizon can be visualized on the charts. Note that latitude is used when discussing the angular displacement of a star from the equator although declination is the proper term. A northern latitude corresponds to a positive declination, and a southern latitude to a negative declination.

There are 24 alternately shaded and unshaded hour segments in the ring just inside the month ring. The arrows indicate the direction of apparent turning of the celestial sphere. A chart may be set for n hours before midnight by first setting it to simulate the midnight sky and then turning it back n hours, i.e., n segments in the direction opposed to the arrows. Likewise, turning a chart set for midnight n hour segments in the direction of the arrows sets it for n hours after midnight.

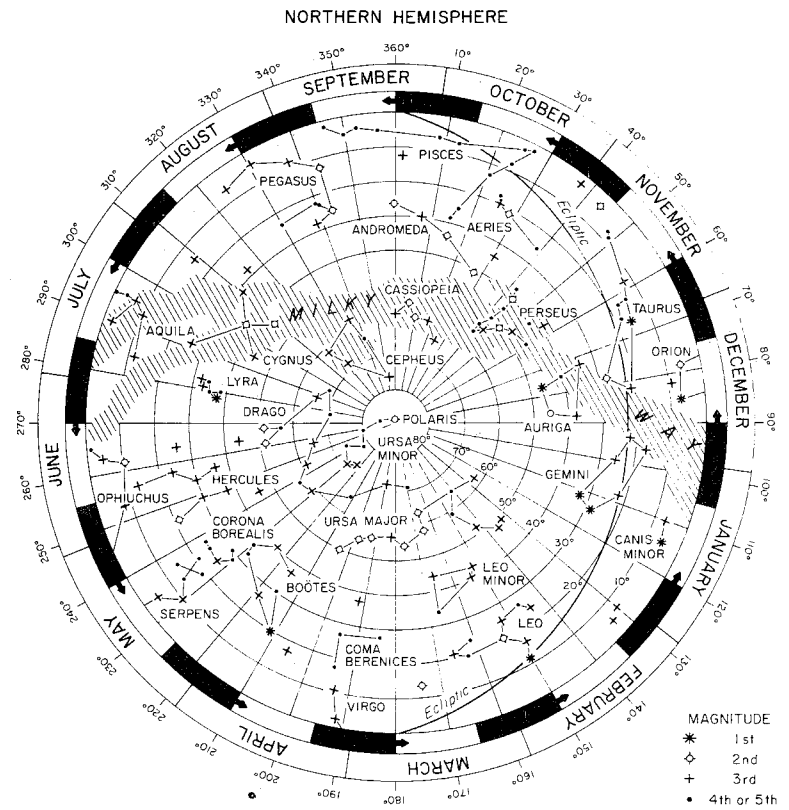


Fig. 0-1. Northern Hemisphere star chart.

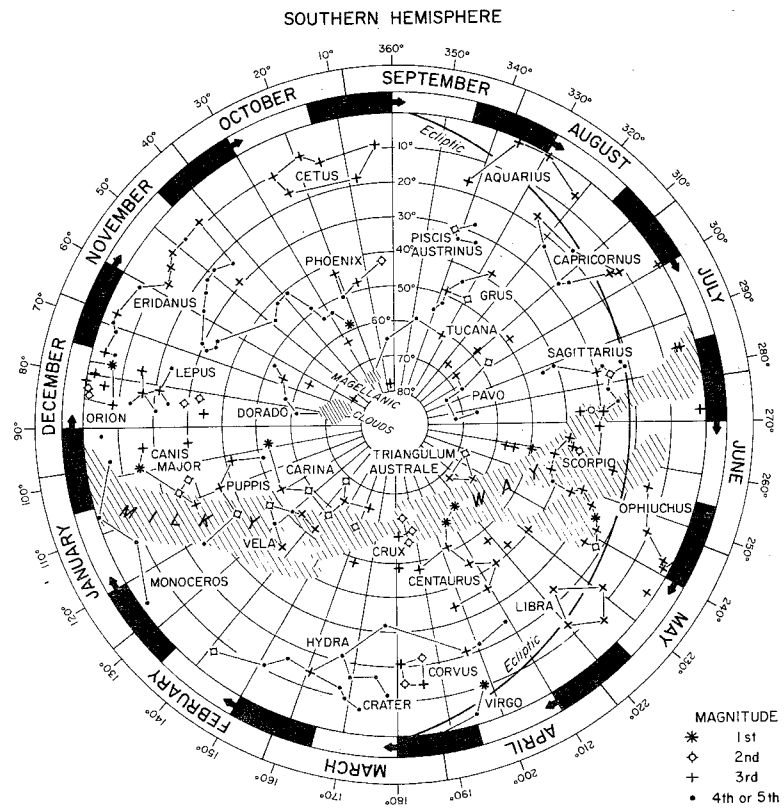


Fig. O-2. Southern Hemisphere star chart.

Part0002 NCAR-TN/IA-99 Scientific Ballooning Handbook - Link Page

[Previous](#)

[PART0001](#)